Chiral Analysis of Baryon Form Factors

PhD thesis by
Tobias A. Gail

summer 2007

Technische Universität München
Physik-Department
Institut für Theoretische Physik T39
Univ.-Prof. Dr. Wolfram Weise

Chiral Analysis of Baryon Form Factors

Dipl.-Phys. Univ. Tobias Andreas Gail

Vollständiger Abdruck der von der Fakultät für Physik der Technischen Universität München zur Erlangung des akademischen Grades eines

Doktors der Naturwissenschaften (Dr. rer. nat.)

genehmigten Dissertation.

Vorsitzender:		Univ.-Prof. Dr. Stephan Paul
Prüfer der Dissertation:	1.	Univ.-Prof. Dr. Wolfram Weise
	2.	Univ.-Prof. Dr. Michael Ratz

Die Dissertation wurde am 02.10.2007 bei der Technischen Universität München eingereicht und durch die Fakultät für Physik am 08.11.2007 angenommen.

Summary

This work presents an extensive theoretical investigation of the structure of the nucleon within the standard model of elementary particle physics. In particular, the long range contributions to a number of various form factors parametrizing the interactions of the nucleon with an electromagnetic probe are calculated. The theoretical framework for those calculations is chiral perturbation theory, the exact low energy limit of Quantum Chromo Dynamics, which describes such long range contributions in terms of a pion-cloud. In this theory, a nonrelativistic leading one loop order calculation of the form factors parametrizing the vector transition of a nucleon to its lowest lying resonance, the Δ, a covariant calculation of the isovector and isoscalar vector form factors of the nucleon at next to leading one loop order and a covariant calculation of the isoscalar and isovector generalized vector form factors of the nucleon at leading one loop order are performed. In order to perform consistent loop calculations in the covariant formulation of chiral perturbation theory an appropriate renormalization scheme is defined in this work. All theoretical predictions are compared to phenomenology and results from lattice QCD simulations. These comparisons allow for a determination of the low energy constants of the theory. Furthermore, the possibility of chiral extrapolation, i.e. the extrapolation of lattice data from simulations at large pion masses down to the small physical pion mass is studied in detail. Statistical as well as systematic uncertainties are estimated for all results throughout this work.

Zusammenfassung

Die vorliegenden Arbeit liefert eine umfassende theoretische Untersuchung der Struktur des Nukleons innerhalb des Standardmodells der Elementarteilchenphysik. Es werden die langreichweitigen Beiträge zu einer Vielzahl von Formfaktoren, die die Wechselwirkung des Nukleons mit einer elektromagnetischen Probe parametrisieren berechnet. Der theoretische Rahmen für diese Rechnungen ist die chirale Störungstheorie, der exakte Niederenergielimes der Quantenchromodynamik, in der diese langreichweitigen Beiträge durch eine Pionwolke beschrieben werden. Eine nichtrelativistische Rechnungen für die Formfaktoren, die den Übergang des Nukleons in seinen niedrigsten angeregten Zustand (das Δ) parametrisieren bis zur führenden Einschleifenordnung, eine kovariante Rechnung der isosvektoriellen und isoskalaren Vektorformfaktoren des Nukleons bis zur nächstführenden Einschleifenordnung und eine kovariante Rechnung der isosvektoriellen und isoskalaren verallgemeinerten Vektorformfaktoren des Nukleons bis zur führenden Einschleifenordnung werden präsentiert. Um wiederspruchsfreie Rechnungen in der kovarianten Formulierung der chiralen Störungstheorie sicher zu stellen wird ein entsprechendes Renormierungsschema für diese Theorie definiert.
Die theoretischen Vorhersagen werden mit Ergebnissen der Phenomenologie sowie von Gittersimulationen verglichen. Diese Vergleiche ermöglichen eine Bestimmung der Niederenergiekonstanten. Des Weiteren wird die Möglichkeit chiraler Extrapolationen, d.h. Extrapolationen der Ergebnisse von Gittersimulationen bei großen Pionmassen hin zur kleinen, physikalischen Pionmasse, ausführlich untersucht. Systematische und statistische Unsicherheiten werden für alle Ergebnisse dieser Arbeit abgeschätzt.

Contents

Introduction **5**

1 Basic Concepts of Chiral Effective Field Theory **9**
1.1 Construction Principles for the Effective Low Energy Lagrangean . . . 9
1.2 Nonrelativistic Limit . . . 12
1.3 Inclusion of Spin-$\frac{3}{2}$ Fields . . . 13

2 The Nucleon-to-Delta Transition Form Factors **15**
2.1 Introduction . . . 15
2.2 Parametrization of the Matrix Element . . . 16
2.3 Effective Field Theory Calculation . . . 18
2.4 Discussion of the Results . . . 23
2.4.1 Fit I: Comparison to previous $\mathcal{O}(\epsilon^3)$ SSE results . . . 23
2.4.2 Fit II: Revised $\mathcal{O}(\epsilon^3)$ SSE analysis . . . 24
2.4.3 The range of applicability of the nonrelativistic $\mathcal{O}(\epsilon^3)$ SSE calculation . . . 29
2.4.4 Chiral extrapolation of the $N\Delta$ transition form factors to $\mathcal{O}(\epsilon^3)$ in nonrelativistic SSE 31
2.5 Conclusions and Outlook . . . 35

3 Renormalization of Covariant BChPT **41**
3.1 Introduction . . . 41
3.2 Infrared Singular- and Regular Parts . . . 41
3.3 An example: Quark Mass Dependence of the Nucleon Mass . . . 48
3.3.1 Input Lagrangeans . . . 48
3.3.2 $\overline{\text{IR}}$ renormalized BChPT calculation of the leading pion-nucleon loop . . . 51
3.3.3 Application of the modified renormalization scheme to a chiral extrapolation of the mass of the nucleon . . . 54
3.4 Concluding Remarks . . . 57

4 The vector Form Factors of the Nucleon **61**
4.1 Introduction . . . 61
4.2 The Form Factors of the Nucleon . . . 62
4.3 Formalism . . . 62
4.3.1 The form factors of the nucleon at next-to-leading one loop order . . . 62
4.3.2 Meson Lagrangean . . . 65
4.3.3 Nucleon Lagrangeans . . . 65
4.4 Isovector Form Factors of the Nucleon . . . 66
4.4.1 The quark mass dependence of the isovector anomalous magnetic moment . . . 66
4.4.2 The quark mass dependence of the slopes of the isovector form factors . . . 67
4.4.3 The momentum dependence of the isovector Sachs form factors . . . 69
4.5 Isoscalar Form Factors of the Nucleon . . . 72

4.5.1 The quark mass dependence of the isoscalar anomalous magnetic moment 72
4.5.2 The quark mass dependence of the slopes of the isoscalar form factors 72
4.5.3 The momentum dependence of the isoscalar form factors 73
4.6 Fit Results 74
4.6.1 Fits based on dipole-extrapolated data 74
4.6.2 Direct fits to the simulation results at finite t 76
4.6.3 A glance at the quark mass dependence in the isoscalar channel 81
4.7 Summary and Conclusions 86

5 The Generalized Form Factors of the Nucleon 89
5.1 Introduction 89
5.2 Extracting the First Moments of GPDs 90
5.2.1 The generalized form factors of the nucleon 90
5.2.2 The generalized form factors of the pion 92
5.3 Formalism 93
5.3.1 Leading order nucleon Lagrangean 93
5.3.2 Consequences for the meson Lagrangean 94
5.3.3 Power-counting in BChPT with tensor fields 95
5.3.4 Next-to-leading order nucleon Lagrangean 96
5.4 The Generalized Isovector Form Factors in $\mathcal{O}(p^2)$ BChPT 97
5.4.1 Moments of the isovector GPDs at $t = 0$ 97
5.4.2 The slopes of the generalized isovector form factors 101
5.4.3 The generalized isovector form factors of the nucleon 103
5.5 The Generalized Isoscalar Form Factors in $\mathcal{O}(p^2)$ BChPT 104
5.5.1 Moments of the isoscalar GPDs at $t = 0$ 104
5.5.2 The contribution of u and d quarks to the spin of the nucleon 106
5.5.3 A first glance at the generalized isoscalar form factors of the nucleon 108
5.6 Summary 111

Summary and Conclusions 115

A Appendices to Chapter 2 119
A.1 Integrals 119
A.2 The Coupling Constant c_A 120

B Appendices to Chapter 3 121
B.1 Basic Integrals 121
B.2 Regulator Functions 122
B.3 Proof of Eq.(3.1) 122

C Appendices to Chapter 4 125
C.1 Regulator Functions 125
C.2 Amplitudes 126
C.3 Explicit Representation of the Form Factors 128
C.3.1 Isovector form factors 128
C.3.2 Isoscalar form factors 130

D Appendices to Chapter 5 **133**
D.1 Regulator Functions 133
D.2 Isovector Amplitudes in $\mathcal{O}(p^2)$ BChPT 135
D.3 BChPT Results in the Isoscalar Channel 136
D.3.1 Isoscalar amplitudes in $\mathcal{O}(p^2)$ BChPT 136
D.3.2 Estimate of $\mathcal{O}(p^3)$ contributions 136

Bibliography **138**

Introduction

Out of the three fundamental interactions of the standard model of elementary particle physics, it is the strong interaction which governs the dynamics of nucleons. In this work we apply an effective field theory (EFT) which is the low energy limit of Quantum Chromo Dynamics (QCD) which, in turn, is the fundamental theory for strong interactions. We access the spacial shape of the nucleon by calculating various form factors within the effective theory. In particular we present a nonrelativistic analysis of the form factors which parametrize the transition of a nucleon to its lowest lying resonance, the $\Delta(1232)$, a covariant calculation of the isoscalar and isovector vector form factors of the nucleon and a discussion of the generalized vector form factors of the nucleon in the same framework. Our calculations systematically extend previous studies of all three types of form factors. To achieve this, we also introduce a consistent renormalization scheme for the covariant formulation of the EFT.

The EFT calculation provides us with momentum transfer and quark mass dependent functions for the observables under discussion. Throughout this work, we study the dependence of our results on both variables with a focus on the quark mass dependence. This variable is of particular interest since QCD in discretized space-time and finite volumes with quark masses far above the physical ones is numerically solved by lattice simulations. To make contact between this theoretical scenario and the physical world, three extrapolations are thus necessary: the extrapolation of lattice results to the continuum, to the infinite volume and to small, physical quark masses. All three extrapolations can be performed in the EFT.

In this work, we focus on the extrapolation of lattice results towards the chiral limit, i.e. through the physical point to the limit of massless quarks. This extrapolation is at present necessary due to the limitation of the calculational power available for lattice collaborations. The calculational costs for lattice simulations scale with a negative power of the quark mass m_q where the lattice community frequently gives empirical formulae for the computational costs which scale like $\frac{1}{m_q^n}$ with $2 < n < 7$, depending on the action used. Present day lattice simulations for nucleon form factors are therefore performed at quark masses corresponding to a pion mass well above $m_\pi = 300$ MeV.

At this point one faces one of the central questions of this field, namely: Up to which values of the pion mass is the effective field theory applicable? Due to its nature as a low energy limit this theory is based on an expansion in the pion mass and thus the assumption that this mass is small. The EFT is therefore bound to break down at some “large” value of the pion mass. We believe that this question is worth a more sophisticated answer than just giving some number for the pion mass which is somehow considered to be large with respect to the scales of the theory. We therefore start our analyses without any bias with regard to this question but hope to find an answer in this work by comparing the results of the theory to data at different quark masses and estimating uncertainties arising due to higher order terms in the low energy expansion which have not yet been included. However, there is not one universal value for the pion mass from which on the low energy expansion cannot lead to trustworthy results anymore. One rather expects the accuracy with which the true quark mass dependence is described by the EFT to decrease with increasing quark mass where the value of the pion mass up to which the theory can provide significant statements about the quark mass dependence depends on the observable under consideration, the particular version of the EFT and on the order of the analysis. In this work, we present real chiral extrapolations, i.e. predictions for the physical values from a combined lattice plus EFT analysis for all those observables for which the quark mass dependence is found to be reliably described by our EFT results up to the quark masses of presently available lattice results.

Not only is the EFT a suitable tool for the interpretation of lattice results but it can also profit from the data provided by simulations on the lattice. The EFT results presented in this work contain quite a number of coupling constants which cannot be determined from the results of experiments yet. However, by fitting our results to the quark mass (and momentum transfer) dependence of lattice data, we are able to give numerical estimates for all coupling constants occurring in the calculations of this work.

This work is organized in five chapters plus this introduction, a summary and four appendices. Each chapter is written such that it can be read independently of all other chapters.
The first chapter gives an introduction to the field theoretical framework in which all calculations presented in this work are performed. Special attention is put on those issues to which we will contribute in the subsequent chapters (like e.g. power-counting, renormalization and the possible inclusion of tensor sources).
In chapter 2 we present an analysis of the electromagnetic $N\Delta$ transition current in the framework of the non-relativistic "small scale expansion" (SSE) to leading one loop order. We discuss the momentum dependence of the magnetic dipole- and the electric- and Coulomb quadrupole transition form factors up to momentum transfers of $Q^2 < 0.25$ GeV^2. Particular emphasis is put on the identification of the role of chiral dynamics in this transition. Our analysis indicates that there is indeed nontrivial momentum dependence in the two quadrupole form factors at small $Q^2 < 0.15$ GeV^2 arising from long distance pion physics, leading for example to negative squared radii in the (real parts of the) quadrupole transition form factors. We compare our results with the EMR(Q^2) and CMR(Q^2) multipole-ratios from pion-electroproduction experiments and find a remarkable agreement up to four-momentum transfers of $Q^2 \approx 0.3$ GeV^2. Finally, we discuss the quark mass dependence of the three transition form factors at $Q^2 = 0$, identifying rapid changes in the (real parts of the) quadrupole transition moments as a function of the pion mass for $m_\pi < 200$ MeV, which arise again from long distance pion dynamics. Our findings indicate that dipole extrapolation methods currently used in lattice QCD analyses of baryon form factors are not applicable for the chiral extrapolation of $N\Delta$ quadrupole transition form factors.
Chapter 3 gives a detailed discussion of general properties of results calculated in covariant Baryon Chiral Perturbation Theory (BChPT) followed by a catalogue of requirements which we demand to be fulfilled by a consistent renormalization scheme for this theory. Driven by the fact that none of the renormalization schemes for covariant BChPT discussed in literature fulfills all of our conditions, we define a new renormalization scheme – which we name $\overline{\text{IR}}$ – by a specific modification of the infrared regularization scheme of reference [BL99]. The second part of this chapter is concerned with a calculation of the mass of the nucleon in this framework and a discussion of the differences between different renormalization schemes on this example. Finally, we apply covariant BChPT up to next-to-leading one loop order for chiral extrapolations of lattice results for the mass of the nucleon, leading to a very satisfying result. Systematic uncertainties of this approach are discussed and are found to be moderate over a quite large range of quark masses. We give a number of arguments, why dependable chiral extrapolations starting from the domain of presently available lattice data necessarily have to rely on the $\overline{\text{IR}}$ renormalization technique. These arguments are supported by the chiral extrapolation functions of all observables discussed in this work. Appendix B collects the necessary technicalities concerning the new renormalization scheme. All integral- and corresponding regulator functions needed for the covariant calculations in this work and a proof for the central equation of chapter 3 are given there.
A calculation of the isovector- and isoscalar Dirac- and Pauli form factors of the nucleon up to next-to-leading one loop order in BChPT using the $\overline{\text{IR}}$ renormalization technique is presented in chapter 4. We analyse both the momentum transfer- and quark mass dependence of our results in the context of data from experiments as well as from lattice simulations. We give estimates for the numerical values of all appearing coupling constants and explore the possibility of chiral extrapolations with these results, including a discussion of systematic and statistical errors. In contrast to previous studies of chiral extrapolation functions for those form factors, we do not only rely on a dipole parametrization in order to extrapolate the lattice results from finite values of the momentum transfer to the forward limit but in addition perform the first fit of a ChPT result to lattice data at different quark masses and different values for the momentum transfer directly. In the isovector sector we find a very good description of the corresponding lattice data and are able to give a reasonable prediction for both nucleon form factors at the physical point. Systematic and statistical errors are again found to be small over a

large range of pion masses. In the isoscalar sector, the analysis is troubled by larger systematic uncertainties and the absence of lattice data at small pion masses. Full analytic expressions for the vector amplitudes and form factors are given in appendix C.
In chapter 5 we present a discussion of the first moments of the parity-even Generalized Parton Distributions (GPDs) in a nucleon corresponding to six generalized vector form factors. We evaluate these fundamental properties of baryon structure at low energies, utilizing the methods of covariant chiral perturbation theory in the baryon sector. Our analysis is performed at leading one loop order in BChPT, predicting both the momentum and the quark mass dependence for the three generalized isovector and three generalized isoscalar form factors which are currently under investigation in lattice QCD analyses of baryon structure. We also study the limit of vanishing four-momentum transfer where the GPD-moments reduce to the well known moments of Parton Distribution Functions (PDFs). For the isovector moment $\langle x \rangle_{u-d}$ our BChPT calculation predicts a new mechanism for chiral curvature, connecting the high values for this moment typically found in lattice QCD studies for large quark masses with the smaller value known from phenomenology. Likewise, we analyse the quark mass dependence of the isoscalar moments in the forward limit and extract the contribution of quarks to the total spin of the nucleon. We close chapter 5 with a first glance at the momentum dependence of the isoscalar C-form factor of the nucleon. Throughout, we again give estimates for the systematic uncertainties of the EFT calculation. The technicalities of the calculation of the generalized form factors are collected in appendix D.
A recent review of the field this work wants to contribute to can be found in reference [PPV06].

Chapter 1

Basic Concepts of Chiral Effective Field Theory

In this chapter we introduce a few basics of Chiral Effective Field Theory (ChEFT). It is the aim of this work to describe strongly interacting systems at low energies. In the following we therefore identify the relevant degrees of freedom of those systems and give a description of their dynamics. Furthermore, we provide the necessary tools for *perturbative* field theoretical calculations based on the effective Lagrangean. The more specific parts of the theory needed for the calculation of the observables discussed in this work are presented in the pertinent chapters.
The basic ideas of this theory have been developed in reference [Wei76] while references [Ber07, BM06, Sch03] give recent reviews and introductions.

1.1 Construction Principles for the Effective Low Energy Lagrangean

Within the standard model of elementary particle physics the strong interaction is described by a non-Abelian SU(3) gauge theory [FGML73] called Quantum Chromo Dynamics (QCD). The three interacting charges of this theory are called colours. Fermions of six different flavours, the quarks, are known to carry this charge. The masses of three of them lie well above the mass of the nucleon and are thus irrelevant for processes at low energies. (Furthermore we restrict ourselves to the sector of two active quark flavours: "up" and "down" quarks.) In QCD the force between coloured objects is mediated by a colour-octet of massless gauge bosons, the gluons. Due to the fact that interactions among these gauge bosons are allowed in a non-Abelian gauge theory, the coupling constant of QCD is small in hard processes but becomes large if soft momenta are mediated between the quarks. At low energies this coupling constant is of order one or even larger, making the standard calculational tool of quantum field theories – i.e. an expansion of amplitudes in powers of the coupling constant – unusable.
Furthermore, no coloured objects can be observed at low energies: The quarks are confined, i.e. they only occur in colour-neutral bound states, so-called hadrons. At present two types of hadrons have been unambiguously observed: mesons (quark-antiquark states) and baryons (three-quark states). It is the spectrum of hadrons which provides the key to a description of strong interaction at low energies in terms of effective degrees of freedom: While there are three pseudoscalar meson states at a mass of about 140 MeV (the pions) the next heavier hadron (the eta) carries a mass of about 550 MeV [Y$^+$06]. Thus the dynamics of a strongly interacting system at low energies is – to a large extent – determined by pion dynamics. Consequently, an effective field theory for QCD at low energies can be constructed as a theory of pions. All physics beyond the effects of dynamical pions is then encoded in the coupling constants of this theory. To be the exact low energy limit of strong interactions, the effective Lagrangean for the pions must preserve all symmetries of the original QCD Lagrangean. It must therefore be invariant under parity- (P), charge conjugation- (C) and time reversal (T) transformations separately. A fourth symmetry leading to very important constraints on the effective field

theory is the chiral symmetry of the QCD Lagrangean in the limit of massless quarks, i.e the left- and right handed components of the quark fields (the components with spin parallel and anti-parallel with respect to the momentum) decouple in this limit and therefore the QCD Lagrangean is invariant under independent global unitary rotations of the left- and right handed fields in flavour space. This symmetry is explicitly broken by the small but nonzero quark masses. Accordingly, the construction principle for the effective theory (called Chiral Perturbation Theory – ChPT) is the demand that the Lagrangean be invariant under chiral rotations and to subsequently account for the finite quark masses by treating them as a small perturbation to this system.
We start the construction of the effective Lagrangean by choosing a nonlinear representation for the pion-field operators $U = \exp\left(i\frac{\tau^i\pi^i}{F_\pi}\right)$, where τ^i with $i = 1,2,3$ are the Pauli matrices acting in isospin space, π^i are the (Klein-Gordon) pion-field operators (with quantum numbers $J^P = 0^-$) and F_π is the pion decay constant. The transformation property of this U field under chiral rotations is found if it is coupled into the original QCD Lagrangean and invariance under chiral rotations is still demanded. In order to be invariant under P-transformations, the effective Lagrangean must consist of terms with even numbers of U fields. To make those terms chirally symmetric, the trace in isospin-space has to be taken. Together with the constraint that the Lagrangean has to be a Lorentz-scalar we find that all structures of the kind [GL84]

$$\text{Tr}\left(UU^\dagger\right),\ \text{Tr}\left(\partial_\mu U\partial^\mu U^\dagger\right),\ \text{Tr}\left(\partial_\mu U\partial_\nu U^\dagger\right)\cdot\text{Tr}\left(\partial_\mu U\partial_\nu U^\dagger\right),\ ... \tag{1.1}$$

and thus an infinite number of terms is allowed in the chiral Lagrangean. The relative prefactors of those terms are not constrained by chiral symmetry but are free parameters of the theory, parametrizing physics not accounted for explicitly in this Lagrangean. It is thus apparent that those coupling constants – which have units of inverse powers of mass – scale with the mass of the lowest lying resonance not included in the effective Lagrangean. Together with the observation that a classification of allowed terms in the effective Lagrangean is possible with respect to the number of derivatives they do contain, we arrive at a consistent hierarchy of terms: Terms with n derivatives scale as $\frac{k_\pi^n}{M_r^n}$ where k_π is a typical pion momentum and M_r is the mass of an arbitrary resonance not explicitly included in the theory. For sufficiently small pion momenta a perturbative expansion of the pion Lagrangean is thus possible.
The next step in our introduction to this theory is to repeat the above steps for arbitrary vector v_μ ($J^P = 1^-$), axial a_μ (1^+), scalar s (0^+) and pseudoscalar p (0^-) external fields (in chapter 5 we introduce external tensor fields in exactly the same fashion). In the following we denote the momenta carried by those fields with Q. The leading part of the Lagrangean, i.e. the parts with minimal number of derivatives (note that the first term in eq.(1.1) is just an unobservable constant) then reads

$$\mathcal{L}^{(2)}_{\pi\pi} = \frac{F_\pi^2}{4}\text{Tr}\left[\nabla_\mu U\nabla^\mu U^\dagger + \chi^\dagger U + U^\dagger\chi\right], \tag{1.2}$$

where we have chosen the prefactor to equal one fourth of the pion decay constant squared and defined the covariant derivative $\nabla_\mu U = \partial_\mu U - i\left(v_\mu + a_\mu\right)U + iU\left(v_\mu - a_\mu\right)$ and the field $\chi = 2B_0(s+ip)$ containing a free parameter B_0. With the help of this construction it is easy to introduce the finite quark masses which break the chiral symmetry explicitly into the effective Lagrangean: One just has to identify $s = \text{diag}(m_u, m_d)$ where m_u is the mass of the up quark, m_d the one of the down quark and finds (with all other external sources set to zero)

$$\mathcal{L}^{(2)}_{\pi\pi} = \frac{1}{2}\partial_\mu\pi^i\partial^\mu\pi^i - B_0(m_u+m_d)\pi^i\pi^i + \mathcal{O}(\vec{\pi}^4), \tag{1.3}$$

which is the Klein-Gordon equation for pions of mass $m_\pi^2 = B_0(m_u+m_d)$. This so called GOR relation was already derived by Gell-Mann, Oakes and Renner from current algebra [GMOR68].
Defining the field strength tensor $F^{L/R}_{\mu\nu} = \partial_\mu F^{L/R}_\nu - \partial_\nu F^{L/R}_\mu - i[F^{L/R}_\mu, F^{L/R}_\nu]$ with $F^{L/R}_\mu = v_\mu \pm a_\mu$ we have now collected all independent building blocks allowed in the construction of the pion Lagrangean. We decide to introduce a hierarchy of terms (i.e. terms with increasing "chiral dimension") in this Lagrangean by taking the standard choice which is to assign chiral dimension one to the structures $\nabla_\mu U$, v_μ and a_μ and

chiral dimension two to the structures s, p and $F_{\mu\nu}^{L/R}$. Note that from this definition we find that the pion mass has chiral dimension one. The contributions of terms with chiral dimension d to a matrix element carry an additional prefactor p^d with $p \in \left\{ \frac{Q}{M_r}, \frac{m_\pi}{M_r} \right\}$ due to this definition and are thus numerically suppressed if there is a sufficiently large mass gap between Q and m_π on one side and M_r on the other side.
Having discussed the hierarchy of terms in the Lagrangean we now turn to a discussion of the hierarchy of loop diagrams in this theory. From the definition of U we find that every pion-vertex of this theory brings a factor $\frac{1}{F_\pi}$. In order to arrive at a dimensionless coupling, this vertex needs another dimensionfull parameter. In this theory either the soft momentum Q or the pion mass m_π are available. Furthermore, for topological reasons, every loop integral brings an additional factor $\frac{1}{(4\pi)}$. Altogether we find that contributions from a Feynman diagram containing n pion vertices carry a prefactor q^n with $q \in \left\{ \frac{Q}{4\pi F_\pi}, \frac{m_\pi}{4\pi F_\pi} \right\}$. This provides a consistent hierarchy of loop diagrams, assuring that the contributions from higher loop orders are parametrically suppressed if the pion masses and momenta are sufficiently small (i.e. $q \ll 1 \Leftrightarrow Q, m_\pi \ll 1.2$ GeV). In this work we follow Weinberg's choice which is to tie together the loop expansion in q and the expansion of the effective Lagrangean in p one-to-one [Wei79] by assigning the chiral dimension one to both of the expansion parameters: $p \approx q$. Therefore we uniformly denote both expansions by an expansion in $\frac{1}{4\pi F_\pi}$ throughout this work. The chiral dimension D of an arbitrary loop diagram can then be calculated as $D = 2 + 2N_L + \sum_d (d-2)N_d$ where N_L is the number of pion loops and N_d the number of vertices with chiral dimension d (i.e. calculated from those pieces of the Lagrangean which are of chiral dimension d). We note that this choice allows for a UV-renormalization of all loop diagrams and leads to renormalization scale independent results. Furthermore, it ensures that for a calculation at a given precision D one only has to know a finite number of terms of the full ChPT Lagrangean.
The final step of this section is now to bring the lowest lying baryons, the nucleons, into the theory and to study their interaction with the pions. In analogy to the procedure described above, one has to determine the transformation properties of the fermion fields Ψ under chiral rotations (the lengthy derivation is done in great detail in reference [Geo84]). One finds that the chiral transformation operator of the nucleon is a function of the pion field. As a consequence, general left-right rotations of the nucleon fields are compensated by the emission or absorption of pions which – within this theory – is the origin of the pion-cloud surrounding the nucleon. Including the (isospin doublet, $J^P = \frac{1}{2}^+$) nucleon fields Ψ one finds the additional chirally invariant, C-, P- and T symmetric building blocks

$$\bar{\Psi} D_\mu \Psi = \bar{\Psi} \left(\partial_\mu + \Gamma_\mu - i v_\mu^{(s)} \right) \Psi, \tag{1.4}$$

$$\bar{\Psi} \gamma_\mu \gamma_5 u^\mu \Psi = i \bar{\Psi} \gamma_\mu \gamma_5 \left(u^\dagger \nabla^\mu u - u \nabla^\mu u^\dagger \right) \Psi, \tag{1.5}$$

where the γ's are the Dirac matrices, the chiral connection is defined as $\Gamma_\mu = \frac{1}{2}[u^\dagger, \partial_\mu u] - \frac{i}{2} u^\dagger \left(v_\mu + a_\mu \right) u - \frac{i}{2} \left(v_\mu - a_\mu \right) u^\dagger$ with $u^2 = U$ and $v_\mu^{(s)}$ is an external isoscalar vector source. We organize the infinite number of possible terms in the Lagrangean by assigning the chiral dimension zero to $\bar{\Psi} A \Psi$ with $A = 1$, γ^μ, $\gamma^\mu \gamma^5$, $\sigma^{\mu\nu}$, $\sigma^{\mu\nu}\gamma_5$, M_0 and chiral dimension one to $\bar{\Psi} B \Psi$ with $B = \gamma_5$, $\left(i \not{D} - M_0 \right)$, D_μ, u_μ, where M_0 is the mass of the nucleon in the limit of massless quarks, i.e. the chiral limit. The leading order chiral pion-nucleon Lagrangean (with chiral dimension one) then reads:

$$\mathcal{L}_{\pi N}^{(1)} = \bar{\Psi} \left[i \not{D} - M_0 + \frac{g_A}{2} \gamma_\mu \gamma_5 u^\mu \right] \Psi, \tag{1.6}$$

where g_A is the axial coupling constant of the nucleon in the chiral limit. All higher order terms can be constructed accordingly from the building blocks. Note, however, that in order to arrive at dimensionless couplings in Feynman diagrams we have now, besides the constructions $\frac{Q}{4\pi F_\pi}$ and $\frac{m_\pi}{4\pi F_\pi}$, the possibility $\frac{M_0}{4\pi F_\pi} \approx 1$ which is not a small quantity! Therefore it is not guaranteed in this theory that contributions from higher order loop diagrams are parametrically suppressed; there is a priori no one-to-one correspondence among the expansions in loop diagrams and parts of the Lagrangean. The historic remedy for this problem is given in the next subsection (and is applied in chapter 2) while we discuss a new solution to this problem in chapter 3 of

this work.
We close this paragraph with another observation from the hadron spectrum: While the QCD Lagrangean displays a (approximate) chiral symmetry, one finds a huge mass gap between chiral partners in the hadron spectrum which is clearly not explicable with the small explicit symmetry breaking quark masses. Therefore we conclude that the symmetry of the QCD Lagrangean under independent rotations of left- and right handed quarks in flavour space ($SU(2)_L \times SU(2)_R$ in the case of two active quark flavours) is spontaneously broken. However, one finds an approximate isospin symmetry in the hadron spectrum leading to the conclusion that the subgroup $SU(2)_{L+R}$ is a symmetry of nature. The Nambu-Goldstone theorem for spontaneously broken symmetries now predicts massless bosons with the quantum numbers of the charge operators of the broken subgroup, i.e. three pseudoscalar bosons. We identify those bosons with the very light pions which have a nonvanishing mass due to the explicit symmetry breaking terms of the Lagrangean and are therefore called quasi Goldstone Bosons. A possible mechanism for the spontaneous breaking of the chiral symmetry is provided by a nonvanishing vacuum expectation value: For the chiral quark condensate we find $\langle 0|\bar{q}q|0\rangle = \langle 0|\frac{\partial \mathcal{H}}{\partial m_q}|0\rangle = -F_\pi^2 B_0$ where $\mathcal{H}$ is the leading order Hamiltonian corresponding to eq.(1.2).

1.2 Nonrelativistic Limit

In order to implement a consistent perturbative expansion of the Lagrangean *and* the loop diagrams in ChPT with baryons – recall that this was troubled by the presence of a second large mass scale M_0, see above – the authors of [JM91] decomposed the nucleon field into a massless dynamical component and a heavy remainder which can consistently be absorbed into the coupling constants of the theory, assuring that terms of the type $\frac{M_0}{4\pi F_\pi} \approx 1$ are absent in loop calculations after this treatment. Therefore, one first has to identify all appearances of the large mass M_0 in the Lagrangean. We find it in the four-momentum of the nucleon $p^\mu = M_0 v^\mu + k_N^\mu$ where we have introduced a velocity vector v_μ with $v^2 = 1$ and a small residual momentum k_N^μ and in the nucleon field $\Psi = e^{-iM_0\, v\cdot x}\,(\mathcal{N} + H)$, where we have decomposed the nucleon field into two components with the help of the projection operators $P_v^\pm = \frac{1}{2}\,(1 \pm \not{v})$ as $\mathcal{N} = e^{iM_0\, v\cdot x} P_v^+ \Psi$ and $H = e^{iM_0\, v\cdot x} P_v^- \Psi$. Inserting those expressions into the Dirac equation we find that $\mathcal{N}$ is massless while H has a mass of twice the mass of the nucleon. The sought after leading order Lagrangean is found if those expressions are inserted into the Lagrangean $\mathcal{L}_{\pi N}^{(2)}$ (see eq.(1.6)), it is then diagonalized in the $\mathcal{N}, H$ basis and the H fields are subsequently integrated out. Finally, in order to avoid nonlocal operators, the Lagrangean has to be expanded in inverse powers of the mass of the nucleon M_0, i.e. expanded in r with $r \in \left\{\frac{m_\pi}{M_0}, \frac{Q}{M_0}\right\}$. As $M_0 \approx 4\pi F_\pi$, the chiral dimension one is assigned to the parameter r and the nonrelativistic Lagrangean is thus organized as a double expansion in p and r. The leading order pion-nucleon Lagrangean takes the form

$$\mathcal{L}_{\pi N}^{(1)} \;=\; \bar{\mathcal{N}}\,[i\, v\cdot D + g_A\, S\cdot u]\,\mathcal{N}. \tag{1.7}$$

Here we have used the Pauli-Lubanski spin vector defined as $S_\mu = \frac{i}{2}\gamma_5\sigma_{\mu\nu}v^\nu$. Note that some parts of the leading order covariant Lagrangean of eq.(1.6) now contribute to the next-to-leading (or even higher order) Lagrangean of this nonrelativistic theory – called Heavy Baryon Chiral Perturbation Theory (HBChPT) – via the additional $\frac{1}{M_0}$ expansion. Counting the additional expansion parameter r on the same footing as p and q: $p \approx q \approx r$, we arrive at a counting rule completely analogous to the one in the meson sector. The chiral dimension D of a Feynman diagram can be calculated as

$$D \;=\; 2N_L + 1 + \sum_d \left[(d-2)N_d^M + (d-1)N_d^{MB}\right], \tag{1.8}$$

where N_L denotes the number of loops in the diagram, N_d^M is the number of vertices from a meson Lagrangean of order d and N_d^{MB} the number of vertices from a meson-baryon Lagrangean of order d. In HBChPT it is guaranteed by construction that diagrams with larger chiral dimension contribute with higher powers of a small parameter.

1.3 Inclusion of Spin-$\frac{3}{2}$ Fields

Scanning the hadron spectrum in search for further relevant degrees of freedom of low energy QCD, one is quickly pointed to the $\Delta(1323)$, a strong paramagnetic nucleon resonance with quantum numbers spin $\frac{3}{2}$ and isospin $\frac{3}{2}$ which is less than ≈ 300 MeV away from its ground state. It is therefore – at least in some channels – advisable to include this degree of freedom explicitly in the calculations. In a theory not including this degree of freedom explicitly it is parametrized in the coupling constants and can thus lead to large values of those constants. In addition one can not be sure a priori, whether the implicit treatment of the $\Delta(1232)$ effects in the coupling constants order by order is a reasonable expansion of the underlying physics. However, in those chapters where we have not included Δ degrees of freedom explicitly we indeed find large values for some of the coupling constants but the respective physics can be described very well by this implicit treatment of the nucleon resonance already at next-to-leading one loop order.
Writing down the chiral Lagrangean with spin $\frac{3}{2}$ states is a straightforward exercise: A field theory of those states was given by Rarita and Schwinger [RS41] and the transformation rules under chiral rotations can be derived in analogy to the one of the nucleon. In order to introduce a consistent hierarchy of loop orders, one can again perform a nonrelativistic expansion of the Lagrangean. At this point however, one has to take a decision: There is a new dimensionfull scale M_Δ (the mass of the Δ) in the theory and the question arises how to treat it with respect to the other mass scales of the theory. Here we follow the choice of reference [HHK98] which is to assign the chiral dimension one to the ratio $\frac{\Delta_0}{4\pi F_\pi}$, where Δ_0 is the nucleon-Δ mass splitting (in the chiral limit): $\Delta_0 = M_\Delta - M_0$. In this theory – the so called "small scale expansion" (SSE) – the Lagrangean and the Feynman diagrams are therefore organized as a series in powers of ϵ with $\epsilon \in \{\frac{Q}{4\pi F_\pi}, \frac{Q}{M_0}, \frac{m_\pi}{4\pi F_\pi}, \frac{m_\pi}{M_0}, \frac{\Delta_0}{4\pi F_\pi}, \frac{\Delta_0}{M_0}\}$.
We start the next chapter – after an introduction to the matrix element under consideration there – with a brief discussion of the lowest order Lagrangeans of this theory.
We emphasize that physical quantities calculated in this theory are guaranteed to *not* depend on any unphysical "off-shell parameter" or gauge parameter of the so called "point symmetry". In ref. [HHK98] it has been shown explicitly that the off-shell parameters do not lead to new structures in the amplitudes and do therefore not give rise to any effects which are observable independent of the counter-terms of the theory. In this work we have therefore chosen to set those parameters to zero which just corresponds to a particular definition of the appearing low energy constants. Furthermore, point symmetry rotations can consistently be factorized and thus be absorbed by a field redefinition.

Chapter 2

The Nucleon-to-Delta Transition Form Factors

2.1 Introduction

$\Delta(1232)$ is the lowest lying baryon resonance with quantum numbers spin $S = \frac{3}{2}$ and isospin $I = \frac{3}{2}$. It can be studied, for example, in the process of pion-photoproduction on a nucleon ($\gamma N \to \pi N$). Therein it shows up both as a clear signal in the cross section and as a pole at $M_\Delta = (1210 - i\,50)$ MeV [Y$^+$06] in the complex W-plane with $W = \sqrt{s}$ denoting the total energy as a function of the Mandelstam variable s. At the position of the resonance the incoming photon can excite the target nucleon into a $\Delta(1232)$ resonant state via a magnetic dipole M1 or an electric quadrupole E2 transition. Assuming Δ pole dominance at the resonance energy, one can relate the pion-photoproduction multipoles describing the final πN state of this process to the strengths of the sought after $\gamma N\Delta$ transition moments. Extensive research over the past decades has produced the result EMR$= -(2.5 \pm 0.1_{\text{stat}} \pm 0.2_{\text{sys}})\%$ [B$^+$00], demonstrating that in this ratio of quadrupole to dipole transition strength the magnetic dipole dominates the transition to the percent level. Extending these studies to pion-electroproduction the incoming virtual photon carries a four-momentum squared $q^2 < 0$ and can also utilize a Coulomb quadrupole C2 transition to excite an intermediate $\Delta(1232)$ resonance. The three electromagnetic multipole transitions M1, E2 and C2 then become functions of momentum transfer squared q^2, analogous to the well known electromagnetic form factors of the nucleon studied in elastic electron scattering off a nucleon target. Extensive experimental studies of pion-electroproduction in the $\Delta(1232)$ resonance region [S$^+$75, B$^+$72, B$^+$68, S$^+$71] have already demonstrated that also for finite q^2 both the electric- and the Coulomb $N\Delta$ quadrupole transitions remain "small" (at the percent level) compared to the dominant magnetic $N\Delta$ dipole transition. However, recently, new high precision studies at continuous beam electron machines [J$^+$02, S$^+$05, P$^+$01, S$^+$06] have been performed in order to quantify the observed dependence of these transitions with respect to q^2. It is hoped that from these new results from experiments one can infer those relevant degrees of freedom within a nucleon which are responsible for the observed (small) quadrupole components in the $\gamma N\Delta$ transition. The theoretical study presented here attempts to identify the active degrees of freedom in these three transition form factors in the momentum region $Q^2 = -q^2 < 0.3$ GeV^2.

Historically the nonzero strength of the $N\Delta$ quadrupole transitions has raised a lot of interest because such transitions are absent in (simple) models for nucleon wave functions with spherical symmetry. The issue of detecting a "deformed shape" of the nucleon via well defined observables in scattering experiments, however, is intriguing to the minds of nuclear physicists up to this day, e.g. see the discussion in ref.[Ber03]. On the theoretical side, most of the work over the past 20 years has focused on the idea that a "natural" explanation for the nonzero $N\Delta$ quadrupole transition moments could arise from pion degrees of freedom present in the nucleon wave function, i.e. from the so-called "pion-cloud" around the nucleon. Many calculations to quantify this hypothesis have been pursued, within the skyrme model ansatz (e.g. see [WW87]), within dynamical pion-nucleon models (e.g see [SL96, SL01a]), within quark-meson coupling models (e.g. see [Buc99]), within

chiral bag models (e.g see [LTW97]), within chiral quark soliton models (e.g. see [SUW$^+$00]), ... to name just a few of them. Around 1990 – based on the works of refs.[GSS88, JM91, BKKM92] – the qualitative concept of the "pion-cloud" around a nucleon could be put on a firm field theoretical footing within the framework of chiral effective field theory (ChEFT) for baryons, for a brief introduction see chapter 1. The pioneering study of the strength of the electric $N\Delta$ quadrupole transition within ChEFT for real photons was performed in ref.[BSS94] and the first calculation of all three $N\Delta$ transition form factors for $Q^2 < 0.2\,\mathrm{GeV}^2$ within the SSE scheme of ChEFT [HHK98] was given in ref.[GHKP99]. In this chapter we present an update and extension of the nonrelativistic $\mathcal{O}(\epsilon^3)$ SSE calculation of the latter reference and compare the results both to results from experiments as well as to recent theoretical calculations [KY99, KYD$^+$01, DHKT99] and will also analyse the quark mass dependence of our results. A comprehensive overview of the field – from the theorist's as well as the experimentalist's point of view – is given in reference [PBe07]
Before we begin the discussion of the general $\gamma N\Delta$ transition matrix element in the next section, we remind the reader, that the "pion-cloud" around the nucleon in ChEFT calculations does not just lead to nonzero quadrupole transition form factors but is also responsible for the fact that *all three $N\Delta$ transition form factors* – unlike the case of the elastic nucleon form factors, see e.g. ref.[BFHM98] and the following chapters – are *complex valued* due to the presence of the open πN channel, in accordance with the parametrization of ref.[JS73]. In the following we continue this chapter with a brief discussion of the effective field theory calculation in section 2.3 and present our results in section 2.4 before summarizing our main findings in section 2.5. A few technical aspects are relegated to appendix A. We have already published the main results of this chapter in references [GH06] and [GH07]

2.2 Parametrization of the Matrix Element

Demanding Lorentz covariance, gauge invariance and parity conservation the matrix element of a $I\left(J^P\right) = \frac{3}{2}\left(\frac{3}{2}^+\right)$ to $\frac{1}{2}\left(\frac{1}{2}^+\right)$ transition can be parametrized in terms of three form factors, i.e. complex valued functions of the momentum transfer squared. For our calculation we follow the conventions of ref.[GHKP99] and choose the definition:

$$\begin{aligned} i\mathcal{M}_{\Delta\to N\gamma} &= +\sqrt{\frac{2}{3}}\,\frac{e}{2M_N}\bar{u}(p_N)\gamma_5\Big[G_1(q^2)(\not{q}\epsilon_\mu - \not{\epsilon}q_\mu) + \frac{G_2(q^2)}{2M_N}(p_N\cdot\epsilon q_\mu - p_N\cdot q\epsilon_\mu) \\ &\quad + \frac{G_3(q^2)}{2\Delta}(q\cdot\epsilon q_\mu - q^2\epsilon_\mu)\Big]u^\mu_\Delta(p_\Delta). \end{aligned} \tag{2.1}$$

Here e denotes the charge of the electron and M_N is the mass of a nucleon at the physical point, $p^\mu_{N/\Delta}$ denotes the relativistic four-momentum of the outgoing nucleon/incoming Δ and q_μ and ϵ^μ are the momentum and polarization vectors of the outgoing photon, respectively. As discussed in ref.[GHKP99] the small scale $\Delta = M_\Delta - M_N$ denoting the nucleon-Delta mass-splitting had to be introduced in front of the $G_3(q^2)$ form factor in order to obtain a consistent matching between the calculated $\Delta \to N\gamma$ amplitudes and the associated $N\Delta$ transition current at leading one loop order in the ChEFT framework of SSE [HHK98]. The dynamics of the outgoing nucleon is described via a Dirac spinor $u(p_N)$ while the associated $\Delta(1232)$ dynamics is parametrized via a Rarita-Schwinger spinor $u_\mu(p_\Delta)$. From the point of view of chiral effective field theory the signatures of chiral dynamics in the $N\Delta$ transition are particularly transparent in the $G_i(q^2)$, $i = 1,2,3$ basis which serves as the analogue of the Dirac- and Pauli form factor basis in the vector current of a nucleon which will be analysed in chapter 4. However, most experiments and most model calculations refer to the multipole basis of the general $N\Delta$ transition current. The allowed magnetic dipole, as well as electric- and Coulomb quadrupole transitions are parametrized via the form factors $\mathcal{G}^*_M(q^2)$, $\mathcal{G}^*_E(q^2)$ and $\mathcal{G}^*_C(q^2)$ defined by Jones and Scadron

[JS73]. They are connected to our choice via the relations

$$\begin{aligned}
\mathcal{G}_M^*(q^2) &= \frac{M_N}{3(M_N+M_\Delta)}\Bigg[\left((3M_\Delta+M_N)(M_\Delta+M_N)-q^2\right)\frac{G_1^\dagger(q^2)}{2M_NM_\Delta}-(M_\Delta^2-M_N^2-q^2)\frac{G_2^\dagger(q^2)}{4M_N^2} \\
&\quad -q^2\frac{G_3^\dagger(q^2)}{2M_N\Delta}\Bigg], \qquad (2.2)\\
\mathcal{G}_E^*(q^2) &= \frac{M_N}{3(M_N+M_\Delta)}\left[(M_\Delta^2-M_N^2+q^2)\frac{G_1^\dagger(q^2)}{2M_NM_\Delta}-(M_\Delta^2-M_N^2-q^2)\frac{G_2^\dagger(q^2)}{4M_N^2}-q^2\frac{G_3^\dagger(q^2)}{2M_N\Delta}\right] \qquad (2.3)\\
\mathcal{G}_C^*(q^2) &= \frac{2M_N}{3(M_N+M_\Delta)}\left[\frac{M_\Delta}{M_N}G_1^\dagger(q^2)-(M_\Delta^2+M_N^2-q^2)\frac{G_2^\dagger(q^2)}{4M_N^2}-(M_\Delta^2-M_N^2+q^2)\frac{G_3^\dagger(q^2)}{4M_N\Delta}\right] \qquad (2.4)
\end{aligned}$$

As these multipole form factors have been defined for the $N\gamma \to \Delta$ reaction they are linear combinations of the hermitian conjugate form factors $G_i^\dagger(q^2)$.
For a comparison with experimental results we also note that the notation of Ash [A$^+$67] is connected to the Jones-Scadron form factors via:

$$\mathcal{G}_M^{*Ash}(q^2) = \frac{1}{\sqrt{1-\frac{q^2}{(M_N+M_\Delta)^2}}}\mathcal{G}_M^{*JS}(q^2). \qquad (2.5)$$

The full information about the rich structure of the general (isovector) $N\Delta$ transition current is hidden in these three *complex* form factors. In experiments this transition is studied in the process $e\,p \to e'\,N\pi$ in the region of the Δ resonance (e.g. see ref.[S$^+$05] and references given therein) which has access to a lot more hadron structure properties than just the $N\Delta$ transition current of eq.(2.1). Based on the observation that the $\gamma^* N \to \pi N$ transition at the resonance energy is dominated by the magnetic dipole transition and under the assumption that intermediate states are dominated by the imaginary part of the Δ propagator, one can relate three of the extracted (complex) pion-electroproduction multipoles in the isospin 3/2 channel $M_{1+}^{I=3/2}(W_{res},q^2)$, $E_{1+}^{I=3/2}(W_{res},q^2)$ and $S_{1+}^{I=3/2}(W_{res},q^2)$ at the position of the resonance W_{res} to the sought after form factors via

$$\begin{aligned}
\text{EMR} &\equiv \text{Re}\left[\frac{E_{1+}^{I=3/2}(W_{res},q^2)}{M_{1+}^{I=3/2}(W_{res},q^2)}\right] \approx -\text{Re}\left[\frac{\mathcal{G}_E^*(q^2)}{\mathcal{G}_M^*(q^2)}\right], \qquad (2.6)\\
\text{CMR} &\equiv \text{Re}\left[\frac{S_{1+}^{I=3/2}(W_{res},q^2)}{M_{1+}^{I=3/2}(W_{res},q^2)}\right] \\
&\approx -\frac{\sqrt{((M_\Delta+M_N)^2-q^2)((M_\Delta-M_N)^2-q^2)}}{4M_\Delta^2}\text{Re}\left[\frac{\mathcal{G}_C^*(q^2)}{\mathcal{G}_M^*(q^2)}\right]. \qquad (2.7)
\end{aligned}$$

Ultimately the validity of this approximate connection between the pion-electroproduction multipoles and the $N\Delta$ transition form factors has to be checked in a full theoretical calculation. At present only nucleon- and Δ pole graphs have been included as intermediate states in calculations of the process $e\,p \to e'\,N\pi$ in the Δ resonance region within chiral effective field theory (e.g. see ref.[PV05]). For such intermediate states eqs.(2.6,2.7) are exact. It remains to be seen to what extent nonresonant intermediate $N\pi$- or $\Delta\pi$ states in the isospin 3/2 channel of this process might lead to a correction[1] in the connection between EMR, CMR and the form factor ratios as given in eqs.(2.6,2.7). As we cannot exclude this possibility at present, we have inserted $\approx$ symbols in eqs.(2.6,2.7).
In the next step we will calculate the form factors of eq.(2.1) using chiral effective field theory and then discuss our results together with data from experiments for $\left|\mathcal{G}_M^{*Ash}(q^2)\right|$, EMR$(q^2)$ and CMR(q^2).

[1] Such contributions arise in a $\mathcal{O}(\epsilon^3)$ SSE calculation of the process $e\,p \to e'\,N\pi$ in the $\Delta(1232)$ resonance region.

2.3 Effective Field Theory Calculation

The isovector $N\Delta$ transition current has been calculated to $\mathcal{O}(\epsilon^3)$ in nonrelativistic SSE in ref.[GHKP99]. Here we briefly review the ingredients of this calculation, the basic concepts of the theory are discussed in chapter 1. The parts of the ChPT Lagrangean needed for a leading one loop calculation of the matrix element eq.(2.1) can be written as a sum of terms with increasing chiral dimension. Divided into parts with different active degrees of freedom they read:

$$\mathcal{L}_{SSE} = \mathcal{L}^{(2)}_{\pi\pi} + \mathcal{L}^{(1)}_{\pi N} + \mathcal{L}^{(1)}_{\pi\Delta} + \mathcal{L}^{(1)}_{\pi N\Delta} + \mathcal{L}^{(2)}_{\gamma N\Delta} + \mathcal{L}^{(3)}_{\gamma N\Delta} + ... \tag{2.8}$$

In order to introduce a hierarchy of terms we utilize a counting scheme called "small scale expansion (SSE) [HHK98]. This framework contains three light (the momentum transfer $|Q|$, the pion mass m_π and the Δ-nucleon mass splitting in the chiral limit Δ_0) and two heavy (the nucleon mass in the chiral limit M_0 and the scale of chiral symmetry breaking $4\pi F_\pi$ where F_π is the pion decay constant) scales and is based on an expansion of the Lagrangean in ratios of a light to a heavy scale. Chiral dimension one is assigned to each of those ratios and the chiral expansion is performed in the small parameter $\epsilon \in \{\frac{|Q|}{4\pi F_\pi}, \frac{m_\pi}{4\pi F_\pi}, \frac{\Delta}{4\pi F_\pi}, \frac{|Q|}{M_0}, \frac{m_\pi}{M_0}, \frac{\Delta}{M_0}\}$. In order to determine the chiral dimension of a particular Feynman diagram we follow the standard power-counting rules of chapter 1

$$D = 2N_L + 1 + \sum_d \left[(d-2)N^M_d + (d-1)N^{MB}_d\right], \tag{2.9}$$

where N_L is the number of independent loop momenta, N^M_d the number of vertices from the meson Lagrangean of order d and N^{MB}_d the number of vertices from the corresponding meson-baryon Lagrangean. At leading order $D = 1$ we have $N_L = 0$ and an arbitrary number of insertions from the leading meson- and meson-baryon Lagrangean. However, the leading $\gamma N\Delta$ coupling is of chiral dimension $d = 2$ and hence there is no $D = 1$ diagram contributing to the transition amplitude. The diagram with $N^{MB}_2 = 1$ and $N_L = 0$ is the only contribution of $D = 2$. It gives rise to counter-term contributions to the chiral limits of $G_1(0)$ and $G_2(0)$. At $D = 3$ first contributions with $N_L \neq 0$ occur. These leading one loop diagrams have $N_L = 1$ and arbitrary values for N^M_2 and N^{MB}_1. The $N_L = 1$ topology only allows diagrams with $(N^{MB}_1, N^M_2) \in \{(3,0),(2,1),(2,0)\}$, the corresponding diagrams shown in figure 2.1. However, we already mention that those diagrams with $N^M_2 = 0$ (i.e. all loop diagrams except for (b) and (c)) vanish in the nonrelativistic limit due to spin- and isospin selection rules. At the same order tree level diagrams contribute via $N_L = 0$, $N^M_2 = N^M_4 = 0$ and $N^{MB}_3 = 1$ giving rise to further counter-term contributions to the chiral limits of $G_1(0)$ and $G_2(0)$ which are now also needed for a renormalization of loop contributions. In this work we stop at $D = 3$ but hope to extend the analysis to $D = 4$ in the future.
The lowest order chiral Lagrangeans are given by [HHK98]:

$$\mathcal{L}^{(2)}_{\pi\pi} = \frac{F^2_\pi}{4}\mathrm{Tr}\left[\nabla_\mu U^\dagger \nabla^\mu U + \chi^\dagger + \chi U^\dagger\right], \tag{2.10}$$

$$\mathcal{L}^{(1)}_{\pi N} = \bar{\mathcal{N}}\left[iv\cdot D + g_A S\cdot u\right]\mathcal{N}, \tag{2.11}$$

$$\mathcal{L}^{(1)}_{\pi\Delta} = -\bar{T}^\mu_i\left[iv\cdot D^{ij} - \delta^{ij}\Delta_0 + g_1 S\cdot u^{ij}\right] g_{\mu\nu} T^\nu_j, \tag{2.12}$$

$$\mathcal{L}^{(1)}_{\pi N\Delta} = c_A\left\{\bar{T}^\mu_i g_{\mu\alpha} u^\alpha_i \mathcal{N} + \bar{\mathcal{N}} u^{\alpha\dagger}_i g_{\alpha\mu} T^\mu_i\right\}. \tag{2.13}$$

g_A, g_1 and c_A denote axial nucleon-, Δ- and $N\Delta$ coupling constants in the chiral limit, respectively. The numerical values of these constants used throughout this work are listed in table 2.1. We are working in a nonrelativistic framework utilizing nonrelativistic nucleon fields $\mathcal{N}$ as well as nonrelativistic Rarita-Schwinger fields T^i_μ for the four Δ states with isospin-indices i, j [HHK98] which is subject to the spin- and isospin constraints $v^\mu T^i_\mu = 0$ and $\tau^i T^i_\mu = 0$ where τ^i are the Pauli matrices. The quasi Goldstone boson pion triplet π^a is collected in the SU(2) matrix valued field $U(x) = u^2$. The associated covariant derivatives for the pions

∇_μ, for the nucleons D_μ and for the Deltas D^{ij}_μ as well as the chiral field tensors χ, u_μ, u^{ij}_μ, u^i_μ are standard and read [HHK98]:

$$
\begin{aligned}
D_\mu &= \partial_\mu + \Gamma_\mu - i v^{(s)}_\mu, && (2.14)\\
\Gamma_\mu &= \frac{1}{2}[u^\dagger, \partial_\mu u] - \frac{i}{2} u^\dagger \left(v_\mu + a_\mu\right) u - \frac{i}{2} u \left(v_\mu - a_\mu\right) u^\dagger, && (2.15)\\
u_\mu &= i u^\dagger \nabla_\mu U u^\dagger \; = \; \tau^i u^i_\mu, && (2.16)\\
\nabla_\mu &= \partial_\mu U - i \left(v_\mu + a_\mu\right) U + i \left(v_\mu - a_\mu\right), && (2.17)\\
D^{ij}_\mu &= \delta^{ij} \left(\partial_\mu + \Gamma_\mu - i v^{(s)}_\mu\right) - 2 i \epsilon^{ijk} \Gamma^k_\mu, && (2.18)\\
u^{ij}_\mu &= \xi^{ik}_{\frac{3}{2}} u_\mu \xi^{kj}_{\frac{3}{2}}, && (2.19)
\end{aligned}
$$

where v_μ and a_μ denote external vector- and axial vector sources, respectively, and $\xi^{ij}_{\frac{3}{2}} = \delta^{ij} - \frac{1}{3}\tau^i\tau^j$ is the isospin $\frac{3}{2}$ projector. Finally we note that v_μ denotes the velocity four-vector of the nonrelativistic baryon and $S_\mu = \frac{i}{2}\gamma_5\sigma_{\mu\nu}v^\nu$ is the Pauli-Lubanski spin-vector of HBChPT [BKM95].
The local operators contributing to the $\gamma N\Delta$ transition up to order ϵ^3 are given in terms of the low energy constants b_1, b_6, E_1 and D_1 (see refs.[HHK98] and [GHKP99]):

$$
\begin{aligned}
\mathcal{L}^{(2)}_{\gamma N\Delta} &= \frac{i b_1}{2M_0} \bar{T}^\mu_i F^{i+}_{\mu\nu} S^\nu N + h.c., && (2.20)\\
\mathcal{L}^{(3)}_{\gamma N\Delta} &= \frac{1}{4M_0^2} \bar{N} \Bigg[D_1 g^\nu_\mu v^\alpha S^\beta F^{i+}_{\nu\beta\alpha} + 2 i \Delta_0 E_1 F^{i+}_{\mu\nu} S^\nu + (b_1 + 2b_6)(S\cdot\overleftarrow{D}) v^\alpha F^{i+}_{\mu\alpha} + \\
&\quad + (b_1 - 2b_6) v^\alpha F^{k+}_{\alpha\mu} \xi^{kj}_{\frac{3}{2}} S\cdot\overrightarrow{D}^{ji} + 2 b_1 F^{k+}_{\alpha\beta} S^\alpha v^\beta \xi^{kj}_{\frac{3}{2}} \overrightarrow{D}^{ji}_\mu \Bigg] T^\mu_i + h.c.. && (2.21)
\end{aligned}
$$

Here we have used the definitions

$$
\begin{aligned}
F^{i+}_{\nu\beta\alpha} &= \frac{1}{2}\mathrm{Tr}\left(\tau^i \left[D_\nu, F^+_{\beta\alpha}\right]\right), && (2.22)\\
F^\pm_{\mu\nu} &= u^\dagger F^R_{\mu\nu} u \pm u F^L_{\mu\nu} u^\dagger, && (2.23)\\
F^{L,R}_{\mu\nu} &= [\partial_\mu - i F^{L,R}_\mu, F^{L,R}_\nu], && (2.24)\\
F^R &= v_\mu + a_\mu, && (2.25)\\
F^L &= v_\mu - a_\mu. && (2.26)
\end{aligned}
$$

The rich counter-term structure contributing in this transition gives already an indication that the relevant scales governing the physics of the $N\Delta$ transition form factors arise from an interplay between long- and short-distance effects, making the detection of genuine signatures of chiral dynamics nontrivial in this transition.
Figure 2.1 shows all Feynman diagrams contributing at $\mathcal{O}(\epsilon^3)$, i.e. leading one loop order in SSE. The strength of the contact terms in figure 2.1 (a) is given by the LECs of eqs.(2.20, 2.21), the vertices and propagators appearing in the loop diagrams are determined by the Lagrangeans eqs.(2.10)-(2.13). For details we are again referring to ref.[GHKP99]. Given that in this chapter we are working in a nonrelativistic field theory, the crucial step is the correct mapping of the $\Delta \to N\gamma$ transition amplitudes calculated from the diagrams of figure 2.1 to the form factors defined in eq.(2.1). Up to $\mathcal{O}(\epsilon^3)$ one obtains (in the rest frame of the Δ) [GHKP99]:

$$
\begin{aligned}
i\mathcal{M}_{\Delta\to\gamma N} &= \sqrt{\frac{2}{3}}\, e\, \bar{u}_v(r_N) \Bigg[S\cdot\epsilon\, q_\mu \frac{G_1(q^2)}{M_N} + S\cdot q\, \epsilon_\mu \left(-\frac{G_1(q^2)}{M_N} - \frac{\Delta_0 G_1(0)}{2M_N^2} \right.\\
&\quad \left. + \frac{\Delta_0 G_2(q^2)}{4M_N^2} + \frac{q^2}{4M_N^2\Delta_0} G_3(q^2) \right) + S\cdot q\, v\cdot\epsilon\, q_\mu \left(\frac{G_1(0)}{2M_N^2} - \frac{G_2(q^2)}{4M_N^2} \right)\\
&\quad - S\cdot q\, \epsilon\cdot q\, q_\mu \frac{G_3(q^2)}{4M_N^2\Delta_0} + \mathcal{O}\left(\epsilon^4\right) \Bigg] u^\mu_{v,\Delta}(0). && (2.27)
\end{aligned}
$$

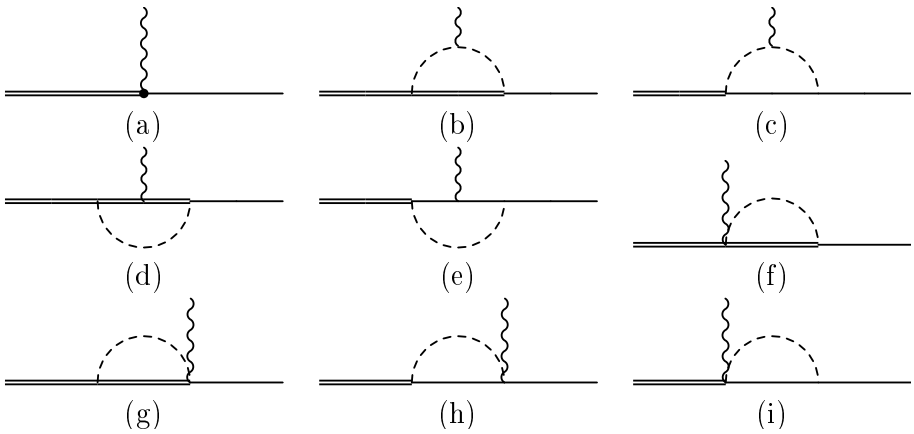

Figure 2.1: The Feynman diagrams contributing to the $\Delta \to N\gamma$ transition at leading one loop order in the SSE formalism [GHKP99]. Double lines represent spin 3/2 states while solid lines stand for nucleon propagators. The dashed lines denote pion-fields and the wiggly line represents the outgoing photon.

Eq.(2.27) provides the central connection between the Feynman diagrams and the sought after form factors. Calculating the $\mathcal{O}(\epsilon^3)$ diagrams of figure 2.1 in nonrelativistic SSE utilizing dimensional regularization one obtains the expressions given in appendix A.1. The finite parts in four dimensions (at renormalization scale λ) still containing a Feynman parameter x read:

$$\begin{aligned} G_1(q^2) &= A(\lambda) + \frac{c_A M_N}{(4\pi F_\pi)^2}\left[\Delta_0\left(\frac{g_A}{3} - \frac{145 g_1}{81}\right) - \frac{4}{9}\Delta_0 \int_0^1 dx\ (5g_1(x-3) - 9g_A(x-1))\, x \log\left(\frac{\tilde{m}}{\lambda}\right)\right. \\ &\quad \left. + \frac{4}{9}\int_0^1 dx\ (5g_1(x-3) I(-x\Delta_0, \tilde{m}) + 9g_A(x-1) I(x\Delta_0, \tilde{m}))\right] + \mathcal{O}(\epsilon^4), \qquad (2.28) \\ G_2(q^2) &= B(\lambda) - C_s q^2 + \frac{c_A M_N^2}{(4\pi F_\pi)^2}\left[\frac{4}{81}(27 g_A - 35 g_1) + \frac{16}{9}(5g_1 - 9g_A)\int_0^1 dx\, x(x-1)\log\left(\frac{\tilde{m}}{\lambda}\right)\right. \\ &\quad \left. + \frac{16}{9}\int_0^1 dx\, \frac{x^2(x-1)}{\tilde{m}^2 - x^2\Delta_0^2}\Delta_0\,(5g_1 I(-x\Delta_0, \tilde{m}) + 9g_A I(x\Delta_0, \tilde{m}))\right] + \mathcal{O}(\epsilon^4), \qquad (2.29) \\ G_3(q^2) &= \frac{8}{9}\frac{c_A M_N^2 \Delta_0}{(4\pi F_\pi)^2}\int_0^1 dx\, \frac{x(2x^2 - 3x + 1)}{\Delta_0^2 x^2 - \tilde{m}^2}\,(5g_1 I(-x\Delta_0, \tilde{m}) + 9g_A I(x\Delta_0, \tilde{m})) + \mathcal{O}(\epsilon^4). \qquad (2.30) \end{aligned}$$

The corresponding $\mathcal{O}(\epsilon^3)$ results in nonrelativistic SSE for the $N\Delta$ multipole transition form factors $\mathcal{G}_M^*(q^2)$, $\mathcal{G}_E^*(q^2)$ and $\mathcal{G}_C^*(q^2)$ are obtained by inserting eqs.(2.28-2.30) into the definitions eqs.(2.2-2.4).
As already mentioned earlier, in $\mathcal{O}(\epsilon^3)$ nonrelativistic SSE only diagrams (b) and (c) of figure 2.1 give nonzero loop contributions to the transition form factors. The contributions from those two diagrams can easily be distinguished: The contributions from diagram (b) are those proportional to the coupling constant g_1 while those from diagram (c) do have a prefactor g_A. Only the latter can give rise to an imaginary part since only in diagram (c) the intermediate states are allowed to simultaneously be onshell – at least for $m_\pi \leq \Delta_0$.
In eqs.(2.28-2.30) we have introduced the quantities $\tilde{m}^2 = m_\pi^2 - q^2 x(1-x)$ and

$$I(\omega, m_\pi) = \begin{cases} \sqrt{\omega^2 - m_\pi^2}\left(\log\left(\frac{\omega}{m_\pi} + \sqrt{\frac{\omega^2}{m_\pi^2} - 1}\right) - i\pi\right) & \frac{\omega}{m_\pi} > 1, \\ \sqrt{m_\pi^2 - \omega^2}\arccos\left(-\frac{\omega}{m_\pi}\right) & \text{for} \quad -1 \leq \frac{\omega}{m_\pi} \leq 1, \\ -\sqrt{\omega^2 - m_\pi^2}\log\left(-\frac{\omega}{m_\pi} + \sqrt{\frac{\omega^2}{m_\pi^2} - 1}\right) & \frac{\omega}{m_\pi} < -1. \end{cases} \qquad (2.31)$$

$A(\lambda)$ and $B(\lambda)$ collect all short range physics contributing to $G_1(0)$ and $G_2(0)$:

$$A(\lambda) = \frac{M_N}{M_0}\left[-\frac{1}{2}b_1 + (2E_1^{(r)}(\lambda) - D_1^{(r)}(\lambda))\frac{\Delta_0}{4M_N}\right], \quad (2.32)$$

$$B(\lambda) = \frac{M_N^2}{M_0^2}\left[2b_6 - D_1^{(r)}(\lambda)\right]. \quad (2.33)$$

The renormalization scale dependence of the counter-terms cancels the one from the loop contributions exactly. We note that the $\mathcal{O}(\epsilon^3)$ structure with the coupling constant E_1 in eq.(2.21) arises naturally in SSE. Its infinite part is required for a complete renormalization of the $\mathcal{O}(\epsilon^3)$ result, whereas its (scale-dependent) finite part $E_1^{(r)}(\lambda)$ cannot be observed independently from the coupling b_1. For nucleon observables the finite parts of terms like $E_1^{(r)}(\lambda)$ are required in order to guarantee the decoupling of the Δ resonance, i.e. those counter-terms are renormalized such that the according loop contributions vanish in the double limit $m_\pi \to 0$ and $\Delta_0 \to \infty$ (see for example the discussion given in ref.[HW02]). In the observables of the $N\Delta$ transition like e.g. $G_1(q^2)$ of eq.(2.28), the finite coupling $E_1^{(r)}(\lambda)$ can be utilized to remove *quark mass independent* short distance physics contributions $\sim \Delta_0$ from loop diagrams contributing to this structure. Implementing this constraint one finds

$$E_1^{(r)}(\lambda) = -\frac{c_A M_N M_0}{324\pi^2 F_\pi^2}\left[36g_A - 139g_1 + 3(35g_1 - 9g_A)\log\left(\frac{2\Delta_0}{\lambda}\right)\right]. \quad (2.34)$$

We emphasize again that this special choice for $E_1^{(r)}(\lambda)$ does not lead to observable consequences[2] in the final result for $G_1(q^2)$. Demanding this decoupling constraint just corresponds to a specific definition of the counter-terms and changing this definition one would only find different numerical values for the coupling constants b_1 and $D_1^{(r)}(\lambda)$. Unfortunately, at $\mathcal{O}(\epsilon^3)$ in SSE we cannot[3] separate the three independent couplings b_1, b_6 and $D_1^{(r)}(\lambda)$ as we only encounter the two linearly independent combinations $A(\lambda)$ and $B(\lambda)$. The strength of these couplings is undetermined in the effective field theory approach and will be determined from phenomenology in the next section.

Finally we comment on the constant C_s in eq.(2.29). To $\mathcal{O}(\epsilon^3)$ in nonrelativistic SSE all counter-terms – i.e. all short distance physics contributions – only appear at $q^2 = 0$, c.f. eqs.(2.28-2.30). All slope parameters of the $G_i(q^2)$ form factors therefore arise as *pure loop effects from the chiral pion dynamics* at this order. While it is expected that the dominant parts of these isovector $N\Delta$ transition slope parameters arise from the pion-cloud, it is also known – for example from calculations of the isovector nucleon form factors (see ref.[BFHM98] and chapter 4) – that short distance contributions in such slope parameters cannot be completely neglected. A short distance contribution to the r_2 slope parameter of the $N\Delta$ transition form factor $G_2(q^2)$ like C_s could, for example, arise from the nonrelativistic reduction of the $\mathcal{O}(\epsilon^5)$ SSE Lagrangean

$$\mathcal{L}_{N\Delta}^{(5)} \sim C_s\bar{\psi}_\mu^i\gamma_5\frac{1}{2}\left(\tau^i\left[D^2, F_+^{\mu\nu}\right]\right)D_\nu\psi_N + h.c.. \quad (2.35)$$

While this contribution is formally suppressed by two orders in the chiral expansion, we will argue in section 2.4.2 that the inclusion of such a short distance coupling is crucial for a comparison with phenomenology. We note that the contribution of eq.(2.35) to the form factor $G_2(q^2)$ was not considered in ref.[GHKP99] and constitutes our main change in terms of formalism compared to those previous results. Short distance effects do of course contribute to the slope parameters of all form factors. However, we have checked that an inclusion of such terms in $G_1(q^2)$ or $G_3(q^2)$ does not lead to significant changes of the best fit curves, indicating that the according contributions to $G_1(q^2)$ and $G_3(q^2)$ do behave as small higher order corrections as suggested by the

[2] This construction ensures that contributions from loops involving $\Delta(1232)$ as an intermediate state get suppressed once the mass of $\Delta(1232)$ gets larger. For a fixed value of the mass of $\Delta(1232)$ this decoupling construction is not necessary.

[3] At $\mathcal{O}(\epsilon^4)$ in SSE one would be able to separate contributions from b_1 and $D_1^{(r)}(\lambda)$ via structurally different contributions to the quark mass dependencies.

power-counting.
At the end of section 2.4.4 we will also discuss the chiral extrapolation of lattice results for the isovector $N\Delta$ transition form factors in the multipole basis at $q^2 = 0$. As the quark mass dependence of $\mathcal{G}_M^*(0)$, $\mathcal{G}_E^*(0)$ and $\mathcal{G}_C^*(0)$ is rather involved (see e.g. the definition equations (2.2-2.4)), the specific form of their chiral extrapolation can only be given numerically. However, the leading quark mass dependence of the $G_i(q^2)$, $i = 1\ldots3$ form factors at $q^2 = 0$ can be given in a closed form and the expansion up to m_π^3 provides a very good approximation of the quark mass dependence of the full result up to $m_\pi = 300$ MeV[4]:

$$\begin{aligned} G_1(0) &= -\frac{1}{2}\frac{M_N}{M_0}b_1 - D_1(\lambda)\frac{\Delta_0}{4M_0} + \frac{ic_A g_A \Delta_0 M_N}{24\pi F_\pi^2} + \frac{c_A M_N m_\pi^2}{576\Delta_0\pi^2 F_\pi^2}\Bigg[9g_A\Bigg(6 - 3\pi^2 + 4i\pi \\ &\quad -4\log\left(\frac{2\Delta_0}{m_\pi}\right)\left(1 + 2i\pi - \log\left(\frac{2\Delta_0}{m_\pi}\right)\right)\Bigg) - 5g_1\Bigg(10 + 3\pi^2 \\ &\quad +4\log\left(\frac{2\Delta_0}{m_\pi}\right) + 12\log^2\left(\frac{2\Delta_0}{m_\pi}\right)\Bigg)\Bigg] + \frac{c_A(5g_1 + 9g_A)M_N m_\pi^3}{216\Delta_0^2\pi F_\pi^2} + ..., \end{aligned} \tag{2.36}$$

$$\begin{aligned} G_2(0) &= (2b_6 - D_1(\lambda))\frac{M_N^2}{M_0^2} - \frac{c_A M_N^2}{162\pi^2 F_\pi^2}\Bigg[5g_1\left(1 + 3\log\left(\frac{2\Delta_0}{\lambda}\right)\right) \\ &\quad +9g_A\left(1 + 3\left(i\pi - \log\left(\frac{2\Delta_0}{\lambda}\right)\right)\right)\Bigg] + \frac{c_A M_N^2 m_\pi^2}{144\Delta_0^2\pi^2 F_\pi^2}\Bigg[9g_A\Bigg(10 - 3\pi(\pi - 4i) \\ &\quad -4\log\left(\frac{2\Delta_0}{m_\pi}\right)\left(3 + 2i\pi - \log\left(\frac{2\Delta_0}{m_\pi}\right)\right)\Bigg) - 5g_1\Bigg(10 + \pi^2 - 12\log\left(\frac{2\Delta_0}{m_\pi}\right) \\ &\quad +4\log^2\left(\frac{2\Delta_0}{m_\pi}\right)\Bigg)\Bigg] + \frac{M_N^2 c_A(5g_1 + 9g_A)m_\pi^3}{27\Delta_0^3\pi F_\pi^2} + ..., \end{aligned} \tag{2.37}$$

$$\begin{aligned} G_3(0) &= \frac{c_A M_N^2}{648\pi^2 F_\pi^2}\left[85g_1 - 9g_A(17 + 6i\pi) + 6(9g_A - 5g_1)\log\left(\frac{2\Delta_0}{m_\pi}\right)\right] - \frac{c_A(5g_1 + 9g_A)M_N^2 m_\pi}{36\Delta_0\pi F_\pi^2} \\ &\quad +\frac{c_A M_N^2 m_\pi^2}{288\Delta_0^2\pi^2 F_\pi^2}\Bigg[9g_A\Bigg(-22 + 9\pi^2 - 20i\pi + 4\log\left(\frac{2\Delta_0}{m_\pi}\right)\left(5 + 6i\pi - 3\log\left(\frac{2\Delta_0}{m_\pi}\right)\right)\Bigg) \\ &\quad +5g_1\left(22 + 3\pi^2 + 4\log\left(\frac{2\Delta_0}{m_\pi}\right)\left(-5 + 3\log\left(\frac{2\Delta_0}{m_\pi}\right)\right)\right)\Bigg] \\ &\quad -\frac{c_A(5g_1 + 9g_A)M_N^2 m_\pi^3}{27\Delta_0^3\pi F_\pi^2} + \ldots. \end{aligned} \tag{2.38}$$

We observe that the leading quark mass (m_q) dependence[5] both for $G_1(0)$ and for $G_2(0)$ is linear in m_q, whereas the leading nonanalytic quark mass behaviour is proportional to $m_q \log m_q$ both for the real- and for the imaginary parts. On the other hand, $G_3(0)$ displays a chiral singularity $\sim \log m_q$ near the chiral limit which will also appear in the Coulomb quadrupole form factor $\mathcal{G}_C^*(0)$ in section 2.4.4. Finally we observe that to $\mathcal{O}(\epsilon^3)$ short distance effects arising from the loop integrals have been removed in eq.(2.36) from the *real* part of $G_1(0)$ via the choice for $E_1^{(r)}(\lambda)$ given in eq.(2.34), whereas the real part of $G_2(0)$ in eq.(2.37) and

[4]Note that the expansion in m_π and the integration over the Feynman parameter x do not commute due to the cuts at $m_\pi = x\Delta_0$ in the full unintegrated results. The above result is only found if the expansion is performed after the integration.

[5]Here we assume the validity of the Gell-Mann, Oakes, Renner relation [GMOR68] given in eq.(2.51) in order to convert the m_π dependence into the m_q dependence.

Parameter	g_A	c_A	g_1	M_N [GeV]	M_Δ [GeV]	m_π [GeV]	F_π [GeV]
Value	1.26	1.5	2.8	0.939	1.210	0.14	0.0924

Table 2.1: The input parameters for our calculation. The nucleon properties g_A and M_N are taken from [Y$^+$06]. For the definition of the mass of $\Delta(1232)$ we are utilizing the T-matrix definition of [Y$^+$06], leading to a (real part) mass of 1210 MeV. The coupling g_1 has been determined in [K$^+$06], whereas the value for c_A is derived in Appendix A.2.

Parameter	A(1GeV)	B(1GeV)	C_s [GeV^{-2}]
Fit I	10.5	15.4	0 (fixed)
Fit II	10.5	15.4	-17.0

Table 2.2: The values for the previously unknown parameters obtained by fitting our results to data from experiments for $\left|\mathcal{G}_M^{*Ash}(Q^2 < 0.2 \text{ GeV}^2)\right|$ and EMR(0) at a regularization scale of $\lambda = 1$ GeV. In Fit I we set $C_s = 0$. We note that the values for $A(\lambda)$ and $B(\lambda)$ do not change significantly between Fit I and Fit II.

all imaginary parts are still affected by quark mass independent short distance physics generated by the loop diagrams of figure 2.1. This nuisance can only be remedied at the next order $\mathcal{O}(\epsilon^4)$. In the present $\mathcal{O}(\epsilon^3)$ SSE calculation this situation is partly responsible for the rather large fit-values we will obtain for $A(\lambda)$ and $B(\lambda)$ in the next section. An interesting observation from the above formulae is that if on uses the SU(6) quark model result $g_1 = \frac{9}{5} g_A$, the two relevant diagrams (diagrams (b) and (c) of figure 2.1) contribute with the same strength to the real parts of the form factors no matter whether the photon couples to a πN or a $\pi\Delta$ loop. Furthermore, in this artificial SU(6) scenario, no UV-divergences, scale dependent logarithms or divergences in the chiral limit are present.

2.4 Discussion of the Results

2.4.1 Fit I: Comparison to previous $\mathcal{O}(\epsilon^3)$ SSE results

The strict $\mathcal{O}(\epsilon^3)$ results of ref.[GHKP99] can be obtained from eqs.(2.28-2.30) by setting $C_s = 0$. For the numerical values of the input parameters we do not follow that reference but instead we utilize the updated values for the couplings given in table 2.1. In Fit I we determine the two unknown parameters $A(\lambda)$ and $B(\lambda)$ by inserting eqs.(2.28)-(2.30) into eqs.(2.2)-(2.4) and fit

- to the experimental data for $\left|\mathcal{G}_M^{*Ash}(Q^2)\right|$ shown in figure 2.2 for momentum transfers of $Q^2 < 0.2$ GeV^2
- and simultaneously to the experimental value for EMR(0) of ref.[B$^+$00] utilizing eq.(2.6).

The resulting values[6] of this Fit I are given in table 2.2 for a regularization scale of $\lambda = 1$ GeV. The dashed curve in figure 2.2 shows that this procedure leads to a satisfying description of $\left|\mathcal{G}_M^{*Ash}(Q^2)\right|$ up to $Q^2 \approx 0.2$ GeV^2. We note that the dotted curve also shown in that figure is the parametrization of the MAID result [TDKY03] which takes into account the fact that this form factor is falling faster than the standard dipole by inserting an extra exponential function:

$$\left|\mathcal{G}_M^{*Ash}(Q^2)\right| = \frac{3}{\left(1 + \frac{Q^2}{0.71\text{GeV}^2}\right)^2} \exp\left(-0.21 \frac{Q^2}{\text{GeV}^2}\right). \tag{2.39}$$

However, while we obtain a reasonable Q^2 dependence for the magnetic $N\Delta$ transition form factor up to $Q^2 \approx 0.2$ GeV^2, we only get the right value of EMR(Q^2) at the photon point $Q^2 = 0$ while the Q^2 dependence

[6] We discuss the numerical size of the two parameters in section 2.4.2.

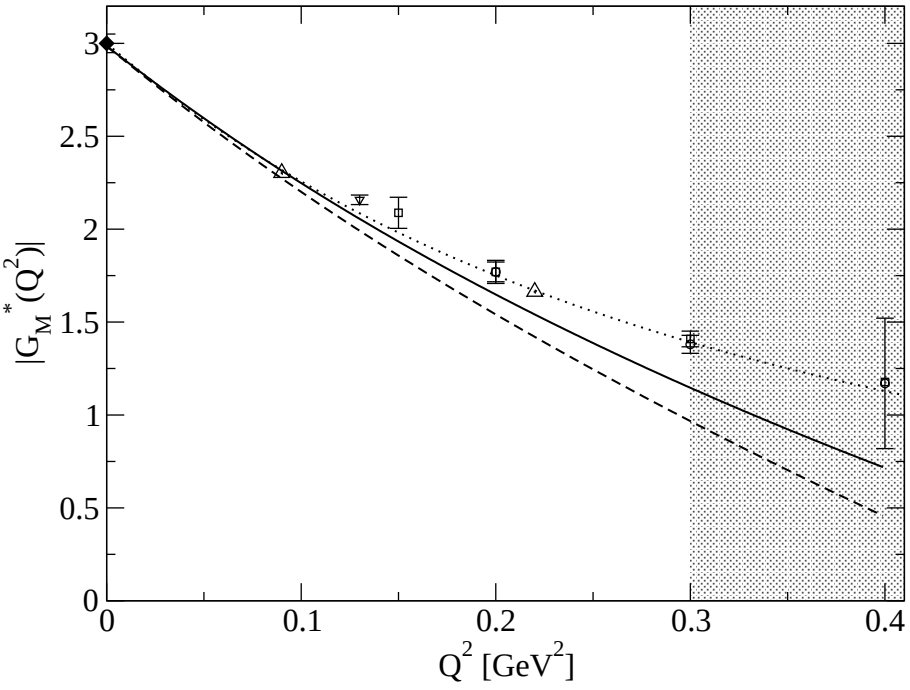

Figure 2.2: The momentum transfer dependence of the absolute value of the magnetic $N\Delta$ transition form factor $\mathcal{G}_M^{*Ash}(Q^2)$ in the convention of eq.(2.5). The solid- (Fit II) and dashed (Fit I) lines show the nonrelativistic $\mathcal{O}(\epsilon^3)$ SSE result while the dotted line corresponds to the MAID parametrization [TDKY03]. The shown experimental data are from [B$^+$00] (diamond), [S$^+$75] (triangle up), [TDKY03] (triangle down), [B$^+$72] (square) and [B$^+$68] (circle). The grey shaded band marks the onset of the domain where one does not expect the low energy expansion to lead to trustworthy results.

of this ratio is far off the experimental data. This can be seen from the dashed curve in fig.2.3. A similarly nonsatisfying picture results for the Q^2 dependence of the CMR-ratio, see fig.2.4. We have analysed the reason for these breakdowns of the $\mathcal{O}(\epsilon^3)$ SSE results of ref.[GHKP99] at very small values of Q^2. According to our new analysis presented here these small ratios are very sensitive to the exact form of the $G_2(Q^2)$ form factor. As it can be seen from the dotted curve of $G_2(Q^2)$ in fig.2.5, in Fit I the momentum transfer dependence of the real part of $G_2(Q^2)$ has an unphysical turning point already at rather low Q^2. It begins to rise again above $Q^2 \approx 0.05$ GeV^2. This "unnatural"[7] behaviour is an indication that important physics is not included in the SSE calculation at the order we are working. Our analysis shows that it is this "unphysical" behaviour of the $G_2(Q^2)$ form factor which is responsible for the poor description of the Q^2 dependence of EMR(Q^2) and CMR(Q^2) in Fit I. In the next section we will present a remedy for this breakdown. In conclusion we must say that for state-of-the-art coupling constants as given in table 2.1 the nonrelativistic $\mathcal{O}(\epsilon^3)$ SSE calculation for the (small) electric- and Coulomb $N\Delta$ quadrupole transition form factors of ref.[GHKP99] is only valid for $Q^2 < 0.05$ GeV^2 while at least the (much larger) magnetic $N\Delta$ transition form factor is described well with the results of ref.[GHKP99] over a larger range in Q^2.

2.4.2 Fit II: Revised $\mathcal{O}(\epsilon^3)$ SSE analysis

The early breakdown of the $\mathcal{O}(\epsilon^3)$ SSE calculation of ref.[GHKP99] discussed in the previous section can be overcome by introducing the parameter C_s in eq.(2.29). As discussed in section 2.3 such a term formally arises

[7] We consider this behaviour to be unphysical since we expect the momentum dependence of a baryon form factor in an effective theory to decrease in magnitude in the momentum range 0.1 GeV$^2 < Q^2 << (4\pi F_\pi)^2 \approx 1$ GeV^2 when the resolution is increased. For further examples of this observed behaviour in the case of nucleon form factors we point to refs.[BFHM98, G$^+$05].

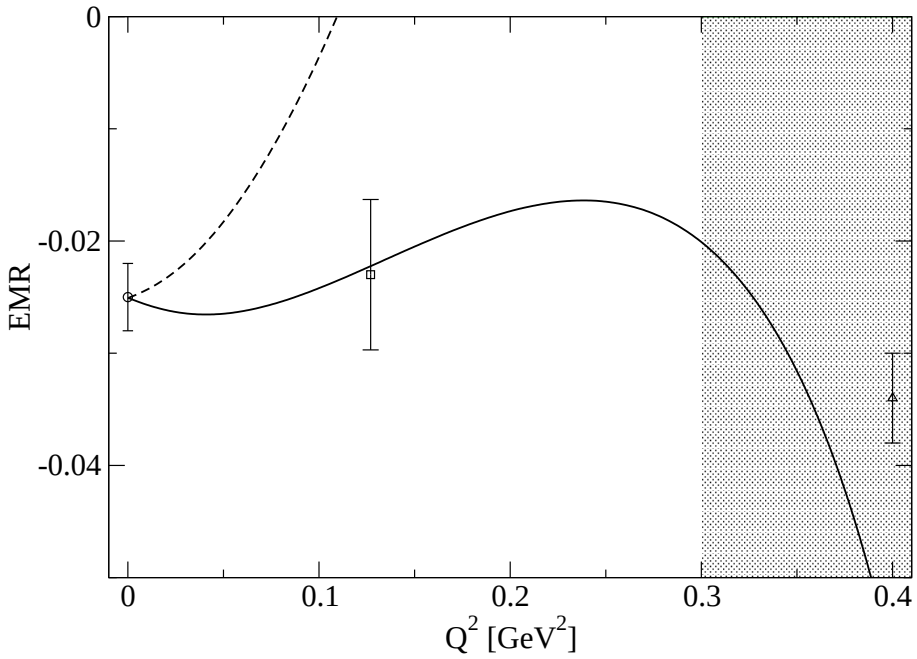

Figure 2.3: EMR(Q^2) of eq.(2.6) at small momentum transfer. Solid line: $\mathcal{O}(\epsilon^3)$ SSE result of Fit II. Dashed line: $\mathcal{O}(\epsilon^3)$ SSE result of Fit I. Experimental data at the real photon point from MAMI [B$^+$00], at $Q^2 = 0.127$ GeV^2 from OOPS [S$^+$05] and at $Q^2 = 0.4$ GeV^2 from CLAS [J$^+$02].

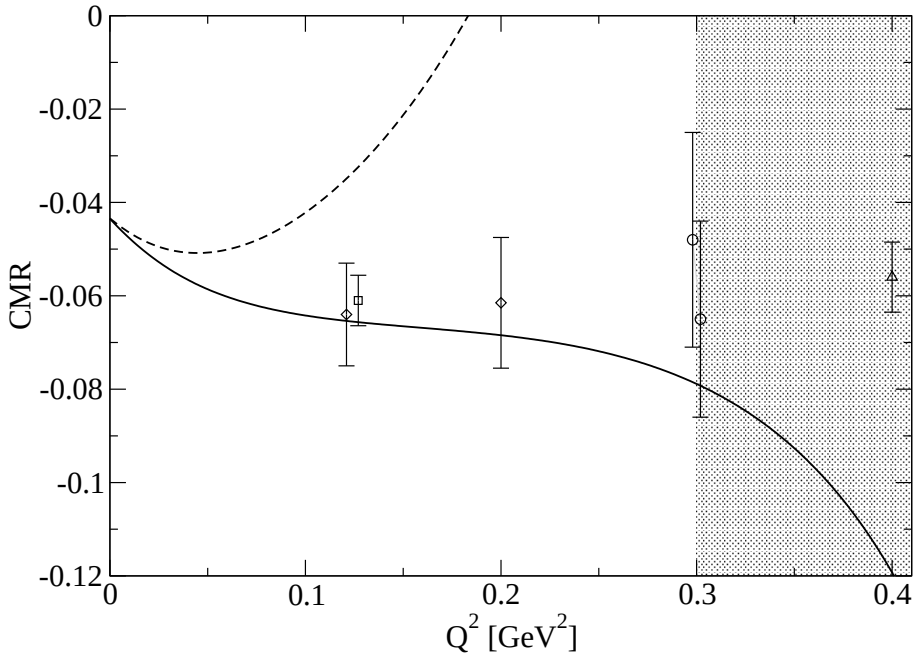

Figure 2.4: CMR(Q^2) of eq.(2.7) at small momentum transfer. Solid line: $\mathcal{O}(\epsilon^3)$ SSE result of Fit II. Dashed line: $\mathcal{O}(\epsilon^3)$ SSE result of Fit I. The data points shown are from refs. [P$^+$01] (diamonds), [S$^+$71] (circles) and [J$^+$02] (triangle).

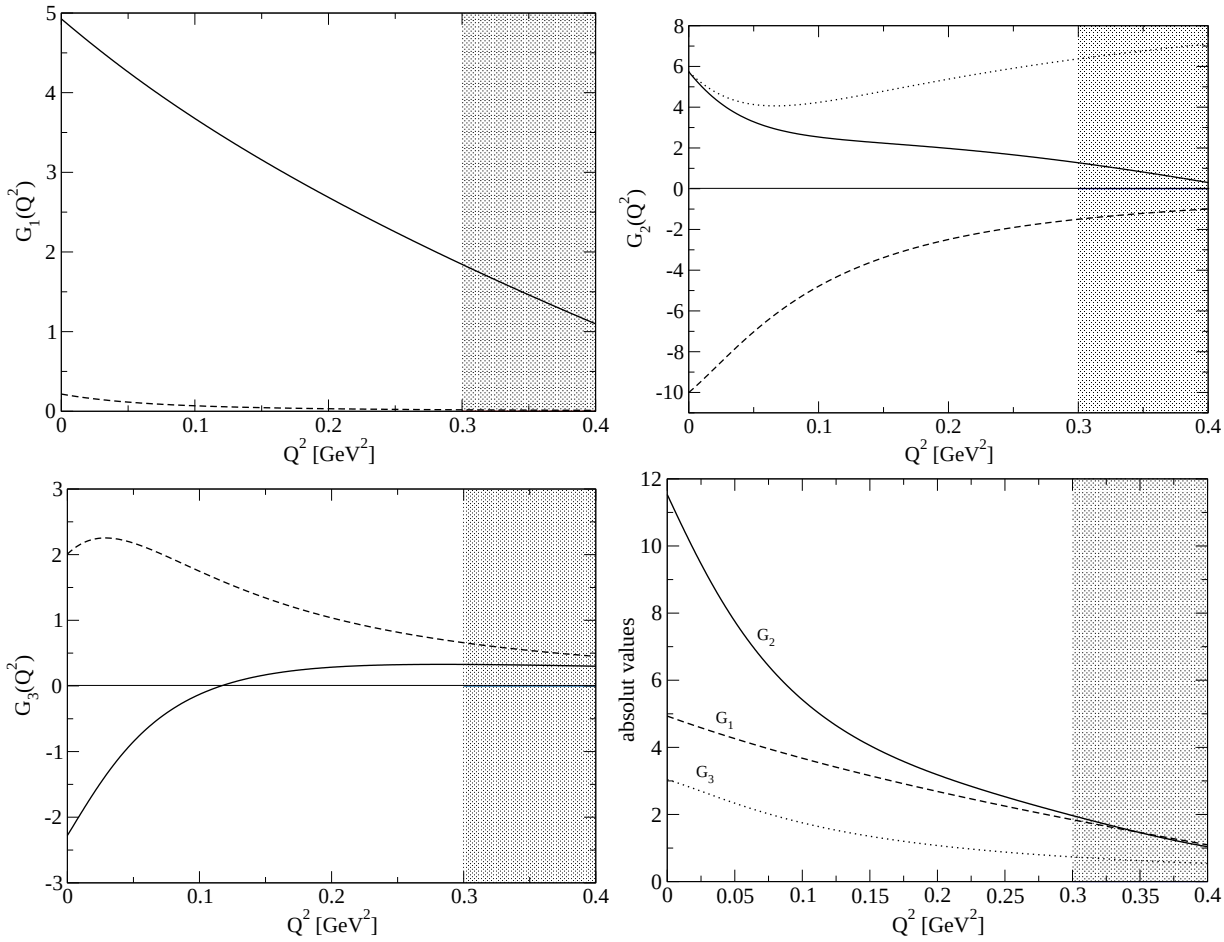

Figure 2.5: The momentum transfer dependence of the transition form factors $G_1(Q^2)$, $G_2(Q^2)$ and $G_3(Q^2)$ (defined in eq.(2.1)) at $\mathcal{O}(\epsilon^3)$ in SSE. Solid lines show real parts, dashed lines imaginary parts. The curves shown are plotted taking the coupling constants at the values determined in Fit II with the only exception being the dotted line in the plot for $G_2(Q^2)$ which corresponds to Fit I.

from higher order couplings in the $\mathcal{O}(\epsilon^5)$ Lagrangean like the one displayed in eq.(2.35). Physically, this term amounts to a small short distance correction in the slope parameter of the form factor $G_2(Q^2)$ which in Fit I is given solely by pion loop contributions. One may wonder why such a contribution, which formally is of higher order in the perturbative chiral calculation, suddenly should play such a prominent role. However, we have to point out that the rather small electric form factor $\mathcal{G}_E^*(Q^2)$ is very sensitive to the $N\Delta$ transition form factor $G_2(Q^2)$. The size of this quadrupole form factor is at the percent level of the dominant magnetic transition form factor $\mathcal{G}_M^*(Q^2)$ – small changes in $G_2(Q^2)$ are therefore disproportionally magnified when looking at EMR(Q^2). In the following we will explicitly include the term C_s in Fit II which now has three unknown parameters $A(\lambda)$, $B(\lambda)$ and C_s. Utilizing the same input parameters as in Fit I (see table 2.1) we insert eqs.(2.28)-(2.30) into eqs.(2.2)-(2.4) and fit again

- to the same experimental data for $\left|\mathcal{G}_M^{*Ash}(Q^2)\right|$ shown in fig.2.2 at momentum transfers of $Q^2 < 0.2$ GeV^2
- and simultaneously to the experimental value for EMR(0) reported in ref.[B$^+$00] utilizing eq.(2.6).

We note that neither in Fit I of the previous section nor in the new Fit II we have used any of the CMR(Q^2) data of fig.2.4. In both fits the resulting sizes and shapes of CMR(Q^2) are a prediction. The same holds for the Q^2 dependence of EMR(Q^2) since only the real photon point of this observable has been used as input for our fits. The numerical values for the three parameters resulting from this new Fit II are given in table 2.2. First we notice that the central values for the parameters $A(1\text{ GeV})$ and $B(1\text{ GeV})$ have not changed significantly compared to Fit I. While the numerical value for the new parameter C_s is quite large, it actually only amounts to a small correction of 0.21 fm in the r_2 slope parameter, in agreement with the expectation from the chiral counting:

$$r_{2,\text{Re}}: \ 1.57\,\text{fm (Fit I)} \quad \rightarrow \quad 1.78\,\text{fm (Fit II)}. \tag{2.40}$$

This small correction in the slope parameter of the $G_2(Q^2)$ form factor leads to a much more physical behaviour[8] in the real part of $G_2(Q^2)$ for $Q^2 < 0.4$ GeV^2, as can clearly be seen from the solid curve in fig.2.5. The resulting changes in the momentum dependence of EMR and CMR as shown by the solid curves of figures 2.3 and 2.4 are quite astonishing. The small change in the slope parameter of $G_2(Q^2)$ has lead to agreement with experimental data both for EMR(Q^2) and CMR(Q^2) up to a four-momentum transfer squared of $Q^2 \approx 0.3$ GeV^2. We note again that none of the experimental data points at *finite* Q^2 in EMR or CMR have been used as input for the determination of the fit-parameters. The significant change of the quadrupole form factors caused by the inclusion of the C_s term which is formally of higher order indicates that its impact is underestimated by naive power counting. At the same time the resulting good accordance with phenomenology shows that this term includes relevant physics into our calculation. These two observations constitute our justification for the inclusion of the coupling C_s at leading one loop order. Similar effects have been observed e.g. in the electric polarizability of the nucleon α_E to $\mathcal{O}(\epsilon^3)$ in SSE (see ref.[HGHP04]) or the contributions beyond the finite one loop result of the process $\gamma\gamma \to \pi^0\pi^0$ in refs.[BC88, DHL88]. For completeness we also note that the resulting absolute value of $\mathcal{G}_M^*(Q^2)$ of Fit II is now also in decent agreement with the experimental data up to $Q^2 \approx 0.2 \ldots 0.3$ GeV^2. We therefore conclude that in Fit II, after the slope parameter correction in $G_2(Q^2)$ has been inserted, it is now the insufficient momentum dependence of $\mathcal{G}_M^*(Q^2)$ *above* $Q^2 \approx 0.25$ GeV^2 that sets the limit in Q^2 for the new nonrelativistic $\mathcal{O}(\epsilon^3)$ SSE result of Fit II presented here. We indicate this limitation by the grey shaded bands in figures 2.2-2.4 and will explore this point further in section 2.4.3.
In table 2.3 we present the findings of Fit II for all six $N\Delta$ transition form factors discussed in this work both at $Q^2 = 0$ and for their (complex) slope parameters r, defined as:

$$G_i(Q^2) \ = \ \text{Re}[G_i(0)]\left[1 - \frac{1}{6}r_{i,\text{Re}}^2 Q^2 + ...\right] + i\,\text{Im}[G_i(0)]\left[1 - \frac{1}{6}r_{i,\text{Im}}^2 Q^2 + ...\right]. \tag{2.41}$$

[8] We note that we do not expect the zero-crossing in the real part of the form factor $G_3(Q^2)$ near $Q^2 = 0.1$ GeV^2, see fig.2.5, to correspond to a physical behaviour. However, the size of $\text{Re}\left[G_3(Q^2)\right]$ for $Q^2 > 0.1$ GeV^2 is so small that this effect does not affect our results in any significant way. For completeness we note that at $\mathcal{O}(\epsilon^4)$ there is a counter term in the SSE Lagrangean which will lead to a momentum independent overall shift in $\text{Re}\left[G_3(Q^2)\right]$ which should correct this presumed artifact.

	$\mathrm{Re}[G_i(0)]$	$r^2_{i,\mathrm{Re}}$ [fm^2]	$\mathrm{Im}[G_i(0)]$	$r^2_{i,\mathrm{Im}}$ [fm^2]	$\lvert G_i(0)\rvert$	$r^2_{i,\mathrm{Abs}}$ [fm^2]
G_1	4.95	0.679	0.216	3.20	4.96	0.678
G_2	5.85	3.15	-10.0	1.28	11.6	1.73
G_3	-2.28	3.39	2.01	-2.26	3.04	0.907
$\mathcal{G}^*_M$	2.98	0.627	-0.377	1.36	3.00	0.630
$\mathcal{G}^*_E$	0.0441	-0.836	-0.249	0.422	0.253	0.388
$\mathcal{G}^*_C$	1.10	-0.729	-1.68	1.90	2.01	1.10

Table 2.3: The values at $Q^2 = 0$ and the slope parameters of the two sets of form factors discussed in this work as obtained in Fit II.

It is interesting to note that the real parts of the slope parameters of both the electric- and the Coulomb $N\Delta$ transition form factors are negative. However, such a behaviour is not too surprising for complex form factors for which the slope parameters cannot be interpreted as radii. As a consequence, the quadrupole $N\Delta$ transition form factors do not behave like dipoles in the low Q^2 region, they look different both from the Sachs form factors of the nucleon and from the common parametrization for $\mathcal{G}^*_M(Q^2)$ of eq.(2.39), see 2.6.
Table 2.3 and figure 2.6 constitute the central results of our analysis of the $N\Delta$ transition. They make clear that the nontrivial Q^2 dependence of EMR(Q^2) and CMR(Q^2) observed in figures 2.3 and 2.4 arises from the quadrupole transition form factors which should therefore be studied independently of $\mathcal{G}^*_M(Q^2)$. Finally we comment on the size of the short distance contributions "sd" parametrized via $A(1\ \mathrm{GeV})$ and $B(1\ \mathrm{GeV})$ versus the long distance contributions from the pion-cloud "pc". Despite the large values for the combinations of LECs (see eqs.(2.32,2.33)), the $N\Delta$ transition form factors are not completely dominated by short distance physics [9] – clear signatures of chiral dynamics are visible. At a scale of $\lambda = 1$ GeV one obtains (at the real photon point):

$$\mathrm{Re}[\mathcal{G}^*_M(0)]|_{\lambda=1\,\mathrm{GeV}} = -1.06|_{pc} + 4.04|_{sd}\,, \tag{2.42}$$
$$\mathrm{Re}[\mathcal{G}^*_E(0)]|_{\lambda=1\,\mathrm{GeV}} = 0.155|_{pc} - 0.110|_{sd}\,, \tag{2.43}$$
$$\mathrm{Re}[\mathcal{G}^*_C(0)]|_{\lambda=1\,\mathrm{GeV}} = 1.47|_{pc} - 0.365|_{sd}\,. \tag{2.44}$$

We note that such a separation into short and long range physics is obviously scale-dependent. However, at a much lower regularization scale of $\lambda = 600$ MeV we have checked that one arrives at the same pattern. Analysing eqs.(2.42-2.44) we conclude that the magnetic $N\Delta$ transition is dominated by short distance physics. Its strength is *reduced* by $\approx 40\%$ due to pion-cloud effects in the magnetic $N\Delta$ transition. This result is very similar to the situation in the isovector magnetic moment of the nucleon (see the discussion in ref.[HW02] and chapter 4), both in sign and in magnitude! While the pion-cloud and the short distance physics are of the same magnitude but of opposite sign for the very small electric quadrupole transition moment, the Coulomb quadrupole moment in our nonrelativistic $\mathcal{O}(\epsilon^3)$ SSE analysis is dominated by the chiral dynamics of the pion-cloud. We note that the smallness of CMR(Q^2) is of purely kinematical origin (see eq.(2.7)), whereas the electric quadrupole form factor in the Jones-Scadron conventions used in this work is intrinsically small relative to the magnetic M1 transition form factor.
The situation is somewhat different for the slope parameters: While we find that approximately 22% of the slope parameter of $G_2(Q^2)$ originate from short range physics, the translation into the Jones-Scadron basis drastically amplifies this contribution to the slope parameters of the quadrupole form factors [10]:

[9] Despite the seemingly large values for $A(\lambda)$ and $B(\lambda)$ as given in table 2.2, the size of the short distance contributions in $\mathcal{G}^*_M(0)$, $\mathcal{G}^*_E(0)$ and $\mathcal{G}^*_C(0)$ is natural as expected (see eqs.(2.42-2.44)).

[10] From eq.(2.41) one can see that the slope parameters are normalized to the the size of the respective form factors at $Q^2 = 0$. The above statements result from just separating the slope parameters into long- and short range physics while keeping the full values for $G_i(Q^2 = 0)$ given in table 2.3.

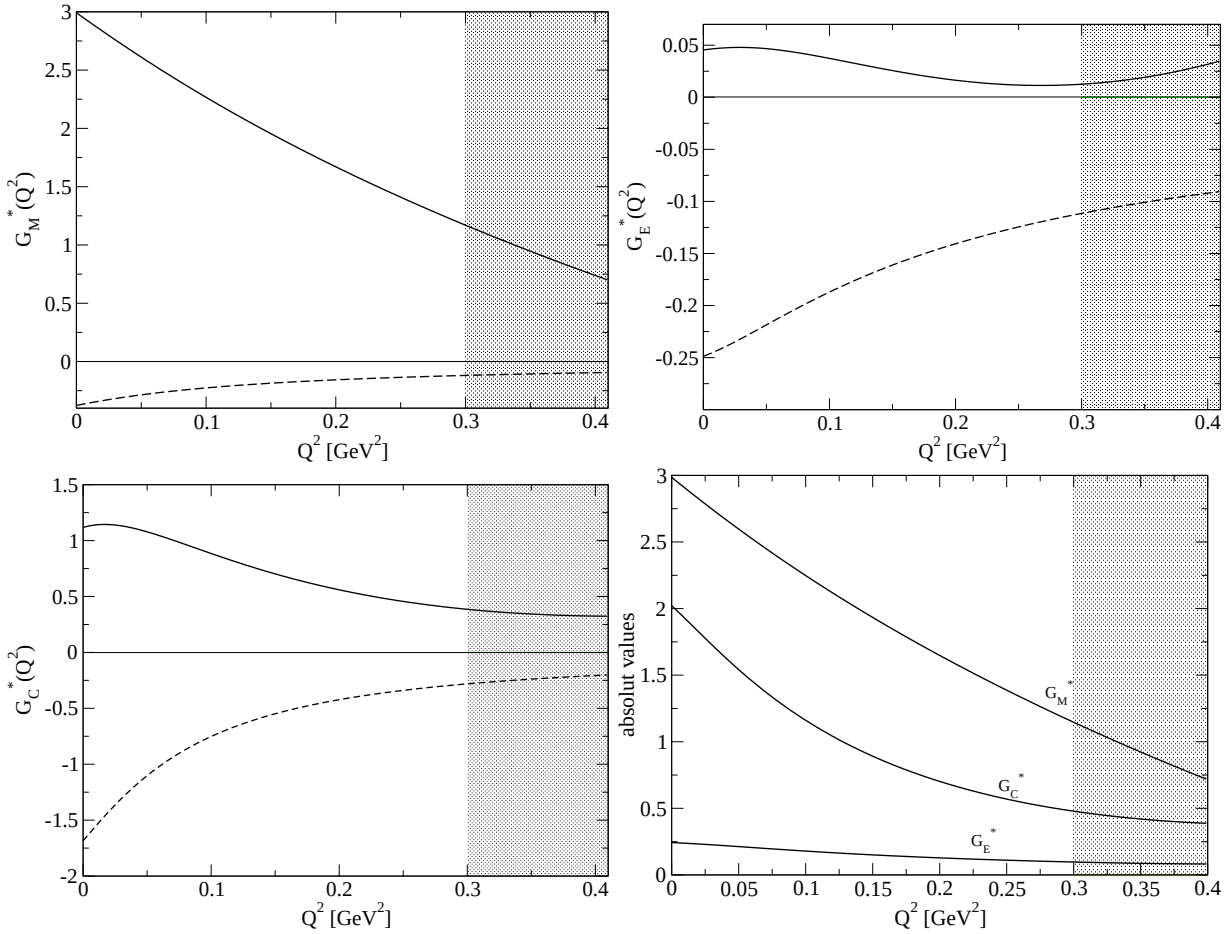

Figure 2.6: $\mathcal{O}(\epsilon^3)$ SSE results of Fit II for the $N\Delta$ transition form factors in the multipole-basis. Solid lines: Real parts. Dashed lines: Imaginary parts.

$$r^2_{M,\mathrm{Re}} = \Big(0.650|_{\mathrm{pc}} - 0.023|_{\mathrm{sd}}\Big)\ \mathrm{fm}^2, \tag{2.45}$$

$$r^2_{E,\mathrm{Re}} = \Big(1.31|_{\mathrm{pc}} - 2.15|_{\mathrm{sd}}\Big)\ \mathrm{fm}^2, \tag{2.46}$$

$$r^2_{C,\mathrm{Re}} = \Big(-0.019|_{\mathrm{pc}} - 0.710|_{\mathrm{sd}}\Big)\ \mathrm{fm}^2. \tag{2.47}$$

All parts marked as short distance contributions in eqs. (2.45)-(2.47) exclusively arise from the local operator contributing to $r^2_{2,\mathrm{Re}}$. From this observation one can see that the G_i basis is clearly preferred for the discussion of chiral signatures in the $N\Delta$ transition as there are fewer kinematical cancellations between large numbers in this basis. At the order of our calculation all effects beyond the linear Q^2 dependence of the form factors and hence the rich structures seen in figures 2.7-2.9 exclusively originate from pion-cloud dynamics.
Before we discuss the quark mass dependence of the form factors we first comment on the range of Q^2 in which the nonrelativistic $\mathcal{O}(\epsilon^3)$ SSE calculation seems applicable.

2.4.3 The range of applicability of the nonrelativistic $\mathcal{O}(\epsilon^3)$ SSE calculation

In nonrelativistic $\mathcal{O}(\epsilon^3)$ SSE calculations the isovector Sachs form factors of the nucleon agree well with dispersion-theoretical results up to a four-momentum transfer of $Q^2 \approx 0.3$ GeV^2 (see e.g. the discussions in

refs.[BFHM98] and [G$^+$05]). On the other hand, it is known that covariant ChEFT calculations of baryon form factors usually do not find enough curvature in the Q^2 dependence of such form factors beyond the term linear in Q^2 (e.g. see ref.[KM01] and the discussion in chapter 4) due to a different organisation of the perturbative ChEFT series. We suspect that this is also the reason why the Q^2 dependence of EMR and CMR reported recently in the covariant ChEFT calculation of refs.[PV05, PV06] is *markedly* different from the one presented here.

In our nonrelativistic $\mathcal{O}(\epsilon^3)$ SSE analysis the limiting factor – as far as the Q^2 dependence is concerned – seems to be the deviation between the result of Fit II for $\mathcal{G}_M^*(Q^2)$ (solid curve in figure 2.2) compared to the data (parametrized by the dotted curve). In order to demonstrate this we present EMR(Q^2) and CMR(Q^2) again in figures 2.8 and 2.9, now with $\mathcal{G}_M^*(Q^2)$ not given by our result of Fit II but with the dipole parametrization of eq.(2.39). One can clearly observe that in both figures the agreement with the experimental results now extends to even larger values of Q^2, giving us confidence that the here calculated results for the electric- and Coulomb $N\Delta$ quadrupole transition form factors – which are the quantities where the impact of chiral dynamics shows up most visibly (see the discussion in section 2.4.2) – have captured the relevant physics up to a momentum transfer $Q^2 \approx 0.3$ GeV^2, similar to the situation for the isovector Sachs form factors of the nucleon in nonrelativistic $\mathcal{O}(\epsilon^3)$ SSE [G$^+$05, BFHM98]. We also note that the slope of the SSE result for CMR at $Q^2 < 0.1$ GeV^2 is highly dominated by πN intermediate states (originating from diagram (c) in figure 2.1). However, the intrinsic Q^2 dependence of this quantity is dressed with a kinematical prefactor which shows a strong momentum transfer dependence at small values of Q^2, see eq.(2.7). This prefactor is responsible for the fast drop-off of CMR(Q^2) at very small momentum transfer and thus hides the effects of the underlying πN dynamics and the interesting behaviour which we found for $\mathcal{G}_C^*(Q^2)$ (see figure 2.5) at small Q^2 cannot be observed in this ratio. The existence and position of the plateau in CMR(Q^2) at higher momentum transfer however is a ChPT prediction and arises due to a balance between loop effects and short range physics with the larger r_2 of Fit II, see eq.(2.40), again being essential.

In addition to these results ChEFT provides us with the knowledge about the structures which can arise in a calculation of the form factors at higher orders. The additional structures contributing to each form factor at lowest order beyond our calculation read:

$$G_1^{(3)}(Q^2) \;\to\; G_1^{(3)}(Q^2) + \frac{Q^2}{(4\pi F_\pi)^2}\delta_1, \tag{2.48}$$

$$G_2^{(3)}(Q^2) \;\to\; G_1^{(3)}(Q^2) + \frac{Q^4}{(4\pi F_\pi)^2 M_N^2}\delta_2, \tag{2.49}$$

$$G_3^{(3)}(Q^2) \;\to\; G_3^{(3)}(Q^2) + \frac{M_N \Delta}{(4\pi F_\pi)^2}\delta_3. \tag{2.50}$$

Here only those contributions which cannot be absorbed via a reparametrization of the three free parameters of our calculation where considered. The uncertainties in the $\mathcal{O}(\epsilon^3)$ calculation due to possible higher order effects are estimated by varying the coefficients δ_i of these structures within their natural size, i.e. between -3 and 3. A stronger constraint is put on the value of δ_1 which dominates the error of the magnetic dipole form factor as we demand the result to be consistent with the input data of our analysis (i.e. $\mathcal{G}_M^*(Q^2)$ at low Q^2). This condition is only fulfilled for $0 < \delta_1 < 2$.

The grey shaded bands around the curves in figures 2.7, 2.8 and 2.9 mark the area in which the set of curves with parameters $0 < \delta_1 < 2$, $-3 < \delta_2 < 3$ and $-3 < \delta_3 < 3$ is located. This band indicates the uncertainties which arise when neglecting higher order effects. A further source of errors lies in the values of those low energy constants already present in the $\mathcal{O}(\epsilon^3)$ calculation which have been kept fixed in the error analysis presented in figures 2.7, 2.8 and 2.9. This is the reason for the fact that the shown error bands for $\mathcal{G}_M^*(Q^2)$ and EMR(Q^2) shrink to zero for $Q^2 \to 0$. As the quality of the determination of the low energy constants depends on the quality of the experimental data used as input, the typical experimental errors of each quantity indicate the possible variation of the ChPT result due to this source of uncertainties. The conclusion from the error analysis presented here is that the calculation at leading one loop order gives a trustworthy prediction of all three transition form factors for momentum transfer Q^2 smaller than 0.2 GeV^2 (note that neither the Q^2 dependence

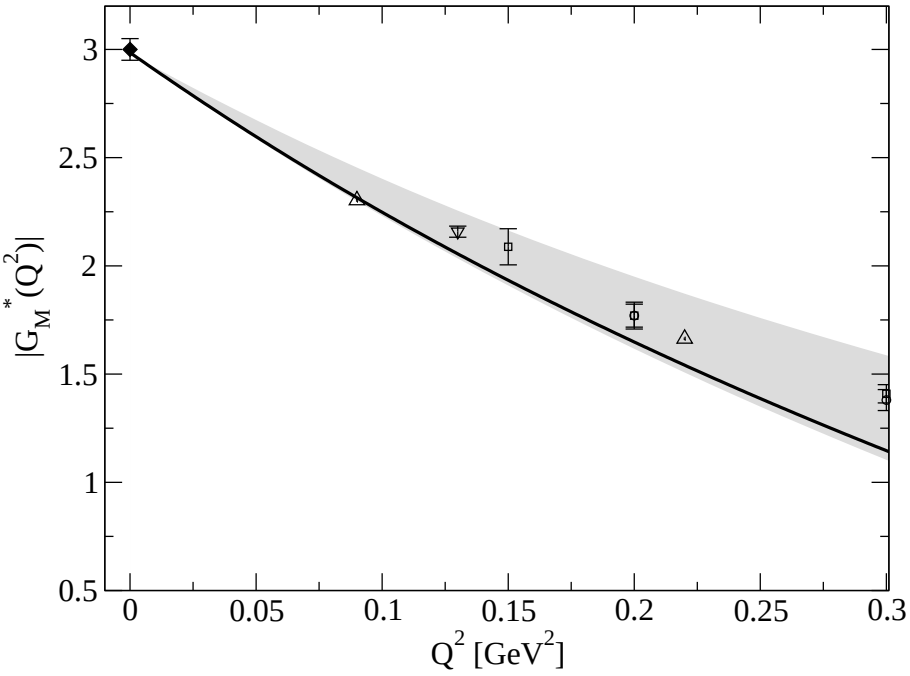

Figure 2.7: The momentum transfer dependence of the magnetic dipole form factor $\mathcal{G}_M^*(Q^2)$: The solid line represents the $\mathcal{O}(\epsilon^3)$ SSE result as discussed in the text, the grey shaded band indicates the uncertainty of this result arising due to possible higher order effects. Data points are taken from [B$^+$00] (diamond), [S$^+$75] (triangle up), [TDKY03] (triangle down), [B$^+$72] (square) and [B$^+$68] (circle).

of EMR nor any information about CMR was used as input for our determination of the low energy constants; the given curves for the quadrupole moments are a prediction). Beyond $Q^2 = 0.2$ GeV^2 higher order effects can – according to this analysis – play a decisive role. We emphasize that due to the uncertainties arising from the extraction of the low energy constants the shown results for the quadrupoles are not in contradiction with most of the models shown in the same figures. E.g., if we where to use the $Q^2 = 0$ values for the quadrupole moments from Sato and Lee [SL96, SL01b] as input for our analysis (instead of the experimental EMR(0) of reference [B$^+$00]), the SSE result would exactly agree with this model prediction (see figure 2.9). Furthermore, we observe that all models (Sato-Lee [SL96, SL01b] and DMT [KY99, KYD$^+$01]) and ChPT calculations (this analysis and the calculation in the δ scheme [PV06]) containing pion-cloud effects coincidingly predict a decreasing EMR at very low Q^2 (where pion-cloud effects should be relevant). We also observe in figure 2.9 that the DMT model of ref.[KY99, KYD$^+$01, DHKT99] shows the same features at low Q^2 as our SSE calculation. It is also interesting to note that the turnover in the Q^2 dependence of EMR near $Q^2 \approx 0.25$ GeV^2 in figure 2.8 may not signal the breakdown of our approach at this (already quite large) momentum transfer but could indicate a real structure effect connecting the OOPS and the CLAS results for EMR(Q^2). In order to decide this issue clearly the next-to-leading one loop order correction to our results has to be calculated. Finally we note again explicitly that the resulting solid curves in figure 2.8 and figure 2.9 have *not* been refit to the data points at finite Q^2, despite their "perfect" agreement with the shown data.

2.4.4 Chiral extrapolation of the $N\Delta$ transition form factors to $\mathcal{O}(\epsilon^3)$ in nonrelativistic SSE

An upcoming task in the description of the nucleon-to-Δ transition in chiral effective field theory is the study of the quark mass dependence of these form factors, extrapolating the recent lattice results of refs. [A$^+$05b] and [A$^+$05a] to the physical point. Figure 2.10 shows – as a first step on this way – the pion mass dependence

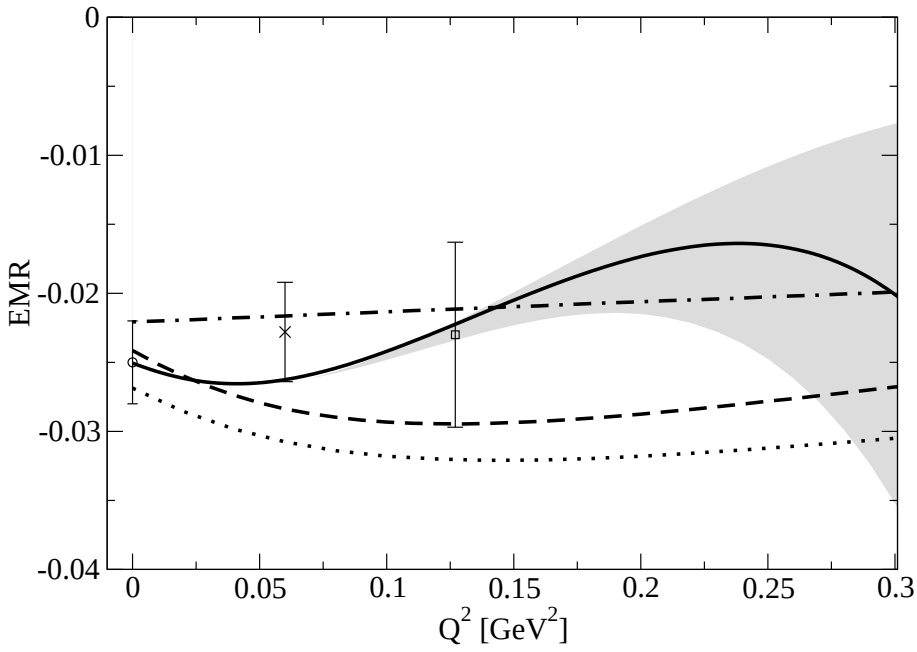

Figure 2.8: The momentum transfer dependence of the ratio of the electric quadrupole to the magnetic dipole form factor EMR(Q^2): The solid line represents the $\mathcal{O}(\epsilon^3)$ SSE result as discussed in the text, the grey shaded band indicates the uncertainty of this result arising due to possible higher order effects. The dashed-dotted (MAID [DHKT99]), dashed (DMT [KY99, KYD$^+$01]) and dotted (Sato-Lee [SL96, SL01b]) curves are model predictions. Experimental date are from MAMI (real photon point [B$^+$00] and $Q^2 = 0.06$ GeV^2 [S$^+$06]) and OOPS [S$^+$05] ($Q^2 = 0.127$ GeV^2).

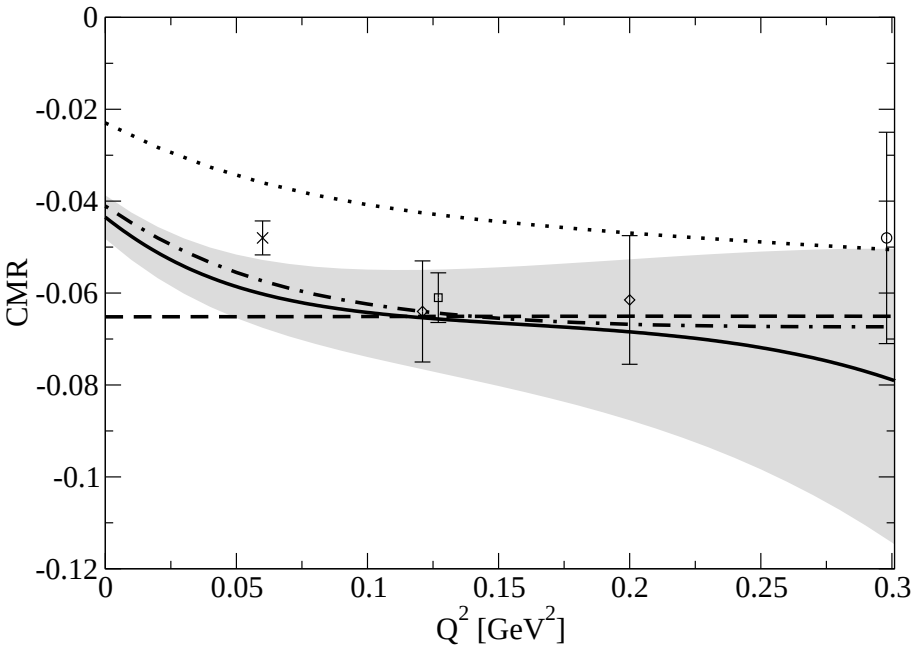

Figure 2.9: The momentum transfer dependence of the ratio of the Coulomb quadrupole to the magnetic dipole form factor CMR(Q^2): The solid line represents the $\mathcal{O}(\epsilon^3)$ SSE result as discussed in the text, the grey shaded band indicates the uncertainty of this result arising due to possible higher order effects. The dashed-dotted (MAID [DHKT99]), dashed (DMT [KY99, KYD$^+$01]) and dotted (Sato-Lee [SL96, SL01b]) curves are model predictions. The data points shown are from refs.[S$^+$06] (cross), [P$^+$01] (diamonds), [S$^+$71] (circles) and [S$^+$05] (square).

of the $N\Delta$ transition form factors in the Jones-Scadron basis of eqs.(2.2-2.4) according to nonrelativistic $\mathcal{O}(\epsilon^3)$ SSE. We note that we did not refit any of the parameters of table 2.2 to produce the extrapolation functions shown. All parameters have been fixed from experimental observables at the physical point as described in sections 2.4.1 and 2.4.2. Both the real and the imaginary parts of the three $N\Delta$ transition form factors develop a quark mass m_q dependence which has been translated into a dependence on the mass of the pion m_π via the GOR-relation [GMOR68]

$$m_\pi^2 \quad = \quad 2\,B_0\,m_q + \mathcal{O}(m_q^2), \tag{2.51}$$

consistent with the order at which we are working. B_0 denotes the magnitude of the chiral condensate. The imaginary parts of all three form factors shown in figure 2.10 are zero[11] for $m_\pi > \Delta_0$ since the $\Delta(1232)$ resonance would become a stable particle at this large pion masses. It is interesting to observe that the quark mass dependence of the magnetic dipole $N\Delta$ transition moment $\mu_{N\Delta} = \mathrm{Re}\,[\mathcal{G}_M^*(0)]$ qualitatively shows the same behaviour as the isovector magnetic moment μ_N^v of the nucleon, studied e.g. in ref.[HW02]. Like its analogue μ_N^v, at the physical point ($m_\pi = 140$ MeV) $\mu_{N\Delta}$ is substantially reduced from its chiral limit value by ≈ 25 percent, dropping further rather quickly in size for increasing quark masses. On the other hand, the quark mass dependence of both the electric- and the Coulomb quadrupole $N\Delta$ transition moments $Q_E^{N\Delta} = \mathrm{Re}\,[\mathcal{G}_E^*(0)]$ and $Q_C^{N\Delta} = \mathrm{Re}\,[\mathcal{G}_C^*(0)]$ is rather unexpected: As can be seen from figure 2.10, $Q_E^{N\Delta}$ even changes its sign around $m_\pi \approx 100$ MeV before approaching a *negative* value in the chiral limit. It will be very interesting to see how the location of this zero-crossing might be affected by corrections at next-to-leading one loop order $\mathcal{O}(\epsilon^4)$ in SSE. In the case of $Q_C^{N\Delta}$ one can observe the effect of $G_3(0)$ of eq.(2.38), leading to a logarithmic divergence of the Coulomb quadrupole transition strength in the chiral limit. Curiously, our nonrelativistic $\mathcal{O}(\epsilon^3)$ SSE calculation indicates that $Q_C^{N\Delta}$ is near a local maximum for physical quark masses. Given the dominance of chiral πN physics in this form factor (see the discussion in section 2.4.3), it would be extremely exciting if such a behaviour could be observed in a lattice QCD simulation. Note that in our discussion we assume all masses appearing in eqs.(2.1-2.4) to be taken at their physical values (see the discussion in ref.[G$^+$05] and after eq.(4.1) of this work regarding this point). However, for a consistent comparison with lattice data, the baryon masses which appear in our ChPT results – mainly through the translation formulae eqs.(2.2)-(2.4) – would have to be evaluated as a function of the pion mass. Regrettably, present state-of-the-art lattice simulations for $N\Delta$ transition form factors take place for $m_\pi > 370$ MeV [A$^+$05b] which is outside the region of applicability of this nonrelativistic leading one loop SSE calculation as indicated by the grey bands in figures 2.10 and 2.11. We hope to extend the range in m_π for which the SSE result provides reasonable chiral extrapolation functions for the $N\Delta$ transition considerably when going to next order in the calculation. We also note that the leading one loop covariant calculation in the δ expansion scheme presented in ref.[PV05] seems to be also stable at pion masses larger than $m_\pi \approx 200$ MeV, presumably due to the additional m_π/M_0 terms present in a covariant approach (see the discussion in the following chapters). However, the stability of the chiral extrapolation functions of both schemes should be tested further by going to next-to-leading one loop order.
Furthermore, we note that there is no need to consider the rather complex structures of EMR(Q^2) or CMR(Q^2) when comparing to lattice QCD results. The intricacies – i.e. the sought after signatures of chiral dynamics – can be studied in a much cleaner fashion when directly comparing ChEFT results to lattice QCD simulations of the $N\Delta$ transition form factors (e.g in the Jones-Scadron basis), see figure 2.10. Nevertheless, for completeness, in figure 2.11 we also show our results[12] for the chiral extrapolation functions of the real parts[13] of

[11] This vanishing is not necessarily a monotonous function of m_π as can be see in the imaginary part of $\mathcal{G}_E^*(0)$ in figure 2.10.

[12] We note again that all chiral extrapolation functions shown in this work *implicitly* assume that all accompanying mass factors in the definition of the $N\Delta$ transition current are held at their physical values. The behaviour of the chiral extrapolation functions changes significantly for $m_\pi > 200$ MeV when the effects of the quark mass dependence of these masses are also included.

[13] Lattice QCD results are obtained in Euclidean space and cannot be connected directly with (complex valued) real world observables in Minkowski space in the case of open decay channels.

EMR(0) and CMR(0) defined as

$$emr = -\frac{\mathrm{Re}[\mathcal{G}_E^*(0)]}{\mathrm{Re}[\mathcal{G}_M^*(0)]}, \tag{2.52}$$

$$cmr = -\frac{M_\Delta^2 - M_N^2}{4M_\Delta^2}\frac{\mathrm{Re}[\mathcal{G}_C^*(0)]}{\mathrm{Re}[\mathcal{G}_M^*(0)]}\,. \tag{2.53}$$

The discussed sign-change in $Q_E^{N\Delta}$ is visible in figure 2.11 in *emr* while the exciting chiral structures of $Q_C^{N\Delta}$ dominate *cmr* for pion masses $m_\pi < 200$ MeV. Above $m_\pi = 200$ MeV the $\mathcal{O}(\epsilon^3)$ SSE results for emr and cmr show a clear breakdown, see fig 2.11. This comes as a consequence of the fact that $\mathrm{Re}[\mathcal{G}_M^*(0)]$ (which is the denominator of those ratios) already becomes very small at those values of the pion mass. Guided by our experience with e.g. the anomalous magnetic moment of the nucleon we would rather expect the real quark mass dependence of $\mathrm{Re}[\mathcal{G}_M^*(0)]$ to plateau at those values of the quark mass[14]. However, we are not surprised by the rapid decrease of our result for the pion mass dependence of $\mathrm{Re}[\mathcal{G}_M^*(0)]$ since the *nonrelativistic* theory leads to similar result for the anomalous magnetic moment of the nucleon, see chapter 4.
As already mentioned, available lattice data of these quantities in refs.[A$^+$05b, A$^+$05a] are unfortunately at too large pion masses to be relevant for the chiral extrapolation functions presented here. However – independent of this (present) limitation of our ChEFT results to the domain of small pion masses – we have to note one important *general caveat* for (future) comparisons of ChEFT results to lattice QCD simulations of $N\Delta$ transition form factors: In figures 2.10 and 2.11 we discuss the chiral extrapolation of the three $N\Delta$ transition moments at $Q^2 = 0$ while lattice QCD results are usually obtained at finite values of momentum transfer. In order to correct for this, one often attempts to connect the lattice results of finite Q^2 to the real photon point by performing global dipole fits with the dipole mass as a free (quark mass dependent) parameter determined from lattice results. While such a procedure may lead to promising results, for example, in the case of the form factors of the nucleon (see the discussion in ref.[G$^+$05] and chapter 4) – and also seems to be applicable to the (monotonously falling) magnetic dipole $N\Delta$ transition form factor $\mathcal{G}_M^*(Q^2)$ – it should not be applied to the study of the sought after electric- and Coulomb quadrupole $N\Delta$ transition form factors due to the nontrivial momentum dependence in these form factors for $Q^2 < 0.15$ GeV^2. This can be clearly concluded from figure 2.6 and from the negative values of (the real parts of) their slope parameters in table 2.3. Global dipole fits connecting lattice QCD results from large Q^2 across the region $Q^2 < 0.15$ GeV^2 to the photon point at $Q^2 = 0$ would just "wash-out" all the interesting chiral physics which dominates the $N\Delta$ quadrupole transition moments $Q_E^{N\Delta}$ and $Q_C^{N\Delta}$ at the physical point! If one wants to study these objects in lattice QCD one has to perform simulations at such small values of momentum transfer that one can directly compare with the ChEFT results for the three $N\Delta$ transition form factors $\mathcal{G}_M^*(Q^2, m_\pi^2)$, $\mathcal{G}_E^*(Q^2, m_\pi^2)$ and $\mathcal{G}_C^*(Q^2, m_\pi^2)$ in the (Q^2, m_π^2) plane and then utilize a function for the momentum dependence down to $Q^2 = 0$ which is consistent with the turning-points generated by chiral πN dynamics. Figure 2.12 shows the nonrelativistic $\mathcal{O}(\epsilon^3)$ SSE result of such a three dimensional function for $\mathcal{G}_M^*(Q^2, m_\pi^2)$, further quantitative studies regarding these chiral extrapolation surfaces are relegated to future work.

2.5 Conclusions and Outlook

The pertinent results of this chapter can be summarized as follows:

1. We have analysed and updated the $\mathcal{O}(\epsilon^3)$ SSE calculation of the isovector $N\Delta$ transition current of ref.[GHKP99] in terms of the magnetic dipole, electric- and Coulomb quadrupole transition form factors in Fit I. It was found that the momentum range of reliability of these results is extremely small (i.e. $Q^2 < 0.05$ GeV^2).

[14]The heuristic argument for this is provided by the observation that pion-cloud effects have usually already been substantially reduced at those large values of m_π and only the contributions from pion mass independent short distance physics remain visible. We will argue in chapter 3 why this effect is nevertheless not observable in nonrelativistic theories.

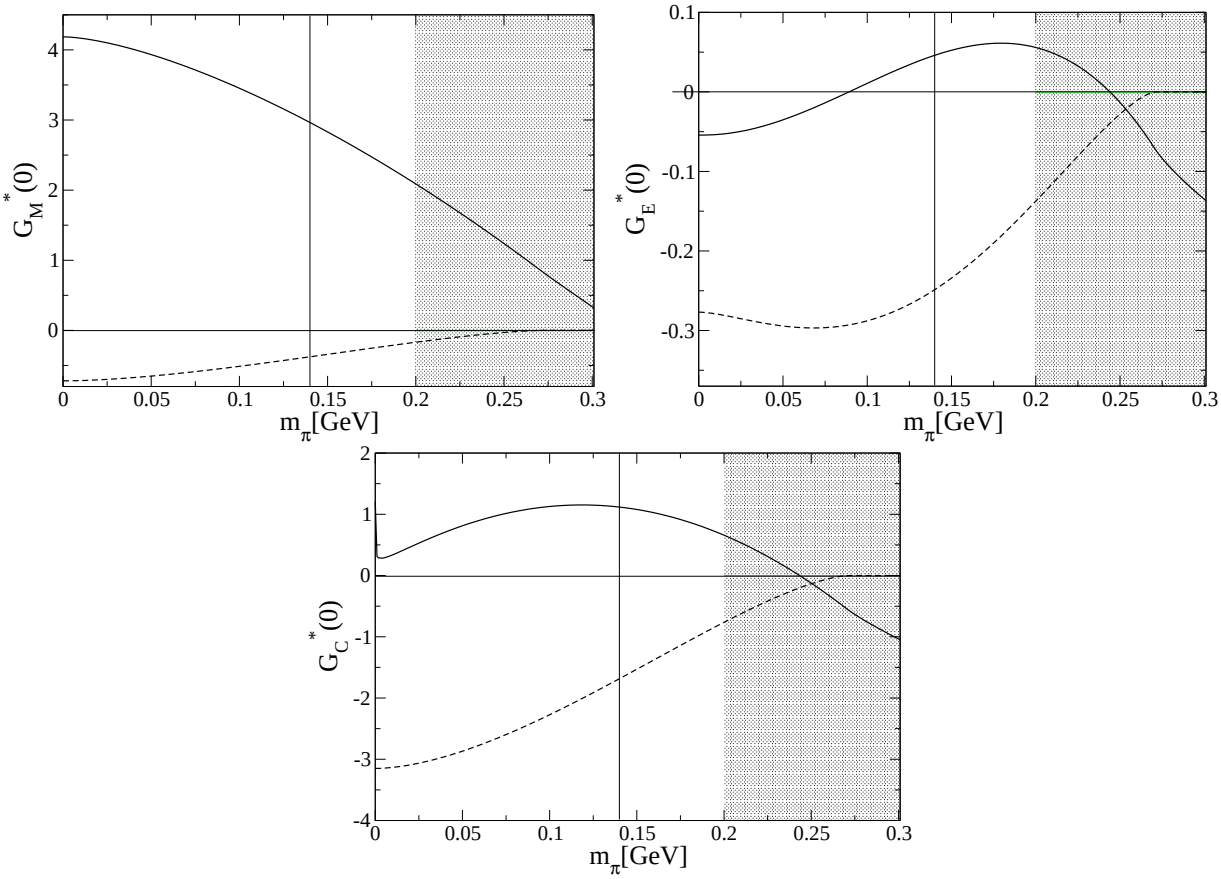

Figure 2.10: The quark mass dependence of the $N\Delta$ transition form factors in the Jones-Scadron basis according to nonrelativistic $\mathcal{O}(\epsilon^3)$ SSE. Solid lines denote the real parts, dashed lines the imaginary parts. All masses appearing in the definitions of the Jones-Scadron multipole form factors are taken at their values at the physical point in order to display *only* the intrinsic quark mass dependence of the transition form factors.

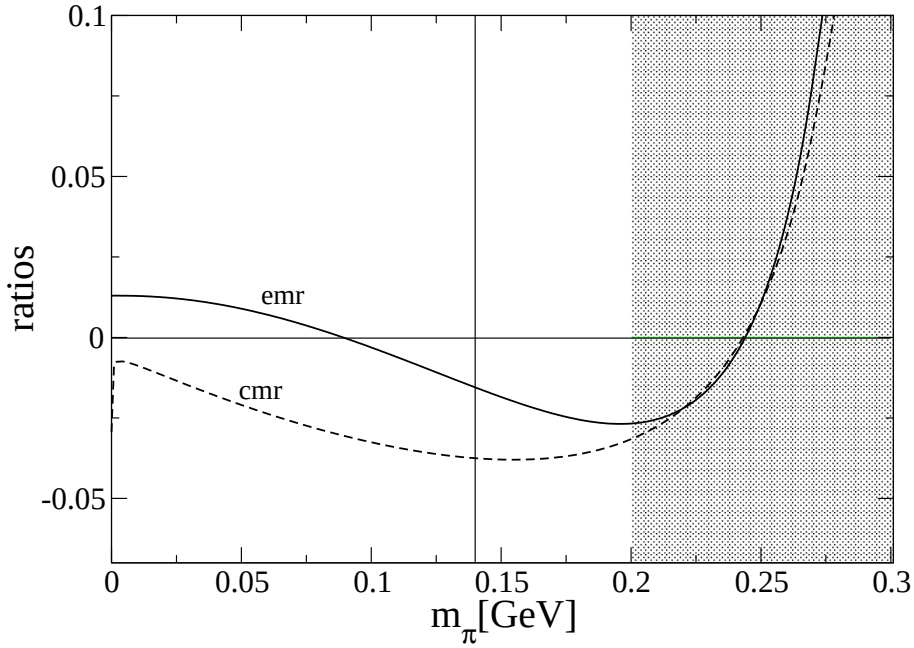

Figure 2.11: m_π dependence of the real parts of emr and cmr as defined in eqs.(2.52,2.53) at $Q^2 = 0$ according to nonrelativistic $\mathcal{O}(\epsilon^3)$ SSE. All masses appearing in the definitions of the Jones-Scadron multipole form factors are taken at their values at the physical point in order to display *only* the intrinsic quark mass dependence of the transition form factors. Note that a clear breakdown of the nonrelativistic results is visible around $m_\pi = 0.2$ GeV.

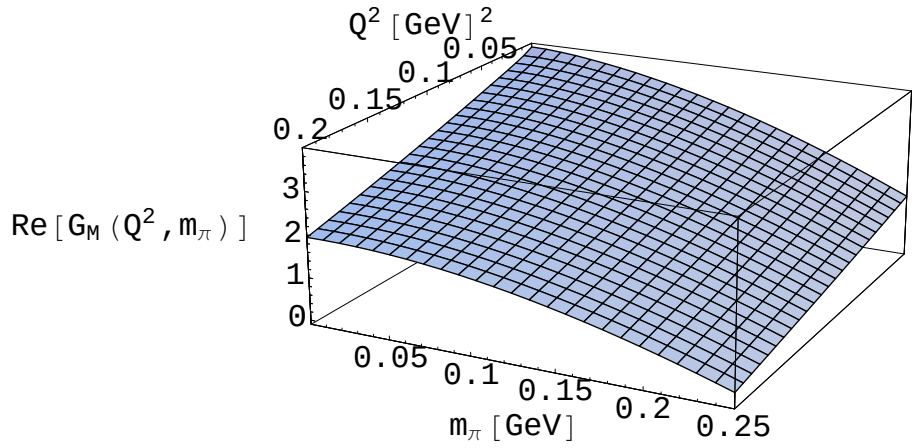

Figure 2.12: Q^2- and m_π dependence of the magnetic dipole $N\Delta$ transition form factor in nonrelativistic $\mathcal{O}(\epsilon^3)$ SSE.

2. We have identified an "unnatural" momentum dependence in the $N\Delta$ transition form factor $G_2(Q^2)$ as the reason for the early breakdown of the results of Fit I. In section 2.4.2 we have demonstrated that the inclusion of a (higher order) counter-term which changes the slope parameter of $G_2(Q^2)$ by 0.21 fm is sufficient to correct the momentum transfer behaviour of this form factor. We have checked that similar correction terms in the slope parameters of $G_1(Q^2)$ and $G_3(Q^2)$ are not significant. The physical origin of the short distance contribution to the slope parameter of $G_2(Q^2)$ parametrized in coupling C_s is not understood at present. The results of Fit II which includes this correction then showed a consistent behaviour in all three form factors up to a momentum transfer squared of $Q^2 = 0.25 \ldots 0.3$ GeV^2.

3. Connecting our results for the transition form factors with ratios of measured pion-electroproduction multipoles via eqs.(2.6,2.7) we have obtained a remarkable agreement between the results of Fit II and experiments up to a momentum transfer squared of $Q^2 = 0.25 \ldots 0.3$ GeV^2 both for EMR(Q^2) and CMR(Q^2).

4. Long distance pion physics was found to be present in all three $N\Delta$ transition form factors. It showed up most prominently in the momentum dependence of the quadrupole form factors for $Q^2 < 0.15$ GeV^2, leading to momentum dependencies which cannot be described via a (modified) dipole ansatz anymore. An observable signal of chiral dynamics in the $N\Delta$ transition could be a minimum in EMR near $Q^2 = 0.05$ GeV^2 and a maximum near $Q^2 = 0.25$ GeV^2. However, it is not clear whether these effects can be identified unambiguously in experiments given the size of current experimental error bars in EMR(Q^2).

5. We have estimated the numerical size of possible higher order contributions to all transition from factors and found that those contributions only start to be relevant above $Q^2 = 0.2$ GeV^2.

6. We have studied chiral extrapolations of the three $N\Delta$ transition form factors at $Q^2 = 0$. We found that the magnetic $N\Delta$ dipole transition moment decreases monotonously with the quark mass, displaying a qualitatively similar behaviour as the isovector magnetic moment of the nucleon. On the other hand, the quark mass dependencies of the quadrupole $N\Delta$ transition moments were found to display rapid changes for pion masses below 200 MeV. While the electric quadrupole transition moment $Q_E^{N\Delta}$ in our analysis even changes its sign near $m_\pi = 0.1$ GeV before approaching a negative chiral limit value, we found that the Coulomb quadrupole transition moment $Q_C^{N\Delta}$ has a local maximum near the physical pion mass and diverges in the chiral limit. State-of-the-art lattice simulations cannot yet reach such small pion masses to test these predictions. On the other hand, our nonrelativistic $\mathcal{O}(\epsilon^3)$ SSE analysis presented here was found to break down for $m_\pi > 0.2$ GeV. In the following chapters we will show that properly renormalized *covariant* ChPT calculations provide a more reliable description of quark mass dependencies in the domain of presently available lattice results. However, the example of the anomalous magnetic moment of the nucleon κ_v given in reference [HW02] teaches us that a considerable improvement concerning the pion mass dependence of SSE[15] results at large quark masses can be achieved when going from $\mathcal{O}(\epsilon^3)$ to $\mathcal{O}(\epsilon^4)$, although this leaves an unpleasant aftertaste concerning the convergence of SSE at larger quark masses.

7. We also point out that lattice studies of the quadrupole $N\Delta$ transition form factors which are performed at finite Q^2 cannot be analysed via a simple dipole ansatz to obtain information about the moments at $Q^2 = 0$ due to the turning-points and structures in the Q^2 dependence of these form factors at $Q^2 < 0.1$ GeV^2.

In the future we are planning to calculate the quark mass dependence of the $N\Delta$ transition form factors at $\mathcal{O}(\epsilon^4)$ in order to extend the range of applicability of these results for chiral extrapolations and to test the stability of the structure effects discussed in this work. In conclusion we can say that we have indeed detected interesting

[15] Note that such an improvement can only be expected in a theory like SSE where besides m_π a second mass scale is involved (here: Δ_0). The arguments for the necessary breakdown of standard HBChPT at large quark masses given in the next chapter are not affected by this observation.

signatures of chiral dynamics in the $N\Delta$ transition, both for the momentum and for the quark mass dependence. In particular we hope that the electric- and Coulomb quadrupole $N\Delta$ transition moments will be tested with higher precision, both on the lattice and in electron scattering experiments in order to verify the signatures of chiral dynamics discussed in this work.

Chapter 3

Renormalization of Covariant BChPT

3.1 Introduction

Motivated by the findings of the previous chapter that the convergence of the chiral expansion at quark masses large compared to the physical one is rather poor in the nonrelativistic theory, we continue our analysis of baryon form factors in the *covariant* formulation of BChPT.
In this chapter we introduce a new renormalization scheme for covariant BChPT. We first develop a catalogue of conditions which a consistent renormalization scheme for covariant BChPT has to fulfill and, subsequently, driven by the observation that none of the renormalization schemes discussed in literature so far is consistent with all of those conditions introduce a new renormalization scheme which we call $\overline{\text{IR}}$ as it is derived starting from the infrared renormalization technique of reference [BL99]. Furthermore, we show that consistent chiral extrapolations exploiting the coupling constants as determined in previous HBChPT analyses are only possible if all of the conditions which we have developed for renormalization schemes are fulfilled, i.e. only in the $\overline{\text{IR}}$ scheme.
After a discussion of basic aspects of renormalization in BChPT, we define the $\overline{\text{IR}}$ scheme and discuss its basic properties. Subsequently, we present an extensive calculation of the mass of the nucleon at next-to-leading one loop order in this new renormalization scheme in section 3.3. This paragraph gives us the possibility to demonstrate the implementation and basic properties of the newly introduced renormalization scheme on a simple example. The last section of this chapter is dedicated to chiral extrapolations of the mass of the nucleon. Readers who are not interested in all the technical details of renormalization in BChPT but want to know how loop diagrams in the new renormalization scheme can be calculated are referred to the framed box in the end of the first section.

3.2 Infrared Singular- and Regular Parts

In the covariant formulation of standard SU(2) BChPT, there are two light- (m_π and q^2) and two heavy mass scales (M_0 and $4\pi F_\pi$). Restricting ourselves to the limit $q^2 = 0$ for simplicity, the contributions to a dimensionless nucleon observable O as a function of those mass scales from a loop diagram of chiral dimension n in dimensional regularization at renormalization scale λ take the general form

$$\begin{aligned} O_{\text{loop}}^{(n)} &= \left(\frac{M_0}{4\pi F_\pi}\right)^n \left[\sum_{i,\text{odd}}^{\infty} o_n^{(n,i\geq n)} \left(\frac{m_\pi}{M_0}\right)^i + \sum_{i,\text{even}}^{\infty} \left(\frac{m_\pi}{M_0}\right)^i \left(o_a^{(n,i)} + o_l^{(n,i\geq n)} \log\frac{m_\pi}{M_0} \right.\right. \\ &\left.\left. + \delta_{i,n} o_d^{(i)} \left(16\pi^2 L + \log\frac{m_\pi}{\lambda}\right)\right) + o_M^{(n,i<n)} \left(16\pi^2 L + \log\frac{M_0}{\lambda}\right) \right], \end{aligned} \tag{3.1}$$

where the index n denotes the order of a specific contribution in[1] $\frac{1}{(4\pi F_\pi)^n}$ and i its order in $\frac{1}{M_0^{i-n}}$. The $o_X^{(n,i)}$ with $X = n, d, l, a, M$ and $c_L^{(i)}$ are dimensionless, quark mass independent prefactors. For a proof of this formula and its properties discussed below see appendix B.3. By normalization with a proper power of a quark mass independent mass scale the reasoning of this chapter can be extended to observables with arbitrary mass dimensions. The generalization to arbitrary values of q^2 can be done by treating q^2 in exactly the same way as we treat m_π^2 in this example.
The full result for the observable O at a certain chiral order m is the sum

$$O = \sum_{n=0}^{m} \left(O_{\text{loop}}^{(n)} + O_{\text{c.t.}}^{(n)} \right) + \mathcal{O}(p^{m+1}), \tag{3.2}$$

where

$$O_{\text{c.t.}}^{(n)} = \begin{cases} c_L^{(n)} \left(\frac{m_\pi}{4\pi F_\pi} \right)^n & n \text{ even}, \\ & \text{if} \\ 0 & n \text{ odd}. \end{cases} \tag{3.3}$$

The six different terms in the above equations are:

- $o_n^{(n,i)}$ are the prefactors of terms which are nonanalytic in the quark mass. Their sizes are determined by the loop calculation in the sense that they are a function of lower order coupling constants.
- $o_d^{(i)}$ is the prefactor of the UV-divergent part of the loop integrals parametrized by L. In dimensional regularization we choose at dimension d: $L = \frac{\lambda^{d-4}}{16\pi^2} \left[\frac{1}{d-4} + \frac{1}{2} \left(\gamma_E - 1 - \log(4\pi) \right) \right]$ where γ_E is the Euler-Mascheroni constant.
- $o_l^{(n,i \geq n)}$ denotes the strength of the logarithmic dependencies of the observable on the pion mass. Again its size is determined by the loop calculation. All coefficients of this type are zero for $i < n$.
- $c_L^{(n)}$ are counter-terms contributing via local operators of chiral dimension n, i.e. they are the *bare* couplings from the Lagrangean $\mathcal{L}_{\pi N}^{(n)}$ contributing via tree level diagrams. The final result eq.(3.2) therefore only contains $c_L^{(n)}$ with even $n \leq m$. In BChPT the size of these couplings is unknown since they parametrize physics beyond the explicit πN dynamics. In practice their numerical values have to be determined from phenomenology. In the $\overline{\text{MS}}$ renormalization program, these terms also serve to absorb the UV-divergences of the loop calculation and the dependencies on the unphysical scale λ.
- $o_a^{(n,i)}$ are the prefactors of the terms analytic in the quark mass. For $i > n$ their sizes are again determined by the loop calculation. For $i = n$ however, there is – due to the presence of $c_L^{(n)}$ – a freedom of choice which terms of the final result for O in eq.(3.2) are considered to come from the loop calculation, i.e the pion-cloud and are written as $o_a^{(n,i)}$ and which terms are part of the local operator, i.e. arise due to short range physics parametrized via $c_L^{(n)}$. Furthermore, the result for O at order $n-1$ already contains all counter-terms $c_L^{(i)}$ with $i < n$. Such, by adding the order n contribution to the order $n-1$ result for O any of the $o_a^{(n,i)}$ with $i \leq n$ meets such a counter-term $c_L^{(i)}$ and therefore at this stage lacks a unique definition. It is this freedom of choice which allows for many different renormalization prescriptions[2] and it is the task of a renormalization prescription to provide a unique separation between long- and short range physics, i.e. a unique definition of the $o_a^{(n,i)}$ and $c_L^{(i)}$.

[1] Following the discussion of the introductory chapter 1 the expansions in p and q (notations of chapter 1) have already been tied together in this expression and are uniformly denoted by $\frac{1}{4\pi F_\pi}$.

[2] The infrared renormalization scheme goes even beyond this by claiming that not only for even n with $i = n$ but for any even value of i there is a chiral order at which the corresponding counter-term $c_L^{(i)}$ appears. Therefore the conclusion of [BL99] is that any of the $o_a^{(n,i)}$ are scheme dependent, even if $i > n$.

- $o_M^{(n,i<n)}$ are the prefactors of logarithms which depend on the mass of the nucleon. They can only be nonzero for $i < n$. Since these terms do not parametrize any nonanalytic quark mass dependencies, they underlie the same scheme dependence as the $o_a^{(n,i)}$.

Note that in the nonrelativistic theory the expression for $O_{\text{loop}}^{(n)}$ given in eq.(3.1) would only contain the terms with $i = n$. Summarizing from a different point of view, one finds that in the final result for O at chiral order m the observable prefactor of a certain even power of $\left(\frac{m_\pi}{M_0}\right)^i$ is

$$\begin{aligned}\frac{M_0^i}{i}\left.\frac{\partial^i O}{\partial m_\pi^i}\right|_{m_\pi\to 0} &= \sum_{n=0}^{m}\left(\frac{M_0}{4\pi F_\pi}\right)^n\left[o_a^{(n,i)}+o_M^{(n,i<n)}\left(16\pi^2 L+\log\frac{M_0}{\lambda}\right)+o_l^{(n,i\geq n)}\log\frac{m_\pi}{M_0}\right]\\ &\quad+\left(\frac{M_0}{4\pi F_\pi}\right)^i\left[o_d^{(i)}\left(16\pi^2 L+\log\frac{m_\pi}{\lambda}\right)+c_L^{(i\leq m)}\right]+\mathcal{O}(p^{m+1}),\end{aligned} \tag{3.4}$$

where only the $o_l^{(n,i\geq n)}$ and $o_d^{(i)}$ are scheme independent since they give the strength of a logarithmic dependence on the quark mass which can only be generated by loop calculations and cannot originate from local operators. However, both loop calculations and local operators can contribute to the other structures and only the sum

$$\sum_{n=0}^{m}\left(\frac{M_0}{4\pi F_\pi}\right)^n\left[o_a^{(n,i)}+o_M^{(n,i<n)}\left(L+\log\frac{M_0}{\lambda}\right)\right]+\left(\frac{M_0}{4\pi F_\pi}\right)^i\left[o_d^{(i\leq m)}L+c_L^{(i\leq m)}\right]+\mathcal{O}(p^{m+1}). \tag{3.5}$$

is observable. In contrast, the prefactors of odd powers of $\left(\frac{m_\pi}{M_0}\right)^i$ are scheme independent. Note that while eq.(3.4) gives the contributions with fixed i (the coefficients of a certain power in m_π) to the final result for O given in eq.(3.2), eq.(3.1) gives the contributions with fixed n (chiral order of the calculated Feynman diagrams, i.e. order in $\frac{1}{4\pi F_\pi}$) to the same result.
We now proceed towards a unique definition of all coefficients appearing in eq.(3.2) by making the expression for O subject to four conditions. Since O as a polynomial in m_π is of course a sum of linear independent terms, these conditions have to be fulfilled by each of the coefficients $\left.\frac{\partial^i O^{(m)}}{\partial m_\pi^i}\right|_{m_\pi\to 0}$ individually.

1. **ultraviolet regularization:** The final result for an observable should be UV-finite and independent of the unphysical renormalization scale λ. Therefore, we require all UV-divergences appearing in the loop calculations (in eqs.(3.1), (3.4) and (3.5) they are contained in L) to be cancelled by corresponding infinite parts of the counter-terms $c_L^{(i)} = c_L^{(i)}(\lambda) - 16\pi^2\beta^{(i)}L$. As L depends on the scale λ, the remaining, finite parts of the counter-terms are consequently also scale dependent and compensate all $\log\frac{m_\pi}{\lambda}$ and $\log\frac{M_0}{\lambda}$ terms of the loop contributions such that $\lambda\frac{\partial}{\partial\lambda}O = 0$. A renormalization scheme designed to fulfill this fundamental condition is $\overline{\text{MS}}$ [GSS88]. In the definitions of eq.(3.2) the renormalization prescription of this scheme is $\left(o_d^{(i)}+\sum_n o_M^{(n,i<n)}\right)16\pi^2 L + c_L^{(i)} \to c_{L^{\overline{\text{MS}}}}^{(i)}(\lambda)$ with $\lambda\frac{\partial}{\partial\lambda}c_L^{(i)}(\lambda) = o_d^{(i)}+\sum_n o_M^{(n,i<n)}$. In the following, we always assume that the UV-divergences have already been cancelled and only discuss the scheme dependence of the finite parts of the counter-terms $c_L^{(i)}(\lambda)$.
   Note that all UV-divergences and scale dependencies appearing in the loop calculation of the observable O up to a certain order can be exactly compensated by the counter-terms available at this order as all UV-divergent and scale dependent contributions to $O^{(n)}$ in eq.(3.1) only appear with $i \leq n$ where corresponding counter-terms occur in eq.(3.2), see appendix B.3.

2. **power counting:** There is a hierarchy of terms in the sum of eq.(3.1): This sum is carried out over increasing powers i of the ratio of the small scale m_π divided by one of the large scales $4\pi F_\pi$ or M_0. Summands with a larger value of the index i are therefore numerically suppressed. Isolating all terms with a nonzero mass dimension, the sum over the index i at fixed n is carried out over terms of the

form $\frac{M_0^{n-i}}{(4\pi F_\pi)^n} m_\pi^i$. But note that for any n those terms start at $i = 0$ and that there is thus no hierarchy amongst contributions with different n! The chiral expansion of eq.(3.2) therefore is not necessarily a reasonable perturbative expansion. Feynman diagrams of any chiral order n are not suppressed [GSS88] but could have arbitrary numerical impact on the final result for O. In order to provide a meaningful power-counting prescription, a consistent renormalization scheme therefore has to link the expansions in i and n in such a way that higher orders in n only contain higher orders of i.
We therefore require all terms with $i < n$ arising in a calculation of a loop diagram of order n to be zero in a renormalization scheme suitable for covariant BChPT. This is possible since all contributions to $O^{(n)}$ of eq.(3.1) with $i < n$ are analytic in the quark mass according to appendix B.3. This condition is thus fulfilled if all contributions of the $o_a^{(n,i)}$ and $o_M^{(n,i<n)}$ with $i < n$ are absorbed into the corresponding $c_L^{(i)}(\lambda)$.
Two renormalization schemes discussed frequently in literature which do have this property are the EOMS scheme [FGJS03] and the infrared renormalization scheme [BL99].

3. **nonrelativistic limit:** In a renormalization scheme fulfilling the previous two conditions which are both necessary for consistent loop calculations in BChPT, eq.(3.5) reduces to $\sum_{n=0}^{i} \left(\frac{M_0}{4\pi F_\pi}\right)^n o_a^{(n,i)} + \left(\frac{M_0}{4\pi F_\pi}\right)^i c_L^{(i\leq m)}(\lambda)$ still leaving a scheme dependence if $i \leq m$. To uniquely define $o_a^{(n,i)}$ and $c_L^{(i)}(\lambda)$ which have the same impact on the final result but are of structurally different origin, we choose to require the segmentation of this sum in covariant BChPT to happen in exactly the same way as in HBChPT, i.e. the $o_a^{(n,i)}$ and $c_L^{(i)}(\lambda)$ must be of same numerical size in both formulations of ChPT. This requirement allows to make contact between covariant BChPT results and the long and successful history of HBChPT. In a scheme fulfilling this condition all coupling constants are defined in the same way and their finite parts do have the same numerical values as in HBChPT. For each diagram, the HBChPT results can be found by an expansion of the corresponding (properly renormalized) covariant result in $\frac{1}{M_0}$.
A renormalization scheme designed to fulfill this condition is the infrared renormalization scheme [BL99].

4. **analyticity:** After conditions 1.-3. all coefficients $o_X^{(n,i)}$ and $c_L^{(i)}(\lambda)$ of the result for O given in eq.(3.2) are uniquely defined. However, there is "in principle" a further scheme dependence: While in a calculation of O at order m only the $c_L^{(i\leq m)}(\lambda)$ with $i \leq m$ are explicitly included, the same expression contains $o_a^{(n,i)}$ with any value of i. By going to higher orders in the chiral expansion, $c_L^{(i)}(\lambda)$ with larger i have to be included and the scheme dependence discussed in condition 3. also pertains the sum $\sum_{n=0}^{i} \left(\frac{M_0}{4\pi F_\pi}\right)^n o_a^{(n,i)} + \left(\frac{M_0}{4\pi F_\pi}\right)^i c_L^{(i)}(\lambda)$ with $i > m$. Apart from the fact that this scheme dependence is only existent "in principle" since those $c_L^{(i)}(\lambda)$ with large values of i are not present at a certain order $n < i$, we require that no unphysical nonanalyticities are generated by the renormalization procedure.
This last condition is relevant with respect to the infrared renormalization scheme [BL99] since this scheme takes advance of this possibility "in principle" but at the end has to deal with unphysical cuts, singularities and imaginary parts at very large quark masses. Although the unphysical singularities in this scheme are located at $m_\pi = 2M_0$ and therefore far outside the region of applicability of the low energy theory, their existence disturbs the convergence properties of the chiral expansion for many observables even for pion masses just above the physical one.

In table 3.1 we give an overview over different renormalization schemes and how they behave with respect to the conditions discussed above. In Figure 3.1 we demonstrate in a schematic sketch how different renormalization schemes treat the double expansion of eq.(3.2), in particular we show which of the $o_X^{(n,i)}$, $X = a, M$ are set to zero in a particular scheme and which are not.
Since we are aiming to work with a renormalization scheme fulfilling all four conditions, we now start with a brief discussion of the infrared renormalization scheme (IR) which fulfills conditions 2. and 3. and subsequently modify it such that it also satisfies our first and fourth condition.

	power counting	analyticity	nonrelativistic limit	ultraviolet regularization
$\overline{\text{IR}}$	✓	✓	✓	✓
standard IR	✓	-	✓	(✓)
$\overline{\text{MS}}$	-	✓	-	✓
EOMS	✓	✓	-	✓

Table 3.1: Overview over several renormalization schemes of BChPT frequently discussed in literature and how they behave with respect to the four conditions discussed in the text. The $\overline{\text{IR}}$ scheme is designed to fulfill all four conditions.

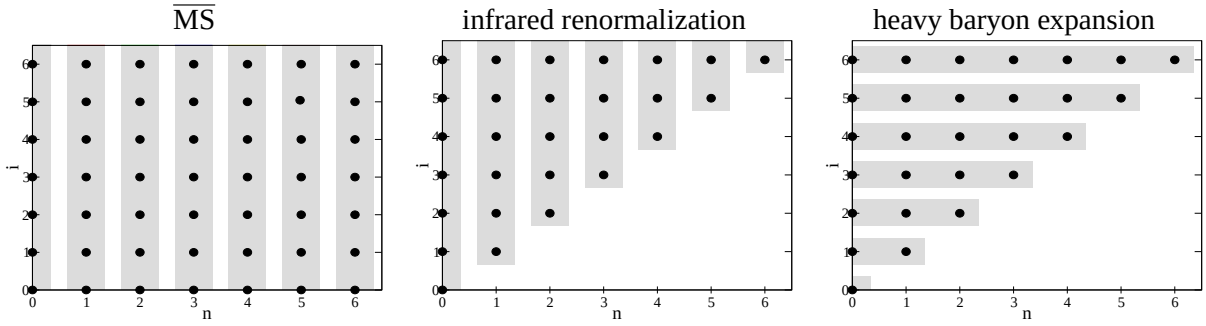

Figure 3.1: A schematic plot demonstrating the different treatments of the double expansion in $\frac{1}{4\pi F_\pi}$ and $\frac{1}{M_0}$ in three different formulations of BChPT. From left to right: $\overline{\text{MS}}$- and infrared renormalized covariant BChPT and HBChPT. From this plot, one can read off at which order in $\frac{1}{(4\pi F_\pi)^n}$ which orders of $\frac{1}{M_0^{i-n}}$ are included. A black dot denotes a nonzero contribution from this structure in the respective scheme while the grey shaded areas pool all those terms which are considered to be of the same chiral order D. The covariant framework identifies $D \sim n$ while the chiral dimension in the heavy baryon expansion can be calculated as $D \sim i$.

The authors of reference [BL99] were able to implement a computational technique which separates results of one loop calculations within BChPT consistently into two parts and showed that one part – called the *infrared singular* part – fulfills conditions 2. and 3. discussed above and the remainder – the *infrared regular* part – is a polynomial in even powers of m_π, i.e. analytic in the quark mass and can therefore be absorbed into the coefficients $c_L^{(i)}(\lambda)$. The identification of the two parts of a one loop integral can be done as follows: With the help of Feynman parameters, the propagator of every intermediate πN state can be expressed in terms of a one-pion-one-nucleon state:

$$H_{11} \;=\; \frac{1}{i}\int \frac{d^dl}{(2\pi)^d}\,\frac{1}{(m_\pi^2-l^2)\left(M_0^2-(p-l)^2\right)}, \tag{3.6}$$

which again using Feynman parametrization can be written as an integral over a single propagator:

$$\frac{1}{i}\int_I dx \int \frac{d^dl}{(2\pi)^d}\,\frac{1}{\left(\tilde{m}^2-l^2\right)^2}, \tag{3.7}$$

where we have introduced the effective mass $\tilde{m}^2=(1-x)m_\pi^2+x^2M_0^2$ and assumed $p^2=M_0^2$ for simplicity. The expressions in eq.(3.6) and eq.(3.7) are analytically equal if the interval of integration is $I=[0,1]$. The *infrared singular* part I_{11} of this integral is projected out if the interval of integration is identified with $I=[0,\infty)$. The difference between eq.(3.6) and eq.(3.7) with this choice of integration bounds – the *infrared regular* part R_{11} – is then the integral over the interval $[1,\infty)$. Writing it down explicitly, one finds[3]:

$$H_{11} \;=\; I_{11}-R_{11} \;=\; \frac{1}{i}\left[\int_0^\infty dx \;-\; \int_1^\infty dx\right]\int \frac{d^dl}{(2\pi)^d}\,\frac{1}{\left(\tilde{m}^2-l^2\right)^2}. \tag{3.8}$$

A loop only containing pion-propagators is completely singular, if it only consists of nucleon-propagators it is completely regular. As already mentioned earlier, I_{11} fulfills the conditions 2. and 3. while R_{11} appears to be an even series in the pion mass $R_{11}=\sum_{j=0}^\infty a_j m_\pi^{2j}$ where the prefactors a_j do not contain any quark mass dependencies. Since at every even power in the pion mass there is a contribution from a contact term $c_L^{(i)}(\lambda)$, recall eq.(3.5), R_{11} can in principle be absorbed into the low energy constants. In other words: The prescription to neglect the infrared regular parts is nothing else but a specific definition of the contact terms $c_L^{(i)}(\lambda)$ and such of $\sum_{n=0}^m o_a^{(n,i)}$ and $\sum_{n=0}^m o_M^{(n,i<n)}$, see eq.(3.5). Therefore, the result of an IR renormalized loop calculation is found when all appearing loop integrals of the type eq.(3.6) are identified with their infrared singular part I_{11}. Writing it down explicitly, the regular part of $O^{(n)}$ of eq.(3.1) is of the form:

$$R\left(O^{(n)}\right) \;=\; \left(\frac{M_0}{4\pi F_\pi}\right)^n \sum_{i,\text{even}}^\infty \left(\frac{m_\pi}{M_0}\right)^i \left[r_a^{(n,i)}+r_M^{(n,i)}\left(16\pi^2L+\log\frac{M_0}{\lambda}\right)\right], \tag{3.9}$$

where one finds

$$r_M^{(n,i)} \;=\; \begin{cases} -o_M^{(n,i<n)} & \\ \text{for} & i<n, \\ o_l^{(n,i>n)} & \end{cases} \tag{3.10}$$

and

$$r_a^{(n,i)} \;=\; -o_a^{(n,i)} \text{ for } i<n. \tag{3.11}$$

While the equations for $i<n$ are necessary to implement our condition 2., the second line of the first equation implements a generalization of our condition 3. to $i>n$ for all terms containing a logarithm.

[3] Note that we define the regular part with a different sign compared to reference [BL99].

If $O^{(n)}_{\text{c.t.}}$ denotes the contributions to $O^{(n)}$ from counter-terms, the IR renormalized result of order m is found by the replacement

$$\sum_{n=0}^{m}\left[O^{(n)}_{\text{c.t.}} - R\left(O^{(n)}\right)\right] \;\rightarrow\; \sum_{n=0}^{m} O^{(n)}_{\text{c.t.}^{\text{IR}}}. \tag{3.12}$$

Such the final result for $O^{(m)}$ in IR renormalization is

$$O^{(m)} \;=\; \sum_{n=0}^{m}\left[O^{(n)}_{\text{c.t.}^{\text{IR}}} + I\left(O^{(n)}\right)\right], \tag{3.13}$$

where $I\left(O^{(n)}\right)$ is the infrared singular part of $O^{(n)}$.
However, this scheme suffers from three deficiencies:

1. As already discussed earlier, the result for an observable O at a certain chiral order m only contains the counter-terms $c_L^{(i)}(\lambda)$ with $i \leq m$. The possibility to absorb terms contained in the infrared regular part with larger values of i is only a possibility "in principle", i.e. a possibility arising at a higher order.

2. The infrared singular piece of a one loop integral can contain divergences and scale dependent logarithms beyond the order of the calculation: The $r_M^{(n,i)}$ are not necessarily zero for $i > m$! As discussed above, there are no corresponding terms $c_L^{(i)}(\lambda)$ present in O for these values of i. Therefore the IR renormalized result for O can contain divergences L and scale dependent logarithms which cannot be absorbed into a corresponding local operator and thus violates our condition 1. The – in our opinion unsatisfactory – remedy proposed in reference [BL99] is to cancel the divergences by hand, again motivated by the possibility "in principle" to absorb these terms into low energy constants which appear at higher orders, and to always set $\lambda = M_0$ to cancel the explicit scale dependence.

3. The infrared regular parts of a loop integral are nonanalytic, they violate our condition 4. This comes due to the fact that the infinite sum $R_{11} = \sum_{j=0}^{\infty} a_j m_\pi^{2j}$ does not converge for all values of m_π.
This point is of particular importance in the application of BChPT results to chiral extrapolations. Although the scheme immanent nonanalyticities which are generated by IR renormalization are located at $m_\pi \geq 2M_0$, the quark mass dependencies of some observables see a strong impact from those effects at pion masses just above the physical one, e.g. start to run into a pole.

The key to a renormalization scheme fulfilling all four conditions is the following observation: While conditions 2. and 3., which are fulfilled by the IR scheme, only affect terms of eq.(3.2) with $i \leq m$, the three deficiencies of IR are due to terms with $i > m$. Therefore, we propose a modified infrared renormalization scheme $\overline{\text{IR}}$ which agrees with the IR prescriptions for all terms with $i \leq m$ but treats all terms with $i > m$ differently. In particular, we overcome all three deficiencies if the infrared regular parts with $i > m$ are not absorbed into counter-terms (which are anyway not present at this order m) in the newly designed renormalization scheme. Note, however, that the determination of those regular parts which are absorbed into the corresponding counter-terms such depends on the order m of the calculation.
In analogy to eq.(3.12) we define the renormalization prescription for a result of chiral order m in the modified infrared renormalization scheme ($\overline{\text{IR}}$) by:

$$\sum_{i=0}^{m}\left[O^{(i)}_{\text{c.t.}} - \frac{m_\pi^i}{i}\sum_{n=0}^{m}\left[\frac{\partial^i}{\partial m_\pi^i} R\left(O^{(n)}\right)\right]_{m_\pi=0}\right] \;\rightarrow\; \sum_{i=0}^{m} O^{(i)}_{\text{c.t.}^{\overline{\text{IR}}}}. \tag{3.14}$$

Using the notations of eq.(3.9) this definition reads

$$\sum_{i=0}^{m}\left[c_L^{(i)} - \sum_{n=0}^{m}\left(\frac{M_0}{4\pi F_\pi}\right)^{n-i}\left[r_a^{n,i} + r_M^{n,i}\left(16\pi^2 L + \log\frac{M_0}{\lambda}\right)\right]\right] \;\rightarrow\; \sum_{i=0}^{m} c^{(i)}_{L^{\overline{\text{IR}}}}(\lambda). \tag{3.15}$$

Let us explain the simple concept behind this rather scary formal definition:
In eq.(3.12) terms of any power i of m_π were absorbed into the counter-terms. This prescription takes advance of this possibility "in principle" that higher powers of m_π can be absorbed into counter-terms which appear at higher orders. However, we refrain from doing so since at a certain chiral order n only the counter-terms with $i \leq n$ are present. In eq.(3.14) the powers of m_π with $i = n$ are projected out of the regular part, ensuring that only those term are absorbed into a local operator which really do have a corresponding counter-term $c_L^{(n)}$. In eq.(3.14) this projection is done with the help of derivatives with respect to m_π. The sum over n in eq.(3.14) is necessary since the regular part of a contribution $O^{(n)}$ which goes like m_π^i with $i > n$ cannot be absorbed into a counter-term at order n but is absorbed at order i. Thus we find all regular contributions of a certain power i of the pion mass appearing at any chiral order $n < i$. The sum over n is necessary to absorb the power-counting violating terms of a contribution of order n into the counter-term of the lower order i.
In table 3.2 we give a short introduction to how a $\overline{\text{IR}}$ renormalization of a loop diagram can be performed in practice. To implement this renormalization scheme in a calculation one does not have to go through eq.(3.14) but can easily find the $\overline{\text{IR}}$ results via

$$O = O^{\text{loop}}_{\overline{\text{MS}}} + O^{\text{(c.t.)}}_{\overline{\text{MS}}} = \underbrace{O^{\text{loop}}_{\overline{\text{MS}}} + R^{\overline{\text{IR}}}\left(O^{\text{loop}}\right)}_{O^{\text{loop}}_{\overline{\text{IR}}}} + \underbrace{O^{\text{(c.t.)}}_{\overline{\text{MS}}} - R^{\overline{\text{IR}}}\left(O^{\text{loop}}\right)}_{O^{\text{(c.t.)}}_{\overline{\text{IR}}}} = O^{\text{loop}}_{\overline{\text{IR}}} + O^{\text{(c.t.)}}_{\overline{\text{IR}}}, \tag{3.16}$$

where $R^{\overline{\text{IR}}}$ has to be understood as the regular part in the sense of $\overline{\text{IR}}$ renormalization, i.e. expanded up to the power of the pion mass at which a corresponding counter-term is available. According to the above equation $\overline{\text{IR}}$ renormalized results can be calculated as the sum of the $\overline{\text{MS}}$ result plus the regular part $O^{\text{loop}}_{\overline{\text{IR}}} = O^{\text{loop}}_{\overline{\text{MS}}} + R^{\overline{\text{IR}}}\left(O^{\text{loop}}\right)$. The regular part can easily be determined with the help of the integrals given in appendix B. The integrals which we give in this appendix are written general enough to be applicable in theories with explicit Δ degrees of freedom, etc.
We note that apart from the different treatment of nucleon recoil effects, the same power-counting analysis can be performed in both HBChPT and $\overline{\text{IR}}$ renormalized covariant BChPT. Thus eq.(1.8) is suitable for a calculation of the chiral dimension of a particular Feynman diagram in both frameworks and both guarantee that diagrams with larger chiral dimension come with a higher power of a small parameter. The operators which are allowed in the Lagrangean and the possible topologies of Feynman diagrams are the same in both formulations of BChPT.
Finally we discuss an advantage of $\overline{\text{IR}}$ renormalization not explicitly named in the four conditions in the beginning of this section. Since in the $\overline{\text{IR}}$ scheme only a very finite number of terms is absorbed from the loop results, the analytic structure of the loop integrals is preserved. In particular, contributions from the pion-cloud are systematically reduced as the pion becomes heavier. In the following chapters we show that this feature is not only in accordance with naive expectations but can be observed on the lattice and is thus essential in a calculation of reliable chiral extrapolation functions. In standard IR renormalization this feature is spoiled by the subtraction of an infinite number of terms which appear to be nonanalytic. HBChPT results do also not show this property since the full loop functions are truncated in the nonrelativistic framework. The reduction of pion-cloud effects for large m_π, however, is analytically realized via an infinite string of $\left(\frac{m_\pi}{M_0}\right)^i$ terms, giving a strong argument for considering all of those contributions to be of the same chiral order.

3.3 An example: Quark Mass Dependence of the Nucleon Mass

3.3.1 Input Lagrangeans

Before we are going to demonstrate the basic properties of the renormalization scheme discussed above by applying it to a calculation of the nucleon self energy and subsequently a chiral extrapolation of lattice data for the mass of the nucleon, this section gives the relevant parts of the chiral Lagrangean needed for a calculation

HOW TO CALCULATE LOOP DIAGRAMS IN $\overline{\text{IR}}$ *- a practitioner's guide -*
1. Calculate all diagrams in $\overline{\text{MS}}$ as usual.
2. The infrared regular part of this result is found if all integrals H_{11} appearing in the $\overline{\text{MS}}$ result are replaced by R_{11} (and analogous for $H_{11}^{(i)}$, Δ_N and Δ_π, see appendix B).
3. The $\overline{\text{IR}}$ renormalized result is found, if the regular part expanded in the pion mass[a] up to the power at which a counter-term is available is added to the $\overline{\text{MS}}$ result.
[a] If the calculation does contain more than one small parameter, e.g. an additional small momentum transfer squared q^2, additional expansions in those small parameters have to be performed.

Table 3.2: The three steps which have to be performed in an $\overline{\text{IR}}$ calculation in practice. The connection between those steps and the definition of the renormalization scheme in eq.(3.14) is provided by eq.(3.16).

of this quantity in BChPT at next-to-leading one loop order, i.e. $\mathcal{O}(p^4)$.
The chiral Lagrangean written as a sum of terms with increasing chiral dimension is:

$$\mathcal{L}_{\text{eff}} = \mathcal{L}_{\pi\pi}^{(2)} + \mathcal{L}_{\pi N}^{(1)} + \mathcal{L}_{\pi N}^{(2)} + \mathcal{L}_{\pi N}^{(3)} + \mathcal{L}_{\pi N}^{(4)} + ... \tag{3.17}$$

The relevant terms for an evaluation of the nucleon self energy up to $\mathcal{O}(p^4)$ are (up to third order from [FMS98], fourth order from [FMMS00]):

$$\mathcal{L}_{\pi\pi}^{(2)} = \frac{F_\pi^2}{4}\left\langle u_\mu u^\mu + \chi_+\right\rangle, \tag{3.18}$$

$$\mathcal{L}_{\pi N}^{(1)} = \bar\Psi\left(i\not{D} - M_0 + \frac{g_A}{2}\not{u}\gamma_5\right)\Psi, \tag{3.19}$$

$$\mathcal{L}_{\pi N}^{(2)} = \bar\Psi\left[c_1\left\langle\chi_+\right\rangle - \frac{c_2}{4M_0^2}\left\langle u_\mu u_\nu\right\rangle\left(D^\mu D^\nu + h.c.\right) + \frac{c_3}{2}\left\langle u_\mu u^\mu\right\rangle\right]\Psi, \tag{3.20}$$

$$\mathcal{L}_{\pi N}^{(4)} = \bar\Psi\left[e_{38}\left\langle\chi_+\right\rangle^2 + \frac{e_{115}}{4}\left\langle\chi_+^2 - \chi_-^2\right\rangle - \frac{e_{116}}{4}\left(\left\langle\chi_-^2\right\rangle - \left\langle\chi_-\right\rangle^2 + \left\langle\chi_+^2\right\rangle - \left\langle\chi_+\right\rangle^2\right)\right]\Psi. \tag{3.21}$$

The quasi Goldstone boson pion triplet is collected in the SU(2) matrix valued field $U(x) = u^2(x)$ and is contained in the chiral vielbein $u_\mu = i\{u^\dagger, \nabla_\mu u\}$, the covariant derivative $D_\mu = \partial_\mu + \Gamma_\mu$ via the chiral connection $\Gamma_\mu = \frac{1}{2}[u^\dagger, \partial_\mu u]$ and the explicit chiral symmetry breaking term $\chi_\pm = u^\dagger\chi u^\dagger \pm u\chi^\dagger u$, for details see chapter 1. Here we use $\chi = 2B_0\mathcal{M}$ where $\mathcal{M} = \text{diag}(m_u, m_d)$ is the quark mass matrix and $B_0 = \frac{\langle\bar qq\rangle}{F_\pi^2}$ is the chiral condensate divided by the pion decay constant squared. Furthermore, $\langle ...\rangle$ denotes the trace in isospin space and M_0 and g_A are the mass- and the axial coupling of the nucleon in the chiral limit. Note that there are no terms of the third order Lagrangean contributing to our analysis of the mass of the nucleon.

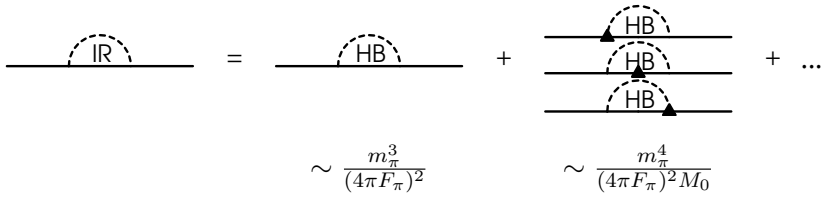

Figure 3.2: A comparison between the Feynman diagrams representing the leading one loop contribution to the nucleon self-energy in IR renormalized covariant BChPT and HBChPT. The triangles denote $\frac{1}{M_0}$ insertion which come from the $\mathcal{O}(p^2)$ Lagrangean of HBChPT. The presence of the diagrams containing those triangles demonstrates that in this scheme higher orders in $\frac{1}{M_0}$ are generated by Feynman diagrams of higher orders.

Figure 3.3: A sketch for the different treatment of the leading one loop diagram contributing to the nucleon self-energy in $\overline{\text{MS}}$- and IR renormalization. The sizes of all coefficients a_n are determined by the definition of the infrared regular part in eq.(3.8).

Figure 3.4: A sketch for the different treatment of the leading one loop diagram contributing to the nucleon self-energy in $\overline{\text{MS}}$- and $\overline{\text{IR}}$ renormalization. The sizes of all coefficients a_n are determined by the definition of the infrared regular part eq.(3.8). Note that in contrast to the sketch in figure 3.3 the sum in the right hand side of this figure is truncated at $i = m$. This displays the main difference between the IR and $\overline{\text{IR}}$ renormalization schemes. Since only the sum of loop diagrams plus local operators is observable – see figure 3.5 – the additional a_i terms can be absorbed via a redefinition of the counter-terms.

3.3.2 $\overline{\text{IR}}$ renormalized BChPT calculation of the leading pion-nucleon loop

In this section the general discussion which was given in section 3.2 for the arbitrary observable O of eq.(3.2) is repeated for the example of the mass of the nucleon $O = M_N$ at leading one loop order $m = 3$.
The full nucleon propagator has a simple pole which is shifted away from M_0 by means of the nucleon self energy $\Sigma(p)$. The location of this pole, the physical mass of the nucleon M_N, is the solution of the equation

$$\left[\not{p} - M_0 - \Sigma(\not{p})\right]_{\not{p}=M_N} \quad = \quad 0. \tag{3.22}$$

Figure 3.5 shows the Feynman diagrams contributing to the *perturbative* solution of this equation for M_N at leading one loop order. Diagram (a) contributes via an insertion from the $\mathcal{O}(p^2)$ Lagrangean leading to the tree level result:

$$M_N \quad = \quad M_0 - 4c_1 m_\pi^2 + \mathcal{O}(p^3). \tag{3.23}$$

Comparing this expression to the general discussion given above, these terms are the $M_{\text{c.t.}}^{(0)}$ and $M_{\text{c.t.}}^{(2)}$ of eq.(3.2). Diagram (b) of figure 3.5 represents the leading pion-nucleon loop from which $M_{\text{loop}}^{(3)}$ is calculated. Its result thus depends on the renormalization scheme applied in the calculation. Writing the outcome of a calculation of diagram (b) in terms of the basic integral of eq.(3.6) one finds [GSS88]:

$$M_{N\,\text{loop}}^{(3)} \quad = \quad \frac{3g_A^2}{2F_\pi^2} M_0 \left(m_\pi^2 H_{11} - \Delta_N\right), \tag{3.24}$$

where Δ_N denotes a loop integral over a single nucleon propagator, see appendix B.
Performing the nonrelativistic expansion of this integral, i.e replacing the nucleon momentum in the integral by $p^\mu = M_0 v^\mu + \mathcal{O}(\vec{p})$, one finds the HBChPT result for this diagram as the leading term of eq.(3.24) in $\frac{1}{M_0}$:

$$M_{N\,\text{loop}}^{(3.\text{HB})} \quad = \quad -\frac{3g_A^2 m_\pi^3}{32\pi F_\pi^2}, \tag{3.25}$$

whereas a $\overline{\text{MS}}$ evaluation of the same loop integrals leads to:

$$\begin{aligned} M_{N\,\text{loop}}^{(3.\overline{\text{MS}})} \quad = \quad & \frac{3g_A^2}{32\pi^2 F_\pi^2 M_0}\Bigg[- m_\pi^3 \sqrt{4M_0^2 - m_\pi^2}\, \arccos\left(\frac{m_\pi}{2M_0}\right) - m_\pi^4 \log\frac{m_\pi}{M_0} \\ & + m_\pi^2 M_0^2 - 2M_0^2\left(m_\pi^2 + M_0^2\right)\log\frac{M_0}{\lambda}\Bigg]. \end{aligned} \tag{3.26}$$

While the HBChPT result eq.(3.25) only contains the leading term in $\frac{1}{M_0}$ and relegates higher orders in $\frac{1}{M_0}$ to diagrams of higher orders, all orders of $\frac{1}{M_0}$ are present at a certain order in $\frac{1}{(4\pi F_\pi)}$ in covariant BChPT. HBChPT assigns the chiral dimension one to $\frac{m_\pi}{M_0}$ and such ties together the expansions in $\frac{1}{M_0}$ and $\frac{1}{(4\pi F_\pi)}$ (i.e. higher orders in $\frac{1}{M_0}$ appear at higher orders in $\frac{1}{4\pi F_\pi}$). Figure 3.2 gives a sketch for the correlation between the expansion in orders of the Feynman diagrams and in orders of $\frac{1}{M_0}$ in HBChPT.
In the $\overline{\text{MS}}$ result of eq.(3.26) the HBChPT result of eq.(3.25) is contained as the leading term of the $\arccos$ structure. Since this leading term occurs at an odd power of m_π, there are no counter-term contributions to this structure and the outcome in the $\overline{\text{MS}}$ scheme must reproduce the corresponding term in HBChPT exactly. Note that this is not ensured if the HBChPT result comes at an even power of the pion mass like e.g. in an $\mathcal{O}(p^4)$ calculation of the mass of the nucleon.
All contributions of the $\arccos$ structure beyond the leading one, as well as the $m_\pi^4 \log\frac{m_\pi}{M_0}$ term of eq.(3.26) are from the viewpoint of HBChPT of higher orders (orders in $\frac{1}{M_0}$) and appear as a consequence of the fact that the covariant formulation of BChPT resumms all orders in $\frac{1}{M_0}$ at a certain order in $\frac{1}{(4\pi F_\pi)}$. However,

due to the presence of positive powers of M_0 in the second row of eq.(3.26) the $\overline{\text{MS}}$ renormalized covariant result for $M_N^{(3.\text{loop})}$ contains terms which are of chiral orders p^2 and even p^0. Such, a Feynman diagram of order p^3 generated terms of lower orders. This example demonstrates that there is no consistent hierarchy of Feynman diagrams in the $\overline{\text{MS}}$ scheme [GSS88]; a diagram of – following the general power-counting formula of BChPT given in eq.(1.8) – arbitrary high order can contribute to an observable with unpredictable size. Contributions from higher order Feynman diagrams are numerically not suppressed. This technical problem of $\overline{\text{MS}}$ renormalized covariant BChPT can be remedied exploiting the following observation: The terms of the second row of eq.(3.26) which violate the power-counting are only observable together with the constants c_1 and M_0, as the full ChPT result for the mass of the nucleon is (in analogy to eq.(3.2))

$$M_N \quad = M_0 - 4c_1 m_\pi^2 + {M_N}_{\text{loop}}^{(3)} + \mathcal{O}(p^4). \tag{3.27}$$

To avoid the appearance of terms which violate power-counting and to ensure the equation

$${M_N}^{(n.\text{covariant})} \quad = \quad {M_N}^{(n.\text{HB})} + \mathcal{O}^{\text{HB}}(p^{n+1}), \tag{3.28}$$

where $\mathcal{O}^{\text{HB}}(p^4)$ denotes terms which are only in the framework of HBChPT considered to be of higher order but in covariant BChPT already appear at order p^3, for any chiral order n with the *same* definition of constants[4] in covariant and nonrelativistic BChPT, the authors of reference [BL99] introduced the IR scheme. In this scheme the integral H_{11} in eq.(3.24) is replaced by I_{11} as defined in eq.(3.8) while the infrared singular part of Δ_N equals zero. One finds:

$${M_N}_{\text{loop}}^{(3.\text{IR})} \quad = \quad \frac{3g_A^2}{32\pi^2 F_\pi^2 M_0}\left[- m_\pi^3 \sqrt{4M_0^2 - m_\pi^2}\,\arccos\left(\frac{-m_\pi}{2M_0}\right) + m_\pi^4\left(\frac{1}{2} - \log\frac{m_\pi}{\lambda}\right)\right]. \tag{3.29}$$

This equation now does not contain any positive powers of M_0, all terms are of order m_π^3 or higher and the lower order terms have been absorbed into the counter-terms. Comparing this result to eq.(3.26) we find an additional m_π^4 term which by construction [BL99] already at order p^3 in the covariant scheme gives the $\mathcal{O}(p^4)$ HBChPT contributions of the type[5] $\frac{1}{M_0}$. The second difference between eq.(3.26) and eq.(3.29) is the sign of the argument of the $\arccos$. In IR it is again designed to reproduce all HBChPT terms of the form $\frac{m_\pi^{i+1}}{(4\pi F_\pi)^2 M_0^i}$ for any i which in HBChPT would only appear at $\mathcal{O}^{\text{HB}}(p^i)$. The difference between the results of loop calculations in the $\overline{\text{MS}}$- and IR renormalization scheme is allowed since it only consists of even powers of the pion mass and such can "in principle" be absorbed into local operators. Figure 3.3 gives a sketch for the different treatment of the leading one loop diagram in $\overline{\text{MS}}$- and IR renormalized BChPT.
However, all three deficiencies of the IR scheme discussed in the previous section can be found in this example:

1. The only local operators present in $M_N^{(3)}$ are M_0 and c_1. All differences between the IR- and $\overline{\text{MS}}$ results beyond m_π^2 can only be absorbed "in principle", i.e strictly speaking at a higher order where the corresponding counter-term becomes available.

2. Eq.(3.29) contains a scale dependence (i.e. $m_\pi^4 \log\frac{m_\pi}{\lambda}$). However, there is no counter-term available at this order which could absorb this scale dependence and the final result for the physical observable M_N thus depends on the unphysical scale λ.

3. The $\arccos$ structure of eq.(3.29) diverges for $m_\pi \to 2M_0$ and becomes complex afterwards. The IR renormalized result for the mass of the nucleon such contains an unphysical singularity. However, for the example of the mass of the nucleon, this singularity becomes numerically relevant only for pion masses above 700 MeV, whereas it appears to play a more prominent role e.g. in the anomalous magnetic moment of the nucleon (see chapter 4).

[4] fulfilling this equation, ${M_N}^{(n.\text{covariant})}$ fulfills conditions 2. and 3. of the previous section.

[5] Note that the full $\mathcal{O}(p^4)$ HBChPT result can – and does – contain m_π^4 structures which are not of the $\frac{1}{M_0}$ type. These additional terms appear in the nonrelativistic theory as well as in the covariant framework at order p^4.

All three deficiencies arise due to the renormalization of terms which are of higher orders in $\frac{1}{M_0}$ and thus do have no corresponding counter-term. In the modified infrared scheme $\overline{\text{IR}}$ they are avoided by only applying the infrared renormalization technique to terms of low orders in $\frac{1}{M_0}$ for which corresponding counter-terms are available. Applying the general definition of the $\overline{\text{IR}}$ scheme eq.(3.14) to the example under discussion – the mass of the nucleon at order p^3 – the infrared regular pieces (see eq.(3.8)) are subtracted from the $\overline{\text{MS}}$ renormalized results up to $\frac{m_\pi^3}{(4\pi F_\pi)^2}$. Not only in this example but in general, this term is exactly of the same order in $\frac{1}{M_0}$ as the corresponding HBChPT result, see eq.(3.25). From this observation one finds the following general pattern in $\overline{\text{IR}}$ renormalization: At leading one loop level the regular parts have to be subtracted from the loop results up to order $\frac{1}{M_0^0}$, while at next-to-leading one loop order all regular parts up to $\frac{1}{M_0^1}$ have to be absorbed into the corresponding counter-terms.
In $\overline{\text{IR}}$ the mass of the nucleon at leading one loop order is renormalized via

$$\begin{aligned} M_0 - 4c_1 m_\pi^2 - R\left(M_N^{(3)}{}_{\text{loop}}\right)_{\mathcal{O}(m_\pi^3)} &= M_0 - 4c_1 m_\pi^2 + \frac{3g_A^2}{32\pi^2 F_\pi^2 M_0}\left[2M_0^4 \log\frac{M_0}{\lambda}\right. \\ &\quad \left. - M_0^2 m_\pi^2\left(1+\log\frac{M_0}{\lambda}\right)\right] \\ &\to M_0 - 4c_1 m_\pi^2. \end{aligned} \tag{3.30}$$

The leading one loop contribution to the mass of the nucleon in $\overline{\text{IR}}$ renormalized BChPT thus reads:

$$M_N^{(3.\overline{\text{IR}})}{}_{\text{loop}} = -\frac{3g_A^2}{32\pi^2 F_\pi^2}\left[m_\pi^3\sqrt{4M_0^2 - m_\pi^2}\arccos\left(\frac{m_\pi}{2M_0}\right) + m_\pi^4 \log\frac{m_\pi}{M_0}\right]. \tag{3.31}$$

It can easily be seen that up to order m_π^3 it coincides with the outcomes of the IR- and HBChPT framework while all terms beyond this order agree with the $\overline{\text{MS}}$ result. Figure 3.4 gives a sketch for the different treatment of the leading one loop diagram in $\overline{\text{MS}}$- and $\overline{\text{IR}}$ renormalization.
To further demonstrate the calculation in $\overline{\text{IR}}$, we proceed to a calculation of the mass of the nucleon at next-to-leading one loop order i.e. $\mathcal{O}(p^4)$. At this order one finds new counter-term contributions from $\mathcal{L}_{\pi N}^{(4)}$:

$$M_N^{(4)}{}_{\text{c.t.}} = 4e_1 m_\pi^4, \tag{3.32}$$

where we have introduced $e_1 = -\left(4e_{38} + \frac{1}{2}e_{115} + \frac{1}{2}e_{116}\right)$. At the same order there are contributions from loop diagrams (c) and (d) of figure 3.6 which after $\overline{\text{MS}}$ renormalization read:

$$\begin{aligned} M_N^{(4.\overline{\text{MS}})}{}_{\text{loop}} &= \frac{3c_1 g_A^2 m_\pi^7}{8\pi^2 F_\pi^2 M_0^2}\arccos\left(\frac{m_\pi}{2M_0}\right) + \frac{3m_\pi^2}{128\pi^2 F_\pi^2 M_0^2}\left[32c_1 g_A^2 M_0^4 + \left(16c_1 g_A^2 + c_2\right)m_\pi^2 M_0^2\right. \\ &\quad -4m_\pi^2\left[4c_1 g_A^2 m_\pi^2 + \left(-8c_1 + c_2 + 4c_3\right)M_0^2\right]\log\frac{m_\pi}{\lambda} \\ &\quad \left. +16c_1 g_A^2\left(m_\pi^2 + 3M_0^2 m_\pi^2 + 6M_0^4\right)\log\frac{M_0}{\lambda}\right]. \end{aligned} \tag{3.33}$$

The regular part of this result up to order m_π^4 – i.e. those pieces of the loop result which are absorbed into the corresponding counter-terms according to the $\overline{\text{IR}}$ prescription – reads:

$$\begin{aligned} -R\left(M_N^{(4)}{}_{\text{loop}}\right)_{\mathcal{O}(m_\pi^4)} &= \frac{3c_1 g_A^2 M_0^2 m_\pi^2}{4\pi^2 F_\pi^2}\left(1+\log\frac{M_0}{\lambda}\right) \\ &\quad -\frac{3g_A^2 m_\pi^4}{64\pi^2 F_\pi^2 M_0}\left[8c_1 M_0 + 3 + \left(24c_1 M_0 + 2\right)\log\frac{M_0}{\lambda}\right], \end{aligned} \tag{3.34}$$

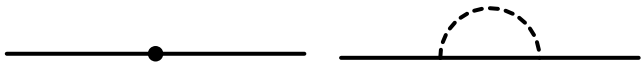

(a) (b)

Figure 3.5: The two Feynman diagrams contributing to the nucleon self-energy at leading one loop order. The solid line represents the propagating nucleon while the dashed line denotes a pion loop. The solid dot in diagram (a) is an insertion from the $\mathcal{O}(p^2)$ Lagrangean. At next-to-leading one loop order an insertion from the $\mathcal{O}(p^4)$ Lagrangean contributes through the very same diagram.

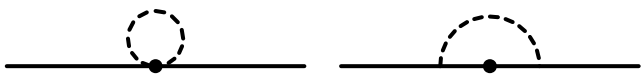

(c) (d)

Figure 3.6: The two next-to-leading one loop order diagrams contributing to the nucleon self energy. The solid dots denote insertions from the Lagrangean $\mathcal{L}^{(2)}_{\pi N}$.

where the regular part of diagram (c) is of course zero since it does not contain a nucleon propagator in the loop. Since at order p^4 the regular parts of $M_{N\,\mathrm{loop}}$ have to be absorbed into the counter-terms up to m_π^4 according to the $\overline{\mathrm{IR}}$ prescription, there is an additional contribution from the $\mathcal{O}(p^3)$ diagram (b) of figure 3.5 which at order p^4 is absorbed into e_1:

$$R\left(M_{N\,\mathrm{loop}}^{(3)}\right)_{\mathcal{O}(m_\pi^4)} = R\left(M_{N\,\mathrm{loop}}^{(3)}\right)_{\mathcal{O}(m_\pi^3)} + \frac{3g_A^2 m_\pi^4}{64\pi^2 F_\pi^2 M_0}\left(3 + 2\log\frac{M_0}{\lambda}\right). \tag{3.35}$$

The $\overline{\mathrm{IR}}$ renormalization prescription for the mass of the nucleon at this order is

$$M_0 - 4c_1 m_\pi^2 + 4e_1^r(\lambda) m_\pi^4 - R\left(M_{N\,\mathrm{loop}}^{(3)} + M_{N\,\mathrm{loop}}^{(4)}\right)\Big|_{\mathcal{O}(m_\pi^4)} \rightarrow M_0 - 4c_1 m_\pi^2 + 4e_1^r(\lambda) m_\pi^4, \tag{3.36}$$

where $|_{\mathcal{O}(m_\pi^4)}$ denotes all contributions of the regular part up to m_π^4.

3.3.3 Application of the modified renormalization scheme to a chiral extrapolation of the mass of the nucleon

Summarizing the previous section, the $\mathcal{O}(p^4)$ $\overline{\mathrm{IR}}$ renormalized BChPT result for the mass of the nucleon is

$$\begin{aligned} M_N(m_\pi) &= M_0 - 4c_1 m_\pi^2 + \frac{3g_A^2 m_\pi^3}{32\pi^2 F_\pi^2 \sqrt{4 - \frac{m_\pi^2}{M_0^2}}}\left(-4 + \frac{m_\pi^2}{M_0^2} + 4c_1\frac{m_\pi^4}{M_0^3}\right)\arccos\left(\frac{m_\pi}{2M_0}\right) \\ &\quad + 4e_1^r(\lambda) m_\pi^4 - \frac{3m_\pi^4}{128\pi^2 F_\pi^2}\left[\left(\frac{6g_A^2}{M_0} - c_2\right) + 4\left(\frac{g_A^2}{M_0} - 8c_1 + c_2 + 4c_3\right)\log\left(\frac{m_\pi}{\lambda}\right)\right] \\ &\quad - \frac{3c_1 g_A^2 m_\pi^6}{8\pi^2 F_\pi^2 M_0^2}\log\frac{m_\pi}{M_0} + \mathcal{O}(p^5). \end{aligned} \tag{3.37}$$

The coupling constants occurring in this formula are described in detail in references [PHW04, AK$^+$04, BHM05, PMW$^+$06]. We now apply this formula for chiral extrapolation of lattice data from reference [AK$^+$04]. Our approach is to extract the coupling constants appearing in the chiral extrapolation function eq.(3.37) from the quark mass dependence of the lattice results and to subsequently give a prediction for the physical value of this observable from the combined lattice plus ChPT analysis. Therefore, we perform a fit with three parameters

(M_0, c_1 and $e_1^r(\lambda)$)[6] to seven lattice points for the mass of the nucleon below $m_\pi = 750$ MeV. Figure 3.7 shows the resulting best fit curve with the physical point included in the fit. The resulting values for the fit parameters are given in table 3.4. In the same figure the $\mathcal{O}(p^3)$ result with the same values for the parameters is shown indicating a very good convergence pattern for this observable in $\overline{\text{IR}}$ renormalized BChPT. For the mass of the nucleon at order p^4 the string of $(m_\pi/M_0)^i$ terms and thus the difference between the standard IR- and $\overline{\text{IR}}$ result becomes numerically relevant only for pion masses above 700 MeV. The values given in table 3.4 as well as the solid curve in figure 3.7 are therefore well consistent with the analyses of references [PHW04, PMW$^+$06] where the $\mathcal{O}(p^4)$ IR renormalized result truncated at order $\frac{m_\pi^5}{(4\pi F_\pi^2)M_0^2}$ was utilized to chirally extrapolate lattice data.

Figure 3.8 shows the $\mathcal{O}(p^4)$ result eq.(3.37) fitted to lattice data only and allows the conclusion that lattice simulations together with BChPT lead to a very reasonable prediction for the physical value of this observable with small systematic and statistical errors (together they are on the 10% level). Not including the physical point we arrive at values for the parameters which are even within statistical errors only well compatible with the ones found in a fit including the physical point, see table 3.4.

We have estimated the systematic uncertainties which arise due to the fact that higher order effects have been neglected as follows: The leading term beyond the chiral order of our analysis is of the form

$$\mathcal{O}(p^5) \quad = \quad \delta_{M_N}^{(5)} \frac{m_\pi^5}{(4\pi F_\pi)^4}. \tag{3.38}$$

The size of the coupling constant $\delta_{M_N}^{(5)}$ would be determined by a $\mathcal{O}(p^5)$ calculation, at the present stage we estimate the size of higher order effects by varying this coupling within natural size, i.e. $-3 < \delta_{M_N}^{(5)} < 3$ and perform the fit to lattice data again. The grey shaded band in figure 3.8 is the area covered by the array of curves resulting from those fits plus statistical errors. For the analyses of statistical errors we rely on the methods described in references [PMW$^+$06] and [Mus05] throughout this work. Note that neither the analysis of the convergence pattern in figure 3.7 nor the estimate of possible higher order effects in figure 3.8 signal a breakdown of our $\mathcal{O}(p^4)$ covariant BChPT results below $m_\pi = 700$ MeV. Thus the application of this result to lattice data at large quark masses clearly seems to be justified.

Finally we comment on two analyses which are concerned with the convergence of the chiral series. The first one has been worked out in references [MB99] and [MB06] where a complete order p^5 analysis of the mass of the nucleon was presented in the framework of HBChPT and the final conclusion was drawn that the chiral series for $M_N(m_\pi)$ breaks down at rather small pion masses if one includes $\mathcal{O}(p^5)$ effects. In the nonrelativistic analysis of reference [MB99] it was found that – apart from recoil corrections which are already present in our covariant results at order p^4 – the only contributions to the mass of the nucleon appearing at order p^5 enter the result by replacing the coupling constants of the $\mathcal{O}(p^3)$ structures (i.e. g_A and F_π) by pion mass dependent functions ($g_A(m_\pi)$ and $F_\pi(m_\pi)$) and include the leading correction to the GOR-relation for $m_\pi(m_q)$. Note that the absence of characteristic p^5 effects in HBChPT does not imply the absence of those effects in a covariant p^5 analysis [SDGS07a, SDGS07b]. Since we cannot rule out such nonzero contributions we do not give a covariant $\mathcal{O}(p^5)$ analysis based in the findings of reference [MB99].

In our opinion the breakdown of the chiral expansion for $M_N(m_\pi)$ diagnosed in reference [MB06] does appear as a consequence of two effects:

1. In the nonrelativistic theory only terms up to a certain power of the pion mass are included. In an $\mathcal{O}(p^5)$ analysis of the mass of the nucleon the highest power of the pion mass appearing in the HBChPT result is m_π^5. Thus, there is always a highest power of the pion mass which from a certain value of m_π on dominates the HBChPT formulae and drives the results to $\pm\infty$. In contrast the $\overline{\text{IR}}$ renormalized covariant

[6] Since the data basis underlying our analyses is not sufficient to determine all appearing low energy constants from the observables discussed in this work, we decide to take values for all those constants from literature which enter our results solely as couplings constants in loop diagrams (i.e. only chiral limit values and the strength of all appearing contact interactions are fitted). The values which we are using as input throughout this work can found in table 3.3.

BChPT results typically contain these terms plus higher $\left(\frac{m_\pi}{M_0}\right)^i$ corrections in the $\arccos$ structure which is a flat function of m_π.

2. Calculating the mass of the nucleon at order p^5 one only picks up the leading quark mass dependencies of g_A, F_π and m_π which are known to be far off the observed quark mass dependencies for pion masses above the physical one (see e.g. [HPW03] and [Lus06]). Obviously the quark mass dependence of the mass of the nucleon can only be described properly by a chiral analysis if the appearing vertex functions do have a realistic quark mass dependence.

We have checked that if we use realistic quark mass dependencies for $g_A(m_\pi)$, $F_\pi(m_\pi)$ and $m_\pi(m_q)$ in our covariant BChPT results for $M_N(m_\pi)$, we arrive at best-fit curves which agree very well with the ones presented in figures 3.7 and 3.8. Following the procedure described here, a breakdown of the chiral expansion for M_N at order p^5 could not be confirmed. Going from $\mathcal{O}(p^4)$ to $\mathcal{O}(p^5)$ we only found some uncertainty[7] in the numerical determination of the counter-term $e_1^r(\lambda)$. In general, we propose to use realistic functions of the quark mass wherever the contributing couplings acquire a quark mass dependence (this is e.g. be done for the corrections to the mass of the nucleon M_0 appearing in the next section). A successful description of quark mass dependencies above the physical point is of course not possible in ChPT if leading order quark mass dependencies for the appearing couplings are used which are known to be far off their physical behaviour at larger quark masses.
We note that the argument given in the above point 1. frequently leads to unsatisfactory quark mass dependencies at large quark masses (i.e. in the domain of presently available lattice data) if results of the nonrelativistic theory are analysed. However, systematic calculations at higher order in the covariant framework would be necessary in order to ultimately test the convergence properties of the chiral series for the mass of the nucleon. A first step on this way was achieved in references [SDGS07a, SDGS07b] where the order p^6 terms which contribute to the mass of the nucleon proportional to m_π^6 were calculated. The presence of a large number of so far undetermined low energy constants in these structures, regrettably, make a detailed numerical analysis of these higher order contributions impossible at presence.
Another critical analysis of the convergence properties of BChPT was given in reference [PMHW07]. In this reference the systematic differences between nonrelativistic ChPT calculations with- or without explicit Δ degrees of freedom were discussed on the example of the axial coupling of the nucleon g_A at leading one loop order. The main conclusions of this analysis were that an interpolation between presently available lattice data for g_A and its physical value based on ChPT at one loop level is only possible if Δ degrees of freedom are included explicitly and that expanding the leading one loop Δ contributions to g_A in powers of m_π around the chiral limit, i.e.matching them to the theory without explicit Δ, one ends up with an asymptotic series if $m_\pi \geq \Delta_0 = M_\Delta - M_0 \lesssim 300$ MeV. Thus, truncating the series at higher and higher powers of the pion mass, i.e at higher and higher chiral orders of the theory without explicit Δ, one does not find a better description of the approximated function but in contrast is faced with uncontrollable deviations. This finding of reference [PMHW07] can even be generalized: An asymptotic series for $m_\pi \geq \Delta_0$ cannot only be found by an expansion of the leading one loop order SSE[8] result for g_A but for any observable calculated within this framework at one loop level since it is a feature of the basic $\pi\Delta$ loop function in the nonrelativistic (see eq.(2.31) and eq.(A.6)) as well as the covariant ($H_{11}(M_\Delta, M_0, m_\pi)$, see appendix B.1) formulation of the theory. Consequently, the available one loop order SSE results for the mass of the nucleon [BHM05], its anomalous magnetic moment [HW02], the slopes of the nucleon form factors [G$^+$05] and the quark contribution to the total spin of the nucleon [CJ02] all lead to an asymptotic series for $m_\pi \geq \Delta_0$ when expanded in powers of m_π around the chiral limit. At the same time, however, the covariant $\mathcal{O}(p^4)$ BChPT results calculated without explicit Δ are flat functions which are in good agreement with lattice data for all those observables even if $m_\pi \geq \Delta_0$ and comparing $\mathcal{O}(p^3)$ with $\mathcal{O}(p^4)$ results we constantly see a clear convergence towards the lattice data over a large

[7] The numbers which we give for the low energy constants in this work – in particular for those constants which only appear at the highest included order – can always be polluted by higher order effects and must therefore only be considered to be rough estimates.

[8] SSE: small scale expansion, a formulation of ChPT with explicit Δ degrees of freedom, see chapters 1 and 2.

g_A	F_π [GeV]	c_2 [GeV^{-1}]	c_3 [GeV^{-1}]	c_4 [GeV^{-1}]
1.2	0.0924	3.2	-3.4	3.6

Table 3.3: Input values used in this chapter for the numerical analyses.

input	M_0 [GeV]	c_1 [GeV^{-1}]	$e_1^r(1\text{GeV})$ [GeV^{-3}]
lattice+phen.	0.889 ± 0.001	-0.815 ± 0.004	1.46 ± 0.01
lattice	0.862 ± 0.04	-0.834 ± 0.03	1.46 ± 0.02

Table 3.4: The values for the parameters M_0, c_1 and $e_1^r(\lambda)$ as extracted in two different fits. The given uncertainties display statistical errors.

range of pion masses and no signal of a breakdown around $m_\pi \approx \Delta_0$. Furthermore, in the final result for an observable, the m_π^i terms resulting from the expansion of the leading $\pi\Delta$ loop are only observable together with a vast number of other structures, see eqs.(3.1) and (3.2). Whether or not the chiral expansion of a result calculated in a theory without Δ inevitably becomes an asymptotic expansion above $m_\pi = \Delta_0$ can therefore not be concluded from the features of the basic $\pi\Delta$ loop. However, we cannot rule out the possibility that the $\mathcal{O}(p^3)$ and $\mathcal{O}(p^4)$ BChPT results presented in this work are low order terms of an asymptotic series and that higher order contributions destroy the good agreement between BChPT and lattice results which we find in our analyses. If this scenario were true, the conclusion form this work would be that covariant BChPT at orders p^3 and p^4 provides a very reasonable approximation of the full result, which then, regrettably, cannot be improved systematically by going to higher orders. Turning back to the example of g_A, however, we have to admit that the weak dependence on the pion mass which is found for this observable on the lattice is in ChPT realized via a cancellation between large contributions from πN- and $\pi\Delta$ loops. We do therefore not expect covariant BChPT without explicit Δ to lead to a very good description of the pion mass dependence of g_A.

3.4 Concluding Remarks

In this chapter we have introduced a new renormalization scheme. This scheme fulfills all necessary conditions which we request to be fulfilled by a consistent renormalization procedure in an effective field theory:

- It allows for a cancellation of all appearing UV-divergences and leads to strictly renormalization scale independent results.
- The results calculated in this scheme follow a consistent hierarchy of terms: The contributions from a certain Feynman diagram are expected to be more and more suppressed, the higher the chiral order of this diagram is. Diagrams of higher order are guaranteed to contribute with a higher power of a small parameter.

Beyond these very basic conditions, the renormalization program discussed in this chapter has further advantages:

- The low energy constants in this scheme are defined in exactly the same way as in HBChPT (and IR renormalized BChPT). Informations on the couplings which have been found in this theory can be used as input in an $\overline{\text{IR}}$ renormalized calculation. A truncation of a such renormalized covariant BChPT result at the proper power in $1/M_0$ always leads to the corresponding HBChPT result.
- In contrast to standard IR, $\overline{\text{IR}}$ renormalized BChPT calculations do not lead to unphysical cuts, singularities or imaginary parts in the results. Furthermore, effects from pion-nucleon loops are systematically reduced in the limit of large pion masses. This second feature is not found in the results of IR renormalized BChPT nor in HBChPT, although it is a necessary condition in order to obtain realistic quark

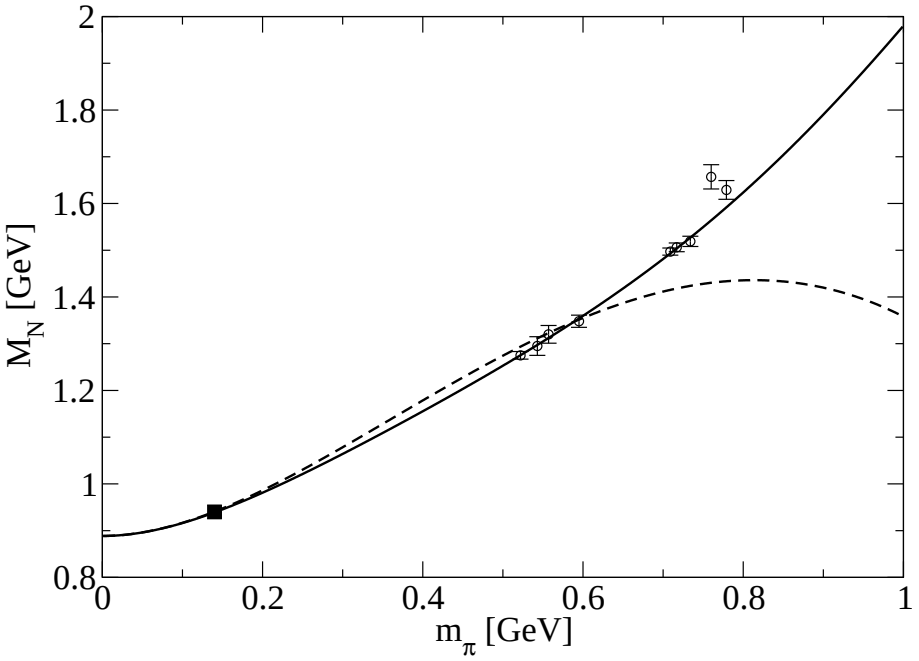

Figure 3.7: The mass of the nucleon as a function of the pion mass. Full line: best fit of the $\mathcal{O}(p^4)$ $\overline{\text{IR}}$ BChPT result to the physical point and the seven lowest lying lattice points; dashed line: $\mathcal{O}(p^3)$ result with the same values for the parameters. The shown lattice data are taken from reference [AK$^+$04]; the black box is the physical point [Y$^+$06].

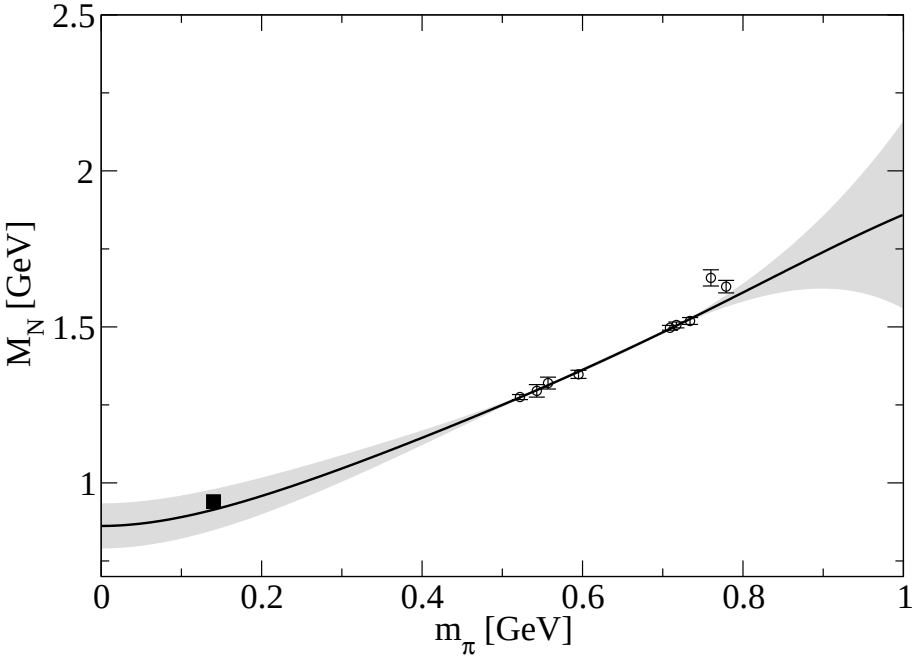

Figure 3.8: The mass of the nucleon as a function of the pion mass. Full line: best fit of the $\mathcal{O}(p^4)$ $\overline{\text{IR}}$ renormalized BChPT result to the seven lowest lying lattice points without the physical point. The grey shaded band indicates the size of statistical plus systematic errors for this fit. The shown lattice data are taken from reference [AK$^+$04].

mass dependencies for pion masses above the physical one and thus for chiral extrapolations of recently available lattice data.

All those properties are *by construction* guaranteed in an $\overline{\text{IR}}$ renormalized BChPT calculation. This was strictly proven in section 3.2 and appendix B.3.
A framed box included in this chapter gives the steps which have to be performed in order to arrive at $\overline{\text{IR}}$ renormalized results. The three steps given there show that the implementation of this scheme for any observable is straightforward and relies on well established calculational techniques. Furthermore, we emphasize that where $\overline{\text{MS}}$ results are already available, the $\overline{\text{IR}}$ result is just a very small step away. All input necessary for this modification can be found in the appendices of this work.
In the second part of this chapter, we presented leading one loop order calculations of the mass of the nucleon in HBChPT, $\overline{\text{MS}}$-, IR- and $\overline{\text{IR}}$ renormalized BChPT, displaying the above discussed properties of $\overline{\text{IR}}$ on a simple example. Furthermore, the next-to-leading one loop order contributions were calculated utilizing the newly defined renormalization prescription. This analysis finally allowed for a successful chiral extrapolation of lattice data for $M_N(m_\pi)$ to the chiral limit. For this chiral extrapolation function, we gave a detailed analysis of systematic and statistical uncertainties as well as an examination of the convergence pattern of the chiral series. A fast convergence as well as a reasonable prediction of the physical value with small errors ($\sim 10\%$) was found. We note that for this first, simple example the $\overline{\text{IR}}$ procedure is not necessary in order to arrive at a satisfying chiral extrapolation function. However, for none of the observables which are studied in the following chapters any of the other ChPT frameworks discussed can give a reasonable description of their quark mass dependencies above the physical pion mass at the one loop order. This observation does not come as a surprise but is expected from many arguments given throughout this chapter (in particular only $\overline{\text{IR}}$ renormalized results are flat, analytic functions of the quark mass where contributions from dynamical pions get weaker as their masses increase). Therefore we are now continuing this work with the first $\overline{\text{IR}}$ calculations of the nucleon form factors (at next-to-leading one loop order) and the generalized nucleon form factors (at leading one loop order). An analysis of our results always includes an examination of its quark mass dependence and systematic errors of the BChPT calculation due to possible higher order effects are always studied in exactly the same way as for the mass of the nucleon in this chapter, see eq.(3.38). The values which we found for the low energy constants in this chapter – see tables 3.3 and 3.4 – are used as input for our studies of nucleon form factors in the following chapters.

Chapter 4

The vector Form Factors of the Nucleon

4.1 Introduction

In this chapter we discuss the isovector- and isoscalar vector form factors of the nucleon. Our analysis is based on a next-to-leading one loop order calculation of these form factors using the methods of $\overline{\text{IR}}$ renormalized covariant BChPT. We analyse both the momentum transfer- and quark mass dependence of the form factors and compare our findings to phenomenology and lattice simulations.
The study of nucleon form factors with the methods of ChPT has a long history: First attempts were made in reference [GSS88] for the case of two active quark flavours and in reference [Kra90] also including strangeness contributions. In those references leading one loop order calculations were presented using $\overline{\text{MS}}$ renormalized covariant BChPT. However, the absence of a consistent power-counting prescription in the $\overline{\text{MS}}$ scheme was revealed by those calculations and hence, throughout the 1990's, chiral analyses of nucleon form factors were only performed using the nonrelativistic formulation of BChPT. Those nonrelativistic studies include calculations with explicit Δ degrees of freedom at the leading one loop level [BFHM98] and in HBChPT with πN degrees of freedom only even at two loop order [Kai03]. After it was shown in reference [BL99] that a consistent power-counting can be implemented in the covariant version of BChPT, next-to-leading one loop order calculations of the nucleon form factors were performed in the IR [KM01] and EOMS [FGS04] renormalization schemes.
Recently, chiral analyses of nucleon form factors have seen renewed interest in the context of chiral extrapolations: Present day lattice simulations [G$^+$05, AKNT06] are performed at quark masses much larger than the physical one and in order to make contact between those theoretical attempts and data from experiments an extrapolation prescription is needed. ChPT provides such an extrapolation prescription since quantities calculated in this theory typically depend on the pion mass which, in turn, can be directly linked to the quark mass. The extrapolation of lattice data for the form factors of the nucleon to the chiral limit is one of the main focuses of this chapter. While chiral extrapolations of the anomalous magnetic moment have been pioneered in reference [HW02] and the possibility of chiral extrapolations for the slopes of the nucleon form factors has been studied in references [G$^+$05, AKNT06], the methods applied in this work allow for the first successful chiral extrapolation of the full isovector form factors.
This chapter is organized as follows: After a brief discussion of the vector current of the nucleon, we give the basic ingredients for our BChPT calculation in section 4.3. The outcomes of the next-to-leading one loop order BChPT analysis for the isovector anomalous magnetic moment and the slopes of the isovector form factors are given in sections 4.4.1 and 4.4.2 while the accordant expressions in the isoscalar sector are given in sections 4.5.1 and 4.5.2. Numerical discussions of our results are given in section 4.4.3 where the Q^2 dependence of the isovector Sachs form factors is discussed and in sections 4.6.1 and 4.6.2 where chiral extrapolations of both lattice data which have been extrapolated to the forward limit using a dipole ansatz and lattice data at finite Q^2 directly are presented. A summary section closes this chapter while the lengthy expressions for the vector amplitudes and the full pion mass- and momentum transfer dependent functions for the form factors are given in appendix C.

g_A	F_π [GeV]	M_0 [GeV]	c_1 [GeV^{-1}]	c_2 [GeV^{-1}]	c_3 [GeV^{-1}]	c_4 [GeV^{-1}]	e_1^r(1GeV) [GeV^{-3}]
1.2	0.0924	0.889	-0.817	3.2	-3.4	3.6	1.44

Table 4.1: Input values used in this chapter for the numerical analysis of the the nucleon form factors.

For a review on the status of the determination of the nucleon form factors in experiments see reference [dJ06].

4.2 The Form Factors of the Nucleon

The vector current of a $J^P = \frac{1}{2}^+$ baryon contains two independent form factors, in covariant Dirac notation typically denoted as "Dirac" $F_1(q^2)$ and "Pauli" $F_2(q^2)$ form factors:

$$\left\langle N \left| V_\mu^a \right| N \right\rangle \;=\; \bar{u}_N(p_2) \left[F_1(q^2)\gamma_\mu + i\frac{F_2(q^2)}{2M^{(n)}}\sigma_{\mu\nu}q^\nu \right] \frac{T^a}{2} u_N(p_1), \tag{4.1}$$

with the four-momentum transfer

$$q \;=\; p_2 - p_1. \tag{4.2}$$

and the quark current

$$V_\mu^a \;=\; \bar{q}\gamma_\mu T^a q, \tag{4.3}$$

where $T^a = (\mathbb{1}, \vec{\tau})$ is an operator in isospin space; $a = 0$ corresponds to the isoscalar- and $a = 1, 2, 3$ to the isovector current. $M^{(n)}$ is a normalizing mass prefactor introduced in order to arrive at a dimensionless Pauli form factor. Throughout this chapter, we either identify it with $M^{(n)} = M_N^{\text{phys}}$ (and call the corresponding Pauli form factor *normalized*) or we identify $M^{(n)} = M_N(m_\pi)$ (and call the corresponding Pauli form factor *unnormalized*). For the quark mass dependence of the mass of the nucleon we employ the findings of chapter 3 where it was analysed at next-to-leading one loop order in covariant BChPT:

$$\begin{aligned} M_N(m_\pi) \;=\;& M_0 - 4c_1 m_\pi^2 + \frac{3g_A^2 m_\pi^3}{8\pi^2 F_\pi^2 \sqrt{4 - \frac{m_\pi^2}{M_0^2}}} \left(-1 + \frac{m_\pi^2}{4M_0^2} + c_1 \frac{m_\pi^4}{M_0^3} \right) \arccos\left(\frac{m_\pi}{2M_0} \right) \\ & + 4e_1^r(\lambda) m_\pi^4 - \frac{3m_\pi^4}{128\pi^2 F_\pi^2} \left[\left(\frac{6g_A^2}{M_0} - c_2 \right) + 4 \left(\frac{g_A^2}{M_0} - 8c_1 + c_2 + 4c_3 \right) \log\left(\frac{m_\pi}{\lambda} \right) \right] \\ & - \frac{3c_1 g_A^2 m_\pi^6}{8\pi^2 F_\pi^2 M_0^2} \log \frac{m_\pi}{M_0} + \mathcal{O}(p^5). \end{aligned} \tag{4.4}$$

The numerical values which we use for the low energy constants appearing in this formula can be found in table 4.1.
Our strategy in this chapter is to evaluate the left hand side of eq.(4.1) in the effective field theory framework with an arbitrary vector source v_μ coupling to this current. We therefore briefly review the necessary ingredients for the field theoretical calculation in the next section.

4.3 Formalism

4.3.1 The form factors of the nucleon at next-to-leading one loop order

We start from the general power-counting formula of Baryon ChPT:

$$D \;=\; 2N_L + 1 + \sum_d (d-2) N_d^M + \sum_d (d-1) N_d^{MB}. \tag{4.5}$$

D denotes the chiral dimension p^D of a particular Feynman diagram, N_L counts the number of loops in the diagram, whereas the variables $N_d^{M,\,MB}$ count the number of vertices of chiral dimension d from the pion (M) and pion-nucleon (MB) Lagrangeans. We emphasize again that the $\overline{\text{IR}}$ renormalization program developed and applied in this work guarantees that diagrams with larger chiral dimension are numerically suppressed.
In this chapter we discuss the vector form factors of the nucleon up to next-to-leading ($N_2^{MB}=1$) one loop ($N_L=1$) order in covariant BChPT. This corresponds to the power of $p^{D=4}$ in the perturbative expansion of Baryon ChPT. To leading order $D=1$ we only have the tree level contributions from the p^1 nucleon Lagrangean of eq.(4.10) with $N_L=0,\ N_2^M=0$ and $N_1^{MB}=1$. This term only gives rise to the contributions $F_1^{(v,s)}(q^2)=1+\mathcal{O}(p^2)$ and $F_2^{(v,s)}(q^2)=0+\mathcal{O}(p^2)$. At next-to-leading order $D=2$ we find an additional tree level contribution from the p^2 Lagrangean of eq.(4.13) with $N_L=0,\ N_2^M=0$ and $N_2^{MB}=1$ leading to the results $F_2^{(v)}(q^2)=\frac{M^{(n)}}{M_0}c_6+\mathcal{O}(p^3)$ and $F_2^{(s)}(q^2)=\frac{M^{(n)}}{M_0}\left(c_6+2c_7\right)+\mathcal{O}(p^3)$.
The first contributions from the pion-cloud enter at $D=3$ with $N_L=1$ and arbitrary values for N_1^{MB} and N_2^M. However, the $N_L=1$ topology only allows diagrams with $(N_1^{MB},N_2^M)\in\{(3,0),(2,1),(2,0),(1,1),(1,0)\}$. The corresponding diagrams are shown in fig.4.1 (a)-(f). In addition, there are loop corrections from the nucleon Z-factor (given in appendix D.2) which at this order only contributes by ensuring charge conservation $F_1^{(s,v)}(q^2=0)=1$, both in the isoscalar- and in the isovector channel. Note that there is an additional possibility of obtaining $D=3$ contributions via $N_L=0,\ N_2^M=0$ and $N_3^{MB}=1$, corresponding to short distance contributions to $F_1^{(v,s)}(q^2)$ which are linear in q^2, see subsection 4.3.3.
In this work we study the nucleon form factors up to next-to-leading one loop order, i.e. up to $D=4$. Aside from the $D=4$ tree level contributions with $N_L=0,\ N_2^M=0$ and $N_4^{MB}=1$ (which contribute proportional to m_π^2 and q^2 to $F_2^{(v,s)}(q^2)$) one encounters loop diagrams with $D=4$ via $N_L=1,\ N_2^{MB}=1$ and possible additional vertices of N_2^M and N_1^{MB} (which again only appear in the combinations given above), the corresponding diagrams are shown in fig. 4.2 (g)-(o). Diagram (o) in this figure represents contributions from the $\mathcal{O}(p^3)$ Z-factor together with coupling constants from the order p^2 Lagrangean, i.e. contributions to $F_2^{(v,s)}(0)$. The additional order p^4 part of the Z-factor again only contributes by ensuring $F_1^{(v,s)}(0)=1$ in the sum of all Feynman diagrams.
The $D=4$ diagrams (j), (k), (l), (m) and (n) of figure 4.2 contribute with pion mass dependent c_1 insertions on the nucleon propagators. The sum of those diagrams plus the $\mathcal{O}(p^3)$ diagrams of the same topology (i.e. the $N_d^{MB}>1$ diagrams: (a), (b), (c) and (d) of figure (4.1)) is just the result of the latter one with the mass of the nucleon M_0 shifted to $M_0-4c_1m_\pi^2$. Strictly speaking, one only finds the leading term of a Taylor series of the $\mathcal{O}(p^3)$ amplitudes around M_0, e.g. $Amp^d+Amp^j=\left(1-4c_1m_\pi^2\frac{\partial}{\partial M_0}\right)Amp^d$. However, we aim to apply our results to chiral extrapolations of lattice data for the nucleon form factors and thus abstain from such a perturbative inclusion of the nucleon mass function since the leading behaviour $M_N=M_0-4c_1m_\pi^2$ is known to only provide a reasonable description of the true quark mass dependence up to the physical pion mass. The perturbative treatment of those effects is therefore bound to spoil the quark mass dependence of the strict $\mathcal{O}(p^4)$ BChPT results for the form factors of the nucleon. In order to overcome this, we account for diagrams (j), (k), (l), (m) and (n) of figure 4.2 by assigning a realistic quark mass dependence to the mass of the nucleon appearing in the corresponding $\mathcal{O}(p^3)$ diagrams. In particular, we choose to use the next-to-leading one loop order result for the mass of the nucleon found in chapter 3, see eq.(4.4). Formally, this corresponds to a resummation of all one loop diagrams with reducible (in the sense that they can be absorbed into the mass of the nucleon) insertions on the nucleon propagators where diagrams (j), (k), (l), (m) and (n) of figure 4.2 are only the very leading contributions. Resuming the discussion of section 3.3.3, we note that a successful chiral extrapolation curve cannot be found in a calculation relying on vertex functions and propagators which are known to not display the correct quark mass dependence up the the quark masses at which one aims to apply the results. We therefore always recommend to follow our example and perform resummations for those vertex functions and propagators.

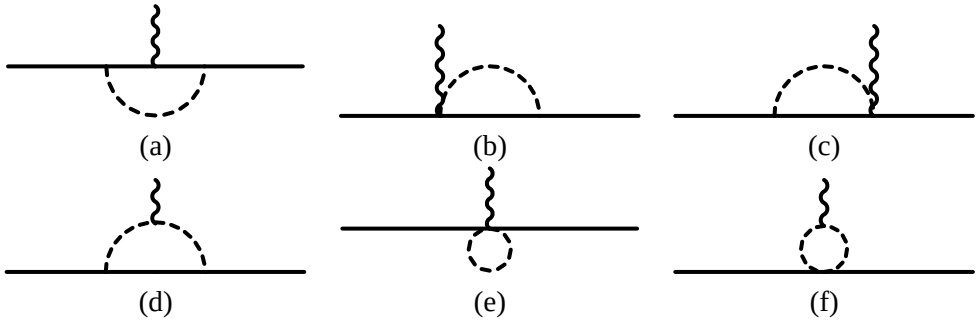

Figure 4.1: The loop diagrams contributing to the nucleon form factors at order p^3. The solid lines denote the propagating nucleon, dashes lines represent pions and the wiggly line is the incoming photon.

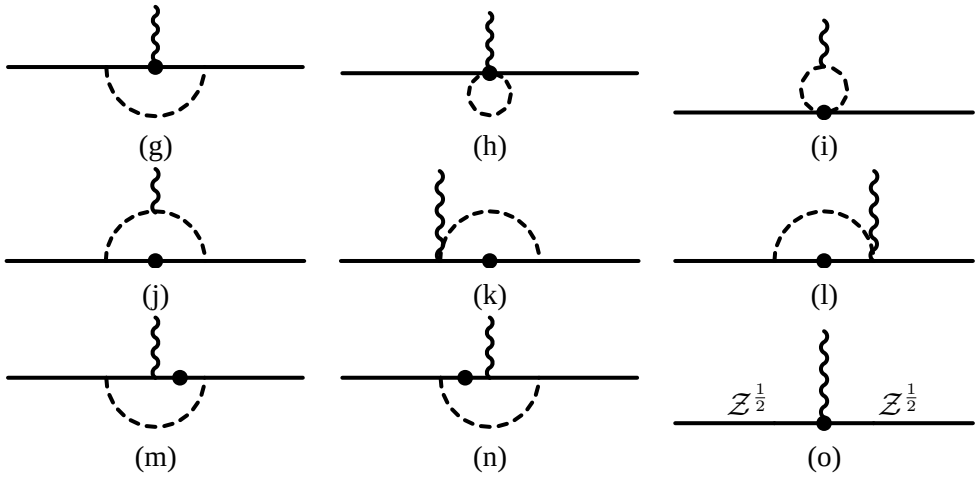

Figure 4.2: The loop diagrams contributing to the nucleon form factors at order p^4. The solid dots denote insertions from the second order Lagrangean of eq.(4.13).

4.3.2 Meson Lagrangean

According to our power-counting analysis given in the previous subsection, we only need to know the chiral meson Lagrangean up to $\mathcal{O}(p^2)$. At this order it reads [GL84]

$$\mathcal{L}_{\pi\pi}^{(2)} = \frac{F_\pi^2}{4}\,\mathrm{Tr}\left[\nabla_\mu U^\dagger \nabla^\mu U + \chi^\dagger U + \chi U^\dagger\right]. \tag{4.6}$$

$U = u^2$ corresponds to a nonlinear realization of the quasi Goldstone boson fields. The covariant derivative $\nabla_\mu U$ is defined as

$$\nabla_\mu U = \partial_\mu U - i\,(v_\mu + a_\mu)\,U + iU\,(v_\mu - a_\mu)\,, \tag{4.7}$$

while v_μ and a_μ denote arbitrary vector- and axial vector background fields, for details see chapter 1. The explicit breaking of chiral symmetry via the finite quark masses is encoded in

$$\chi = 2\,B_0\,(s + i\,p)\,, \tag{4.8}$$

if one switches off the external pseudoscalar background field p and assigns the two flavour quark mass matrix $\mathcal{M} = \mathrm{diag}(m_u, m_d)$ to the scalar background field s. To the order we are working at, we obtain the resulting pion mass m_π via

$$m_\pi^2 = 2\,B_0\,\hat{m} + \mathcal{O}({m_q}^2), \tag{4.9}$$

where $\hat{m} = (m_u + m_d)/2$ and B_0 corresponds to the value of the chiral condensate. The other free parameter at this order F_π can be identified with the value of the pion-decay constant (in the chiral limit).

4.3.3 Nucleon Lagrangeans

The well known leading order Lagrangean in BChPT is given as [GSS88]

$$\mathcal{L}_{\pi N}^{(1)} = \bar{\Psi}_N\left[i\gamma^\mu D_\mu - M_0 + \frac{g_A}{2}\gamma^\mu\gamma_5 u_\mu\right]\Psi_N, \tag{4.10}$$

with

$$\begin{aligned} D_\mu\Psi_N &= \left[\partial_\mu - iv_\mu^{(s)} + \frac{1}{2}\left[u^\dagger, \partial_\mu u\right] - \frac{i}{2}u^\dagger\,(v_\mu + a_\mu)\,u - \frac{i}{2}u\,(v_\mu - a_\mu)\,u^\dagger\right]\Psi_N, && (4.11)\\ u_\mu &= iu^\dagger\nabla_\mu U u^\dagger. && (4.12)\end{aligned}$$

Ψ_N is the nucleon field operator, the coupling constant g_A denotes the axial-coupling of the nucleon (in the chiral limit), M_0 corresponds to the mass of the nucleon (in the chiral limit) and $v_\mu^{(s)}$ is the isosinglet vector background field.
According to subsection 4.3.1 we need to know the nucleon Lagrangean up to $\mathcal{O}(p^4)$. The relevant terms are [FMS98, FMMS00]

$$\begin{aligned} \mathcal{L}_{\pi N}^{(2)} &= \bar{\Psi}_N\Bigg[c_1\langle\chi_+\rangle - \frac{c_2}{8M_0^2}\left(\langle u_\mu u_\nu\rangle\{D^\mu D^\nu\} + h.c.\right) + \frac{ic_4}{4}\sigma^{\mu\nu}[u_\mu, u_\nu] + \frac{c_6}{8M_0}\sigma^{\mu\nu}F_{\mu\nu}^+ \\ &\quad + \frac{c_7}{8M_0}\sigma^{\mu\nu}\langle F_{\mu\nu}^+\rangle\Bigg]\Psi_N, && (4.13)\\ \mathcal{L}_{\pi N}^{(3)} &= \bar{\Psi}_N\left[\frac{id_6}{2M_0}\left([D^\mu, \hat{F}_{\mu\nu}^+]D_\nu + h.c.\right) + \frac{id_7}{2M_0}\left([D^\mu, \langle F_{\mu\nu}^+\rangle]D_\nu + h.c.\right)\right]\Psi_N, && (4.14)\\ \mathcal{L}_{\pi N}^{(4)} &= \bar{\Psi}_N\Bigg[-\frac{e_{54}}{2}\left[D^\lambda, [D_\lambda, \langle F_{\mu\nu}^+\rangle]\right]\sigma^{\mu\nu} - \frac{e_{74}}{2}\left[D^\lambda, [D_\lambda, \hat{F}_{\mu\nu}^+]\right]\sigma^{\mu\nu} - \frac{e_{105}}{2}\langle F_{\mu\nu}^+\rangle\langle\chi_+\rangle\sigma^{\mu\nu} \\ &\quad - \frac{e_{106}}{2}\hat{F}_{\mu\nu}^+\langle\chi_+\rangle\sigma^{\mu\nu}\Bigg]\Psi_N, && (4.15)\end{aligned}$$

where we have used the definitions $F^+_{\mu\nu} = u^\dagger F_{\mu\nu} u + u F_{\mu\nu} u^\dagger$ with the field strength tensor $F_{\mu\nu} = \partial_\mu v_\nu - \partial_\nu v_\mu$ and the explicit chiral symmetry breaking term $\chi_+ = u^\dagger \chi u^\dagger + u \chi u$. Furthermore $\langle ... \rangle$ denotes the trace in isospin space and $\hat{A} = A - \frac{1}{2}\langle A \rangle$ is a traceless SU(2) operator.

4.4 Isovector Form Factors of the Nucleon

Calculating the Feynman diagrams shown in figures 4.1 and 4.2 with the nucleon- and pion dynamics as well as their couplings to the incoming photon field determined by the Lagrangeans given in the previous section, we arrive at the amplitudes given in appendix C.2. The rather lengthy explicit analytic expressions for the isovector form factors $F_1^v(t)$ and $F_2^v(t)$ are given in appendix C.3.
We start the discussion of those results by analysing the quark mass dependence of their lowest moments in $q^2 = t$, namely the isovector anomalous magnetic moment of the nucleon κ_v and the slopes ρ_1^v and ρ_2^v of those form factors defined via

$$F_1^v(t) = 1 + \rho_1^v t + \mathcal{O}(t^2), \tag{4.16}$$

$$F_2^v(t) = \kappa_v + \rho_2^v t + \mathcal{O}(t^2). \tag{4.17}$$

A numerical discussion of these results in the context of chiral extrapolations of lattice data is given in section 4.6.
Note that due to the presence of the small parameter q^ν in the current of eq.(4.1) and the prefactors t attached to the slopes in the above definitions, the contributions of a BChPT calculation at chiral dimension D to these structures are of chiral dimensions $D-2$ for κ_v, $D-3$ for ρ_1 and $D-4$ for ρ_2. Systematic uncertainties due to possible higher order effects are therefore accordingly larger for those quantities.

4.4.1 The quark mass dependence of the isovector anomalous magnetic moment

The BChPT result for the isovector anomalous magnetic moment of the nucleon κ_v written as a sum of contributions from order p^3 ($\delta\kappa_v^{(3)}$) and p^4 ($\delta\kappa_v^{(4)}$) as well as the pertinent contributions from local operators (with couplings c_6 and $e^r_{106}(\lambda)$) reads (here and throughout this chapter we fix the renormalization scale at $\lambda = M_0$):

$$\kappa_v = \frac{M^{(n)}}{M_0}\Big[c_6 - 16 M_0 m_\pi^2 e^r_{106}(M_0) + \delta\kappa_v^{(3)} + \delta\kappa_v^{(4)} + \mathcal{O}_{\kappa_v}(p^5)\Big], \tag{4.18}$$

with

$$\begin{aligned}\delta\kappa_v^{(3)} = {} & \frac{g_A^2 m_\pi^2 M_0}{8\pi^2 F_\pi^2 M^3}\Big[\left(3m_\pi^2 - 7M^2\right)\log\frac{m_\pi}{M} - 3M^2\Big] \\ & - \frac{g_A^2 m_\pi M_0}{8\pi^2 F_\pi^2 M^3\sqrt{4M^2 - m_\pi^2}}\Big[3m_\pi^4 - 13M^2 m_\pi^2 + 8M^4\Big]\arccos\Big(\frac{m_\pi}{2M}\Big),\end{aligned} \tag{4.19}$$

and

$$\begin{aligned}\delta\kappa_v^{(4)} = {} & -\frac{m_\pi^2}{32\pi^2 F_\pi^2 M_0^2}\Big[4g_A^2\left(c_6+1\right)M_0^2 - g_A^2\left(5c_6 m_\pi^2 + 28M_0^2\right)\log\frac{m_\pi}{M_0} \\ & + 4M_0^2\left(2c_6 g_A^2 + 7g_A^2 + c_6 - 4c_4 M_0\right)\log\frac{m_\pi}{M_0}\Big] \\ & - \frac{g_A^2 c_6 m_\pi^3}{32\pi^2 F_\pi^2 M_0^2\sqrt{4M_0^2 - m_\pi^2}}\left(5m_\pi^2 - 16M_0^2\right)\arccos\left(\frac{m_\pi}{2M_0}\right).\end{aligned} \tag{4.20}$$

While the leading chiral contributions beyond our analysis take the form

$$\mathcal{O}_{\kappa_v}(p^5) = \delta_{\kappa_v}\frac{M_0 m_\pi^3}{(4\pi F_\pi)^4} + ... \tag{4.21}$$

The prefactor δ_{κ_v} would be determined in a full $\mathcal{O}(p^5)$ calculation. At the level of our $\mathcal{O}(p^4)$ analysis, we estimate the possible impact of higher order contributions to our results by varying this parameter within natural size, i.e. $-3 < \delta_{\kappa_v} < 3$, for a numerical analysis see sections 4.6.1 and 4.6.2.
Note that according to the discussion at the end of section 4.3.1, the mass function M in eq.(4.19) is to be understood as

$$M = M_0, \tag{4.22}$$

if one truncates eq.(4.18) already at $\mathcal{O}(p^3)$, whereas at $\mathcal{O}(p^4)$ it starts to acquire an intrinsic quark mass dependence given in eq.(4.4):

$$M = M_N(m_\pi). \tag{4.23}$$

The mass parameter $M^{(n)}$ in eq.(4.18) appears as a consequence of the normalization of $F_2(q^2)$ in the current of eq.(4.1). For comparison with experiment and normalized lattice data one would have to choose $M^{(n)} = M_N^{\text{phys}}$ while a comparison with raw, unnormalized lattice data has to be performed using $M^{(n)} = M_N(m_\pi)$.
Comparing the results presented in this chapter to the findings of reference [KM01] where the nucleon form factors have been calculated using the standard IR renormalization technique of reference [BL99] at the same order p^4, one observes a difference of the form $\kappa_v^{\text{this work}} - \kappa_v^{[\text{KM01}]} = \frac{M_0^2}{(4\pi F_\pi)^2} \sum_{i=2}^{\infty} a_i \left(\frac{m_\pi}{M_0}\right)^{2i}$, i.e. an infinite sum of even powers of the pion mass starting from m_π^4. In principle these terms can be absorbed into higher order coupling constants and each one such becomes unobservable at a sufficiently high order of the chiral analysis. They appear as a consequence of the different regularization prescriptions used here and in [KM01]. From the viewpoint of applicability for chiral extrapolations our choice of the renormalization scheme is motivated by the fact that the $\overline{\text{IR}}$ scheme utilized here shows a much better convergence pattern for pion masses $m_\pi > m_\pi^{\text{phys}}$ and provides smooth extrapolation functions, where contributions from πN loops are systematically reduced for large pion masses in agreement with observations from the lattice but in contrast to the standard IR result, see figure 4.7. In addition there are some more formal arguments – see chapter 3 – motivating our choice.
Performing an additional $\frac{1}{M_0}$ expansion of the above expressions one finds

$$\delta\kappa_v^{(3)} = -\frac{g_A^2 M m_\pi}{4\pi F_\pi^2} - \frac{g_A^2 m_\pi^2 \left(1 + 7\log\frac{m_\pi}{M_0}\right)}{8\pi^2 F_\pi^2} + ..., \tag{4.24}$$

$$\delta\kappa_v^{(4)} = -\frac{m_\pi^2}{8\pi^2 F_\pi^2}\left[(c_6+1)\, g_A^2 + \left(2c_6 g_A^2 + c_6 - 4c_4 M_0\right)\log\frac{m_\pi}{M_0}\right] + ... \tag{4.25}$$

and such recovers the $\mathcal{O}(p^3)$ HBChPT result [BFHM98] (which is the first term of eq.(4.24)) while the terms $\sim m_\pi^2$ constitute the accordant $\mathcal{O}(p^4)$ HBChPT contributions. Note that the second term in eq.(4.24) is of order p^3 in the covariant framework but only appears at order p^4 in the nonrelativistic formulation of BChPT. The leading, linear dependence of κ_V on the pion mass is long-known from current algebra [CP74].

4.4.2 The quark mass dependence of the slopes of the isovector form factors

The slope of the isovector Dirac form factor again written as a sum of $\mathcal{O}(p^3)$ and $\mathcal{O}(p^4)$ loop contributions plus a counter-term from the order p^3 Lagrangean reads:

$$\rho_1^v = B_{c1} + \rho_1^{v\,(3)} + \rho_1^{v\,(4)} + \mathcal{O}_{\rho_1^v}(p^5), \tag{4.26}$$

with

$$
\begin{aligned}
B_{c1} &= -2d_6^r(\lambda = M_0), && (4.27)\\
\rho_1^{v\,(3)} &= -\frac{1}{96\pi^2 F_\pi^2 M^4}\Big[7g_A^2M^4 + 2\left(5g_A^2+1\right)M^4\log\frac{m_\pi}{M_0} + M^4 - 15g_A^2m_\pi^2M^2 \\
&\quad +g_A^2m_\pi^2\left(15m_\pi^2 - 44M^2\right)\log\frac{m_\pi}{M}\Big] \\
&\quad +\frac{g_A^2m_\pi}{96\pi^2F_\pi^2M^4\sqrt{4M^2-m_\pi^2}}\Big[15m_\pi^4 - 74m_\pi^2M^2 + 70M^4\Big]\arccos\left(\frac{m_\pi}{2M}\right), && (4.28)\\
\rho_1^{v\,(4)} &= -\frac{c_6g_A^2m_\pi^2}{32\pi^2F_\pi^2M_0^4\sqrt{4M_0^2-m_\pi^2}}\Bigg[m_\pi\left(m_\pi^2-3M_0^2\right)\arccos\left(\frac{m_\pi}{2M_0}\right) \\
&\quad +\sqrt{4M_0^2-m_\pi^2}\Big[M_0^2+\left(M_0^2-m_\pi^2\right)\log\frac{m_\pi}{M_0}\Big]\Bigg], && (4.29)\\
\mathcal{O}_{\rho_1^v}(p^5) &= \delta_{\rho_1^v}\frac{m_\pi^2}{(4\pi F_\pi)^4} + ... && (4.30)
\end{aligned}
$$

where the last line is again not part of the order p^4 result but represents the leading contribution beyond the order of our analysis and allows for an estimate of higher order effects. Expanding our results in powers of $\frac{1}{M_0}$ we again find the according HBChPT results ($\frac{m_\pi^0}{M_0^0}$ terms correspond to order p^3 in HBChPT while the terms carrying a factor $\frac{m_\pi}{M_0}$ are of order p^4 in this framework):

$$
\begin{aligned}
\rho_1^{v\,(3)} &= -\frac{1}{96\pi^2F_\pi^2}\left[7g_A^2+1+2\left(5g_A^2+1\right)\log\frac{m_\pi}{M}\right] + \frac{35g_A^2m_\pi}{192\pi F_\pi^2M_0} + ..., && (4.31)\\
\rho_1^{v\,(4)} &= \mathcal{O}\left(\frac{m_\pi^2}{M_0^2}\right). && (4.32)
\end{aligned}
$$

The leading, pion mass independent term given as the first term in eq.(4.31) was first found in the nonrelativistic ChPT analysis of reference [BKKM92].
Likewise one finds for the slope of the isovector Pauli form factor:

$$
\rho_2^v = \frac{M^{(n)}}{M_0}\left(B_{c2} + \rho_2^{v\,(3)} + \rho_2^{v\,(4)} + \mathcal{O}_{\rho_2^v}(p^5)\right), \qquad (4.33)
$$

where

$$
\begin{aligned}
B_{c2} &= 4M_0e_{74}^r(M_0), && (4.34)\\
\rho_2^{v\,(3)} &= \frac{g_A^2M_0}{96\pi^2F_\pi^2M^5\left(m_\pi^2-4M^2\right)}\Bigg[-124M^6 + 105m_\pi^2M^4 - 18m_\pi^4M^2 \\
&\quad +6\left(3m_\pi^6 - 22M^2m_\pi^4 + 44M^4m_\pi^2 - 16M^6\right)\log\frac{m_\pi}{M}\Bigg] \\
&\quad +\frac{g_A^2M_0}{48\pi^2F_\pi^2M^5m_\pi\left(4M^2-m_\pi^2\right)^{\frac{3}{2}}}\Big[9m_\pi^8 - 84M^2m_\pi^6 + 246M^4m_\pi^4 \\
&\quad -216M^6m_\pi^2 + 16M^8\Big]\arccos\left(\frac{m_\pi}{2M}\right), && (4.35)
\end{aligned}
$$

$$\begin{aligned}
\rho_2^{v\,(4)} &= -\frac{g_A^2 c_6 m_\pi^3}{96\pi^2 F_\pi^2 M_0^4 \left(4M_0^2 - m_\pi^2\right)^{\frac{3}{2}}}\left[4m_\pi^4 - 27m_\pi^2 M_0^2 + 42M_0^4\right]\arccos\left(\frac{m_\pi}{2M_0}\right) \\
&+\frac{1}{96\pi^2 F_\pi^2 M_0^4\left(m_\pi^2 - 4M_0^2\right)}\Bigg[16c_4 M_0^7 + 52g_A^2 M_0^6 - 4c_4 m_\pi^2 M_0^5 - 14c_6 g_A^2 m_\pi^2 M_0^4 \\
&-13g_A^2 m_\pi^2 M_0^4 + 8\left(3g_A^2 - c_4 M_0\right)\left(m_\pi^2 - 4M_0^2\right)M_0^4 \log\frac{m_\pi}{M_0} + 4c_6 g_A^2 m_\pi^4 M_0^2 \\
&-g_A^2\left(m_\pi^2 - 4M_0^2\right)\left(4c_6 m_\pi^4 - 3c_6 m_\pi^2 M_0^2 + 24M_0^4\right)\log\frac{m_\pi}{M_0}\Bigg]. \qquad (4.36)
\end{aligned}$$

In order to estimate higher order contributions to this observable we use

$$\mathcal{O}_{\rho_2^v}(p^5) = \delta_{\rho_2^v}\frac{M_0 m_\pi}{(4\pi F_\pi)^2} + ... \qquad (4.37)$$

The corresponding HBChPT results can again be found by an additional expansion in $\frac{1}{M_0}$ and read:

$$\rho_2^{v\,(3)} = \frac{g_A^2 M}{48\pi F_\pi^2 m_\pi} + \frac{g_A^2}{96\pi^2 F_\pi^2}\left(29 + 24\log\frac{m_\pi}{M_0}\right) + ..., \qquad (4.38)$$

$$\rho_2^{v\,(4)} = -\frac{1}{96\pi^2 F_\pi^2}\left(3g_A^2 + 4c_4 M_0 + 8c_4 M_0 \log\frac{m_\pi}{M_0}\right) + ... \qquad (4.39)$$

where the second term in $\rho_2^{v\,(3)}$ would be of order p^4 according to the counting in the nonrelativistic framework and the first term in this equation was already found in reference [BKKM92].
Note that the slopes of both isoscalar form factors are singular in the chiral limit. While ρ_1^v displays a logarithmic divergence, see eq.(4.31), ρ_2^v behaves as $\frac{1}{m_\pi}$, see eq.(4.38). The mass function M appearing in the $\mathcal{O}(p^3)$ expressions of eqs.(4.28,4.35) depends again on the chiral order at which eqs.(4.26) and (4.33) are studied.

4.4.3 The momentum dependence of the isovector Sachs form factors

In this section we discuss the momentum transfer $Q^2 = -t$ dependence of the isovector electric- and magnetic Sachs form factors. They are related to the previously discussed Dirac- and Pauli form factors via

$$G_E(Q^2) = F_1(Q^2) - \frac{Q^2}{4M_N^2}F_2(Q^2), \qquad (4.40)$$

$$G_M(Q^2) = F_1(Q^2) + F_2(Q^2). \qquad (4.41)$$

The Q^2 dependence of those form factors in $\mathcal{O}(p^4)$ BChPT at $m_\pi = 140$ MeV is shown in figures 4.3 and 4.4. In those plots we have used the input values given in table 4.1 and have adjusted the parameters c_6, B_{c1} and B_{c2} such that we reproduce the anomalous magnetic moment and the slopes of the the parametrization of reference [FW03] given in table 4.3. The resulting values for those parameters are given in table 4.2. The Q^2 dependence of the phenomenological parametrization is also shown in figures 4.3 and 4.4. A comparison allows us to conclude a good description of phenomenology by $\mathcal{O}(p^4)$ covariant BChPT up to momentum transfers of about $Q^2 \approx 0.25$ GeV^2 where we find more curvature and a better agreement of $\mathcal{O}(p^4)$ BChPT with the phenomenological parametrization for $G_E^v(Q^2)$ but a still satisfying description of $G_M^v(Q^2)$ at low momenta. To get an impression of the convergence properties of the chiral expansion for those form factors, we also show the $\mathcal{O}(p^3)$ results for the Sachs form factors. Whereas $G_E^v(Q^2)$ receives moderate corrections when going from $\mathcal{O}(p^3)$ to $\mathcal{O}(p^4)$, the next-to-leading one loop order has a huge impact on the magnetic Sachs form factor. These large $\mathcal{O}(p^4)$ contributions to $G_M^v(Q^2)$ come as a result of two effects which – at a renormalization $\lambda = M_0$ – can be interpreted as follows: Short distance contributions to the radius of this form factor arise at this order, the term $\sim B_{c2}$ considerably changes the Q^2 dependence of the magnetic form factor. The large

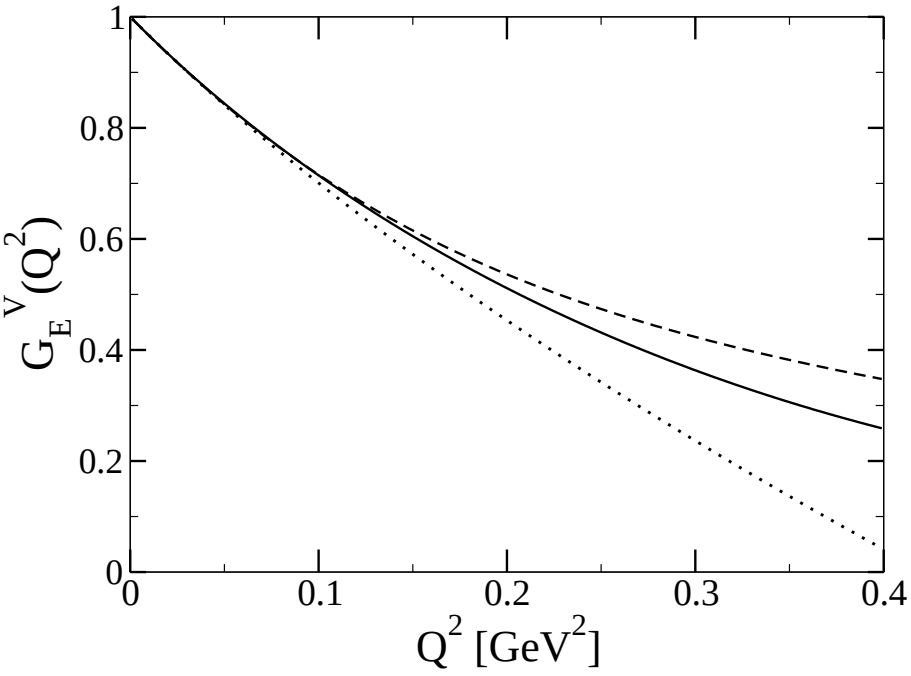

Figure 4.3: The momentum transfer dependence of the isovector electric Sachs form factor of the nucleon in $\mathcal{O}(p^4)$ BChPT (solid), $\mathcal{O}(p^3)$ BChPT (dotted) and the phenomenological parametrization of reference [FW03] (dashed).

values for the coupling constants of the second order Lagrangean give the second, albeit less important reason for the large $\mathcal{O}(p^4)$ contributions. These coupling constants are known to parametrize contributions from the Δ resonance and thus their impact on the magnetic form factor does not come as a surprise [BFHM98]. However, a convergence of the BChPT results towards phenomenology is clearly signaled by the comparison of the different orders of our calculation.

A quantitative estimate for systematic uncertainties of the $\mathcal{O}(p^4)$ BChPT calculation can be given as follows: The leading contributions of order p^5 to the nucleon form factors (which cannot be absorbed at the physical point by a shift in c_6, B_{c1} and B_{c2}) are proportional to Q^4. Again assuming the prefactors of these structures to be within natural size (i.e. between -3 and 3), the systematic uncertainties of our analysis of $G_E^v(Q^2)$ and $G_M^v(Q^2)$ exceed the 30% level above $Q^2 = 0.3$ GeV^2 but are below 10% for $Q^2 < 0.2$ GeV^2. Within those errors BChPT and phenomenology are perfectly consistent.

Given the good agreement between the phenomenological parametrization and the $\mathcal{O}(p^4)$ BChPT result for $G_E^v(Q^2)$ at low momentum transfer, we to study the deviation of the Q^2 dependence of this form factors from the standard dipole form

$$G_{\rm D}(Q^2) \quad = \frac{1}{\left(1+\frac{Q^2}{0.71\text{GeV}^2}\right)^2}. \tag{4.42}$$

The result is shown in figure 4.5 as a function of $|Q|$. Even in this high-resolution plot, the good agreement between $\mathcal{O}(p^4)$ BChPT and the parametrization of reference [FW03] holds, supporting the claims made about the deviations of the nucleon form factors from the dipole shape in this reference[1]. In the same plot, we show the result of the radius approximation, i.e. $F_i^v(Q^2) \approx F_i^v(0) - \rho_i^v Q^2$, demonstrating that the full $\mathcal{O}(p^4)$ BChPT result contains important structures beyond this approximation.

[1]Note that the "bumps" observed in reference [FW03] are only visible in the charge channels, whereas in the isovector channel discussed here, one would – according to reference [FW03] – only find a decline below the dipole behaviour in the Q^2 dependence of the form factors.

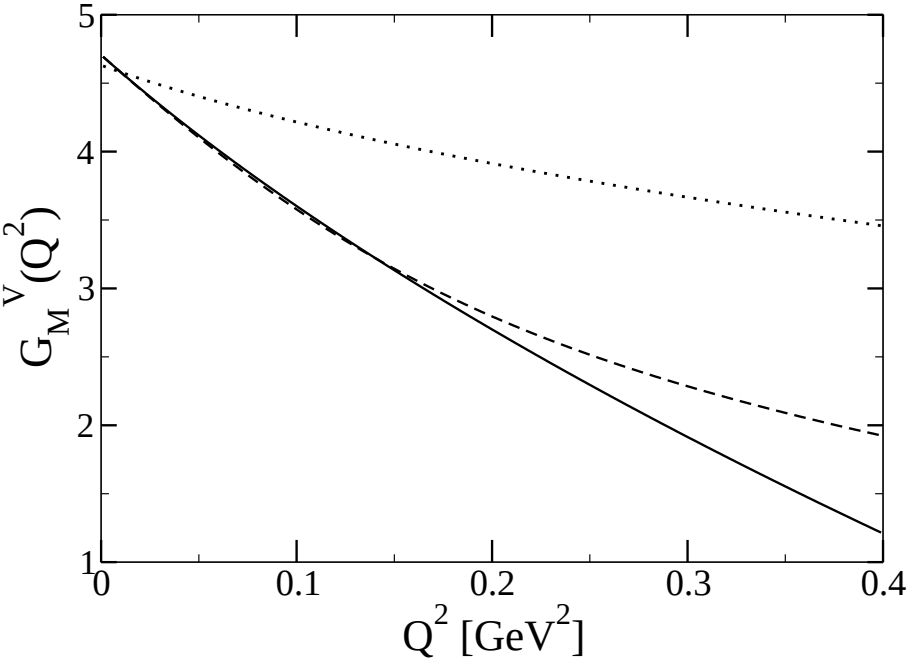

Figure 4.4: The momentum transfer dependence of the isovector magnetic Sachs form factor of the nucleon in $\mathcal{O}(p^4)$ BChPT (solid), $\mathcal{O}(p^3)$ BChPT (dotted) and the phenomenological parametrization of reference [FW03] (dashed).

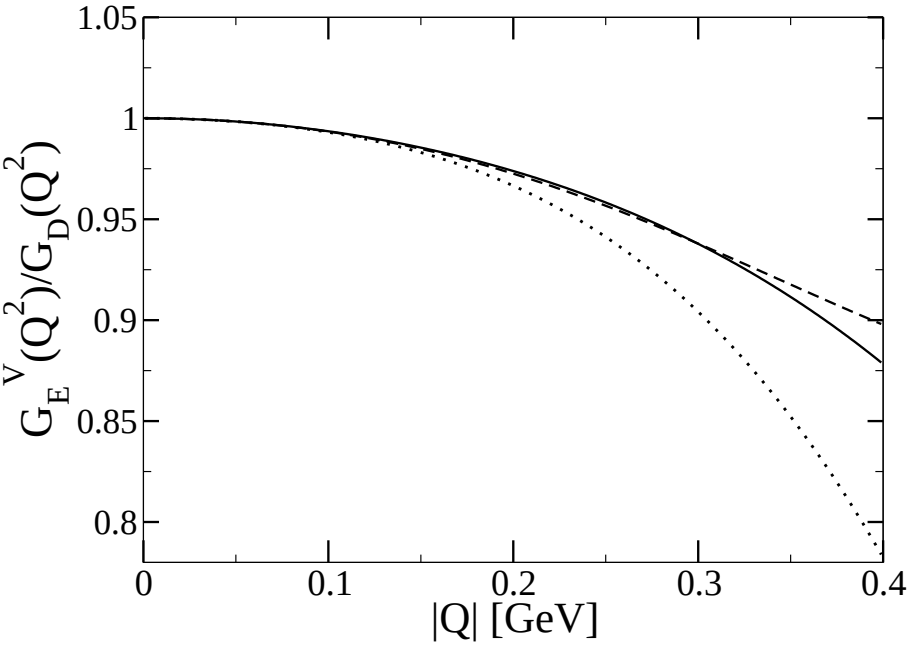

Figure 4.5: The isovector electric Sachs form factor of the nucleon normalized to the standard dipole: $\mathcal{O}(p^4)$ BChPT result (solid), radius approximation (dotted) and the phenomenological parametrization of reference [FW03] (dashed).

4.5 Isoscalar Form Factors of the Nucleon

Contributions to the isoscalar form factors of the nucleon arise from diagrams (a), (g) and (h) of figure 4.1. The resulting amplitudes can again be found in appendix C.2 while explicit analytic expressions for $F_1^s(t)$ and $F_2^s(t)$ are given in appendix C.3. We start the discussion of these form factors again by analysing the quark mass dependence of their lowest moments in t defined via

$$F_1^s(t) = 1 + \rho_1^s t + \mathcal{O}(t^2), \tag{4.43}$$
$$F_2^s(t) = \kappa_s + \rho_2^s t + \mathcal{O}(t^2). \tag{4.44}$$

A first glance at the numerical implications of our results can be found in section 4.6.

4.5.1 The quark mass dependence of the isoscalar anomalous magnetic moment

The BChPT result for the isoscalar anomalous magnetic moment of the nucleon κ_s written as a sum of contributions from order p^3 ($\delta\kappa_s^{(3)}$) and p^4 ($\delta\kappa_s^{(4)}$) as well as the pertinent contributions from local operators (with couplings $\kappa_s^0 = c_6 + 2c_7$ and $e_{105}^r(\lambda)$) reads:

$$\kappa_s = \frac{M^{(n)}}{M_0}\Big[\kappa_s^0 - 16M_0 m_\pi^2 e_{105}^r(M_0) + \delta\kappa_s^{(3)} + \delta\kappa_s^{(4)} + \mathcal{O}_{\kappa_s}(p^5)\Big], \tag{4.45}$$

with

$$\delta\kappa_s^{(3)} = -\frac{3g_A^2 m_\pi^2 M_0}{8\pi^2 F_\pi^2 M^3}\left[\frac{m_\pi\left(m_\pi^2 - 3M^2\right)}{\sqrt{4M^2 - m_\pi^2}}\arccos\left(\frac{m_\pi}{2M}\right) + M^2 + \left(M^2 - m_\pi^2\right)\log\frac{m_\pi}{M}\right], \tag{4.46}$$

and

$$\begin{aligned}\delta\kappa_s^{(4)} = \frac{3g_A^2 m_\pi^2}{32\pi^2 F_\pi^2 M_0^2}\Bigg[&4M_0^2 + \kappa_s^0\left(3m_\pi^2 - 4M_0^2\right)\log\frac{m_\pi}{M_0} \\ &-\kappa_s^0\frac{m_\pi\left(3m_\pi^2 - 8M_0^2\right)}{\sqrt{4M_0^2 - m_\pi^2}}\arccos\left(\frac{m_\pi}{2M_0}\right)\Bigg].\end{aligned} \tag{4.47}$$

The leading chiral contributions to κ_s beyond our analysis take the form:

$$\mathcal{O}_{\kappa_s}(p^5) = \delta_{\kappa_s}\frac{M_0 m_\pi^3}{(4\pi F_\pi)^4} + ... \tag{4.48}$$

The corresponding results of the nonrelativistic HBChPT framework can again be found by an expansion of our covariant results in $\frac{1}{M_0}$. In HBChPT one does not find any loop contributions at order p^3. At $\mathcal{O}(p^4)$ one finds

$$\delta\kappa_s^{\text{loop}} = -\frac{3g_A^2 m_\pi^2}{8\pi^2 F_\pi^2}\left(\kappa_s^0 + 1\right)\log\frac{m_\pi}{M_0} + \mathcal{O}^{\text{HB}}(p^5). \tag{4.49}$$

4.5.2 The quark mass dependence of the slopes of the isoscalar form factors

Writing the slopes of the isoscalar form factors of the nucleon as a sum of contributions of different chiral dimension, we find

$$\rho_1^s = B_{c1}^s + \rho_1^{s\,(3)} + \rho_1^{s\,(4)} + \mathcal{O}_{\rho_1^s}(p^5), \tag{4.50}$$

with

$$B^s_{c1} = -4d_7, \tag{4.51}$$

$$\rho_1^{s\,(3)} = \frac{g_A^2 m_\pi^2}{32\pi^2 F_\pi^2 M^4 (m_\pi^2 - 4M^2)}\Bigg[5m_\pi^2 M^2 - 18M^4 + \frac{m_\pi\left(5m_\pi^4 - 34M^2m_\pi^2 + 54M^4\right)}{\sqrt{4M^2 - m_\pi^2}} \times \arccos\left(\frac{m_\pi}{2M}\right) - \left(m_\pi^2 - 4M^2\right)\left(5m_\pi^2 - 4M^2\right)\log\frac{m_\pi}{M}\Bigg], \tag{4.52}$$

$$\rho_1^{s\,(4)} = \frac{3g_A^2\kappa_s^0 m_\pi^2}{32\pi^2 F_\pi^2 M_0^4}\left[M_0^2 + \left(M_0^2 - m_\pi^2\right)\log\frac{m_\pi}{M_0} + \frac{m_\pi\left(m_\pi^2 - 3M_0^2\right)}{\sqrt{4M_0^2 - m_\pi^2}}\arccos\left(\frac{m_\pi}{2M_0}\right)\right], \tag{4.53}$$

$$\mathcal{O}_{\rho_1^s}(p^5) = \delta_{\rho_1^s}\frac{m_\pi^2}{(4\pi F_\pi)^2} + ... \tag{4.54}$$

And likewise

$$\rho_2^s = \frac{M^{(n)}}{M_0}\left(B^s_{c2} + \rho_2^{s\,(3)} + \rho_2^{s\,(4)} + \mathcal{O}_{\rho_2^s}(p^5)\right), \tag{4.55}$$

with

$$B^s_{c2} = 8M_0 e_{54}, \tag{4.56}$$

$$\rho_2^{s\,(3)} = \frac{g_A^2 m_\pi^2 M_0}{16\pi^2 F_\pi^2 M^5 (4M^2 - m_\pi^2)}\Bigg[\frac{m_\pi\left(3m_\pi^4 - 20M^2m_\pi^2 + 30M^4\right)}{\sqrt{4M^2 - m_\pi^2}}\arccos\left(\frac{m_\pi}{2M}\right) - 2\Big(10M^4 - 3m_\pi^2M^2 + \left(4M^2 - m_\pi^2\right)\left(2M^2 - 3m_\pi^2\right)\log\frac{m_\pi}{M}\Big)\Bigg], \tag{4.57}$$

$$\rho_2^{s\,(4)} = \frac{\kappa_s^0 g_A^2 m_\pi^2}{32\pi^2 F_\pi^2 M_0^4\left(m_\pi^2 - 4M_0^2\right)}\Bigg[-\frac{m_\pi\left(4m_\pi^4 - 27M_0^2m_\pi^2 + 42M_0^4\right)}{\sqrt{4M_0^2 - m_\pi^2}}\arccos\left(\frac{m_\pi}{2M_0}\right) + 14M_0^4 - 4m_\pi^2M_0^2 + \left(m_\pi^2 - 4M_0^2\right)\left(4m_\pi^2 - 3M_0^2\right)\log\frac{m_\pi}{M_0}\Bigg]. \tag{4.58}$$

$$\mathcal{O}_{\rho_2^s}(p^5) = \delta_{\rho_2^s}\frac{M_0 m_\pi}{(4\pi F_\pi)^2} + ... \tag{4.59}$$

In the heavy baryon expansion all the above pion-cloud contributions to the slopes of the isoscalar form factors only appear at higher orders and at order p^4 one would only find the counter-term contributions.
Finally we emphasize again that the mass-function M in eqs.(4.46,4.52,4.57) depends on the chiral order at which the respective quantities are studied. It has to be identified with $M = M_0$ in an analysis at $\mathcal{O}(p^3)$ but with $M = M_N(m_\pi)$ in a $\mathcal{O}(p^4)$ result.

4.5.3 The momentum dependence of the isoscalar form factors

After the coupling constants κ_s, $e^r_{105}(M_0)$, B^s_{c1} and B^s_{c2} are adjusted such that the isoscalar anomalous magnetic moment and the slopes of the parametrization of reference [FW03] given in table 4.3 are reproduced, the Q^2 dependence of the $\mathcal{O}(p^4)$ BChPT result for the isoscalar form factors is completely dominated by short distance physics. Although we do find rich analytic structures resulting from the pion-cloud, their sizes are numerically negligible compared to the contributions from local operators. Thus, we basically only find a linear dependence of the isoscalar form factors on Q^2 and no substantial curvature. Therefore, $\mathcal{O}(p^4)$ BChPT cannot provide a good description of experimental data for these form factors beyond $Q^2 = 0.1$ GeV^2. However, due to isospin and parity conservation, the corresponding spectral functions do have a cut starting at $Q^2 = -(3m_\pi)^2$ [Kai03] and thus essential contributions to the isoscalar form factors arise from two loop effects (containing three pion lines in the loop), starting at order p^5.

4.6 Fit Results

In this section we give a numerical discussion of our $\mathcal{O}(p^4)$ covariant BChPT results in the context of chiral extrapolations, i.e. the extrapolations of lattice data at large values of m_π through the physical point to the chiral limit.
Simulations of the nucleon form factors on the lattice are not only performed at large pion masses but also at finite values of the momentum transfer which in former days did lie clearly outside the range of applicability of BChPT. The standard tool to extract observables like the anomalous magnetic moment and the slopes of the nucleon form factors from simulation results at large Q^2 is a fit of the dipole ansatz to those lattice data. Thus, by fitting the dipole formula to the lattice results for $F_1(Q^2)$ and $F_2(Q^2)$ at every value of m_π separately, values for κ, ρ_1 and ρ_2 at the respective pion mass can be given.
The simulation of reference [AKNT06] now for the first time provides us with (quenched) lattice results for $F_1^v(Q^2)$ and $F_2^v(Q^2)$ at $Q^2 \lesssim 0.3$ GeV^2, values for which the previous section gives us some confidence that the chiral expansion for the isovector nucleon form factors has already well converged at next-to-leading one loop level. We therefore perform two different types of analyses: One is to extract the values for our couplings by a fit of the $\mathcal{O}(p^4)$ formulae given in sections 4.4.1 and 4.4.2 to data for κ_v, ρ_1^v and ρ_2^v gained via a dipole-Q^2-extrapolation (see section 4.6.1). The second approach discussed in section 4.6.2 is a fit of our extrapolation functions directly to the outcome of lattice simulations at finite Q^2. In both paragraphs we do not include the physical point in the fits but give predictions for the physical values of the isovector anomalous magnetic moment and the slopes of the form factors including an analysis of statistical as well as systematic errors.

4.6.1 Fits based on dipole-extrapolated data

In this section we present fits of our $\mathcal{O}(p^4)$ BChPT results for κ_v, ρ_1^v and ρ_2^v (given in sections 4.4.1 and 4.4.2) to data resulting from lattice simulations of $F_1^v(Q^2)$ and $F_2^v(Q^2)$ which have been extrapolated to low values of Q^2 using a dipole ansatz [AKNT06]. As fit parameters we choose the BChPT couplings entering our results through tree level diagrams[2]: c_6, $e_{106}^r(\lambda)$, B_{c1} and B_{c2}. Their numerical values are determined by a fit of the $\mathcal{O}(p^4)$ BChPT results for κ_v (see eqs.(4.18)-(4.21)) and the slopes ρ_1^v (eqs.(4.26)-(4.30)) and ρ_2^v (eqs.(4.33)-(4.37)) to dipole-Q^2-extrapolated results of dynamical- and quenched lattice simulations, each performed at three pion masses between 300 MeV$< m_\pi <$ 700 MeV. The resulting values for the fit parameters can be found in table 4.2. The values for all other couplings entering our results are taken from chapter 3 and the literature and are given in table 4.1. The numbers which we find for c_6 and B_{c1} in this fit are well consistent with what we found by an adjustment to the parametrization of reference [FW03] in section 4.4.3 while we find a small deviation for B_{c2}.
Figures 4.6, 4.8 and 4.9 show the quark mass dependencies of the isovector anomalous magnetic moment of the nucleon and the slopes of the Dirac- and the Pauli form factor, respectively. For all three quantities we find very satisfactory chiral extrapolation curves connecting the lattice results at large quark masses with data from phenomenology (which have not been used as input in the fits) in a smooth fashion. All three extrapolation curves do only show a very weak dependence on the quark mass in the domain of the available lattice data but see stronger and stronger influences of the pion-cloud as the pion mass gets to lower values and due to this effect, the physical values for κ_v, ρ_1^v and ρ_2^v are found to be considerably larger then the results found on the lattice – but smaller than the corresponding chiral limit values. Having fixed the fit parameters with the help of lattice data, we are able to predict the values of κ_v, ρ_1^v and ρ_2^v at the physical pion mass. The resulting values, each given with the corresponding statistical error can be found in table 4.3. For all three observables we find very good agreement between the predictions from chirally extrapolated lattice data and phenomenology. However, we have to admit that the phenomenological situation for the slopes is ambiguous since there is quite some inconsistency between the two analyses [FW03, BHM07] to which we compare our results. We find good agreement with both references for ρ_1^v but only with [BHM07] for ρ_2^v. Furthermore, comparing our findings

[2] However, note that the coupling c_6, determining the chiral limit value of κ_v, not only enters our results via a local operator at $\mathcal{O}(p^2)$ but also contributes as a coupling constant in $\mathcal{O}(p^4)$ loop diagrams.

to data from experiments, one has to be aware of the fact that one thereby compares the results of a theory with two active quark flavours to the physical world with an additional, moderately light strange quark. Slight differences between both are therefore expected.
Addressing the question of the range of applicability of ChPT, we conclude from the following three observations which can be made in figures 4.6, 4.8 and 4.9 that our $\mathcal{O}(p^4)$ covariant BChPT results may be applicable for pion masses as large as $m_\pi = 600$ MeV and a breakdown cannot be observed before $m_\pi = 700$ MeV:

- For κ_v and ρ_1^v the $\mathcal{O}(p^3)$ results are found very close to the $\mathcal{O}(p^4)$ results leading us to the conclusion that for those observables BChPT has already converged well at this order. The different orders do not start to deviate significantly below $m_\pi \approx 700$ MeV.
  In contrast, the convergence of the chiral series for ρ_2^v is slower, originating in the fact that in a calculation of the matrix element eq.(4.1) the slope of the Pauli form factor is identified as the prefactor of the structure $\sim \sigma_{\mu\nu} q^\nu q^2$. Three powers of the small momentum q are thus factorized out and a $\mathcal{O}(p^n)$ calculation of the matrix element starts to contribute to ρ_2^v at the power m_π^{n-4}. As a consequence, the quark mass independent counter-term B_{c2} entering this quantity is of order p^4. The appearance of this counter-term is responsible for the large difference between the $\mathcal{O}(p^3)$ and $\mathcal{O}(p^4)$ results for ρ_2^v observed in figure 4.9. The size of order p^4 *pion-cloud* contributions to ρ_2^v is small (at $\lambda = M_0$) and in accordance with expectations from the power-counting analysis below $m_\pi \approx 700$ MeV.

- In eqs. (4.21), (4.30) and (4.37) we give terms which allow for an estimate of possible higher order contributions to κ_v, ρ_1^v and ρ_2^v: Varying the coefficients δ_{κ_v}, $\delta_{\rho_1^v}$ and $\delta_{\rho_1^v}$ of eqs. (4.21), (4.30) and (4.37) between -3 and 3 and performing the fits again, we arrive at arrays of curves which are indicated by the grey shaded bands in figures 4.6, 4.8 and 4.9. In addition to those systematic uncertainties of the ChPT analysis at the next-to-leading one loop level, the considerably smaller statistical uncertainties resulting from the determination of the low energy constants in the fits are also included in the grey shaded bands. Following this analysis we do not expect large higher order contributions to κ_v, ρ_1^v and ρ_2^v for $m_\pi < 700$ MeV.
  Due to the large absolute value of ρ_2^v, the error band in figure 4.9 looks a bit small. We note that for this intrinsically large observable the assumption $-3 < \delta_{\rho_2^v} < 3$ might be too optimistic and the true systematic uncertainty for this quantity may be a bit larger than the one indicated.

- As discussed in detail in chapter 3, the $\overline{\text{IR}}$ renormalization program leads to flat chiral extrapolation functions and πN loops are systematically reduced in this framework as the pion mass takes on larger values. This is in good agreement with the results from lattice simulations at large pion masses where κ_v, ρ_1^v and ρ_2^v do only show very weak pion mass dependence. However, around $m_\pi = 700$ MeV, our BChPT result for the isovector anomalous magnetic moment as a function of the quark mass begins to raise, see figure 4.6. This behaviour, which we consider to be unphysical and such to signal the breakdown of our approach, appears as a consequence of the fact that the subtle balance between different chiral contributions to this observable gets disturbed at very large pion masses. First signals for the breakdown of our approach can thus be seen around $m_\pi \approx 700$ MeV.

Besides the results of covariant BChPT, we show the quark mass dependence of the corresponding $\mathcal{O}(p^4)$ HBChPT results for κ_v, ρ_1^v and ρ_2^v given in eqs.(4.24,4.25), (4.31,4.32) and (4.38,4.39) as the dotted lines in figures 4.7, 4.8 and 4.9. For κ_v and ρ_1^v the curves from the nonrelativistic- and covariant approach start to deviate even below the physical pion mass. This observed early breakdown of the HBChPT results does not allow for chiral extrapolations of presently available lattice data. This comes as a consequence of the fact that the $\left(\frac{m_\pi}{M_0}\right)^i$ terms which sum to flat functions and are all considered to be of the same order in our covariant approach are artificially expanded in the HBChPT framework which such assigns a low order polynomial in $\frac{m_\pi}{M_0}$ to all (Q^2 independent) observables. HBChPT results are thus bound to be acceleratedly in- or decreasing from a certain pion mass on. Typically – see the examples in this chapter and the following one – this value of the pion mass lies around the physical one and the breakdown of HBChPT already occurs at rather small pion

	c_6	$e^r_{106}(\lambda = M_0)$ [GeV^{-3}]	B_{c1} [GeV^{-2}]	B_{c2} [GeV^{-2}]
adjusted to [FW03] (see section 4.4.3)	4.56	0.08 (fixed)	-1.13	5.16
dipole-Q^2-extrapolated (see section 4.6.1)	4.51 ± 0.06	0.06 ± 0.03	-1.17 ± 0.04	7.06 ± 0.25
direct fit (see section 4.6.2)	4.46 ± 0.05	0.10 ± 0.02	-1.31 ± 0.02	4.47 ± 0.16

Table 4.2: The values for the fit parameters determined in three different ways.

masses.
At first sight, the $\mathcal{O}(p^4)$ HBChPT curve for ρ_2^v given in figure 4.9 seems to contradict this general reasoning. However, at the next-to-leading one loop order, the low order polynomial in m_π which is found in HBChPT for this observable only consists of the terms $\sim \frac{1}{m_\pi}$ and ~ 1, see eqs.(4.38,4.39). Thus, the arguments given above apply for ρ_2^v only from order p^5 on where first positive powers of m_π and such again the early breakdown are expected to occur in the HBChPT result. Note, however, that for the numerical comparison of covariant- and nonrelativistic BChPT we use the values for the parameters which we found in the fit of $\mathcal{O}(p^4)$ covariant BChPT results to lattice data[3]. The statements about the early breakdown of HBChPT are therefore made under the assumption that these fits lead to a reasonable estimate of the true value of those coupling constants. In our results we can find a hint which justifies this assumption: Going from $\mathcal{O}(p^3)$ to $\mathcal{O}(p^4)$ in our calculation, we encounter no new fit parameter in ρ_1^v. We can thus study the stability of the value of the parameter B_{c1} by comparing its value in the fit of our $\mathcal{O}(p^4)$ result with the one it would get in a fit of the corresponding $\mathcal{O}(p^3)$ result to lattice data. This analysis confirms the value which we give for B_{c1} since we find that between the two fits this constant only differs about 10% (as can easily be seen comparing the solid and dashed lines in figure 4.8). Furthermore, we note that there are no pion mass dependent counter-terms present in the slopes of the form factors at the order we are working. It is thus obvious from figure 4.8, that no set of parameters can be found which allows to make contact between lattice simulations and phenomenology for ρ_1^v using the $\mathcal{O}(p^4)$ HBChPT results. For κ_v we find a similar behaviour: There is no set of parameters that leads to a reasonable chiral extrapolation curve for this observable based on $\mathcal{O}(p^4)$ HBChPT. In nonrelativistic SSE, a formulation of ChPT with explicit Δ degrees of freedom, however, it is at least possible to reasonably describe the quark mass dependence of κ_v up to larger values of the quark mass [HW02]. The interpolation function calculated in this reference is – within errors – consistent with the analysis presented here.
Finally we also show the $\mathcal{O}(p^4)$ covariant BChPT result for κ_v calculated in standard IR renormalization [KM01] in figure 4.7. The unphysical singularity which can appear in this renormalization program shows up very drastically in this figure and dominates the quark mass dependence of κ_v already slightly above the physical pion mass. This renormalization prescription thus clearly does not lead to a reliable description of quark mass dependencies above the physical pion mass.

4.6.2 Direct fits to the simulation results at finite t

In this section we present a fit of our $\mathcal{O}(p^4)$ BChPT results for $F_1^v(t, m_\pi)$ and $F_2^v(t, m_\pi)$ given in appendix C.3 to lattice data at finite Q^2 and large m_π directly. The fit parameters are again c_6, $e^r_{106}(\lambda)$, B_{c1} and B_{c2}. The available lattice data are located at $Q^2 \approx 0.17$ GeV^2, $Q^2 \approx 0.33$ GeV^2 and larger values of Q^2. The results of section 4.4.3 clearly allow the conclusion that the lowest of these values lies well within the region of applica-

[3] All low energy constants are defined in exactly the same way in both HBChPT and $\overline{\text{IR}}$ renormalized covariant BChPT and are thus bound to ultimately have the same size in both frameworks, see chapter 3.

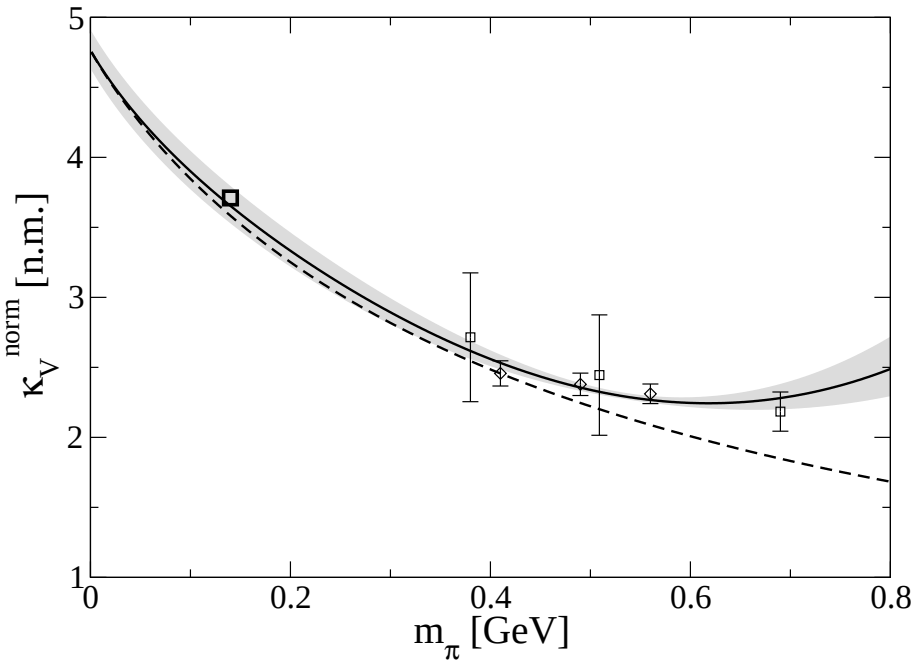

Figure 4.6: The quark mass dependence of the normalized isovector anomalous magnetic moment of the nucleon in covariant BChPT (solid: covariant $\mathcal{O}(p^4)$ BChPT result fitted to the shown dipole-Q^2-extrapolated lattice data; dashed: corresponding $\mathcal{O}(p^3)$ curve with the same set of parameters) and lattice QCD [AKNT06] (squares: dynamical simulations, diamonds: quenched simulations). The bold square represents the physical point [Y$^+$06] not included in the fit. The grey shaded band is an estimate of statistical plus systematic BChPT errors and originates from fits with $\delta_{\kappa_v} = \pm 3$ (see eq.(4.21)) to the data.

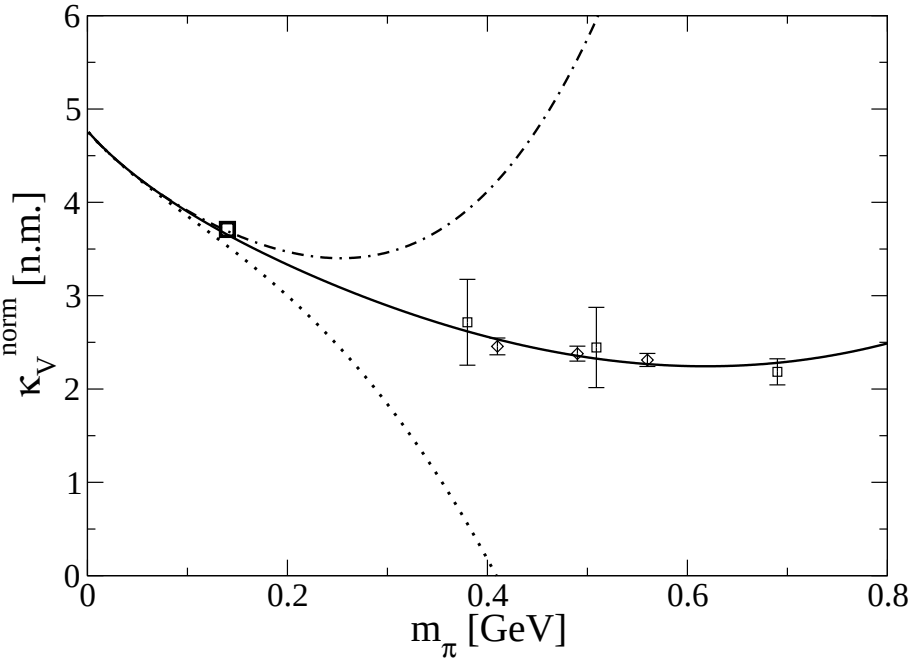

Figure 4.7: The quark mass dependence of the normalized isovector anomalous magnetic moment of the nucleon in three different ChPT frameworks. Solid: $\overline{\text{IR}}$ renormalized covariant BChPT, dashed-dotted: standard IR renormalized BChPT, dotted: HBChPT. All three curves correspond to results at next-to-leading one loop order and are plotted using the same set of parameters, see tables 4.1 and 4.2.

bility of our $\mathcal{O}(p^4)$ BChPT calculation while the second Q^2 value is on the borderline. Therefore, we would like to determine our parameters from a fit to lattice data at $Q^2 \approx 0.17$ GeV^2 and find that this is absolutely sufficient in the case of $F_1(Q^2, m_\pi)$. However, the curves representing the unnormalized $F_2(Q^2, m_\pi)$ for the three different pion masses just happen to cross each other in the vicinity of this value of Q^2. Therefore, to avoid huge uncertainties in the fit, we perform the fit with four free parameters to nine lattice points (at three different quark masses for $F_1^v(Q^2 \approx 0.17$ GeV$^2)$ and three each for $F_2^v(Q^2 \approx 0.17$ GeV$^2)$ and $F_2^v(Q^2 \approx 0.33$ GeV$^2)$). The numerical values for the fit parameters resulting from this fit can again be found in table 4.2. The values for c_6 and $e_{106}^r(\lambda)$ are in good agreement with both the results of the fit to dipole-Q^2-extrapolated data and the adjustment to the phenomenological parametrization of reference [FW03].
The predictions for the physical values of κ_v, ρ_1^v and ρ_2^v resulting from our chiral extrapolation curves can be found in table 4.3. We note that in this table we only give statistical errors; the larger systematic uncertainties are estimated at the end of this section. Keeping this in mind, we find good agreement between the BChPT fits to both dipole-Q^2-extrapolated data and to lattice results directly on the one side and phenomenology on the other side for κ_v, ρ_1^v and – with larger systematic uncertainties – for ρ_2^v. For ρ_1^v, the direct fit leads to a value which is a bit smaller than the one found in the fit to dipole-Q^2-extrapolated data. This difference is even more pronounced in the slope of $F_2^v(Q^2)$. A reason for this is given by the fact that (as can be seen in figure 4.10) the dipole ansatz shows more curvature in the Q^2 dependence of these form factors than the $\mathcal{O}(p^4)$ BChPT result does. To describe the same data at finite Q^2, this effect is compensated by smaller values for the slopes in $\mathcal{O}(p^4)$ BChPT. These curves are therefore not as steep at very low Q^2 and do not bend upwards as strongly as the ones based on a dipole ansatz.
Figure 4.10 shows the resulting Q^2 dependence of the $\mathcal{O}(p^4)$ BChPT result for $F_1^v(Q^2, m_\pi)$ at the physical pion mass and the three pion masses for which lattice data are available at low Q^2. For comparison we also show the phenomenological parametrization of reference [FW03]. The Q^2 dependence of the $\mathcal{O}(p^4)$ BChPT result for $F_2^v(Q^2)$ at the pion masses of the lattice simulations and the corresponding curve at the physical pion

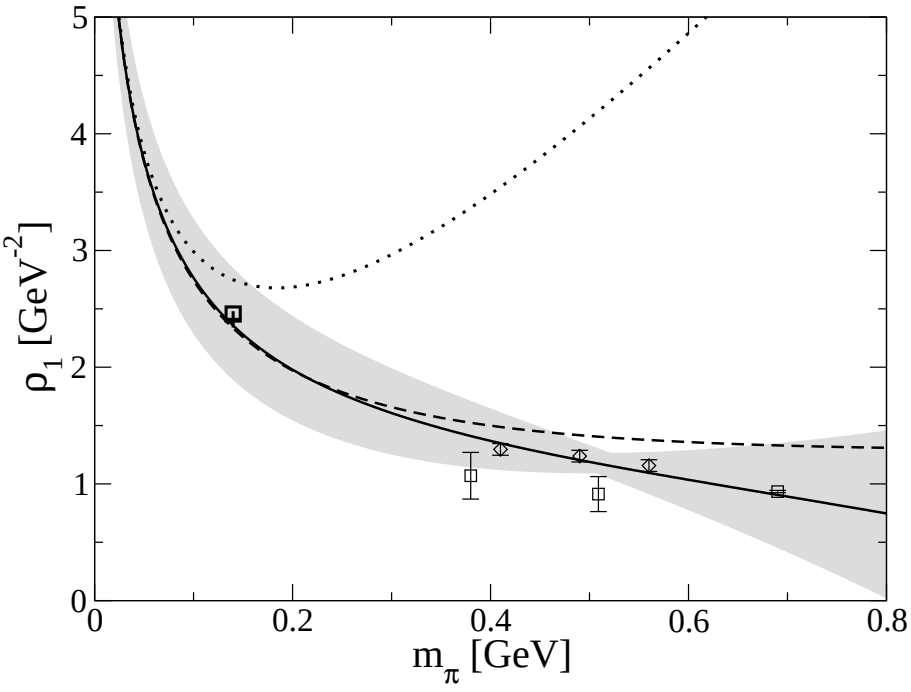

Figure 4.8: The quark mass dependence of the slope of the isovector Dirac form factor in covariant BChPT (solid: covariant $\mathcal{O}(p^4)$ BChPT result fitted to the shown dipole-Q^2-extrapolated lattice data, dashed: corresponding $\mathcal{O}(p^3)$ curve, dotted: $\mathcal{O}(p^4)$ HBChPT result, all with the same set of parameters) and lattice QCD [AKNT06]. The points for physical quark masses are from the analyses of references [FW03] (cross) and [BHM07] (square). The grey shaded band indicates the size of statistical plus systematic ChPT errors estimated via fits with $\delta_{\rho_1^v} = \pm 3$ (see eq.(4.30)) to the data.

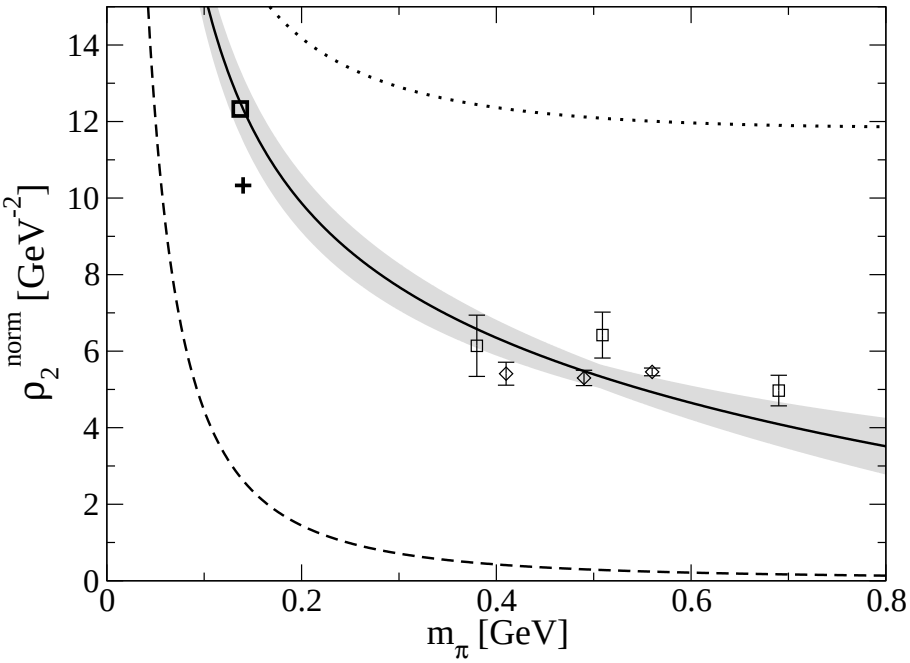

Figure 4.9: The quark mass dependence of the slope of the normalized isovector Pauli form factor in covariant BChPT (solid: covariant $\mathcal{O}(p^4)$ BChPT result fitted to the shown dipole-Q^2-extrapolated lattice data, dashed: corresponding $\mathcal{O}(p^3)$ curve, dotted: $\mathcal{O}(p^4)$ HBChPT result, all with the same set of parameters) and lattice QCD [AKNT06]. The points for physical quark masses are from the analyses of references [FW03] (cross) and [BHM07] (square). The grey shaded band indicates the size of statistical plus systematic ChPT errors estimated via fits with $\delta_{\rho_2^v} = \pm 3$ (see eq.(4.37)) to the data.

mass again together with the findings of reference [FW03] can be found in figure 4.11. In those figures one can observe that $\mathcal{O}(p^4)$ BChPT bridges the broad gap between the lattice results and phenomenology for both form factors and that the predicted Q^2 dependencies of the form factors at the physical point are in reasonable agreement (see the discussion of systematic uncertainties below) with the parametrization of ref.[FW03] up to $Q^2 \approx 0.3$ GeV ^{2}. Moreover, one can see in figure 4.10 that at larger values of Q^2 the lattice results show more curvature in the Q^2 dependence of the Dirac form factor than the corresponding $\mathcal{O}(p^4)$ BChPT results.
In figure 4.12 we show the quark mass dependence of κ_v in $\mathcal{O}(p^4)$ covariant BChPT resulting from an extraction of the low energy constants at finite Q^2 directly and compare it to the findings of the previous section where dipole-Q^2-extrapolated data were used as input. This figure demonstrates that the lattice data would lie a bit lower if one were to use ChPT instead of the dipole ansatz in order to extrapolate them down to $Q^2 = 0$.
The grey shaded bands around the BChPT results in figures 4.10, 4.11 and 4.12 indicate the size of statistical errors. However, since the shown lattice data which serve as input for our analysis were all found on the same lattice, the errors attached to those data are presumably correlated. Our analysis of statistical errors in contrast assumes uncorrelated errors on the input data and thus probably leads to too optimistic estimates for the statistical errors.
In addition to those errors which arise solely due to the statistics of the fits, there are of course systematic errors from both lattice simulations and the BChPT analysis. One source for systematic uncertainties lies in the possibility of lattice artifacts like finite size effects and discretization errors. The following procedure might give an estimate for the size of those uncertainties:
The direct fits have been performed to unnormalized data for $F_2^v(t, m_\pi)$, i.e. data which have been projected out of the matrix element eq.(4.1) at the local mass of the nucleon $M^{(n)} = M_N(m_\pi)$. However, comparing the quark mass dependence of M_N given in reference [AKNT06] with the one gained in chapter 3 by a fit to lattice data from reference [AK$^+$04], we find slight inconsistencies which can only arise due to such lattice artifacts. Thus the normalization of the lattice results which we use to fit the form factors is – numerically – done slightly different than the one of our ChPT results. Fitting our normalized formula directly to normalized lattice data we find $\kappa_v = 3.83 \pm 0.1$, $B_{c1} = (-1.57 \pm 0.015)$ GeV^{-2} and $B_{c2} = (4.95 \pm 0.07)$ GeV^{-2}, indicating that in addition to the statistical errors, there is an approximate 10% uncertainty due to the specific conditions of lattice simulations.
Furthermore, there are of course uncertainties arising from the fact that higher chiral orders have been neglected in our analysis. The leading contributions beyond the next-to-leading one loop order are for $F_1^v(t, m_\pi)$ of the form $\frac{m_\pi^2 t}{(4\pi F_\pi)^4}$ and $\frac{t^2}{(4\pi F_\pi)^4}$; for $F_2^v(t, m_\pi)$ they are $\frac{M^{(n)} m_\pi t}{(4\pi F_\pi)^4}$ and $\frac{M^{(n)} m_\pi^3}{(4\pi F_\pi)^4}$. Assuming couplings of natural size in front of these structures (i.e. couplings with numerical values between -3 and 3), the possible variation of the form factors due to those terms at the (Q^2, m_π) values at which we fixed our parameters is in average on the 20% level. This value gives an indication for the size of the systematic errors of the $\mathcal{O}(p^4)$ ChPT analysis which have to be attached to our predictions given in table 4.2. The best premise for an improvement of the precision of predictions from chiral extrapolations would be the existence of lattice data at lower values of m_π since e.g. the error for the $\mathcal{O}(p^4)$ BChPT result for κ_v scales with m_π^3. The systematic uncertainties of the chiral extrapolation functions can of course also be diminished if the ChPT analyses are carried out at higher orders. However, a ChPT calculation of the form factors at higher orders would contain a number of so far undetermined low energy constants and the smaller systematic uncertainties would therefore have to be paid with larger statistical errors.
Given the present accuracy of our chiral analysis of lattice data and the ambiguous situation for the phenomenology of the slopes of the nucleon form factors, we find good agreement between the predictions from chiral extrapolations and phenomenology for all examined quantities. This leads us to the conclusion that lattice simulations together with BChPT are a powerful and trustworthy tool for predictions of physical observables.

4.6.3 A glance at the quark mass dependence in the isoscalar channel

In this section we present a brief numerical discussion of the quark mass dependence of the isoscalar nucleon form factors. In particular we examine the $\mathcal{O}(p^4)$ BChPT results for the observables κ_s, ρ_1^s and ρ_2^s given in

	κ_v	ρ_1 [GeV^{-2}]	ρ_2 [GeV^{-2}]
direct fit	3.58 ± 0.06	2.22 ± 0.03	9.60 ± 0.3
dipole-Q^2-extrapolated	3.65 ± 0.06	2.37 ± 0.04	12.3 ± 0.3
reference [FW03]	3.71	2.41	10.3
reference [BHM07]	3.71	2.46	12.3

Table 4.3: The predictions resulting from the different fits to lattice data. The errors are purely statistical errors and do not take into account any systematic uncertainties.

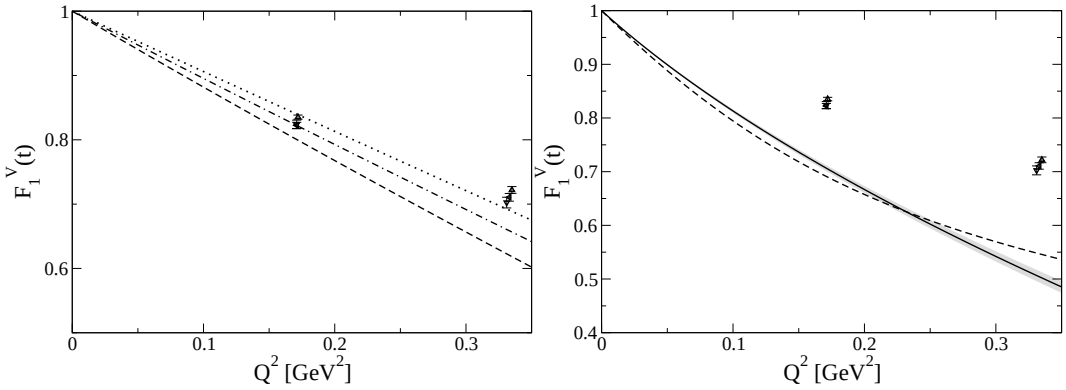

Figure 4.10: Left Panel: The $\mathcal{O}(p^4)$ BChPT result for the momentum transfer dependence of the Dirac form factor. The shown curves correspond to pion masses of 410 MeV (dashed), 490 MeV (dashed-dotted) and 560 MeV (dotted). Right Panel: The $\mathcal{O}(p^4)$ BChPT prediction for the Dirac form factor at the physical pion mass resulting from a fit to lattice data at finite Q^2 directly. The tiny grey shaded area indicates statistical errors. For comparison we show the parametrization of reference [FW03] (dashed curve). Lattice data are from [Ale].

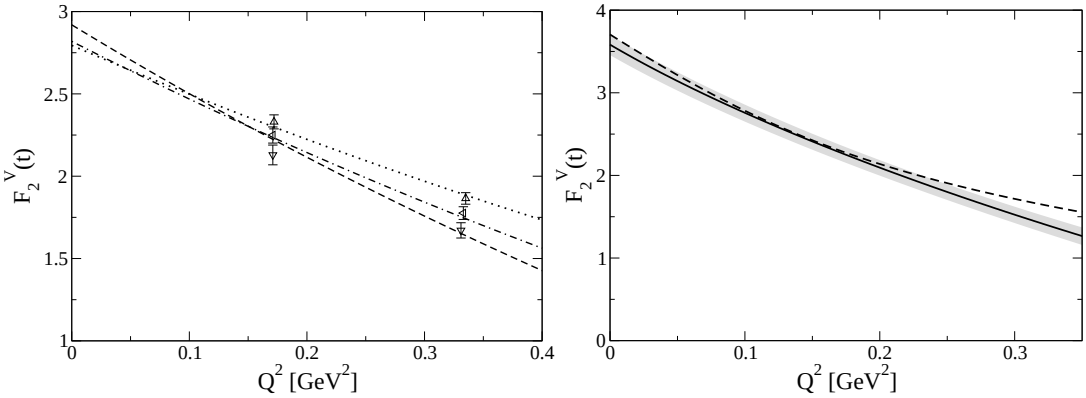

Figure 4.11: Left Panel: The $\mathcal{O}(p^4)$ BChPT result for the momentum transfer dependence of the unnormalized Pauli form factor. The shown curves correspond to pion masses of 410 MeV (dashed), 490 MeV (dashed-dotted) and 560 MeV (dotted). Right Panel: The prediction for the momentum transfer dependence of the Pauli form factor at the physical pion mass as resulting from the combined fit of the $\mathcal{O}(p^4)$ BChPT result to lattice data at finite Q^2 (black) and the corresponding statistical errors (grey shaded). For comparison we also show the parametrization of reference [FW03] (dashed). Lattice data are from [Ale].

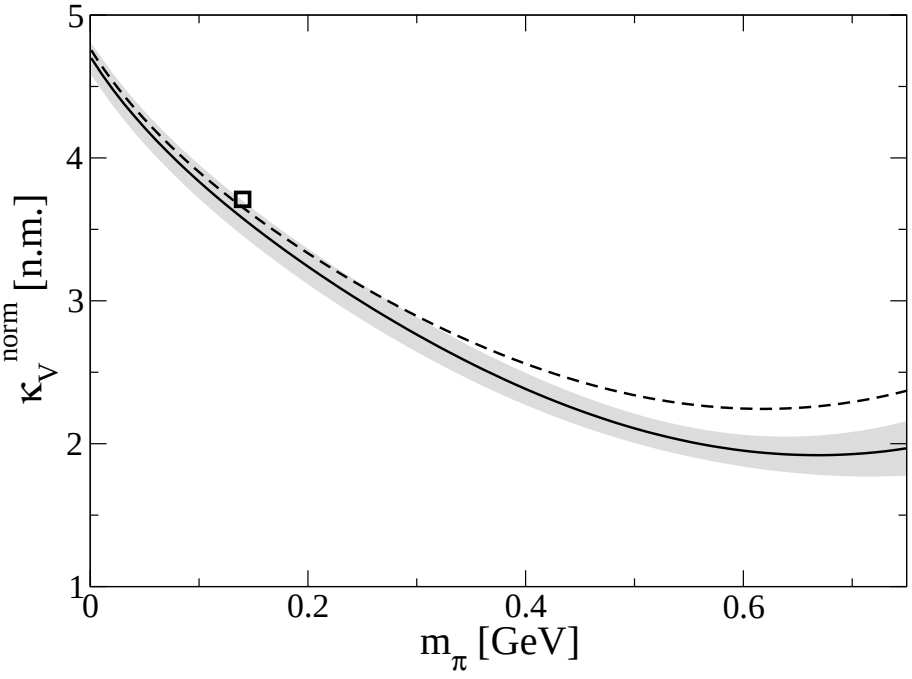

Figure 4.12: The quark mass dependence of the isovector anomalous magnetic moment of the nucleon in covariant BChPT. The solid line corresponds to a fit of $\mathcal{O}(p^4)$ BChPT to quenched lattice data at finite Q^2. The grey shaded band indicates the statistical error for this fit. For comparison we give the result of the fit to dipole-Q^2-extrapolated data (dashed line).

κ_s	$e^r_{105}(M_0)$ [GeV^{-3}]	B^s_{c1} [GeV^{-2}]	B^s_{c2} [GeV^{-2}]
-0.20	0.46	2.92	-0.334

Table 4.4: The values for the parameters entering the isoscalar form factors estimated via a comparison to the phenomenological parametrization of reference [FW03]. Due to the very weak dependence of the results at physical pion masses on $e^r_{105}(\lambda)$, we have again used the quark mass dependence of κ_s to determine the size of this coupling.

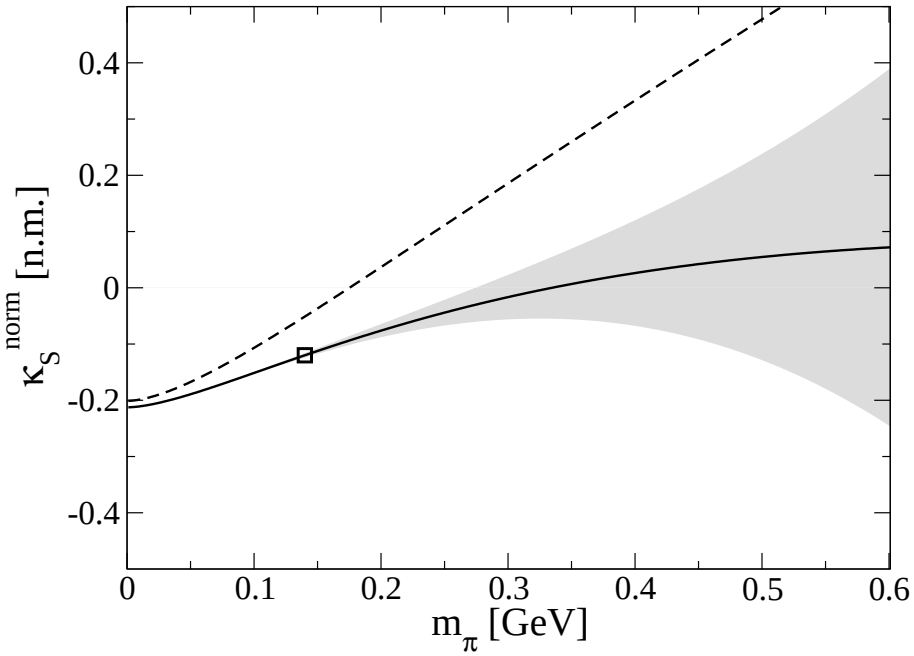

Figure 4.13: The quark mass dependence of the normalized isoscalar anomalous magnetic moment of the nucleon in covariant BChPT (solid: $\mathcal{O}(p^4)$, dashed: $\mathcal{O}(p^3)$). The unknown counter-term $e^r_{105}(\lambda)$ is varied around the value which generates a plateau in the function $\kappa_s(m_\pi)$. The grey shaded band indicates the size of possible chiral corrections arising at $\mathcal{O}(p^5)$, its boundaries are curves with $\delta_{\kappa_s} = \pm 3$ (see eq.(4.48)).

sections 4.5.1 and 4.5.2, respectively. As already mentioned earlier we only find small contributions from the pion-cloud at one loop order and assume two loop effect to play an important role in the isoscalar sector. Since the *relative* size of higher order effects might therefore be large in the isoscalar sector, we abstain from a similarly elaborate discussion as for the isovector form factors. All results presented in this section really just constitute a first glance at the quark mass dependence of the isoscalar form factors. However, two loop contributions are suppressed by powers of m_π^n divided by some large scale where $n = 3$ in the case of κ_s, $n = 2$ in the case of ρ_1^s and $n = 1$ for ρ_2^s. Therefore, the next-to-leading one loop order results can at least give a reliable description of the quark mass dependence in a region close to the chiral limit.

Figure 4.13 shows the quark mass dependence of the isoscalar anomalous magnetic moment of the nucleon as it is predicted by $\mathcal{O}(p^4)$ BChPT. The couplings κ_s^0 and $e^r_{105}(\lambda)$ have been adjusted such that the phenomenological value of this quantity at the physical pion mass [Y$^+$06] is reproduced and that the curve plateaus at large pion masses. Figures 4.14 and 4.15 show the quark mass dependencies of the slopes of the isoscalar Dirac- and Pauli form factor, respectively. The numerical values for the counter-terms B^s_{c1} and B^s_{c2} are determined by the condition that – at the physical point – those curves hit the values given in reference [FW03] for those quantities. All resulting values for the ChPT couplings can be found in table 4.4.

The position of the plateau which we find for κ_s, see figure 4.13, is consistent with the results of the lattice simulations at very large pion masses [G$^+$05]. However, disconnected diagrams (diagrams where the incoming photon does not couple to a valence quark directly) can contribute to isoscalar observables but are neglected in present day lattice simulations of nucleon form factors leading to uncontrolled systematic errors in the lattice results.

As already discussed in section 4.5.3 the pion-cloud contributions to ρ_1^s and ρ_2^s are small at the order we are working, resulting in an only weak dependence of those quantities on the pion mass.

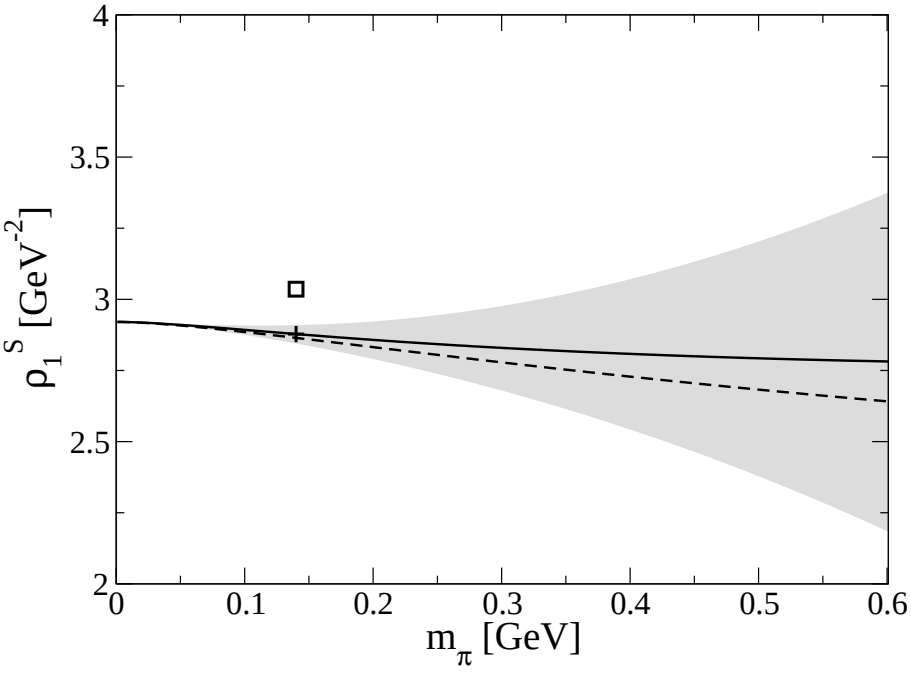

Figure 4.14: The quark mass dependence of the slope of the isoscalar Dirac form factor in covariant BChPT (solid: $\mathcal{O}(p^4)$, dashed: $\mathcal{O}(p^3)$). The points at the physical quark masses are from the analyses of references [FW03] (cross) and [BHM07] (square). The grey shaded band indicates the size of possible chiral corrections arising at $\mathcal{O}(p^5)$, its boundaries are curves with $\delta_{\rho_1^s} = \pm 3$ (see eq.(4.54)).

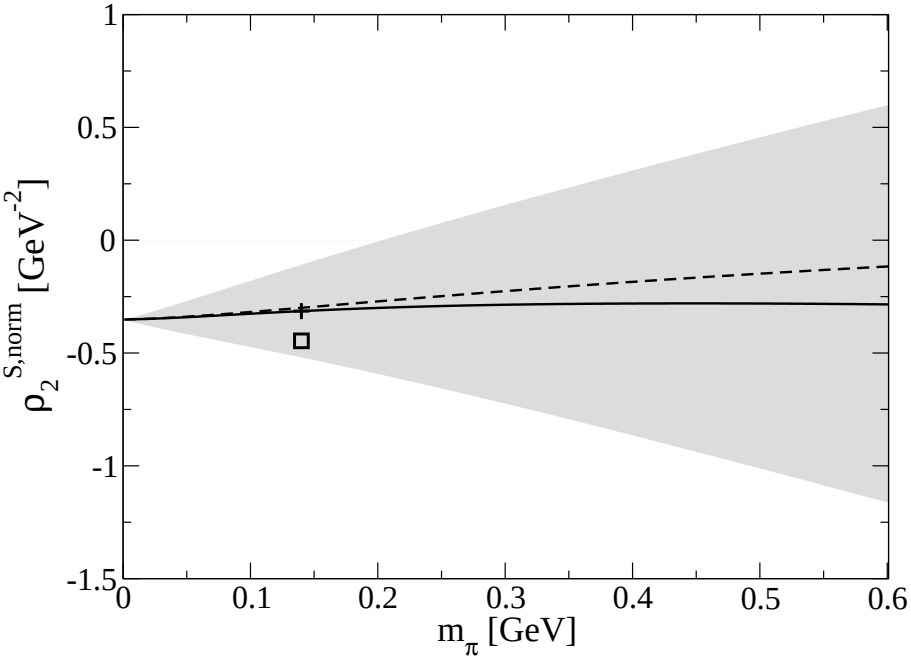

Figure 4.15: The quark mass dependence of the slope of the normalized isoscalar Pauli form factor in covariant BChPT (solid: $\mathcal{O}(p^4)$, dashed: $\mathcal{O}(p^3)$). The points at the physical quark masses are from the analyses of references [FW03] (cross) and [BHM07] (square). The grey shaded band indicates the size of possible chiral corrections arising at $\mathcal{O}(p^5)$, its boundaries are curves with $\delta_{\rho_2^s} = \pm 3$ (see eq.(4.59)).

4.7 Summary and Conclusions

The pertinent results of this chapter can be summarized as follows:

1. We have calculated the isoscalar- and isovector vector form factors of the nucleon up to next-to-leading one loop order – corresponding to order p^4 – in covariant BChPT using the $\overline{\text{IR}}$ renormalization prescription developed in the previous chapter. Analytic results for the full momentum transfer- and quark mass dependence of the form factors are given in the appendix of this work, the anomalous magnetic moments and the slopes of the form factors as a function of the pion mass are given in this chapter. Together with the covariant results, we always presented the corresponding expressions in HBChPT.

2. Covariant BChPT predicts the isovector observables κ_v, ρ_1^v and ρ_2^v to decrease, with decreasing gradient, as a function of the quark mass and to finally take on values which are considerably smaller than the physical ones, in accordance with lattice simulations. The Q^2 dependence of the BChPT result for the isovector form factors shows less curvature at small Q^2 than the analyses in other approaches.

3. In the isoscalar sector we found short distance contributions – at least at order p^4 – to dominate the BChPT results. In our approach we therefore found the isoscalar form factors to be linear in Q^2 and an only very weak dependence of ρ_1^v and ρ_2^v on the pion mass.

4. The quark mass dependence of the mass of the nucleon entered our results in two ways: Firstly, it appeared in the prefactor of the Pauli form factor in the vector current of the nucleon and hence as an overall prefactor in all cases where we compared our results to unnormalized lattice data for the Pauli form factor. Secondly, at order p^4 first pion mass dependent corrections to the mass of the nucleon occurred in the loop calculations. We have accounted for those effects by a resummation of all quark mass dependent insertions on the nucleon propagator, i.e. identified $M_N = M_N(m_\pi)$ as the propagating nucleon mass since we considered a comparison of BChPT results depending on the leading quark mass dependence of the nucleon – which is known to only describe the true quark mass dependence at very low values of the pion mass – with lattice data at large pion masses to be inconsistent.

5. We have compared the $\mathcal{O}(p^4)$ BChPT results for the isovector electromagnetic Sachs form factors with the phenomenological parametrization of reference [FW03] and found the ChPT result to provide a satisfactory description of the momentum transfer dependence of the nucleon form factors at the physical pion mass up to $Q^2 \approx 0.25$ GeV^2. We showed that the chiral expansion does display a clear convergence towards the phenomenological parametrization and that the deviations between both are within the accuracy of the effective field theory calculation at this order.

6. Comparing our findings to the standard dipole parametrization for the momentum transfer dependence of the form factors, we found slight deviations between this ansatz and $\mathcal{O}(p^4)$ BChPT in the momentum transfer dependence of the Dirac form factor.

7. We have performed chiral extrapolations of lattice data for the isovector nucleon form factors in two different ways: The first was to extrapolate lattice data at finite Q^2 to the forward limit using a dipole ansatz and to subsequently perform chiral extrapolations for the anomalous magnetic moment and the slopes of the form factors. The second approach was to directly fit the $\mathcal{O}(p^4)$ BChPT result to lattice data at different values of m_π and Q^2 and to perform chiral extrapolations for the full momentum transfer dependent functions.

8. Chiral extrapolations of lattice data for the isovector anomalous magnetic moment and the slopes of the isovector form factors were performed using the $\mathcal{O}(p^4)$ covariant BChPT results. The findings were satisfactory in many ways: First of all, the predictions of chirally extrapolated lattice data were in every case in good agreement with phenomenology. Secondly, systematic uncertainties of the chiral analysis were found to be small over a large range of pion masses and, thirdly, a good convergence pattern of the chiral expansion was found for all observables under consideration.

9. We have studied the quark mass dependence of the $\mathcal{O}(p^4)$ HBChPT and IR renormalized BChPT results for κ_v and the $\mathcal{O}(p^4)$ HBChPT results for ρ_1^v and ρ_2^v. We diagnosed a breakdown of all those results in the vicinity of the physical pion mass and found that lattice data for those quantities cannot be chirally extrapolated in these frameworks. We therefore consider covariant calculations in the $\overline{\text{IR}}$ renormalization scheme to be essential in order to arrive at reliable chiral extrapolation functions.

10. We have performed the first fits of ChPT results to lattice data for the isovector form factors at finite Q^2. The resulting chiral extrapolation curves were again satisfactory and allow for a prediction of the momentum transfer dependence of the nucleon form factors at the physical point with a 20% uncertainty up to $Q^2 \approx 0.3$ GeV^2.

11. The prediction of $\mathcal{O}(p^4)$ covariant BChPT for the quark mass dependence of the isoscalar form factors of the nucleon was discussed. Due to a lack of reliable lattice data and the expectation that two loop effects might be essential in this channel we did not perform chiral extrapolations for isoscalar quantities.

12. The values for the fit parameters determined in the different fits throughout this chapter are all in reasonable agreement and within natural size.

In conclusion, covariant BChPT at next-to-leading one loop order provides – at least in the isovector sector – very reasonable chiral extrapolation functions which may be applicable at quark masses as large as $m_\pi = 600$ MeV. All observables discussed in this chapter support the statement that trustworthy predictions for physical observables using lattice results as input can be obtained in this framework. Therefore, our hope is that future studies of nucleon form factors on the lattice rely on covariant $\overline{\text{IR}}$ renormalized BChPT in order to make contact between the domain of large quark masses and the physical world.

Chapter 5

The Generalized Form Factors of the Nucleon

5.1 Introduction

About a decade ago the concept of Generalized Parton Distributions (GPDs) has emerged among theorists, constituting a universal framework bringing a host of seemingly disparate nucleon structure observables like form factors, moments of parton distribution functions, etc. under one theoretical roof. For reviews of this very active field of research we refer to references [Ji98, Die03, BR05].
Working in twist-two approximation, the parity-even part of the structure of the nucleon is encoded in two Generalized Parton Distribution functions $H^q(x,\xi,t)$ and $E^q(x,\xi,t)$. For a process where the incoming (outgoing) nucleon carries the four-momentum p_1^μ (p_2^μ) we define two new momentum variables

$$q^\mu = p_2^\mu - p_1^\mu; \quad \bar{p} = (p_1^\mu + p_2^\mu)/2. \tag{5.1}$$

The GPDs can e.g. be accessed in Deeply Virtual Compton Scattering (DVCS) off the nucleon where – in the parton model of the nucleon – the GPD variable x can be interpreted as the fraction of the total momentum of the nucleon carried by the probed quark q. $t = q^2$ denotes the total four-momentum transfer squared to the nucleon, whereas the "skewdness" variable $\xi = -n \cdot q/2$ with $n \cdot \bar{p} = 1$ interpolates between the t- and the x dependence of the GPDs, for details see the reviews [Ji98, Die03, BR05].
The three-dimensional parameter space of GPDs is vast and rich in information about nucleon structure. The experimental program for their determination is only at the beginning at laboratories like CERN, Desy, JLAB, etc. [Ji98, Die03, BR05]. However, moments of GPDs can be interpreted much easier and are connected to well established hadron structure observables. E.g. the zeroth order Mellin moments in the variable x correspond to the contribution of quark q to the well known Dirac- and Pauli form factors $F_1(t)$ and $F_2(t)$ of the nucleon which were discussed in the previous chapter:

$$\int_{-1}^{1} dx\, H^q(x,\xi,t) = F_1^q(t), \tag{5.2}$$

$$\int_{-1}^{1} dx\, E^q(x,\xi,t) = F_2^q(t). \tag{5.3}$$

In this chapter we focus on the *first* moments in x of these nucleon GPDs

$$\int_{-1}^{1} dx\, x\, H^q(x,\xi,t) = A_{2,0}^q(t) + (-2\xi)^2 C_{2,0}^q(t), \tag{5.4}$$

$$\int_{-1}^{1} dx\, x\, E^q(x,\xi,t) = B_{2,0}^q(t) - (-2\xi)^2 C_{2,0}^q(t), \tag{5.5}$$

where one encounters *three generalized form factors* $A_{2,0}^q(t)$, $B_{2,0}^q(t)$ and $C_{2,0}^q(t)$ of the nucleon for each quark flavour q. For the case of two light flavours the *generalized isoscalar and isovector form factors* have been analysed in a series of papers at leading one loop order in the nonrelativistic framework of HBChPT, starting with

the pioneering analyses of Chen and Ji as well as Belitsky and Ji [CJ02, BJ02, ACK06, DMS06a, DMS06b]. In this chapter we provide the first analysis of these generalized form factors utilizing the methods of covariant Baryon Chiral Perturbation Theory (BChPT) for two light flavours pioneered in reference [GSS88]. The leading one loop order calculation presented here again relies on the $\overline{\text{IR}}$ renormalization prescription introduced in chapter 3 which we consider to be inevitable for a consistent analysis of quark mass dependencies in BChPT. However, a disclaimer has to be added: Since the calculation presented here is only performed at leading one loop order, systematic errors due to possible higher order effects are of course larger then they were in the previous chapter where an analysis at next-to-leading one loop order was presented and the convergence properties of the chiral expansion for the pion-cloud effects cannot be studied in this chapter. Therefore we cannot give an as elaborate discussion of chiral extrapolations as in the previous chapter, although we show that – at least for some observables – a satisfying description of the quark mass dependencies up to the domain of presently available lattice data with moderate errors is already possible at this stage.
Since we are going to compare our findings to the previous analyses in the nonrelativistic theory throughout this chapter, we note again that (at $t = 0$) a covariant BChPT calculation differs from a nonrelativistic one – provided both are performed at the same chiral order D – by an infinite series of terms $\sim (m_\pi/M_0)^i$ where M_0 denotes the mass of the nucleon in the chiral limit, estimated to be around 890 MeV, see chapter 3. As already observed in chapter 4, such terms quickly become relevant once the pion mass m_π takes on values larger than 140 MeV, as it typically occurs in present day lattice QCD simulations of generalized form factors. Aside from this resummation property in $(1/M_0)^i$, we emphasize again, that the power-counting analysis determining possible operators and allowed topologies for loop diagrams at a particular chiral order (see section 5.3.3) is *identical* between covariant and nonrelativistic frameworks. Both schemes organize a perturbative calculation as a power series in $(1/(4\pi F_\pi))^D$. Finally we note that the first moments of nucleon GPDs have also been studied in constituent quark models (e.g. see ref.[BPT03]) and chiral quark soliton models (e.g. see ref.[G$^+$07]) of the nucleon which – in contrast to ChEFT – can also provide dynamical insights into the short-distance structure present in the generalized form factors.
This chapter is organized as follows: In the next section we specify the operators with which we are going to obtain information on the three generalized isoscalar and the three generalized isovector form factors of the nucleon. In section 5.3 we portray the effective chiral Lagrangean required for the calculation, immediately followed by the sections containing our leading one loop order results of the generalized form factors in the isovector (section 5.4) and in the isoscalar (section 5.5) matrix elements. A summary of the main results concludes this chapter while a few technical details regarding the calculation of the amplitudes in covariant BChPT are relegated to the appendix section D. We have already published the main results of this chapter in reference [DGH07].

5.2 Extracting the First Moments of GPDs

5.2.1 The generalized form factors of the nucleon

In eqs.(5.4,5.5) of the introduction of this chapter it was shown that the first moments of nucleon GPDs are connected to three generalized form factors. In lattice QCD one can directly access the contribution of quark flavour q to these generalized form factors of the nucleon by evaluating the matrix element of the QCD energy-momentum (and angular-momentum density) tensor for this quark flavour [Ji98, Die03, BR05]

$$i\langle p_2|\overline{q}\gamma_{\{\mu}\overleftrightarrow{D}_{\nu\}}\,q|p_1\rangle \;=\; \overline{u}(p_2)\left[A^q_{2,0}(q^2)\gamma_{\{\mu}\overline{p}_{\nu\}} - \frac{B^q_{2,0}(q^2)}{2M_N}\,q^\alpha i\sigma_{\alpha\{\mu}\overline{p}_{\nu\}} + \frac{C^q_{2,0}(q^2)}{M_N}\,q_{\{\mu}q_{\nu\}}\right]u(p_1). \tag{5.6}$$

The brackets $\{\ldots\}$ denote the completely symmetrized and traceless combination of all indices: $a_{\{\mu}b_{\nu\}} = a_\mu b_\nu + a_\nu b_\mu - \frac{2}{d}g_{\mu\nu}a\cdot b$. In eq.(5.6), $u\,(\overline{u})$ is a Dirac spinor of the incoming (outgoing) nucleon of mass M_N

for which the quark matrix element is evaluated (recall the discussion after eq.(4.1) [1]) and the generalized form factors $A(q^2)$, $B(q^2)$ and $C(q^2)$ are real functions of the momentum transfer squared. In ChEFT we employ the same philosophy and also extract information about the first moments of nucleon GPDs of eq.(5.4,5.5) via a calculation of the generalized form factors according to eq.(5.6). We evaluate the current on the right hand side of eq.(5.6) using the methods of covariant BChPT in complete analogy to the calculation of the vector current given in eq.(4.1) with the only difference being that, in this chapter, not an external vector source v_μ but an external (symmetric an traceless) tensor source $v_{\mu\nu}$ is coupling to the current.
Studying a strongly interacting system with two light flavours in the nonperturbative regime of QCD with the methods of ChEFT one works in the basis of singlet (s) and triplet (v) contributions of the quarks to the three form factors:

$$i\langle p_2|\overline{q}\gamma_{\{\mu}\overleftrightarrow{D}_{\nu\}}\,q|p_1\rangle_{u+d} = \overline{u}(p_2)\left[A^s_{2,0}(q^2)\gamma_{\{\mu}\overline{p}_{\nu\}} - \frac{B^s_{2,0}(q^2)}{2M_N}\,q^\alpha i\sigma_{\alpha\{\mu}\overline{p}_{\nu\}} + \frac{C^s_{2,0}(q^2)}{M_N}\,q_{\{\mu}q_{\nu\}}\right]\frac{\mathbb{1}}{2}\,u(p_1), \tag{5.7}$$

$$i\langle p_2|\overline{q}\gamma_{\{\mu}\overleftrightarrow{D}_{\nu\}}\,q|p_1\rangle_{u-d} = \overline{u}(p_2)\left[A^v_{2,0}(q^2)\gamma_{\{\mu}\overline{p}_{\nu\}} - \frac{B^v_{2,0}(q^2)}{2M_N}\,q^\alpha i\sigma_{\alpha\{\mu}\overline{p}_{\nu\}} + \frac{C^v_{2,0}(q^2)}{M_N}\,q_{\{\mu}q_{\nu\}}\right]\frac{\tau^a}{2}\,u(p_1). \tag{5.8}$$

Note that the 2×2 unit matrix $\mathbb{1}$ and the Pauli matrices τ^a with $a = 1, 2, 3$ on the right hand sides of eqs.(5.7,5.8) operate in the space of a (proton,neutron) doublet field.
At present not much is known yet experimentally about the momentum dependence of these 6 form factors. The main source of information at the moment is provided by lattice QCD studies of these objects (e.g. see refs.[G$^+$04, H$^+$03, E$^+$06, H$^+$07]). Given that present day lattice simulations work with quark masses much larger than those realized for u and d quarks in the standard model, one also needs to know the quark mass dependence of all 6 form factors in order to extrapolate the lattice QCD results down to the real world of light u and d quarks. This information is also encoded in the ChEFT results, typically expressed in form of a pion mass dependence of the observables under study. For the quark mass dependence of the generalized form factors we again perform a double tracked analysis: On one side we extract numerical values for presently unknown ChPT coupling constants by a fit of the pion mass dependent BChPT results to lattice data at different quark masses. On the other side, the EFT framework provides an extrapolation function bridging the gap between the domain of large quark masses used in present day lattice simulations and the physical world of small quark masses. With this combined lattice plus ChPT analysis we are again able to give predictions for physical observables and in the case of the generalized form factors of the nucleon some of theses prediction come prior to first results from experiments.
Allowing variable quark masses in the currents eqs.(5.7,5.8) leads to a further complication in the analysis: One needs to be aware that it is *common practice in current lattice QCD analyses* that the mass parameter M_N in those currents does *not* correspond to the physical mass of a nucleon, instead, it represents a larger nucleon mass consistent with the values of the quark masses employed in the simulation. In order to compare BChPT results with the outcome of lattice simulations one therefore has to know the quark mass dependence of the mass of the nucleon appearing in the currents eqs. (5.7) and (5.8).

[1] In this chapter we do not indicate the normalizing mass in the currents independent of the other appearing masses like we did in the previous chapter but use the local nucleon mass $M_N(m_\pi)$ as the normalizing mass in the above definitions of the form factors throughout this chapter.

g_A	F_π [GeV]	M_0 [GeV]	c_1 [GeV^{-1}]	c_2 [GeV^{-1}]	c_3 [GeV^{-1}]	e_1^r(1GeV) [GeV^{-3}]
1.2	0.0924	0.889	-0.817	3.2	-3.4	1.44

Table 5.1: Input values used in this chapter for the numerical analysis of the chiral extrapolation functions.

In this chapter we utilize the $\mathcal{O}(p^4)$ BChPT result found in chapter 3:

$$\begin{aligned} M_N(m_\pi) &= M_0 - 4c_1 m_\pi^2 + \frac{3g_A^2 m_\pi^3}{8\pi^2 F_\pi^2 \sqrt{4-\frac{m_\pi^2}{M_0^2}}}\left(-1+\frac{m_\pi^2}{4M_0^2}+c_1\frac{m_\pi^4}{M_0^3}\right)\arccos\left(\frac{m_\pi}{2M_0}\right) \\ &\quad +4e_1^r(\lambda)m_\pi^4 - \frac{3m_\pi^4}{128\pi^2F_\pi^2}\left[\left(\frac{6g_A^2}{M_0}-c_2\right)+4\left(\frac{g_A^2}{M_0}-8c_1+c_2+4c_3\right)\log\left(\frac{m_\pi}{\lambda}\right)\right] \\ &\quad -\frac{3c_1 g_A^2 m_\pi^6}{8\pi^2F_\pi^2M_0^2}\log\left(\frac{m_\pi}{M_0}\right)+\mathcal{O}(p^5). \end{aligned} \tag{5.9}$$

Possible effects of higher orders can be estimated as $\mathcal{O}(p^5) \sim \delta_M \frac{m_\pi^5}{(4\pi F_\pi)^4}$ where δ_M could be varied within natural size estimates $-3 < \delta_M < +3$ and were found to be small below $m_\pi \approx 700$ MeV in chapter 3.
We note that the trivial, purely kinematical effect of $M_N = M_N(m_\pi)$ in eqs.(5.7,5.8) could induce quite a strong quark mass dependence into the form factors $B_{2,0}^{s,v}(t)$ and $C_{2,0}^{s,v}(t)$ and might even be able to mask any "intrinsic" quark mass dependence in these form factors. We are reminded of the analysis of the Pauli form factors $F_2^{s,v}(t)$ in ref.[G$^+$05] and chapter 4 where the absorption of the analogous effect into a "normalized" magneton even led to a different slope (!) for the isovector anomalous magnetic moment $\kappa_v = F_2^v(t=0)$ when compared to the quark mass dependence of the "unnormalized" lattice data. We therefore urge the readers that this effect should be taken into account in any quantitative (future) analysis of the quark mass dependence of the generalized form factors $B_{2,0}^{s,v}(t)$ and $C_{2,0}^{s,v}(t)$ as well. For convenience we give the numerical values for the appearing coupling constants again in table 5.1 and emphasize that we use the same values for all parameters throughout this work. Finally we note that in the forward limit $t \to 0$ the generalized form factors $A_{2,0}^{s,v}(t=0)$ can be understood as moments of the ordinary Parton Distribution Functions (PDFs) $q(x)$ and $\bar{q}(x)$ [Ji98, Die03, BR05]:

$$\langle x \rangle_{u\pm d} = A_{2,0}^{s,v}(t=0) = \int_0^1 dx\, x\, (q(x)+\bar{q}(x))_{u\pm d}\,. \tag{5.10}$$

Experimental results exist for $\langle x \rangle$ in proton- and "neutron" targets, from which one can estimate the isoscalar and isovector quark contributions at the physical point [xpr] at a regularization scale μ. In this work we choose $\mu = 2$ GeV for our comparisons with phenomenology[2]. In section 5.4.1 we attempt to connect the physical value for $\langle x \rangle_{u-d}$ with recent lattice QCD results from the LHPC collaboration [H$^+$07], whereas in section 5.5.1 we analyse the quark mass dependence of $\langle x \rangle_{u+d}$ with (quenched) lattice QCD results from the QCDSF collaboration [G$^+$04].

5.2.2 The generalized form factors of the pion

The first moment of a generalized parton distribution function in a pion $H_\pi^q(x,\xi,t)$ can be defined analogously to the case of the nucleon discussed above. One obtains [Ji98, Die03, BR05]

$$\int_{-1}^1 dx\, x\, H_\pi^q(x,\xi,t) = A_\pi^q(t) + (-2\xi)^2 C_\pi^q(t). \tag{5.11}$$

[2]Note that this μ dependence is not part of the ChEFT framework, as it clearly involves short-distance physics. However, all chiral tensor couplings specified in section 5.3 carry an implicit μ dependence (which we do not indicate) as soon as they are fitted to lattice QCD data or phenomenological values which do depend on this scale.

The two functions $A_\pi^q(t)$ and $C_\pi^q(t)$ are the generalized form factors of the pion, generated by contributions of quark flavour q. In the forward limit one recovers the first moment of the ordinary parton distribution functions in a pion:

$$\langle x \rangle_\pi \quad = \quad A_\pi^q(t=0) = \int_0^1 dx\, x\, (q(x) + \bar{q}(x))\,. \tag{5.12}$$

In the analysis of the isoscalar GPD moments of a nucleon we encounter tensor fields directly interacting with the pion-cloud of the nucleon. One therefore needs to understand the relevant pion-tensor couplings in terms of the two generalized form factors $A_\pi(t)$ and $C_\pi(t)$. We note that the two generalized form factors of the pion have been analysed at one loop level already in ref.[DL91] for the total sum of quark and gluon contributions, whereas the quark contribution to the form factors as defined in eq.(5.11) has been the focus of the more recent works [KP02, DMS05].

5.3 Formalism

5.3.1 Leading order nucleon Lagrangean

In this section we briefly introduce the relevant parts of the chiral Lagrangean which are necessary for an evaluation of the tensor currents eqs.(5.7,5.8) at leading one loop level.
The well known leading order Lagrangean in BChPT is given as [GSS88]

$$\mathcal{L}_{\pi N}^{(1)} = \bar{\Psi}_N \left[i\gamma^\mu D_\mu - M_0 + \frac{g_A}{2}\gamma^\mu\gamma_5 u_\mu \right] \Psi_N, \tag{5.13}$$

with

$$D_\mu \Psi_N \quad = \quad \left\{ \partial_\mu - i v_\mu^{(s)} + \frac{1}{2}\left[u^\dagger, \partial_\mu u\right] - \frac{i}{2} u^\dagger \left(v_\mu + a_\mu\right) u - \frac{i}{2} u \left(v_\mu - a_\mu\right) u^\dagger \right\} \Psi_N, \tag{5.14}$$

$$u_\mu \quad = \quad i u^\dagger \nabla_\mu U u^\dagger. \tag{5.15}$$

$U = u^2$ corresponds to a nonlinear realization of the quasi Goldstone boson fields while v_μ and a_μ denote arbitrary vector- and axial vector background fields and $v_\mu^{(s)}$ is the isosinglet vector background field, for details see chapter 1. The covariant derivative $\nabla_\mu U$ is defined as

$$\nabla_\mu U = \partial_\mu U - i\left(v_\mu + a_\mu\right) U + i U \left(v_\mu - a_\mu\right). \tag{5.16}$$

Finally we note that the coupling g_A denotes the axial-coupling of the nucleon (in the chiral limit), whereas M_0 corresponds to the nucleon mass (in the chiral limit).
We now extend this Lagrangean to the interaction between *external tensor fields* and a strongly interacting system at low energies. In this work we focus on *symmetric, traceless tensor fields* with positive parity in order to calculate the generalized form factors of the nucleon. In particular, we utilize the chiral tensor structures

$$\begin{aligned} V_{\mu\nu}^{\pm} \quad &= \quad \frac{1}{2}\left(g_{\mu\alpha}g_{\nu\beta} + g_{\mu\beta}g_{\nu\alpha} - \frac{2}{d} g_{\mu\nu}g_{\alpha\beta} \right) \times \left(u^\dagger V_R^{\alpha\beta} u \pm u V_L^{\alpha\beta} u^\dagger \right), \\ V_{\mu\nu}^{0} \quad &= \quad \frac{1}{2}\left(g_{\mu\alpha}g_{\nu\beta} + g_{\mu\beta}g_{\nu\alpha} - \frac{2}{d} g_{\mu\nu}g_{\alpha\beta} \right) v_{(s)}^{\alpha\beta} \frac{\mathbb{1}}{2}\,. \end{aligned} \tag{5.17}$$

The right- and left handed fields $V_{\alpha\beta}^{(R,L)}$ are related to the symmetric *isovector* tensor fields of definite parity $v_{\alpha\beta}^i$ and $a_{\alpha\beta}^i$ with $i = 1,2,3$ via

$$\begin{aligned} V_{\alpha\beta}^R \quad &= \quad \left(v_{\alpha\beta}^i + a_{\alpha\beta}^i\right) \times \frac{\tau^i}{2}\,, \\ V_{\alpha\beta}^L \quad &= \quad \left(v_{\alpha\beta}^i - a_{\alpha\beta}^i\right) \times \frac{\tau^i}{2}\,, \end{aligned} \tag{5.18}$$

while $v^{(s)}_{\alpha\beta}$ denotes the symmetric *isoscalar* tensor field of positive parity. In order to study possible interactions with external tensor fields originating from the leading order Lagrangean eq.(5.13), we rewrite it into the equivalent form

$$\mathcal{L}_{t\pi N} = \bar{\Psi}_N \left[\frac{1}{2} \left(i\gamma^\mu \widetilde{g_{\mu\nu}} \overrightarrow{D}^\nu - i\overleftarrow{D}^\nu \widetilde{g_{\mu\nu}} \gamma^\mu \right) - M_0 + \ldots \right] \Psi_N, \tag{5.19}$$

where we have introduced

$$\widetilde{g_{\mu\nu}} = g_{\mu\nu} + a^s_{2,0} V^0_{\mu\nu} + \frac{a^v_{2,0}}{2} V^+_{\mu\nu}. \tag{5.20}$$

The coupling $a^s_{2,0}$ ($a^v_{2,0}$) has been defined such that it corresponds to the chiral limit value of $(\langle x \rangle_{u+d})$ $(\langle x \rangle_{u-d})$ defined in eq.(5.10). We note that the coupling $a^s_{2,0}$ is allowed to be different from unity, as we only sum over the $u+d$ quark contributions in the isoscalar moments but neglect the contributions from gluons. While this separation between quark- and gluon contributions does not occur in nature where one obtains the sum rule for the total angular momentum $A^{q+g}_{2,0}(0) = 1$, it can be implemented in lattice QCD analyses at a fixed renormalization scale (e.g. see refs.[G$^+$04, H$^+$03, E$^+$06, H$^+$07]).
Although the construction of the parity-even tensor interactions with a strongly interacting system started from the $\mathcal{O}(p^1)$ BChPT Lagrangean, an inspection of the resulting Lagrangean eq.(5.19) reveals that the leading interactions actually start out at $\mathcal{O}(p^0)$. This appears as a consequence of the fact that we do not assign a nonzero chiral dimension p^n, $n \geq 1$ to any of the tensor fields. Furthermore, symmetries allow the addition of the parity-odd tensor interaction $\sim V^-_{\mu\nu}$. We finally obtain

$$\begin{aligned} \mathcal{L}^{(0)}_{t\pi N} = \frac{1}{2}\bar{\Psi}_N \Bigg[& i\gamma^\mu \left(a^s_{2,0} V^0_{\mu\nu} + \frac{a^v_{2,0}}{2} V^+_{\mu\nu} + \frac{\Delta a^v_{2,0}}{2} V^-_{\mu\nu}\gamma_5 \right) \overrightarrow{D}^\nu \\ & - i\overleftarrow{D}^\nu \gamma^\mu \left(a^s_{2,0} V^0_{\mu\nu} + \frac{a^v_{2,0}}{2} V^+_{\mu\nu} + \frac{\Delta a^v_{2,0}}{2} V^-_{\mu\nu}\gamma_5 \right) \Bigg] \Psi_N, \end{aligned} \tag{5.21}$$

with the coupling $\Delta a^v_{2,0}$ corresponding to the chiral limit value of the axial quantity $\langle \Delta x \rangle_{u-d}$ [DH]. The $\mathcal{O}(p^1)$ part of the leading order pion-nucleon Lagrangean in the presence of external symmetric, traceless tensor fields with positive parity then reads

$$\begin{aligned} \mathcal{L}^{(1)}_{t\pi N} = \bar{\Psi}_N \Bigg\{ & i\gamma^\mu D_\mu - M_0 + \frac{g_A}{2}\gamma^\mu\gamma_5 u_\mu + \frac{b^v_{2,0}}{8M_0} \left(i\sigma_{\alpha\mu} \left[\overrightarrow{D}^\alpha, V^{\mu\nu}_+ \right] \overrightarrow{D}_\nu + h.c. \right) \\ & + \frac{b^s_{2,0}}{4M_0} \left(i\sigma_{\alpha\mu} \left[\overrightarrow{\nabla}^\alpha, V^{\mu\nu}_0 \right] \overrightarrow{D}_\nu + h.c. \right) + \ldots \Bigg\} \Psi_N, \end{aligned} \tag{5.22}$$

where we have introduced $\nabla^\alpha = \partial^\alpha - i v^\alpha_{(s)}$. The two new couplings $b^v_{2,0}$ and $b^s_{2,0}$ can be interpreted as the chiral limit values of isovector- and isoscalar anomalous gravitomagnetic moments $B^v_{2,0}(0)$ and $B^s_{2,0}(0)$. No further structures enter our calculation at this order[3]. Finally we note that the coupling $b^s_{2,0}$ is only allowed to exist because we do not sum over the quark- *and gluon* contributions in the isoscalar moments, otherwise the anomalous gravitomagnetic moment is bound to vanish in the forward limit $B^{q+g}_{2,0}(t=0) = 0$ [Ter99].

5.3.2 Consequences for the meson Lagrangean

The choice of assigning the chiral power p^0 to the symmetric tensor fields $V^{L,R,0}_{\mu\nu}$ also has the consequence that the well known leading order chiral Lagrangean for two light flavours in the meson sector [GL84] is modified:

$$\mathcal{L}^{(2)}_{t\pi\pi} = \frac{F^2_\pi}{4} \, \mathrm{Tr} \left[\nabla_\mu U^\dagger \left(g^{\mu\nu} + 4x^0_\pi V^{\mu\nu}_0 \right) \nabla_\nu U + \chi^\dagger U + \chi U^\dagger \right]. \tag{5.23}$$

[3]We only show those terms where the tensor fields couple at tree level without simultaneous emission of pions, photons, etc., as these are the relevant terms for our $\mathcal{O}(p^2)$ calculation of the form factors according to the power-counting analysis of subsection 5.3.3.

We note that the new coupling x_π^0 has been defined such that it corresponds to the chiral limit value of $\langle x \rangle_\pi$ of eq.(5.12). It is allowed to differ from unity because we only sum over the quark-distribution functions in the isoscalar channel and neglect the contributions from gluons.
The explicit breaking of chiral symmetry via the finite quark masses is encoded via

$$\chi = 2\, B_0\, (s + ip)\,, \tag{5.24}$$

if one switches off the external pseudoscalar background field p and identifies the two flavour quark mass matrix $\mathcal{M} = \text{diag}(m_u, m_d)$ with the scalar background field s. To the order we are working here we obtain the resulting pion mass m_π via

$$m_\pi^2 = 2\, B_0\, \hat{m} + \mathcal{O}({m_q}^2), \tag{5.25}$$

where $\hat{m} = (m_u + m_d)/2$ and B_0 corresponds to the value of the chiral condensate. The other free parameter at this order F_π can be identified with the value of the pion-decay constant (in the chiral limit).

5.3.3 Power-counting in BChPT with tensor fields

We start from the general power-counting formula of Baryon ChPT:

$$D \;\; = \;\; 2N_L + 1 + \sum_d (d-2) N_d^M + \sum_d (d-1) N_d^{MB}. \tag{5.26}$$

Here D denotes the chiral dimension p^D of a particular Feynman diagram, N_L counts the number of loops in the diagram, whereas the variables $N_d^{M,\,MB}$ count the number of vertices of chiral dimension d from the pion (M) and pion-nucleon (MB) Lagrangeans. To leading order[4] $D = 0$ we only have the tree level contributions from the order p^0 Lagrangean of eq.(5.21) with $N_L = 0$, $N_2^M = 0$ and $N_0^{MB} = 1$. At next-to-leading order $D = 1$ we find additional tree level contributions from the order p^1 Lagrangean of eq.(5.22) with $N_L = 0$, $N_2^M = 0$ and $N_1^{MB} = 1$. The first loop contributions enter at $D = 2$ with $N_L = 1$, $N_2^M = 0$ and $N_0^{MB} = 1$ plus possible contributions from N_1^{MB}. The corresponding diagrams are shown in fig.5.1. Diagram (e) in that figure represents loop corrections from the nucleon Z-factor (given in appendix D.2) which at this order only renormalizes the tree level tensor couplings of the order p^0 Lagrangean. Note that there is an additional possibility of obtaining $D = 2$ contributions via $N_L = 0$, $N_2^M = 0$ and $N_2^{MB} = 1$, corresponding to further tree level contributions discussed in the next subsection.
In this work we stop with our analysis of the generalized form factors at the $D = 2$, i.e. $\mathcal{O}(p^2)$ level, corresponding to a leading one loop order calculation. The next-to-leading one loop effects of $D = 3$ are postponed to a later communication. The (perhaps) surprising finding of this power-counting analysis is the observation that the tensor coupling to the pion field controlled by the coupling x_π^0 in eq.(5.23) does *not* contribute at leading one loop order! Here it only starts to enter at $D = 3$ via $N_L = 1$, $N_2^M = 1$ and $N_1^{MB} = 1$ or 2. (The corresponding diagram for $N_1^{MB} = 2$ is shown in fig.5.2 while the not-shown diagram for $N_1^{MB} = 1$ is expected to sum to zero due to isospin-symmetry.) We therefore note that the generalized form factors of the nucleon behave quite different from the standard Dirac- and Pauli form factors of the nucleon where the pion-cloud interactions with the external source à la fig.5.2 are part of the leading one loop order result and play a prominent role in the final result. We discuss the impact of this particular $D = 3$ contribution further in section 5.5.3 when we try to estimate the possible size of higher order corrections to our $\mathcal{O}(p^2)$ analysis.
Note that the discussion given above refers to the chiral dimension of the contributing loop diagrams and thus of the currents in eqs.(5.8,5.7) and not necessarily to the chiral dimension of the respective contributions to the generalized form factors. If the currents are evaluated at a chiral dimension D, the corresponding contributions to $B_{2,0}(q^2)$ are of chiral dimension $D-1$, the contributions to $C_{2,0}(q^2)$ are of chiral dimension $D-2$ due to the presence of one power of a small parameter in front of $B_{2,0}(q^2)$ and two powers of a small parameter in front of $C_{2,0}(q^2)$ in the currents (while $A_{2,0}(q^2)$ does not carry such a small prefactor). At the $D = 2$ level systematic

[4]Note that in contrast to the analyses presented in the previous chapters where the leading order contributions were of chiral dimension $D = 1$, the calculation in this chapter starts at $D = 0$ due to the presence of external fields with zero chiral dimension.

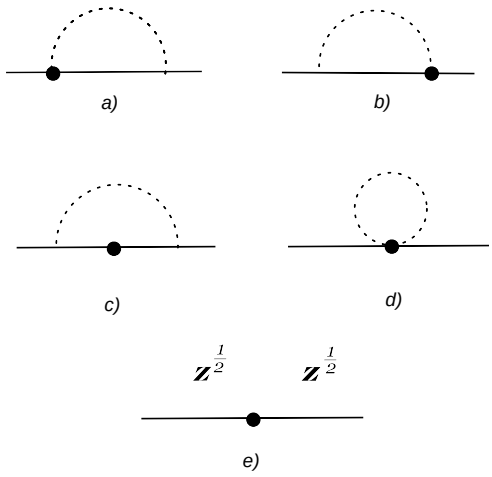

Figure 5.1: The loop diagrams contributing to the first moments of the GPDs of a nucleon at leading one loop order in BChPT. The solid- and dashed lines represent nucleon and pion propagators, respectively. The solid dot denotes a coupling to a tensor field from the $\mathcal{O}(p^0)$ Lagrangean of eq.(5.21).

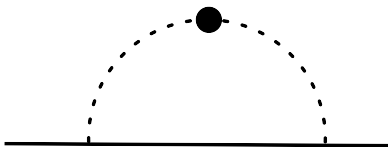

Figure 5.2: (Isoscalar) tensor field coupling to the pion-cloud of the nucleon. This process only starts to contribute at next-to-leading one loop order in BChPT.

uncertainties due to possible higher order effects are therefore expected to be already moderate for $A_{2,0}(q^2)$ but still large for $C_{2,0}(q^2)$. We now move on to a discussion of the tensor interactions in the $\mathcal{O}(p^2)$ Lagrangean which contribute to the generalized form factors at $D = 2$ according to our power-counting analysis.

5.3.4 Next-to-leading order nucleon Lagrangean

At next-to-leading order the covariant BChPT Lagrangean for two flavour QCD contains seven independent terms in the presence of general scalar, pseudoscalar, vector- and axial vector background fields, governed by the couplings $c_1, \ldots, c_7$ [BKM95] which contributed to our results for the mass and the form factors of the nucleon in the previous chapters. Extending this scenario to *symmetric* and *traceless* tensor background fields with positive parity, symmetries allow the construction of *six* additional, independent terms which describe the coupling of a tensor field to the nucleon at next-to-leading order tree level:

$$
\begin{aligned}
\mathcal{L}^{(2)}_{t\pi N} =& \frac{c_8}{4M_0^2}\,\bar{\Psi}_N\Big\{\mathrm{Tr}(\chi_+)V^+_{\mu\nu}\gamma^\mu i\overrightarrow{D}^\nu + h.c.\Big\}\Psi_N \\
&+ \frac{c_9}{2M_0^2}\,\bar{\Psi}_N\Big\{\mathrm{Tr}(\chi_+)\gamma^\mu i\overrightarrow{D}^\nu + h.c.\Big\}\Psi_N V^0_{\mu\nu} \\
&+ \frac{c^v_{2,0}}{2M_0}\bar{\Psi}_N\Big\{\big[\overrightarrow{D}^\mu,[\overrightarrow{D}^\nu,V^+_{\mu\nu}]\big]\Big\}\Psi_N \\
&+ \frac{c^s_{2,0}}{M_0}\bar{\Psi}_N\Big\{\big[\overrightarrow{\nabla}^\mu,[\overrightarrow{\nabla}^\nu,V^0_{\mu\nu}]\big]\Big\}\Psi_N \\
&+ \frac{c_{12}}{4M_0^2}\bar{\Psi}_N\Big\{\big[\overrightarrow{D}^\alpha,[\overrightarrow{D}_\alpha,V^+_{\mu\nu}]\big]\gamma^\mu i\overrightarrow{D}^\nu + h.c.\Big\}\Psi_N \\
&+ \frac{c_{13}}{2M_0^2}\bar{\Psi}_N\Big\{\gamma^\mu i\overrightarrow{D}^\nu + h.c.\Big\}\Psi_N\,\big[\overrightarrow{\nabla}^\alpha,[\overrightarrow{\nabla}_\alpha,V^0_{\mu\nu}]\big] \\
&+ \ldots
\end{aligned}
\tag{5.27}
$$

with $\chi_+ = u^\dagger\chi u^\dagger + u\chi^\dagger u$. The physics behind these couplings c_i where $i = 8,\ldots 13$ with respect to the generalized form factors of the nucleon is quite simple: c_8 and c_9 govern the leading quark mass insertion in $\langle x\rangle_{u-d}$ and $\langle x\rangle_{u+d}$, respectively, whereas the couplings c_{10} and c_{11} give the values of the generalized form factors $C^v_{2,0}(0)$ and $C^s_{2,0}(0)$ in the double limit $t\to 0$ and $m_\pi \to 0$. We can therefore denote them as $c^v_{2,0}$ and $c^s_{2,0}$. Finally the couplings c_{12} and c_{13} parametrize the contributions of short-distance physics to the slopes of the generalized form factors $A^v_{2,0}(t)$ and $A^s_{2,0}(t)$ in the chiral limit. Note that the operator controlled by the coupling c_9 is not allowed to exist when we add the gluon-contributions on the left hand side of eq.(5.7) [H$^+$]. After laying down the necessary effective Lagrangeans for our calculation, we are now proceeding to the results of our calculation.

5.4 The Generalized Isovector Form Factors in $\mathcal{O}(p^2)$ BChPT

5.4.1 Moments of the isovector GPDs at $t = 0$

In this subsection we present our results for the generalized isovector form factors of the nucleon at $t = 0$. For the PDF-moment $A^v_{2,0}(t=0)$ we obtain to $\mathcal{O}(p^2)$ in $\overline{\mathrm{IR}}$ renormalized BChPT

$$
\begin{aligned}
A^v_{2,0}(0) &= \langle x\rangle_{u-d} \\
&= a^v_{2,0} + \frac{a^v_{2,0}m_\pi^2}{(4\pi F_\pi)^2}\Bigg[-(3g_A^2+1)\log\frac{m_\pi^2}{\lambda^2} - 2g_A^2 + g_A^2\frac{m_\pi^2}{M_0^2}\left(1+3\log\frac{m_\pi^2}{M_0^2}\right) \\
&\quad -\frac{1}{2}g_A^2\frac{m_\pi^4}{M_0^4}\log\frac{m_\pi^2}{M_0^2} + g_A^2\frac{m_\pi}{\sqrt{4M_0^2-m_\pi^2}}\left(14-8\frac{m_\pi^2}{M_0^2}+\frac{m_\pi^4}{M_0^4}\right)\arccos\left(\frac{m_\pi}{2M_0}\right)\Bigg] \\
&\quad +\frac{\Delta a^v_{2,0}g_A m_\pi^2}{3(4\pi F_\pi)^2}\Bigg[2\frac{m_\pi^2}{M_0^2}\left(1+3\log\frac{m_\pi^2}{M_0^2}\right) - \frac{m_\pi^4}{M_0^4}\log\frac{m_\pi^2}{M_0^2} + \frac{2m_\pi(4M_0^2-m_\pi^2)^{\frac{3}{2}}}{M_0^4}\arccos\left(\frac{m_\pi}{2M_0}\right)\Bigg] \\
&\quad +4m_\pi^2\frac{c_8^{(r)}(\lambda)}{M_0^2} + \mathcal{O}(p^3).
\end{aligned}
\tag{5.28}
$$

Many of the parameters in this expression are well known from analyses of chiral extrapolation functions. Numerical estimates for their chiral limit values can be found in table 5.1. Furthermore, in a first fit to lattice data we constrain the coupling $\Delta a^v_{2,0}$ from the phenomenological value of $\langle\Delta x\rangle^{phen.}_{u-d} \approx 0.21$ via [DH]

$$
\langle\Delta x\rangle_{u-d} = \Delta a^v_{2,0} + \mathcal{O}(m_\pi^2) \tag{5.29}
$$

	Fit I (4 points - 2 parameter)	Fit II (6+1 points - 3 parameter)
$a^v_{2,0}$	0.157 ± 0.006	0.141 ± 0.0057
$\Delta a^v_{2,0}$	0.210 (fixed)	0.144 ± 0.034
c^r_8(1GeV)	-0.283 ± 0.011	-0.213 ± 0.03

Table 5.2: The values of the coupling constants resulting from the two fits of the $\mathcal{O}(p^2)$ BChPT result given in eq.(5.28) to the LHPC lattice data for $\langle x \rangle_{u-d}$. The errors shown are of only statistical origin and do neither include uncertainties from possible higher order corrections in ChEFT nor from systematic uncertainties connected with the lattice simulation.

and perform a fit with two parameters: The couplings $a^v_{2,0}$ and $c^{(r)}_8(1\text{GeV})$ at the regularization scale $\lambda = 1$ GeV. We fit to the LHPC data for this quantity as given in ref.[H$^+$07], including lattice data up to effective pion masses of $m_\pi \approx 600$ MeV. The resulting values for the fit parameters together with their statistical errors are given in table 5.2. The resulting chiral extrapolation function is shown as the solid line in figure 5.3. We note that the extrapolation curve tends towards smaller values for small quark masses but does not quite reach the phenomenological value at the physical point which was *not* included in the fit. We therefore again estimate possible corrections to the solid curve arising from higher orders. From dimensional analysis we know that the leading chiral contribution to $\langle x \rangle_{u-d}$ beyond our calculation takes the form $\mathcal{O}(p^3) \sim \delta_A \frac{m_\pi^3}{(4\pi F_\pi)^2 M_0} + ...$ Repeating the fit with values for δ_A between[5] $-1, \ldots, +1$ and accounting for statistical errors one ends up with an array of curves covering the grey shaded area of figure 5.3. Reassuringly, the phenomenological value for $\langle x \rangle_{u-d}$ lies well within that band of uncertainties due to possible next-order corrections, giving us *no indication* that something may be inconsistent with the large values for $\langle x \rangle_{u-d}$ typically found in lattice QCD simulations at large quark masses. The resulting values for the couplings $a^v_{2,0}$ and $c^{(r)}_8(1\text{ GeV})$ of Fit I are also well within expectations. This analysis allows the conclusion that the physical value of this observable can be predicted with a precision of approximately 30% by a combined (leading one loop order) BChPT plus lattice analysis. Note that the lattice results which we use in this chapter to determine the low energy constants are calculated with $2+1$ flavours. Our SU(2) ChPT calculation is if course applicable to a scenario with a large, fixed strange quark mass since such effects are encoded in the coupling constants of the theory. Therefore however, the numbers which we find for those constants might differ from the ones in a pure two flavour scenario.
We note that the mechanism of the downward-bending at small quark masses in $A^v_{2,0}(0)$ found in eq.(5.28), see figure 5.4, is quite different from what has been discussed in literature so far within the nonrelativistic HBChPT framework (e.g. see ref.[DMN$^+$01]). In order to demonstrate this we truncate eq.(5.28) at leading order in $1/M_0$ to obtain the exact $\mathcal{O}(p^2)$ HBChPT limit of our results, agreeing with the findings of references [AS02, CJ01]:

$$\begin{aligned} A^v_{2,0}(0)|^{p^2}_{HBChPT} &= a^v_{2,0}\left\{1 - \frac{m_\pi^2}{(4\pi F_\pi)^2}\left(2g_A^2 + (3g_A^2+1)\log\frac{m_\pi^2}{\lambda^2}\right)\right\} + 4m_\pi^2 \frac{c^{(r)}_8(\lambda)}{M_0^2} \\ &\quad + \mathcal{O}\left(\frac{m_\pi^3}{16\pi^2 F_\pi^2 M_0}\right). \end{aligned} \tag{5.30}$$

As proven in chapter 3, the covariant BChPT scheme used in this work is able to exactly reproduce the corresponding nonrelativistic HBChPT result at the same order by the appropriate truncation of the $1/M_0$ expansion. At leading one loop order no recoil effects are included in HBChPT loop results and our covariant results have thus to be truncated at order $\left(\frac{1}{M_0}\right)^0$ in order to obtain the according nonrelativistic limit. In the following we therefore denote this truncation by $1/M_0 \to 0$. All differences between the HBChPT limits presented in this

[5]The natural scale of all couplings in the observables considered here is below one, as all coupling estimates in this section refer to a moment of a parton distribution itself normalized to unity. This expectation is confirmed by the fit values of tables 5.2 and 5.3 found for the investigated coupling constants.

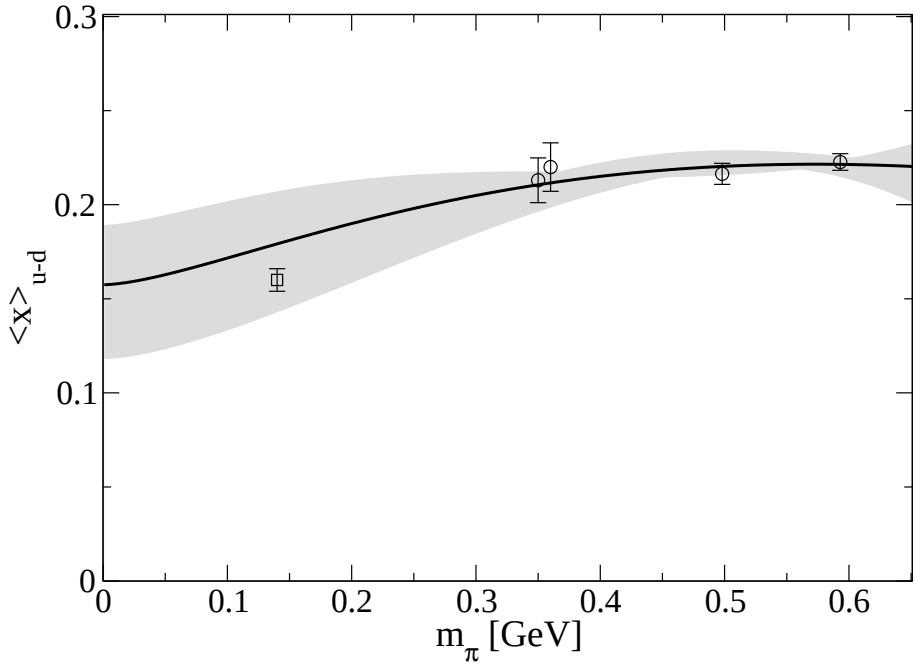

Figure 5.3: The quark mass dependence of the isovector parton distribution in a nucleon. The solid line displays the best fit curve of the $\mathcal{O}(p^2)$ result of eq.(5.28) to the LHPC lattice data of ref.[H$^+$07]. The corresponding parameters are given in Table 5.2. Note that the phenomenological value at the physical pion mass was not included in the fit. The grey band indicates the size of possible $\mathcal{O}(p^3)$ corrections as discussed in the text.

chapter and the findings of previous HBChPT studies [AS02, CJ01, ACK06, DMS06a, DMS06b] are due to the inclusion of selected terms of higher order, i.e. terms with $D = 3$ (and even larger values of D) according to the counting formula eq.(5.26) in those references.
Fit I is certainly constricted by the assumption that we use the physical value of $\langle \Delta x \rangle_{u-d}^{phen.} \approx 0.21$ for the coupling $\Delta a_{2,0}^v$ which presumably takes a value in the chiral limit which is a bit smaller than the phenomenological value at the physical point [DH]. Furthermore, in order to also numerically compare the $\mathcal{O}(p^2)$ HBChPT result of eq.(5.30) with the $\mathcal{O}(p^2)$ covariant BChPT result of eq.(5.28) we perform a second fit: We fit the covariant expression for $\langle x \rangle_{u-d}$ of eq.(5.28) again to the LHPC lattice data, this time however, we constrain the coupling $\Delta a_{2,0}^v$ in such a way that the resulting chiral extrapolation curve reproduces the phenomenological value of $\langle x \rangle_{u-d}^{phen.} = 0.160 \pm 0.006$ [xpr] exactly for physical quark masses. The parameter values for this Fit II are again given in table 5.2, whereas the resulting chiral extrapolation curve of the covariant $\mathcal{O}(p^2)$ expression of eq.(5.28) is shown as the solid line in fig.5.4. First, we emphasize that the curve looks very reasonable, connecting the physical point with the lattice data of the LHPC collaboration in a smooth fashion. Second, we note that the resulting values for the coupling constants $a_{2,0}^v$ and $\Delta a_{2,0}^v$ underlying this curve are very reassuring, indicating that both $\langle x \rangle_{u-d}$ and $\langle \Delta x \rangle_{u-d}$ are slightly smaller in the chiral limit than at the physical point! Likewise, the unknown quark mass insertion $c_8^{(r)}(\lambda)$ contributes in a strength just as expected from natural size estimates. For the comparison with HBChPT we now utilize the very same values[6] for $a_{2,0}^v$ and $c_8^{(r)}(\lambda)$ of Fit II as given in table 5.2. The resulting curve based on the $\mathcal{O}(p^2)$ HBChPT formula of eq.(5.30) is shown as the dashed curve in fig.5.4. One observes that this leading one loop HBChPT expression agrees with the covariant result between the chiral limit and the physical point but is not able to extrapolate on towards the lattice data. This behaviour of the two flavour HBChPT result is completely analogous to the corresponding leading one loop HBChPT

[6] We emphasize again that due to the definition of the $\overline{\text{IR}}$ renormalization scheme – see chapter 3 – the numerical values of the ChPT coupling constants have to be the same in HBChPT and $\overline{\text{IR}}$ renormalized covariant BChPT.

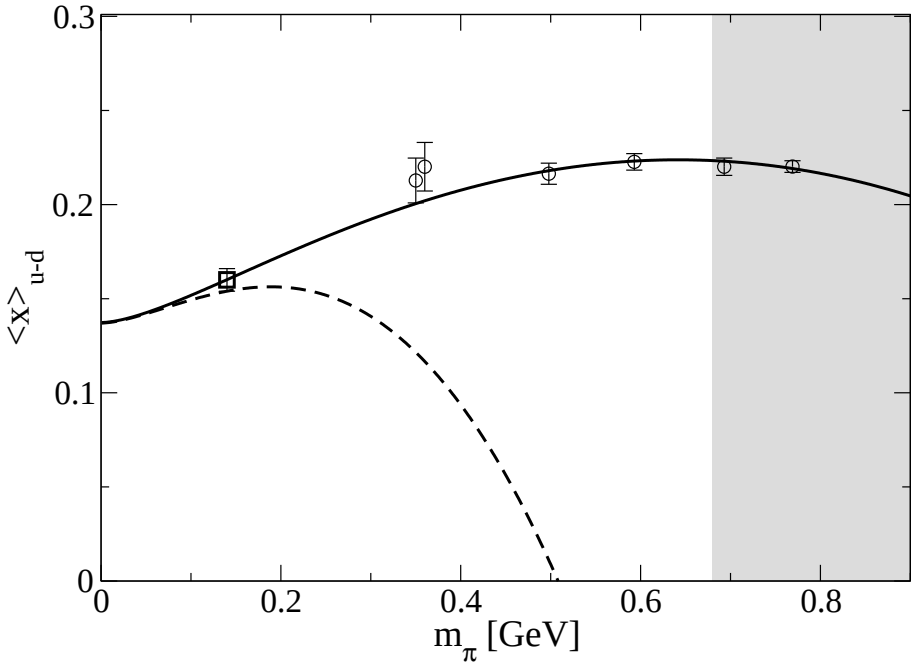

Figure 5.4: "Fit II" of the $\mathcal{O}(p^2)$ BChPT result of eq.(5.28) to the LHPC lattice data of ref.[H$^+$07] *and* to the physical point (solid line). The corresponding fit-parameters are given in table 5.2. The dashed curve shown corresponds to the $\mathcal{O}(p^2)$ result in the HBChPT truncation (see eq.(5.30)). The shaded area indicates the region where one does not expect that ChEFT can provide a trustworthy chiral extrapolation function due to the large pion masses involved.

expressions for the axial coupling constant of the nucleon [HPW03], for the anomalous magnetic moments of the nucleon [HW02], the nucleon radii and also for the transition form factors of chapter 2. It appears to be a pattern that such leading HBChPT extrapolation formulae only describe the quark mass dependence between the chiral limit and the physical point. Possible reasons for this have been given in chapter 3 of this work.
However, we note that all our *numerical* comparisons with HBChPT results shown in the figures of section 5.4 and 5.5 are based on the assumption that the $D = 2$ fit values found in tables 5.2 and 5.3 are already reliable estimates of the true, correct values of these couplings in low energy QCD. Clearly, the shown HBChPT curves might have to be revised if future $D = 3$ analyses [DGHH] lead to substantially different numerical values for these couplings. The true range of applicability of HBChPT versus covariant BChPT can only be determined once the stability of the employed couplings is guaranteed. A study of higher order effects is therefore essential also in this respect. Note, however, that there is no set of parameters for which the $\mathcal{O}(p^2)$ HBChPT result for $\langle x \rangle_{u-d}$ provides a reasonable chiral extrapolation function at the quark masses of the lattice data shown in figures 5.3 and 5.4. At this point we conclude that the smooth extrapolation behaviour of the covariant $\mathcal{O}(p^2)$ BChPT expression for $\langle x \rangle_{u-d}$ of eq.(5.28) between the chiral limit and the region of present lattice QCD data is due to an *infinite tower* of $\left(\frac{m_\pi}{M_0}\right)^i$ terms. According to our analysis the chiral curvature resulting from the logarithm of eq.(5.30) governing the leading nonanalytic quark mass behaviour of this moment is *not* responsible for the rising behaviour of the chiral extrapolation function as has been hypothesized in ref.[DMN$^+$01].
In figure 5.4 we have marked the values of the quark mass at which we do not expect our $\mathcal{O}(p^2)$ BChPT analysis to provide a trustworthy chiral extrapolation function. The decision to indicate the onset of this domain clearly above $m_\pi = 600$ MeV is based on two observations: First, as can be seen in figure 5.3, higher order contributions to our analysis of $\langle x \rangle_{u-d}$ only become sizable above $m_\pi = 600$ MeV. Second, the only indication for a breakdown of our approach is the downward-bending of our extrapolation curve for $\langle x \rangle_{u-d}$ starting around $m_\pi = 700$ MeV. This effect results from an unbalancing of different chiral contributions to our results and

does surely not display any real physical contribution of the pion-cloud since dynamical pions should not play a prominent role at these large quark masses.
Finally we are discussing the $\mathcal{O}(p^2)$ BChPT results at $t = 0$ for the remaining two generalized isovector form factors of the nucleon at twist-two level. One obtains

$$\begin{aligned} B^v_{2,0}(t=0) &= b^v_{2,0}\frac{M_N(m_\pi)}{M_0} + \frac{a^v_{2,0}\, g_A^2 m_\pi^2}{(4\pi F_\pi)^2}\left[\left(3+\log\frac{m_\pi^2}{M_0^2}\right) - \frac{m_\pi^2}{M_0^2}\left(2+3\log\frac{m_\pi^2}{M_0^2}\right)\right. \\ &\left. + \frac{m_\pi^4}{M_0^4}\log\frac{m_\pi^2}{M_0^2} - \frac{2m_\pi}{\sqrt{4M_0^2-m_\pi^2}}\left(5-5\frac{m_\pi^2}{M_0^2}+\frac{m_\pi^4}{M_0^4}\right)\arccos\left(\frac{m_\pi}{2M_0}\right)\right] + \mathcal{O}(p^3) \quad (5.31) \\ C^v_{2,0}(t=0) &= c^v_{2,0}\frac{M_N(m_\pi)}{M_0} + \frac{a^v_{2,0} g_A^2 m_\pi^2}{12(4\pi F_\pi)^2}\left[-1+2\frac{m_\pi^2}{M_0^2}\left(1+\log\frac{m_\pi^2}{M_0^2}\right)\right. \\ &\left. - \frac{m_\pi^4}{M_0^4}\log\frac{m_\pi^2}{M_0^2} + \frac{2m_\pi}{\sqrt{4M_0^2-m_\pi^2}}\left(2-4\frac{m_\pi^2}{M_0^2}+\frac{m_\pi^4}{M_0^4}\right)\arccos\left(\frac{m_\pi}{2M_0}\right)\right] + \mathcal{O}(p^3) \quad (5.32) \end{aligned}$$

As one can easily observe, one encounters plenty of nonanalytic terms and even chiral logarithms in these covariant $\mathcal{O}(p^2)$ BChPT results. However, we note that in the HBChPT limit to the same chiral order $\mathcal{O}(p^2)$ one would only obtain the chiral limit values $b^v_{2,0}$ and $c^v_{2,0}$, nothing else [Dor05]. E.g. the chiral logarithms calculated in ref.[BJ02] for $B^v_{2,0}(t=0)$ and $C^v_{2,0}(t=0)$ would only show up in a full $\mathcal{O}(p^3)$, respectively $\mathcal{O}(p^4)$ BChPT calculation of the generalized form factors. From the viewpoint of power-counting in BChPT they are to be considered part of higher order corrections (i.e. $D > 2$) to the full $\mathcal{O}(p^2)$ results given in eqs.(5.31,5.32). Regrettably, at this point no information from experiments exists for these two structure quantities of the nucleon. From phenomenology one would expect that $B^v_{2,0}(t=0)$ has a "large" positive value at $m_\pi = 140$ MeV, as it corresponds to the next-higher moment of the *isovector* Pauli form factor $F_2^v(t=0) = \kappa_v = 3.71$ n.m. (Compare eq.(5.5) and eq.(5.3) at $\xi = 0$). Lattice QCD analyses seem to support this expectation [G$^+$04, H$^+$03, H$^+$07]. In contrast, the value of $C^v_{2,0}(t=0)$ cannot be estimated from information known about nucleon form factors. State-of-the-art lattice QCD analyses (e.g. see ref.[H$^+$07]) suggest that it is consistent with zero. In fig.5.5 we have indicated how the corresponding extrapolation curves based upon this information might look like. As a caveat we note that in both form factors the intrinsic quark mass dependence is small and we would see a dominant influence of the quark mass dependence stemming from the kinematical factor $M_N(m_\pi)$ in eqs.(5.31) and (5.32), if the corresponding chiral limit values $b^v_{2,0}$ and $c^v_{2,0}$ are nonzero. A further observation is that the uncertainties connected with possible higher order corrections from $\mathcal{O}(p^3)$ to $B^v_{2,0}(t=0)$ and $C^v_{2,0}(t=0)$ could already become substantial for pion masses around 300 MeV. For both quantities they can be estimated via $\mathcal{O}(p^3) \sim \delta_{B,C}\frac{m_\pi^2 M_N(m_\pi)}{(4\pi F_\pi)^2 M_0}$ where $-1 < \delta_{B,C} < 1$. In order to ultimately test the stability of the results in eqs.(5.31,5.32) it will be very useful to extend this analysis to next-to-leading one loop order. Due to the fact that the systematic errors of our calculation of $B^v_{2,0}(t=0)$ and $C^v_{2,0}(t=0)$ already become large at the lowest pion masses at which lattice data are available, we abstain from a study of those two observables based on fits to lattice data. However, such a discussion of the BChPT results presented in this work including an analysis of statistical errors can be found in reference [H$^+$07].

5.4.2 The slopes of the generalized isovector form factors

In order to discuss the generalized isovector form factors $A^v_{2,0}(t)$, $B^v_{2,0}(t)$ and $C^v_{2,0}(t)$ at nonzero values of t, we first analyse their slopes ρ_X, defined via

$$X^v_{2,0}(t) = X^v_{2,0}(0) + \rho^v_X\, t\, + \mathcal{O}(t^2); \qquad X = A, B, C. \quad (5.33)$$

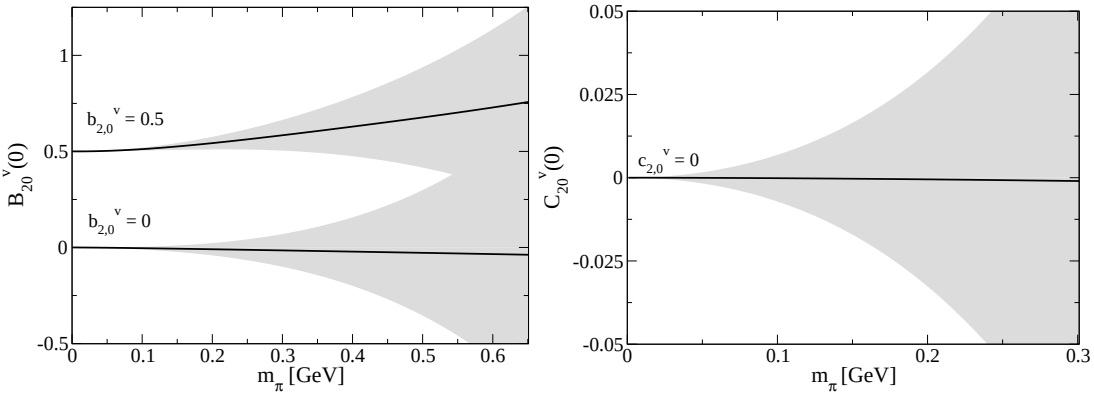

Figure 5.5: Quark mass dependence of the isovector moments $B^v_{2,0}(t=0)$ and $C^v_{2,0}(t=0)$. In $B^v_{2,0}(t=0)$ we have varied the (unknown) chiral limit value $b^v_{2,0}$ between 0 and $+0.5$, as lattice analyses [G$^+$04, H$^+$03, H$^+$07] suggest that this moment has a large positive value. For the chiral limit value $c^v_{2,0}$ of $C^v_{2,0}(t=0)$ we have chosen the value zero, as preliminary lattice QCD analyses suggest that this moment is consistent with zero [H$^+$07]. The grey bands shown indicate the size of possible higher order corrections to these $\mathcal{O}(p^2)$ results.

To $\mathcal{O}(p^2)$ in BChPT we find

$$\begin{aligned}
\rho^v_A &= \frac{c_{12}}{M_0^2} - \frac{a^v_{2,0} g_A^2}{6(4\pi F_\pi)^2}\,\frac{m_\pi^2}{(4M_0^2-m_\pi^2)}\left\{26 + 8\log\frac{m_\pi^2}{M_0^2} - \frac{m_\pi^2}{M_0^2}\left(30 + 32\log\frac{m_\pi^2}{M_0^2}\right)\right. \\
&\quad + \frac{m_\pi^4}{M_0^4}\left(6 + \frac{39}{2}\log\frac{m_\pi^2}{M_0^2}\right) - 3\frac{m_\pi^6}{M_0^6}\log\frac{m_\pi^2}{M_0^2} \\
&\quad \left. - \frac{m_\pi}{\sqrt{4M_0^2-m_\pi^2}}\left(90 - 130\frac{m_\pi^2}{M_0^2} + 51\frac{m_\pi^4}{M_0^4} - 6\frac{m_\pi^6}{M_0^6}\right)\arccos\left(\frac{m_\pi}{2M_0}\right)\right\} + \frac{m_\pi \delta^t_A}{(4\pi F_\pi)^2 M_0}, \qquad (5.34)
\end{aligned}$$

$$\begin{aligned}
\rho^v_B &= \frac{a^v_{2,0} g_A^2}{18(4\pi F_\pi)^2}\,\frac{1}{(4M_0^2-m_\pi^2)}\left\{4M_0^2 + m_\pi^2\left(83 + 24\log\frac{m_\pi^2}{M_0^2}\right) - 114\frac{m_\pi^4}{M_0^2}\left(1 + \log\frac{m_\pi^2}{M_0^2}\right)\right. \\
&\quad + \frac{m_\pi^6}{M_0^4}\left(24 + 75\log\frac{m_\pi^2}{M_0^2}\right) - 12\frac{m_\pi^8}{M_0^6}\log\frac{m_\pi^2}{M_0^2} - \frac{6m_\pi^3}{\sqrt{4M_0^2-m_\pi^2}}\left(50 - 80\frac{m_\pi^2}{M_0^2} + 33\frac{m_\pi^4}{M_0^4} - 4\frac{m_\pi^6}{M_0^6}\right) \\
&\quad \left. \times \arccos\left(\frac{m_\pi}{2M_0}\right)\right\} + \delta^t_B\,\frac{M_N(m_\pi)}{(4\pi F_\pi)^2 M_0}, \qquad (5.35)
\end{aligned}$$

$$\begin{aligned}
\rho^v_C &= \frac{a^v_{2,0} g_A^2}{180(4\pi F_\pi)^2}\,\frac{1}{(4M_0^2-m_\pi^2)}\left\{4M_0^2 - 13m_\pi^2 + 12\frac{m_\pi^4}{M_0^2}\left(4 + 3\log\frac{m_\pi^2}{M_0^2}\right)\right. \\
&\quad - 3\frac{m_\pi^6}{M_0^4}\left(4 + 11\log\frac{m_\pi^2}{M_0^2}\right) + 6\frac{m_\pi^8}{M_0^6}\log\frac{m_\pi^2}{M_0^2} + \frac{6m_\pi^3}{\sqrt{4M_0^2-m_\pi^2}}\left(10 - 30\frac{m_\pi^2}{M_0^2} + 15\frac{m_\pi^4}{M_0^4} - 2\frac{m_\pi^6}{M_0^6}\right) \\
&\quad \left. \times \arccos\left(\frac{m_\pi}{2M_0}\right)\right\} + \delta^t_C\,\frac{M_N(m_\pi)}{(4\pi F_\pi)^2 M_0}. \qquad (5.36)
\end{aligned}$$

The parameters δ^t_A, δ^t_B and δ^t_C are not part of the covariant $\mathcal{O}(p^2)$ result. They are only given to indicate the size of possible higher order corrections from $\mathcal{O}(p^3)$. A numerical analysis of the formulae given above suggests that the size of pion-cloud contributions to the slopes of the *generalized isovector* form factors is very small! The physics governing the size of these objects seems to be hidden in the counter-term contributions c_{12}, δ^t_B and δ^t_C which dominate numerically when assuming natural size estimates $-1 < c_{12},\, \delta^t_B,\, \delta^t_C < +1$. We note that this situation reminds us of the *isoscalar Dirac- and Pauli* form factors of the nucleon $F^s_1(t)$ and $F^s_2(t)$, where the t dependence in SU(2) ChEFT calculations is also dominated by counter-terms (e.g. see the

discussion in chapter 4 or reference [BFHM98]).
Finally truncating the covariant results of eqs.(5.34-5.36) at leading order in $1/M_0$ we obtain the (trivial) HBChPT expressions to $\mathcal{O}(p^2)$:

$$\rho_A^v = \frac{c_{12}}{M_0^2} + \mathcal{O}(p^3), \tag{5.37}$$

$$\rho_B^v = 0 + \mathcal{O}(p^3), \tag{5.38}$$

$$\rho_C^v = 0 + \mathcal{O}(p^3). \tag{5.39}$$

As already mentioned, the nonzero slope results found in the HBChPT calculations of refs.[ACK06, DMS06a, DMS06b] are of higher order from the point of view of our power-counting. Most of them can already be added systematically to our covariant $\mathcal{O}(p^2)$ results of eqs.(5.34-5.36) at $\mathcal{O}(p^3)$.

5.4.3 The generalized isovector form factors of the nucleon

In this subsection we present the full t dependence of the generalized isovector form factors of a nucleon to $\mathcal{O}(p^2)$ in BChPT. We note that for all three generalized form factors at this order only the amplitude of diagram c) of fig.5.1 depends on t. The resulting expressions at this order are therefore quite simple:

$$A_{2,0}^v(t) = A_{2,0}^v(0) + \frac{a_{2,0}^v g_A^2}{192\pi^2 F_\pi^2} F_{2,0}^v(t) + \frac{c_{12}}{M_0^2}\, t + \mathcal{O}(p^3), \tag{5.40}$$

with $A_{2,0}^v(0)$ given above and

$$\begin{aligned} F_{2,0}^v(t) = {} & t - \frac{2m_\pi^3\left(50M_0^4 - 43m_\pi^2 M_0^2 + 8m_\pi^4\right)}{M_0^4\sqrt{4M_0^2 - m_\pi^2}} \arccos\left(\frac{m_\pi}{2M_0}\right) \\ & + \int_{-\frac{1}{2}}^{\frac{1}{2}} du \Bigg\{ \frac{2m_\pi^3 M_0^2}{\tilde{M}^8\sqrt{4\tilde{M}^2 - m_\pi^2}} \Big[-10\tilde{M}^6 + \left(17m_\pi^2 + 60M_0^2\right)\tilde{M}^4 - 4m_\pi^2\left(m_\pi^2 + 15M_0^2\right)\tilde{M}^2 \\ & + 12m_\pi^4 M_0^2\Big] \arccos\left(\frac{m_\pi}{2\tilde{M}}\right) + \frac{2\left(M_0^2 - \tilde{M}^2\right)}{M_0^2\tilde{M}^6}\Big[12m_\pi^4 M_0^4 + 2m_\pi^2\left(4m_\pi^2 - 9M_0^2\right)M_0^2\tilde{M}^2 \\ & + \left(m_\pi^2 - 2M_0^2\right)\left(8m_\pi^2 + M_0^2\right)\tilde{M}^4\Big] + \frac{2M_0^2}{\tilde{M}^8}\Big[2\tilde{M}^8 + 3m_\pi^2\left(3m_\pi^2 + 4M_0^2\right)\tilde{M}^4 \\ & - 4m_\pi^4\left(m_\pi^2 + 9M_0^2\right)\tilde{M}^2 + 12m_\pi^6 M_0^2\Big] \log\left(\frac{\tilde{M}}{M_0}\right) + \frac{2m_\pi^2}{M_0^4\tilde{M}^8}\Big[m_\pi^4\Big(-12M_0^8 + 4\tilde{M}^2 M_0^6 \\ & + 8\tilde{M}^8\Big) + 9m_\pi^2\tilde{M}^2\left(4M_0^8 - \tilde{M}^2 M_0^6 - 3\tilde{M}^6 M_0^2\right) + 12M_0^4\tilde{M}^4\left(\tilde{M}^4 - M_0^4\right)\Big] \log\left(\frac{m_\pi}{M_0}\right)\Bigg\}, \end{aligned} \tag{5.41}$$

where we have introduced $\tilde{M}^2 = M_0^2 + \left(u^2 - \frac{1}{4}\right)t$. Note that $F_{2,0}^v(t=0) = 0$ by construction. A conservative estimate for the size of possible higher order corrections indicated in eq.(5.40) can be obtained via $\mathcal{O}(p^3) \sim \delta_A \frac{m_\pi^3}{(4\pi F_\pi)^2 M_0} + \delta_A^t \frac{m_\pi}{(4\pi F_\pi)^2 M_0}\, t$, in complete analogy to the discussion in the two previous subsections. For the

remaining two generalized isovector form factors we obtain

$$\begin{aligned} B^v_{2,0}(t) &= b^v_{2,0}\,\frac{M_N(m_\pi)}{M_0} + \frac{a^v_{2,0} g_A^2 M_0^2}{48\pi^2 F_\pi^2}\int_{-\frac{1}{2}}^{\frac{1}{2}} \frac{du}{\tilde{M}^8}\Bigg\{ \left(M_0^2-\tilde{M}^2\right)\tilde{M}^6 + 9m_\pi^2 M_0^2\tilde{M}^4 \\ &\quad -6m_\pi^4 M_0^2\tilde{M}^2 + 6m_\pi^2 M_0^2\left(m_\pi^4 - 3m_\pi^2\tilde{M}^2 + \tilde{M}^4\right)\log\frac{m_\pi}{\tilde{M}} \\ &\quad -\frac{6m_\pi^3 M_0^2}{\sqrt{4\tilde{M}^2-m_\pi^2}}\left[m_\pi^4 - 5m_\pi^2\tilde{M}^2 + 5\tilde{M}^4\right]\arccos\left(\frac{m_\pi}{2\tilde{M}}\right)\Bigg\} \\ &\quad +\delta_B\,\frac{m_\pi^2 M_N(m_\pi)}{(4\pi F_\pi)^2 M_0} + \delta^t_B\,\frac{M_N(m_\pi)}{(4\pi F_\pi)^2 M_0}\,t, \end{aligned} \tag{5.42}$$

$$\begin{aligned} C^v_{2,0}(t) &= c^v_{2,0}\frac{M_N(m_\pi)}{M_0} + \frac{a^v_{2,0} g_A^2 M_0^2}{48\pi^2 F_\pi^2}\int_{-\frac{1}{2}}^{\frac{1}{2}} \frac{du\,u^2}{\tilde{M}^8}\Bigg\{ 2\left(M_0^2-\tilde{M}^2\right)\tilde{M}^6 - 3m_\pi^2 M_0^2\tilde{M}^4 \\ &\quad +6m_\pi^4 M_0^2\tilde{M}^2 - 6m_\pi^4 M_0^2\left(m_\pi^2 - 2\tilde{M}^2\right)\log\frac{m_\pi}{\tilde{M}} \\ &\quad +\frac{6m_\pi^3 M_0^2}{\sqrt{4\tilde{M}^2-m_\pi^2}}\left[m_\pi^4 - 4m_\pi^2\tilde{M}^2 + 2\tilde{M}^4\right]\arccos\left(\frac{m_\pi}{2\tilde{M}}\right)\Bigg\} \\ &\quad +\delta_C\,\frac{m_\pi^2 M_N(m_\pi)}{(4\pi F_\pi)^2 M_0} + \delta^t_C\,\frac{M_N(m_\pi)}{(4\pi F_\pi)^2 M_0}\,t. \end{aligned} \tag{5.43}$$

The parameters δ_B, δ_C, δ^t_B and δ^t_C have again been inserted to study the possible corrections of higher orders to our $\mathcal{O}(p^2)$ results. Varying these parameters between -1 and +1, we conclude that a full $\mathcal{O}(p^3)$ calculation is required before one wants to make any strong claims regarding the t dependence of $B^v_{2,0}(t)$ and $C^v_{2,0}(t)$ *beyond* the linear t dependence discussed in the previous subsection. On the other hand, the predicted t dependence of the form factor $A^v_{2,0}(t)$ of eq.(5.40) appears to be more reliable at this order, as possible higher order contributions only affect terms beyond the leading linear dependence on t. However, due to the unsettled situation in the t dependence of those form factors at leading one loop level, we only present fits to dipole-Q^2-extrapolated lattice data throughout this chapter and do not dare to fit to lattice data directly before the next-to-leading one loop order effects are calculated. To get a rough idea about such direct fits in the sector of generalized nucleon form factors the reader is again pointed to reference [H$^+$07].

5.5 The Generalized Isoscalar Form Factors in $\mathcal{O}(p^2)$ BChPT

5.5.1 Moments of the isoscalar GPDs at $t = 0$

To $\mathcal{O}(p^2)$ in two flavour covariant BChPT the only nonzero loop contributions to the isoscalar moment $A^s_{2,0}(t = 0)$ (see eq.(5.10)) arise from diagrams c) and e) in fig.5.1. One obtains

$$\begin{aligned} A^s_{2,0}(0) &= \langle x\rangle_{u+d} \\ &= a^s_{2,0} + 4m_\pi^2\frac{c_9}{M_0^2} - \frac{3a^s_{2,0}g_A^2 m_\pi^2}{16\pi^2 F_\pi^2}\Bigg[\frac{m_\pi^2}{M_0^2} + \frac{m_\pi^2}{M_0^2}\left(2-\frac{m_\pi^2}{M_0^2}\right)\log\left(\frac{m_\pi}{M_0}\right) \\ &\quad +\frac{m_\pi}{\sqrt{4M_0^2-m_\pi^2}}\left(2-4\frac{m_\pi^2}{M_0^2}+\frac{m_\pi^4}{M_0^4}\right)\arccos\left(\frac{m_\pi}{2M_0}\right)\Bigg] + \mathcal{O}(p^3). \end{aligned} \tag{5.44}$$

Eq.(5.44) should provide a similarly successful chiral extrapolation function for $\langle x\rangle_{u+d}$ as the covariant $\mathcal{O}(p^2)$ BChPT result of eq.(5.28) did for the LHPC lattice data for $\langle x\rangle_{u-d}$ in section 5.4.1. The uncertainty arising

from higher orders can be estimated to scale as $\mathcal{O}(p^3) \sim \delta_A^0 \frac{m_\pi^3}{(4\pi F_\pi)^2 M_0}$ where δ_A^0 should again be a number between $-1, \ldots, +1$, according to natural size estimates. We note that the coupling $\Delta a_{2,0}^v$ which played an essential role in the chiral extrapolation function of $\langle x \rangle_{u-d}$ is *not* present in the quark mass dependence of the isoscalar moment $\langle x \rangle_{u+d}$. The resulting chiral extrapolation function is therefore presumably quite different from the one in the isovector channel. The absence of a chiral logarithm $\sim m_\pi^2 \log m_\pi$ in $\langle x \rangle_{u+d}$ (compare eq.(5.30) and eq.(5.45)) presumably only leads to a difference in the chiral extrapolation functions between the isovector- and the isoscalar moment for $m_\pi < 140$ MeV.
Note that from eq.(5.44) in the limit $1/M_0 \to 0$ we reproduce the leading HBChPT result for $\langle x \rangle_{u+d}$ of ref.[AS02] which found a complete cancellation of the nonanalytic quark mass dependent terms in this channel:

$$A_{2,0}^s(0)|_{HBChPT}^{p^2} = a_{2,0}^s + 4m_\pi^2 \frac{c_9}{M_0^2} + \mathcal{O}\left(\frac{m_\pi^3}{16\pi^2 F_\pi^2 M_0}\right). \tag{5.45}$$

The coupling c_9 is therefore scale independent (in dimensional regularization) and constitutes the leading correction to the chiral limit value $a_{2,0}^s$ of $\langle x \rangle_{u+d}$.
At $t = 0$ we also find nontrivial results for the two other generalized isoscalar form factors of the nucleon. To order p^2 in the covariant calculation they read

$$\begin{aligned} B_{2,0}^s(0) &= b_{2,0}^s \frac{M_N(m_\pi)}{M_0} - \frac{3\, a_{2,0}^s\, g_A^2 m_\pi^2}{(4\pi F_\pi)^2}\left[\left(3 + \log\frac{m_\pi^2}{M_0^2}\right) - \frac{m_\pi^2}{M_0^2}\left(2 + 3\log\frac{m_\pi^2}{M_0^2}\right)\right. \\ &\quad \left. + \frac{m_\pi^4}{M_0^4}\log\frac{m_\pi^2}{M_0^2} - \frac{2m_\pi}{\sqrt{4M_0^2 - m_\pi^2}}\left(5 - 5\frac{m_\pi^2}{M_0^2} + \frac{m_\pi^4}{M_0^4}\right)\arccos\left(\frac{m_\pi}{2M_0}\right)\right] \\ &\quad + \delta_B^0 \frac{m_\pi^2 M_N(m_\pi)}{(4\pi F_\pi)^2 M_0}, \end{aligned} \tag{5.46}$$

$$\begin{aligned} C_{2,0}^s(0) &= c_{2,0}^s \frac{M_N(m_\pi)}{M_0} - \frac{a_{2,0}^s g_A^2 m_\pi^2}{4(4\pi F_\pi)^2}\left[-1 + 2\frac{m_\pi^2}{M_0^2}\left(1 + \log\frac{m_\pi^2}{M_0^2}\right) - \frac{m_\pi^4}{M_0^4}\log\frac{m_\pi^2}{M_0^2}\right. \\ &\quad \left. + \frac{2m_\pi}{\sqrt{4M_0^2 - m_\pi^2}}\left(2 - 4\frac{m_\pi^2}{M_0^2} + \frac{m_\pi^4}{M_0^4}\right)\arccos\left(\frac{m_\pi}{2M_0}\right)\right] + \delta_C^0 \frac{m_\pi M_N(m_\pi)}{(4\pi F_\pi)^2}. \end{aligned} \tag{5.47}$$

The parameters δ_B^0 and δ_C^0 have been added "by hand" to these results in order to indicate possible effects of higher order (i.e. $\mathcal{O}(p^3)$) corrections. Presumably they take on values $-1, \ldots, +1$. Note that our $\mathcal{O}(p^2)$ BChPT prediction for $C_{2,0}^s(0)$ is strongly affected by possible corrections from higher orders. This is due to the fact that one only receives a nonzero result for this form factor starting at $\mathcal{O}(p^2)$ – the order we are working at. Eq.(5.47) should therefore only be considered to provide a rough estimate for the quark mass dependence of this form factor at $t = 0$. For a true, quantitative analysis of its chiral extrapolation behaviour the complete[7] $\mathcal{O}(p^3)$ corrections should first be added. In order to obtain a *rough estimate* of the chiral extrapolation functions resulting from eqs.(5.44,5.46) we utilize the quenched[8] data of the QCDSF collaboration [G$^+$04] as input. A similar analysis of the here presented $\mathcal{O}(p^2)$ BChPT results together with recent LHPC data can be found in reference [H$^+$07] leading to the same qualitative statements.
However, in particular in the isoscalar channel, there are several sources of systematic errors in the lattice simulation whose impact is hard to estimate at present. The generalized form factors of the nucleon have not been simulated at different lattice spacings and volumes at small pion masses yet. In order to control possible finite size and discretization effects in the lattice results further simulations are therefore needed. Furthermore, in the isoscalar channel disconnected diagrams (all processed where the incoming external field is not directly

[7] The most prominent correction from $\mathcal{O}(p^3)$ arises from the triangle diagram of fig.5.2 and is given in appendix D.3.2 via $\Delta C_{h.o.}^s(t = 0, m_\pi)$. We note, however, that this is not the only next-order correction.

[8] The quark masses employed in ref.[G$^+$04] are so large that one does not expect to find differences between quenched and dynamical simulations, see e.g. the discussion in reference [HW02]. Note that we are utilizing the lattice data of reference [G$^+$04] with the scale set by r_0, as we consider the alternative way of scale-setting (via a *linear* extrapolation to the physical mass of the nucleon) also discussed in ref.[G$^+$04] to be obsolete in the light of the detailed chiral extrapolation studies of refs.[PHW04, AK$^+$04, BHM05, PMW$^+$06].

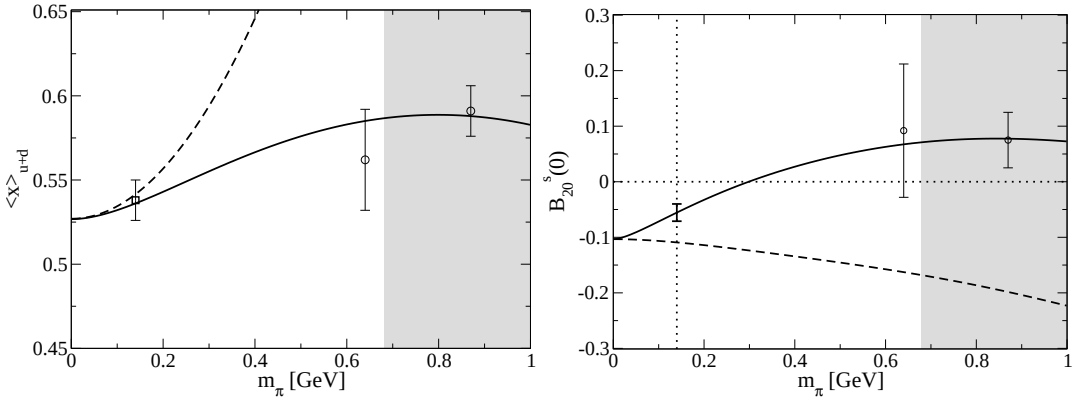

Figure 5.6: Solid lines: The quark mass dependence of the $\mathcal{O}(p^2)$ BChPT result for $\langle x\rangle_{u+d}$ of eq.(5.44) and $B^s_{2,0}(0)$ of eq.(5.46). The values for the three previously unknown parameters resulting from a *combined* fit to the shown QCDSF data of ref.[G$^+$04] and to the phenomenological value for $\langle x\rangle_{u+d}$ [xpr] are given in table 5.3. At the physical point we obtain $B^s_{2,0} = -0.056 \pm 0.016$, with the shown error only being statistical. Due to the poor data situation with its unknown systematic errors, however, these results should only be considered as a rough estimate of the true quark mass dependence. The dashed lines correspond to the respective HBChPT results at this order which are again found to only be applicable for very low pion masses.

coupled to a valence quark) contribute to three point functions but are due to large calculational expenses connected with these processes frequently neglected in lattice simulations. The lattice results for isoscalar form factors at present therefore come with an uncontrollable systematic error.
Performing a combined fit of eqs.(5.44,5.46) to the lattice data shown in fig.5.6 and including the phenomenological value of $\langle x\rangle_{u+d} \sim 0.54$ [xpr], we obtain the two solid curves shown in fig.5.6. The resulting parameters of the fit are given in table 5.3. Interestingly, despite the large quark masses and the huge error bars in the data of ref.[G$^+$04] we obtain reasonable chiral extrapolation curves with natural size coupling constants. The analysis of the QCDSF data in combination with the physical value for $\langle x\rangle_{u+d}$ suggests that the chiral limit value of this isoscalar PDF-moment is smaller than the value at the physical point, leading to a monotonically rising chiral extrapolation function as shown in the left panel of fig.5.6. As a second observation we note that the value for the generalized form factor $B^s_{2,0}(t=0)$ could take on a *small negative* value at the physical point according to the right panel of fig.5.6, albeit with a large uncertainty due to the poor data situation and large systematic errors of the BChPT calculation at this order. Because of the small (negative!) value of the isoscalar Pauli form factor $F^s_2(t=0) = \kappa_s = -0.12$ n.m., it is somewhat expected that the next higher moment yields a value close to zero. However, fig.5.6 now opens the possibility that $B^s_{2,0}(t=0) \approx -0.06$ might be as large as 50% of its $F^s_2(t=0)$ analogue. It will be very interesting to observe whether this feature can be reproduced when the new data of QCDSF [LQ] at small pion masses and a next-to-leading one loop order BChPT calculation of the generalized form factors become available. Fig.5.6 also demonstrates that the corresponding $\mathcal{O}(p^2)$ HBChPT results are again not sufficient for a chiral extrapolation at this order. However, we note again that the true range of applicability of HBChPT versus covariant BChPT can only be determined once the stability of the employed couplings is guaranteed, see the similar discussion for $\langle x\rangle_{u-d}$ in section 5.4.1.

5.5.2 The contribution of u and d quarks to the spin of the nucleon

In the past few years a lot of interest in generalized isoscalar form factors of the nucleon has focused on the values of $A^s_{2,0}$ and $B^s_{2,0}$ at the point $t=0$ since one can determine the contribution of quarks to the total spin of the nucleon via these two structures [Ji97]:

$$J_{u+d} \;=\; \frac{1}{2}\big[A^s_{2,0}(t=0) + B^s_{2,0}(t=0)\big]. \tag{5.48}$$

$a^s_{2,0}$	$b^s_{2,0}$	c_9	$\langle x\rangle^{phen.}_{u+d}(\mu = 2\text{GeV})$
0.527 ± 0.007	-0.103 ± 0.016	0.147 ± 0.002	0.538 ± 0.012 (fixed)

Table 5.3: The values for the three tensor coupling constants entering $A^s_{2,0}(t)$ and $B^s_{2,0}(t)$ at order p^2 as extracted from a combined fit to the lattice results for $A^s_{2,0}(0)$ and $B^s_{2,0}(0)$ [G$^+$04] shown in fig.5.6 and to the physical point of $A^s_{2,0}(t = 0, m_\pi = 0.14\text{ GeV}) = \langle x\rangle^{phen.}_{u+d}$. Note that we have obtained a small negative value for $b^s_{2,0}$. The indicated uncertainties are the statistical errors arising in the fit of eqs.(5.44) and (5.46) to the data of references [G$^+$04, xpr] and do not reflect the much larger systematic uncertainties from both the lattice simulations (which e.g. neglect all contributions from disconnected diagrams) and possible higher order contributions to our chiral analysis.

To $\mathcal{O}(p^2)$ in BChPT we find

$$\begin{aligned} J_{u+d} &= \frac{1}{2}\Bigg\{ a^s_{2,0} + b^s_{2,0}\,\frac{M_N(m_\pi)}{M_0} + \frac{a^s_{2,0} m_\pi^2}{(4\pi F_\pi)^2}\Bigg[\frac{3g_A^2 m_\pi}{\sqrt{4M_0^2 - m_\pi^2}}\left(8 - 6\frac{m_\pi^2}{M_0^2} + \frac{m_\pi^4}{M_0^4}\right)\arccos\frac{m_\pi}{2M_0} \\ &\quad -3g_A^2\left(3 - \frac{m_\pi^2}{M_0^2} + \left(2 - 4\frac{m_\pi^2}{M_0^2} + \frac{m_\pi^4}{M_0^4}\right)\log\frac{m_\pi}{M_0}\right)\Bigg] + 4m_\pi^2\frac{c_9}{M_0^2}\Bigg\} + \mathcal{O}(p^3). \end{aligned} \tag{5.49}$$

Note that despite the plethora of nonanalytic quark mass dependent terms contained in the $\mathcal{O}(p^2)$ BChPT result of eq.(5.49), the two chiral logarithms calculated in ref.[CJ02] within the HBChPT framework are *not yet* contained in our result. Both terms ($\sim a_{(q)\pi}$, $b_{(q)N}$ in the notation of ref.[CJ02]) are part of the complete $\mathcal{O}(p^3)$ result according to our power-counting and will appear in the calculation of the next order[9]. We further note that the two logarithms of ref.[CJ02] are UV-divergent and are accompanied by a counter-term, whereas the $\mathcal{O}(p^2)$ BChPT result of eq.(5.49) happens to be UV-finite to the order we are working. In ref.[CJ02] the authors also reported that the two chiral logarithms (of $\mathcal{O}(p^3)$) which they describe presumably are canceled *numerically* by pion-cloud contributions around an intermediate $\Delta(1232)$ state. We can confirm that this possibility exists, as the described Δ contributions also start at $\mathcal{O}(p^3)$, assuming a power-counting where the nucleon-Δ mass difference in the chiral limit is counted as a small parameter of chiral dimension one $\sim p^1$ (as it has been done in chapter 2, see ref.[BHM03] for details).
Utilizing the $\mathcal{O}(p^2)$ BChPT result of eq.(5.49) and the fit parameters of table 5.3, we obtain a first estimate for the contribution of u and d quarks to the spin of a nucleon:

$$J_{u+d}(t = 0,\, m_\pi = 0.14\,\text{GeV}) \approx 0.24 \pm 0.05, \tag{5.50}$$

which is only about half of the total spin of the nucleon! We emphasize that this number is just a rough estimate, as we are assuming that the true error is dominated by *systematic* errors from both the lattice input to our analysis and the possible higher order corrections to our chiral calculation[10]. However, the same chiral analysis performed on a different set of lattice data lead the authors of reference [H$^+$07] to a result which is consistent with the value given here – within statistical errors.
Based on the same input, we can also predict the quark mass dependence of J_{u+d}. The result is displayed as the solid line in fig.5.7. Note that in contrast to the analysis given in ref.[G$^+$04], we do not obtain a flat chiral extrapolation function between the lattice data and the physical point. The $\mathcal{O}(p^2)$ BChPT analysis suggests that the value at the physical point lies *lower* than the values obtained in the QCDSF simulation at large quark masses. Following the above discussion, this curve obviously can only be a first estimate of the true result.

[9] The contribution $\sim a_{(q)\pi}$ is already contained in the function $\Delta B_{h.o.}(t = 0, m_\pi)$ discussed in subsection 5.5.3.

[10] The size of the statistical error read off from the fit of table 5.3 is ± 0.01 and therefore negligible. The small value of this statistical error is of course heavily influenced by the error assigned to the phenomenological value of $\langle x\rangle_{u+d}$ given in table 5.3. Note, however, that the size of statistical errors will increase once we extend our analysis to next-to-leading one loop order due to the presence of several so far unknown counter-terms at this order.

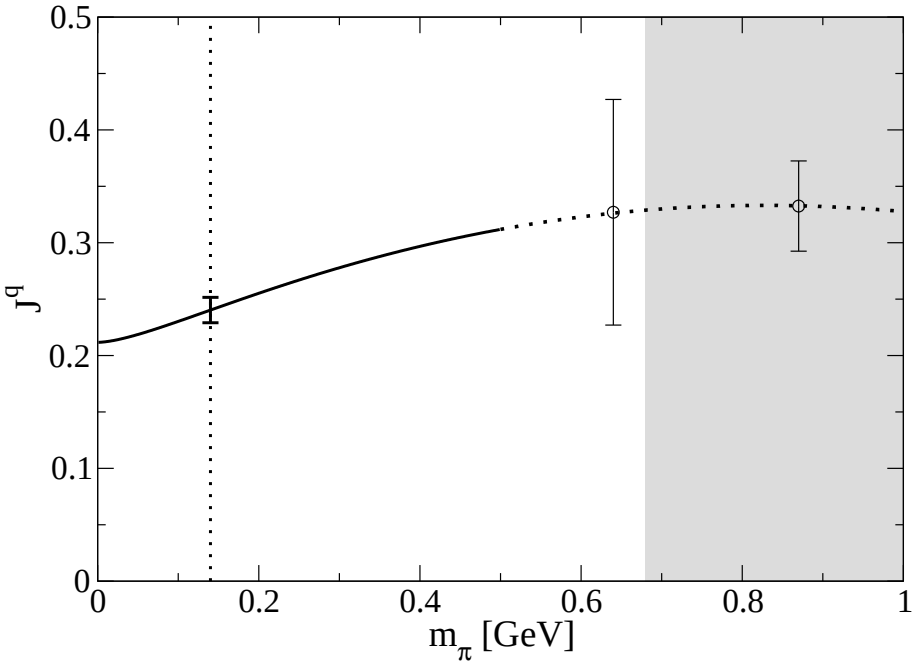

Figure 5.7: The contribution of $u+d$ quarks to the spin of a nucleon as function of the effective pion mass. The $\mathcal{O}(p^2)$ BChPT result shown as the solid line is a prediction of eq.(5.49) which utilizes the fit-parameters of table 5.3. For comparison we have also plotted simulation data from QCDSF [G$^+$04] in the figure. At the physical point one can read off $J_{u+d} \approx 0.24$. (The error bar shown at the physical point is only statistical, i.e. arises due to the errors attached to the parameters in table 5.3, and does not reflect any systematic uncertainties.)

5.5.3 A first glance at the generalized isoscalar form factors of the nucleon

In this section we present the results for the momentum- and quark mass dependence of the generalized form factors of the nucleon for the isoscalar flavour combination $u+d$ at $\mathcal{O}(p^2)$ in BChPT. We note that at this order the only nonzero loop contributions to the three isoscalar form factors arise from diagrams c) and e) of figure 5.1, as the coupling of the isoscalar tensor field to the nucleon is not affected by chiral rotations. One obtains

$$A^s_{2,0}(t) \;=\; A^s_{2,0}(0) - \frac{a^s_{2,0} g_A^2}{64\pi^2 F_\pi^2} F^s_{2,0}(t) + \frac{c_{13}}{M_0^2}\, t + \mathcal{O}(p^3)\,, \tag{5.51}$$

with $A^s_{2,0}(0)$ given in eq.(5.44) and $F^s_{2,0}(t=0)=0$ by construction. Interestingly, to the order we are working here, the t dependence of this isoscalar form factor $A^s_{2,0}(t)$ is given by the same function

$$F^s_{2,0}(t) \;=\; F^v_{2,0}(t) + \mathcal{O}(p^3), \tag{5.52}$$

that controls its isovector analogue eq.(5.41) albeit with *larger* numerical prefactors (compare eq.(5.51) to eq.(5.40)). We note that $F^s_{2,0}(t)$ does not depend on the scale λ of dimensional regularization for the loop diagrams. The chiral coupling c_{13} is therefore also scale-independent[11], parametrizing the quark mass independent short-distance contributions to the slope of $A^s_{2,0}(t)$. The unknown contributions from higher orders in the chiral expansion can be estimated from a calculation of the triangle diagram displayed in figure 5.2. Due to the coupling of the tensor field to the (long-range) pion-cloud of the nucleon, among all the contributions at the next chiral order this diagram should give the most important t dependent correction to the covariant $\mathcal{O}(p^2)$ result of eq.(5.51), resulting in the estimate $\mathcal{O}(p^3) \sim \Delta A^s_{h.o.}(t, m_\pi)$. This assumption is motivated by the findings

[11] We note again that this scale-independence refers to the UV-scales of the ChEFT calculation, not to be confused with the scale- and scheme dependence of the quark-operators on the left hand side of eq.(5.6) which is completely outside the framework of ChEFT.

of chapters 2 and 4 and the heuristic argument that the dynamics of the πN loop is much stronger affected if the incoming momentum is transferred to a propagating pion as if it is transferred to the much heavier nucleon. The explicit expression for the function $\Delta A^s_{h.o.}(t, m_\pi)$ can be found in appendix D.3.2. For completeness, we also note that in the limit $1/M_0 \to 0$ we obtain the corresponding $\mathcal{O}(p^2)$ HBChPT result

$$A^s_{2,0}(t)|^{p^2}_{HBChPT} \;=\; a^s_{2,0} + 4m_\pi^2 \frac{c_9}{M_0^2} + \frac{c_{13}}{M_0^2}\, t + \mathcal{O}(1/(16\pi^2 F_\pi^2 M_0))\,, \tag{5.53}$$

which is just a string of tree level couplings.
To order $\mathcal{O}(p^2)$ in covariant BChPT the two other isoscalar form factors read

$$\begin{aligned} B^s_{2,0}(t) \;=\;& b^s_{2,0}\,\frac{M_N(m_\pi)}{M_0} - \frac{a^s_{2,0} g_A^2 M_0^2}{16\pi^2 F_\pi^2}\int_{-\frac{1}{2}}^{\frac{1}{2}} \frac{du}{\tilde{M}^8}\Big\{ \left(M_0^2 - \tilde{M}^2\right)\tilde{M}^6 + 9m_\pi^2 M_0^2 \tilde{M}^4 \\ & -6m_\pi^4 M_0^2 \tilde{M}^2 + 6m_\pi^2 M_0^2\left(m_\pi^4 - 3m_\pi^2\tilde{M}^2 + \tilde{M}^4\right)\log\frac{m_\pi}{\tilde{M}} \\ & -\frac{6m_\pi^3 M_0^2}{\sqrt{4\tilde{M}^2 - m_\pi^2}}\left[m_\pi^4 - 5m_\pi^2\tilde{M}^2 + 5\tilde{M}^4\right]\arccos\left(\frac{m_\pi}{2\tilde{M}}\right)\Big\} \\ & +\Delta B^s_{h.o.}(t, m_\pi), \end{aligned} \tag{5.54}$$

$$\begin{aligned} C^s_{2,0}(t) \;=\;& c^s_{2,0}\frac{M_N(m_\pi)}{M_0} - \frac{a^s_{2,0} g_A^2 M_0^2}{16\pi^2 F_\pi^2}\int_{-\frac{1}{2}}^{\frac{1}{2}} \frac{du\,u^2}{\tilde{M}^8}\Big\{ 2\left(M_0^2 - \tilde{M}^2\right)\tilde{M}^6 - 3m_\pi^2 M_0^2 \tilde{M}^4 \\ & +6m_\pi^4 M_0^2 \tilde{M}^2 - 6m_\pi^4 M_0^2\left(m_\pi^2 - 2\tilde{M}^2\right)\log\frac{m_\pi}{\tilde{M}} \\ & +\frac{6m_\pi^3 M_0^2}{\sqrt{4\tilde{M}^2 - m_\pi^2}}\left[m_\pi^4 - 4m_\pi^2\tilde{M}^2 + 2\tilde{M}^4\right]\arccos\left(\frac{m_\pi}{2\tilde{M}}\right)\Big\} \\ & +\Delta C^s_{h.o.}(t, m_\pi), \end{aligned} \tag{5.55}$$

with $\tilde{M}$ defined in appendix D.2 (c.f. eq.(D.14)). $M_N(m_\pi)$ again denotes the (quark mass dependent) mass function of the nucleon eq.(5.9), introduced via eq.(5.7). In the limit $1/M_0 \to 0$ we obtain the corresponding $\mathcal{O}(p^2)$ HBChPT results for $B^s_{2,0}(t)$ and $C^s_{2,0}(t)$ which at this order only consist of the tree level coupling constants $b^s_{2,0}$ and $c^s_{2,0}$. As in the case of $A^s_{2,0}(t)$ we have estimated the contributions from higher orders via $\mathcal{O}(p^3) \sim \Delta B^s_{h.o.}(t, m_\pi)$, $\Delta C^s_{h.o.}(t, m_\pi)$, assuming that the dominant t dependent higher order corrections to our covariant $\mathcal{O}(p^2)$ BChPT results of eqs.(5.54,5.55) originate from the $\mathcal{O}(p^3)$ triangle diagram displayed in fig.5.2. Explicit expressions are given in appendix D.3.2. We note that the nonanalytic quark mass dependent terms in $A^s_{2,0}(t)$, $B^s_{2,0}(t)$ and $C^s_{2,0}(t)$ calculated in reference [BJ02] with the help of the HBChPT formalism[12] correspond to the leading terms in a $1/M_0$ expansion of the $\mathcal{O}(p^3)$ BChPT corrections $\Delta X_{h.o.}(t, m_\pi)$ where $X = A, B, C$.
At this point we refrain from a detailed numerical analysis of the t dependence of the generalized isoscalar form factors $A^s_{2,0}(t)$ and $B^s_{2,0}(t)$. On the one hand very few lattice data for this flavour combination have been published so far for pion masses below 600 MeV. Moreover, available lattice data neglect contributions from disconnected diagrams and are therefore accompanied by an unknown systematic uncertainty which is very hard to estimate. On the other hand, in the t dependence both of $A^s_{2,0}(t)$ and of $B^s_{2,0}(t)$ we encounter chiral couplings (c_{13} at $\mathcal{O}(p^2)$ in eq.(5.51) and B_{34} at $\mathcal{O}(p^3)$ in $\Delta B^s_{h.o.}(t, m_\pi)$ of eq.(D.22)) connected with presently unknown short-distance physics and systematic uncertainties can therefore not be guaranteed to be

[12] In refs.[ACK06, DMS06a, DMS06b] additional terms have been calculated within the HBChPT approach. While some terms correspond to $\mathcal{O}(p^3)$ and $\mathcal{O}(p^4)$ contributions according to our power-counting, expanding the covariant $\mathcal{O}(p^2)$ result of eq.(5.54) to the order $\frac{1}{(4\pi F_\pi)^2 M_0^1}$ one can e.g. also recognize a term $\sim a^s_{2,0}\, m_\pi^2$ present in ref.[ACK06]. However, as far as we can see, neither ref.[ACK06] nor ref.[DMS06a, DMS06b] presents a *complete* $\mathcal{O}(p^3)$ HBChPT calculation of the *matrix element* eq.(5.7).

small at the order we are working here. We are therefore postponing this discussion until further information is available, in particular from a calculation of the effects of next-to-leading one loop order. Disregarding the doubts mentioned here the authors of reference [H$^+$07] have attempted a study of the t dependence of the $\mathcal{O}(p^2)$ BChPT results for the isoscalar generalized form factors and report quite satisfactory findings. In the meantime we are preparing a full (next-to-leading one loop) $\mathcal{O}(p^3)$ BChPT analysis of the isoscalar moments of the GPDs which (in addition to several other diagrams!) also contains the contributions from the triangle diagram shown in fig.5.2, already presented in appendix D.3.2.

Before finally proceeding to the summary of this chapter, we take a look at the third generalized isoscalar form factor $C^s_{2,0}(t)$ of eq.(5.55). According to our power-counting, short distance contributions to the radius of this form factor are suppressed and only start to enter at $\mathcal{O}(p^4)$, both in HBChPT and in BChPT. After adding the $\mathcal{O}(p^3)$ *estimate* $\Delta C^s_{h.o.}(t, m_\pi)$ to the $\mathcal{O}(p^2)$ BChPT result of eq.(5.55), we can hope to catch a first glance of the t dependence of this elusive nucleon structure. Utilizing $a^s_{2,0}$ of table 5.3 and assuming $x^0_\pi \approx \langle x\rangle^s_\pi \approx 0.5$ at a renormalization scale $\mu^2 = 4$ GeV^2 [GRS99] we can determine its slope

$$\begin{aligned}
\rho^s_C &= \frac{d\,C^s_{2,0}(t)}{d\,t}|_{t=0} \\
&= \frac{g_A^2}{640\pi^2 F_\pi^2 M_0^6}\Bigg\{4a^s_{2,0}m_\pi^4\left(2m_\pi^2-3M_0^2\right)\log\frac{m_\pi}{M_0}+a^s_{2,0}\left(m_\pi^6-8m_\pi^4M_0^2+2m_\pi^2M_0^4-\frac{2}{3}M_0^6\right) \\
&\quad +x^0_\pi M_0 M_N(m_\pi)\left(7m_\pi^4-27m_\pi^2M_0^2+\frac{20}{3}M_0^4\right)-2x^0_\pi\frac{M_N(m_\pi)}{M_0}\left(4m_\pi^6-21m_\pi^4M_0^2\right. \\
&\quad \left.+20m_\pi^2M_0^4+5M_0^6\right)\log\frac{m_\pi}{M_0}-\frac{1}{m_\pi^3-4m_\pi M_0^2}\Bigg[a^s_{2,0}\left(m_\pi^8-4M_0^2m_\pi^6+2M_0^4m_\pi^4\right) \\
&\quad -x^0_\pi M_0 M_N(m_\pi)\left(m_\pi^6-7m_\pi^4M_0^2+9m_\pi^2M_0^4+8M_0^6\right)-\frac{1}{\sqrt{4M_0^2-m_\pi^2}}\Bigg(4a^s_{2,0}m_\pi^4\left(-2m_\pi^6\right. \\
&\quad \left.+15m_\pi^4M_0^2-30m_\pi^2M_0^4+10M_0^6\right)+2x^0_\pi\frac{M_N(m_\pi)}{M_0}\left(4m_\pi^{10}-45M_0^2m_\pi^8+170m_\pi^6M_0^4\right. \\
&\quad \left.\left.-225m_\pi^4M_0^6+30m_\pi^2M_0^8+32M_0^{10}\right)\Bigg)\Bigg]\arccos\left(\frac{m_\pi}{2M_0}\right)\Bigg\}.
\end{aligned} \tag{5.56}$$

At the physical point this would give us $\rho^s_C(m_\pi = 0.14\text{GeV}) = -0.77$ GeV^{-2}. Truncating eq.(5.56) in $1/M_0$ we reproduce the chiral singularity $\sim m_\pi^{-1}$ found in ref.[BJ02][13]

$$\rho^s_C = -\frac{g_A^2 x^0_\pi M_N(m_\pi)}{160\pi F_\pi^2 m_\pi}-\frac{g_A^2}{960\pi^2F_\pi^2}\left[a^s_{2,0}+x^0_\pi\frac{M_N(m_\pi)}{M_0}\left(-13+15\log\frac{m_\pi}{M_0}\right)\right]+... \tag{5.57}$$

This amounts to a slope of $\rho^s_C|_\chi = -1.12$ GeV^{-2} which is 45% larger than the BChPT estimate of eq.(5.56). Interestingly, among the terms $\sim m_\pi^0$ shown in eq.(5.57) it is the $1/M_0$ suppressed corrections to the leading HBChPT result of ref.[BJ02] that dominate numerically. This gives a strong indication that a *covariant* calculation of $\Delta C^s_{h.o.}(t, m_\pi)$ as given in appendix D.3.2 is advisable, automatically containing *all* associated $(1/M_0)^i$ corrections.

The quark mass dependence of the slope function ρ^s_C of eq.(5.56) already suggests that one obtains an interesting variation of the t dependence of this form factor as a function of the quark mass! We therefore close this discussion with a look at fig.5.8. There we have fixed the only unknown parameter $c^s_{2,0} = -0.41 \pm 0.1$ such that the BChPT result coincides with the dipole parametrization of the QCDSF collaboration at $t = 0$ [G$^+$04] for the lightest pion mass in the simulation, i.e. $m_\pi = 640$ MeV. We note explicitly that this coupling

[13] Note that due to a different definition of the covariant derivative in the quark-operator on the left hand side of eq.(5.6) our definition of the third isoscalar form factor differs from ref.[BJ02] by a factor of 4: $C_2^{BJ}(t) = 4C^s_{2,0}(t)$.

only affects the overall normalization of this form factor but does not impact its momentum dependence. It is therefore quite remarkable to observe that the resulting t dependence of this form factor according to this ChEFT estimate agrees quite well with the phenomenological dipole-parametrization of the QCDSF data at this large quark mass, even over quite a long range in four-momentum transfer. The result is rather close to a straight line which is a consequence of the fact that in the renormalization scheme introduces and applied in this work, pion-cloud effects are switched off at large pion masses (see fig.5.8). We remind the reader that the value of this form factor at $t = 0$ and $m_\pi = 0.14$ GeV determines the strength of the so-called D-term of the nucleon, playing a decisive role in the analysis of DVCS experiments [Ji98, Die03, BR05]. Utilizing the extracted value of $c^s_{2,0}$, we can now study the C-form factor also at the physical point, with the result also shown in fig.5.8. At this low value of the pion mass one can suddenly observe a nonlinear t dependence for low values of four-momentum transfer *due to the pion-cloud of the nucleon.* This is a very interesting observation because such a mechanism would allow for a more negative value of $C^s_{2,0}(t = 0)$ at the physical point than previously extracted from lattice QCD analyses via dipole extrapolations (e.g. see ref.[G$^+$04]). We obtain

$$C^s_{2,0}\,(t = 0, m_\pi = 140\,\mathrm{MeV}) \approx\ -0.36 \pm 0.1, \tag{5.58}$$

The assigned error corresponds to the fit error of $C^s_{2,0}(m_\pi = 0.64\,\mathrm{GeV}, \mathrm{t} = 0)_{\mathrm{QCDSF}}$ given in ref.[G$^+$04], as it directly influences our unknown coupling $c^s_{2,0}$. However, we note that the (unknown) systematic uncertainties, both from the quenched simulation results of ref.[G$^+$04] and possible further $\mathcal{O}(p^3)$ contributions (beyond $\Delta C^s_{h.o.}(t, m_\pi)$) to our BChPT results are not accounted for in this error bar.
With this value we can finally obtain the first estimate for the radius of this elusive form factor:

$$\begin{aligned}(r^s_C)^2 &= \frac{6}{C^s_{2,0}(t = 0,\, m_\pi = 140\,\mathrm{MeV})}\,\rho^s_C(m_\pi = 140\,\mathrm{MeV}) \\ &\approx (0.5 \pm 0.1)\,\mathrm{fm}^2.\end{aligned} \tag{5.59}$$

We compare this result with the radii of the isovector Dirac- and Pauli form factors of the nucleon which are also dominated by pion-cloud effects. Interestingly, with $(r^v_1)^2 = 0.51$ fm^2 and $(r^v_2)^2 = 0.73$ fm^2 (averages of the numbers discussed in the previous chapter) the estimated value for $(r^s_C)^2$ seems to lie in the same order of magnitude! We note, however, that our numerical estimate for the slope ρ^s_C of eq.(5.56) given above is *significantly* smaller than the corresponding slopes of the isovector Pauli- and Dirac form factors, as expected from general arguments and as already observed in lattice QCD simulations with dynamical fermions [L$^+$04] (at very large quark masses).
However, before we can go into a more detailed numerical analysis of these interesting new form factors of the nucleon, one should first complete the $\mathcal{O}(p^3)$ calculation of the generalized isoscalar form factors, as there are additional diagrams next to fig.5.2 possibly also affecting the t dependence, albeit presumably in a weaker fashion [DGHH].

5.6 Summary

The pertinent results of this chapter can be summarized as follows:

1. We have constructed the effective chiral Lagrangean for symmetric, traceless tensor fields of positive parity up to $\mathcal{O}(p^2)$ in the covariant framework of Baryon Chiral Perturbation Theory for two light quark flavours.

2. Within this covariant framework we have calculated the generalized isovector- and isoscalar form factors of the nucleon $A^{v,s}_{2,0}(t, m^2_\pi)$, $B^{v,s}_{2,0}(t, m^2_\pi)$ and $C^{v,s}_{2,0}(t, m^2_\pi)$ up to $\mathcal{O}(p^2)$ which corresponds to leading one loop order. Our results were again $\overline{\mathrm{IR}}$ renormalized and we can thus exactly reproduce the corresponding nonrelativistic $\mathcal{O}(p^2)$ results previously obtained in Heavy Baryon ChPT by taking the limit $1/M_0 \to 0$. Several HBChPT results published recently could not yet be reproduced, as they correspond to partial, nonrelativistic results from the higher orders $\mathcal{O}(p^3, p^4, p^5)$.

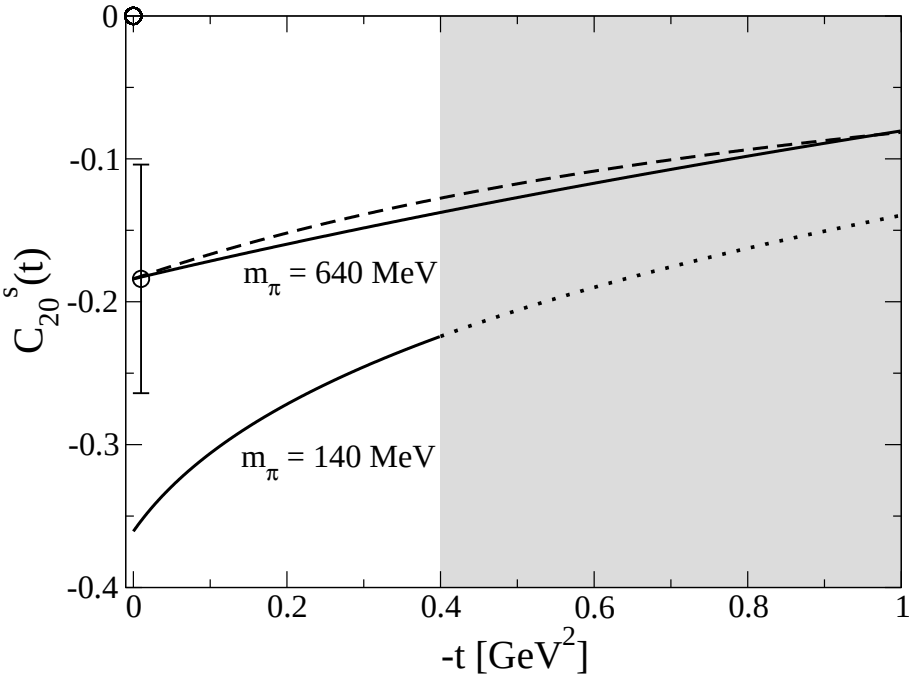

Figure 5.8: Momentum dependence of the form factor $C^s_{2,0}(t)$. The quasi linear t dependence of the $\mathcal{O}(p^2)$ BChPT result at $m_\pi = 640$ MeV (solid line) has been normalized to the dipole parametrization of the QCDSF data of ref.[G$^+$04] (dashed line), the shown data point gives the result of this reference at $t = 0$ and $m_\pi = 640$ MeV. The resulting nonlinear t dependence in this form factor for smaller values of m_π is then due to the coupling of the tensor field to the pion-cloud, providing an interesting mechanism to obtain "large" negative values at $t = 0$ and $m_\pi = 140$ MeV.

3. According to our numerical analysis of the quark mass dependence of the generalized form factors, we have noted that for $B^{s,v}_{2,0}(t)$ and $C^{s,v}_{2,0}(t)$ the observable quark mass dependencies could be dominated by the (well known) quark mass dependence of the mass of the nucleon $M_N(m_\pi)$. This mass function appears in several places in the chiral results due to kinematical factors in the matrix element used in the definition of the generalized form factors. Such a "trivial" but numerically significant effect is already known from the analysis of lattice QCD data for the Pauli form factors of the nucleon.

4. The pion-cloud contributions to all three generalized *isovector* form factors only show a very weak dependence on t. The momentum transfer dependence of these structures seems to be dominated by presently unknown short distance contributions. The situation in this isovector channel reminds us of an analogous role played by chiral dynamics in the isoscalar Dirac- and Pauli form factors of the nucleon. At this point we are therefore not able to give predictions for the *numerical* size of the slopes of these interesting nucleon structure quantities. It is hoped that a global fit to new lattice QCD data at small pion masses and small values of t – extrapolated to the physical point with the help of the formulae presented in this work – will lead to first insights into this new field of baryon structure physics. A first step on this way has already been achieved in reference [H$^+$07].

5. The leading one loop order covariant BChPT results for the generalized *isoscalar* form factors $A^s_{2,0}(t)$ and $B^s_{2,0}(t)$ are quite surprising. As far as the topology of possible Feynman diagrams is concerned, one is reminded of the isovector Dirac- and Pauli form factors of the nucleon. A power-counting analysis, however, told us that those diagrams (e.g see fig.5.2) which one would naively expect to strongly depend on both the momentum transfer and the quark mass only start to contribute at next-to-leading one loop order. Our analysis therefore suggests that the momentum dependence at low values of t is dominated by

short-distance physics.

6. It is the value of $\langle x \rangle_\pi$ of a pion in the chiral limit that controls the magnitude of those long-distance pion-cloud effects in the generalized isoscalar form factors of the nucleon, pointing to the need of a simultaneous analysis of pion- and nucleon structure on the lattice and in ChEFT.

7. In the forward limit, the isovector form factor $A^v_{2,0}(t \to 0)$ reduces to $\langle x \rangle_{u-d}$. Our covariant $\mathcal{O}(p^2)$ BChPT result for this isovector moment provides a smooth chiral extrapolation function between the high values at large quark masses from the LHPC collaboration and the lower value known from phenomenology. The required chiral curvature according to this new analysis does *not* originate from the chiral logarithm of the leading nonanalytic quark mass dependence of this moment – as had been speculated in the literature for the past few years – but is due to an infinite tower of terms $(m_\pi/M_0)^i$ with well constrained coefficients (see eq.(5.28)). The well known leading one loop HBChPT result for $\langle x \rangle_{u-d}$ of eq.(5.30) was found to be not applicable for chiral extrapolations above the physical pion mass, as expected.

8. For $\langle x \rangle_{u-d}$ we have also studied the possibility of a real chiral extrapolation of lattice data with the help of our order p^2 BChPT result, i.e. we have studied the quark mass dependence of our result for this quantity with all unknown parameters determined from lattice data only. In addition the possible impact of higher order corrections on this extrapolation function was examined leading us to the conclusion that a reasonable prediction of this observable with a $\sim 30\%$ uncertainty is possible from presently available lattice data if one relies on the leading one loop order BChPT result in order to extrapolate to physical quark masses.

9. Judging from the (quenched) lattice data of the QCDSF collaboration, our $\mathcal{O}(p^2)$ BChPT result of eq.(5.44) for $A^s_{2,0}(t = 0) = \langle x \rangle_{u+d}$ also provides a very stable chiral extrapolation function out to quite large values of effective pion masses.

10. A study of the forward limit in the isoscalar sector has led to a first estimate of the contribution of the u and d quarks to the total spin of a nucleon $J_{u+d} \approx 0.24$. This low value compared to previous determinations arises from the possibility of a small negative contribution of $B^s_{2,0}(t = 0) \approx -0.06$ at the physical point, driven by pion-cloud effects. However, at the moment the uncertainty in such a determination is rather large.

11. In a first glance at the third generalized isoscalar form factor $C^s_{2,0}(t)$ the quark mass dependence was found to be qualitatively different from $A^s_{2,0}(t)$ and $B^s_{2,0}(t)$. Its slope contains a chiral singularity $\sim m_\pi^{-1}$ and the influence of short distance contributions is suppressed. A first numerical estimate of its slope gives $\rho^s_C \approx -0.75$ GeV^2 which is much smaller than the slopes of the corresponding Dirac- or Pauli form factors. At low t we have also observed significant changes in the momentum dependence of this form factor as a function of the quark mass, resulting in the estimate $C^s_{2,0}(t = 0) \approx -0.35$ at the physical point.

12. Throughout this chapter we have indicated how to estimate possible corrections of higher orders to our leading one loop order BChPT results. The associated theoretical uncertainties of our $\mathcal{O}(p^2)$ calculation have been discussed in detail. Ultimately, in order to judge the stability of our results it is mandatory that we analyse the complete next-to-leading one loop order.

Finally we note that the tensor Lagrangeans constructed in section 5.3 invite a host of further studies, pertaining both to generalized axial form factors of the nucleon [DH] and to the energy-momentum-tensor of the nucleon [H$^+$]. The BChPT results for the generalized isovector form factors presented in this chapter have already been applied in a detailed analysis of recent lattice data in reference [H$^+$07].

Summary and Conclusions

The pertinent results of the separate chapters have been summarized individually in a summary section at the end of each chapter. In this paragraph, we want to highlight again the most important findings of this work and draw conclusions by a comparison of the results of different chapters.

After a brief introduction to the methods of Chiral Perturbation Theory (ChPT) in chapter 1, we discussed the form factors parametrizing the transition of a nucleon to its lowest lying resonance, the $\Delta(1232)$ in chapter 2. Our analysis of this transition was based on a nonrelativistic calculation of the according matrix element at leading one loop order in the small scale expansion (SSE). The central result of this chapter was that our SSE results for the three complex form factors $\mathcal{G}_M^*(Q^2)$, $\mathcal{G}_E^*(Q^2)$ and $\mathcal{G}_C^*(Q^2)$ parametrizing the magnetic dipole-, electric- and Coulomb quadrupole transitions, respectively, are in good agreement with results from experiments up to momentum transfers of $Q^2 \approx 0.25$ GeV^2. Furthermore, the SSE calculation allowed for a prediction of the Q^2 dependence of the ratio EMR$(Q^2) \sim \mathcal{G}_E^*(Q^2)/\mathcal{G}_M^*(Q^2)$ and the size and shape of CMR$(Q^2) \sim \mathcal{G}_C^*(Q^2)/\mathcal{G}_M^*(Q^2)$. The relative sizes of the quadrupole compared to the dipole transitions were found to be on the percent level in accordance with phenomenology. Interesting signatures of the pion-cloud could be found in the Q^2 dependencies of the real parts of $\mathcal{G}_E^*(Q^2)$ and $\mathcal{G}_C^*(Q^2)$, leading to negative slope parameters and turning points at low momentum transfer in those form factors. Regrettably, these structures are washed out in the EMR and CMR ratios – which are preferred by experimentalists – and only a turning point in EMR(Q^2) remains as an exciting prediction from SSE. Recent results from experiments are in agreement with this prediction, however, their error bars are too large to unambiguously confirm it. An analysis of systematic uncertainties of our chiral analysis, i.e. the possible impact of contributions of higher orders, lead us to the conclusion that such higher order effects should only become relevant above $Q^2 = 0.2$ GeV^2 and that the interesting structures predicted by $\mathcal{O}(\epsilon^3)$ SSE for the Q^2 dependence of the form factors at the leading one loop order should not be affected decisively by higher order effects.

Note, however, that we only presented a ChPT calculation for the $N\Delta$ transition form factors and hence had to rely on an approximate connection in order to compare our findings for those quantities with results from pion-electroproduction experiments. It remains an open issue to connect the $N\Delta$ transition current with the pion-electroproduction multipoles in a ChPT calculation.

On the lattice, in contrast, the $N\Delta$ transition can be directly accessed. Therefore, we have also studied the quark mass dependence of the transition form factors encoded in the ChPT results via a dependence on the mass of the pion m_π. Again, interesting structures were predicted by the SSE calculation which was, however, found to only be applicable for pion masses below $m_\pi = 200$ MeV. Our nonrelativistic analysis therefore did not allow to make contact between present-day lattice simulations of the $N\Delta$ transition form factors at large quark masses and their chiral limits.

In order to systematically extend the range of pion masses at which ChPT is applicable, we performed all subsequent ChPT calculations in the covariant formulation of this theory. The difference between nonrelativistic- and covariant calculations in Baryon ChPT (BChPT) is that the latter considers the variable $(q/M_0)^i$, where M_0 is the mass of the nucleon in the chiral limit and q is a small momentum or mass, to be of the same chiral order for any value of i. In contrast, the chiral dimension i is assigned to $(q/M_0)^i$ in the nonrelativistic theory which is thus organized as an expansion in q/M_0 where contributions with higher powers of q/M_0 appear at higher orders of the chiral analysis. However, for consistent loop calculations in the covariant framework, we had to introduce a new renormalization scheme for covariant BChPT first. In chapter 3, we developed four condi-

tions which necessarily have to be fulfilled by a consistent renormalization scheme for covariant BChPT. Those conditions were that, firstly, the results of a properly renormalized BChPT calculation should be UV-finite and independent of the renormalization scale. Secondly, they should be in accordance with the power-counting of ChPT, i.e. higher order loop diagrams should be parametrically suppressed. Thirdly, the low energy constants (LECs) should be defined in exactly the same way in both the covariant and the Heavy Baryon (HBChPT) formulation of ChPT. Covariant results fulfilling this requirement do have the advantageous features that an expansion in q/M_0 leads to the corresponding HBChPT result and a numerical value found for a LEC in one of the schemes can also be utilized in the other one. Fourthly, we demand that no nonanalytic functions are absorbed into the counter-terms of the theory since such a procedure leads to unphysical cuts, singularities and imaginary parts in BChPT results.

A renormalization scheme named $\overline{\text{IR}}$, fulfilling all four conditions, was constructed in chapter 3 by a modification of the infrared renormalization scheme of reference [BL99]. In this new framework the $(q/M_0)^i$ terms sum to flat functions where contributions from dynamical pions are reduced as the pion mass is increased. These features are spoiled in HBChPT since the sum over the $(q/M_0)^i$ terms is truncated and the analytic structure of loop integrals is thus destroyed in this approach.

As a first application of the new renormalization scheme, we also presented a $\overline{\text{IR}}$ renormalized next-to-leading one loop order ($\mathcal{O}(p^4)$) BChPT calculation of the mass of the nucleon M_N in chapter 3. Using this result to chirally extrapolate lattice results for the mass of the nucleon from pion masses above 500 MeV down to the physical point, we arrived at a prediction for this observable which was in remarkable agreement with phenomenology. We have also studied the possible impact of higher order effects on our result, only leading to a small uncertainty in our prediction for the physical value of M_N. This gives us confidence that our next-to-leading one loop order result for M_N may be applicable for pion masses even around $m_\pi = 600$ MeV. This last statement was supported by an analysis of the convergence of the chiral series for M_N.

Chapter 4 subsequently was dedicated to the first calculation of the isovector- and isoscalar vector form factors of the nucleon in $\overline{\text{IR}}$ renormalized BChPT at next-to-leading one loop order. In the isovector sector we found large contributions from the pion-cloud while our analysis showed that the isoscalar form factors – at least on the one loop level – are dominated by short distance physics. We therefore extensively studied the Q^2- as well as the m_π dependence of the $\mathcal{O}(p^4)$ BChPT results for the isovector form factors. The momentum transfer dependence of these results, examined in the basis of the Sachs form factors, was found to be in good agreement with the phenomenological parametrization of reference [FW03] up to $Q^2 = 0.25$ GeV^2, although the BChPT curves showed less curvature than the phenomenological parametrization. Above $Q^2 = 0.25$ GeV^2 the deviations between the BChPT results and phenomenology as well as the systematic uncertainties of our chiral analysis grew considerably.

In chapter 4 we have also performed two different analyses of the chiral extrapolation functions for the isovector vector form factors of the nucleon resulting from our $\mathcal{O}(p^4)$ BChPT analysis: One was to use lattice data as input which were extrapolated to $Q^2 = 0$ GeV^2 using a dipole ansatz and to study the resulting m_π dependence of the isovector anomalous magnetic moment κ_v and the slopes of the isovector form factors ρ_1^v and ρ_2^v. Our second approach was to fit the quark mass and momentum transfer dependent $\mathcal{O}(p^4)$ BChPT results for the form factors of the nucleon to lattice data at finite Q^2 directly. The results of both analyses were well consistent and both bridged the gap between presently available lattice data and phenomenology in a convincing way for all observables under consideration. Again, we studied systematic uncertainties of our chiral analysis and found that – utilizing next-to-leading one loop order covariant BChPT results – the form factors of the nucleon at $m_\pi = 140$ MeV and $Q^2 \lesssim 0.3$ GeV^2 can be predicted from lattice data above $m_\pi = 350$ MeV with an uncertainty of $\approx 20\%$. Small systematic uncertainties and a fast convergence of the chiral series – two features which were observed over a large range of pion masses for all quantities discussed – may furthermore be an indication that $\mathcal{O}(p^4)$ covariant BChPT possibly provides a trustworthy description of the quark mass dependence of the isovector form factors of the nucleon up to $m_\pi \approx 600$ MeV. The quark mass dependencies of κ_v, ρ_1^v and ρ_2^v were found to display some similarities: At large quark masses the values of all three observables are considerably smaller than the physical ones and our ChPT results as well as lattice data only display a very weak dependence on the pion mass. Approaching smaller values of the pion mass, the chiral extrapolation

functions for all three quantities start to increase and such connect the lattice results at large quark masses with the larger phenomenological values. Below the physical pion mass, κ_v, ρ_1^v and ρ_2^v still increase as a function of the pion mass and in the chiral limit κ_v finally takes on a value which is considerably larger then the one at the physical point while the slopes are singular in the chiral limit.
We also gave a first glance at the m_π dependence of the isoscalar anomalous magnetic moment of the nucleon and the slopes of the isoscalar form factors. The variation of those quantities as a function of the pion mass was found to only be weak due to the small contributions of dynamical pions in this sector. It could therefore not be excluded that the *relative* size of higher order contributions is large for the isoscalar form factors. Furthermore, at present, no lattice results at small values of m_π are available for the isoscalar form factors. Moreover, the presently available simulation results at large quark masses come with an uncontrollable systematic uncertainty since contributions from disconnected diagrams have been neglected in those simulations. We therefore did not perform chiral extrapolations of the isoscalar form factors of the nucleon in this work.
In chapter 5 we finally presented a leading one loop order calculation of the isovector- and isoscalar generalized vector form factors of the nucleon $A_{2,0}(Q^2)$, $B_{2,0}(Q^2)$ and $C_{2,0}(Q^2)$ in $\overline{\text{IR}}$ renormalized covariant BChPT. Since we performed the first covariant analysis of those nucleon observables we first had to construct the relevant parts of the chiral Lagrangean including external tensor fields. Subsequently, we applied our results for a chiral extrapolation of recent lattice data for the moment of the parton distribution function $A_{2,0}^v(0) = \langle x \rangle_{u-d}$ and were able to connect the lattice data at quark masses above $m_\pi = 350$ MeV with the value found for this observable in experiments. An estimate of higher order effects showed that the physical value of this quantity can be predicted with a 30% uncertainty by leading one loop order BChPT if so far unknown low energy constants are determined with the help of lattice data. We also performed chiral extrapolations of lattice data for $A_{2,0}^s(0) = \langle x \rangle_{u+d}$ and $B_{2,0}^s(0)$ and were thus able to estimate the contributions of up- and down quarks to the spin of the nucleon: $J_{u+d} = \frac{1}{2}\left(A_{2,0}^s(0) + B_{2,0}^s(0)\right) \approx 0.24$. However, as the lattice data which we used as input in the isoscalar sector were found in simulations at very large pion masses and come with an uncontrollable systematic uncertainty due to the fact that disconnected diagrams have been neglected, we did not perform an analysis of systematic uncertainties for the isoscalar form factors but surely expect them to be large. The value which we give for J_{u+d} therefore has to be considered to be a very rough estimate. Furthermore, we also showed that a combined lattice plus ChPT analysis allows for an estimate of the size of the C-form factor of the nucleon which plays an important role in the analysis of Deeply Virtual Compton Scattering (DVCS) experiments.
We close this summary section with a discussion of two effects which have been observed on many examples throughout this work:

- Neither HBChPT- nor standard IR renormalized covariant BChPT results were able to reasonably describe the quark mass dependence above the physical pion mass for any of the observables discussed in this work (except for the mass of the nucleon). We therefore conclude that $\overline{\text{IR}}$ renormalization is the most promising framework for calculating chiral extrapolation functions which may be applicable up to the pion masses of state-of-the-art lattice simulations.

- $\overline{\text{IR}}$ renormalized BChPT results at one loop order allowed for a reasonable description of quark mass dependencies with in most cases small, in some cases only moderate systematic uncertainties up to pion masses around $m_\pi = 600$ MeV. Up to this large value of the pion mass the differences between the results at orders p^3 and p^4 were found to be small for all (isovector) observables under consideration. In this work, no signal for a breakdown of our results could be found below $m_\pi \approx 700$ MeV. The size of systematic uncertainties of a ChPT analysis of a certain observable of course depends on the chiral dimension at which the corresponding matrix element is calculated and on the powers of small quantities (typically momenta q) which are contained in the prefactor of this observable in the matrix element.

We hope that – as has already been done for our results for the generalized form factors of the nucleon in reference [H$^+$07] – future studies of lattice results will include chiral extrapolations relying on the methods and calculations presented in this work. Ultimately, in our opinion, it is a rewarding goal to study as many

observables as possible in the same chiral framework since this would allow for a consistent combined fit of all those observables to lattice data which, in turn, would lead to a simultaneous determination of many low energy constants with small statistical errors and hence to precise predictions for many physical observables. We hope that we were able to convince our readers that $\overline{\text{IR}}$ renormalized covariant BChPT at next-to-leading one loop order provides a suitable framework for such an analysis.

Accordant results for the mass- and the vector form factors of the nucleon have already been made available in this work. The $\mathcal{O}(p^3)$ calculation for the generalized form factors of the nucleon is in preparation and even the $N\Delta$ transition form factors are analysed at next-to-leading one loop order in $\overline{\text{IR}}$ renormalized covariant BChPT at present.

Appendix A

Appendices to Chapter 2

A.1 Integrals

The result of the nonrelativistic $\mathcal{O}(\epsilon^3)$ SSE calculation for the $N\Delta$ transition form factors defined in eq.(2.1) written in terms of standard loop integrals reads:

$$\begin{aligned}
G_1(q^2) &= \frac{2c_A M_N}{F_\pi^2}\int_0^1 dx\left[g_A(x-1)J_2'(x\Delta_0,\tilde{m}^2)-\frac{5}{3}g_1\left(1-\frac{d-3}{d-1}x\right)J_2'(-x\Delta_0,\tilde{m}^2)\right] \\
&\quad -\frac{1}{2}b_1+(2E_1-D_1)\frac{\Delta_0}{4M_N} \qquad \text{(A.1)} \\
G_2(q^2) &= \frac{8c_A M_N^2}{F_\pi^2}\int_0^1 dx\left[g_A x(x-1)J_1'(x\Delta_0,\tilde{m}^2)-\frac{5}{3}g_1 x(x-1)\frac{d-3}{d-1}J_1'(-x\Delta_0,\tilde{m}^2)\right] \\
&\quad +2b_6-D_1 \qquad \text{(A.2)} \\
G_3(q^2) &= \frac{4c_A M_N^2\Delta_0}{F_\pi^2}\int_0^1 dx\Big[g_A x(x-1)(1-2x)J_0'(x\Delta_0,\tilde{m}^2)- \\
&\quad \frac{5}{3}g_1 x(x-1)(2x-1)\frac{d-3}{d-1}J_0'(-x\Delta_0,\tilde{m}^2)\Big]. \qquad \text{(A.3)}
\end{aligned}$$

The basic loop integrals (in dimensional regularization) are defined as:

$$\begin{aligned}
\frac{1}{i}\int\frac{d^dl}{(2\pi)^d}\frac{1}{m_\pi^2-l^2} &= \Delta_\pi = 2m_\pi^2\left(L+\frac{1}{16\pi^2}\ln\frac{m_\pi}{\lambda}\right) \qquad \text{(A.4)} \\
\frac{1}{i}\int\frac{d^dl}{(2\pi)^d}\frac{1}{(v\cdot l-\omega)(m_\pi^2-l^2)} &= J_0(\omega,m_\pi^2). \qquad \text{(A.5)}
\end{aligned}$$

For the nonrelativistic one-nucleon-one-pion loop integral one finds:

$$\begin{aligned}
J_0(\omega,m_\pi^2) &= -4L\omega+\frac{\omega}{8\pi^2}\left(1-2\ln\frac{m_\pi}{\lambda}\right) \\
&\quad -\frac{1}{4\pi^2}\begin{cases}\sqrt{\omega^2-m_\pi^2}\left(\ln\left(\frac{\omega}{m_\pi}+\sqrt{\frac{\omega^2}{m_\pi^2}-1}\right)-i\pi\right) & \frac{\omega}{m_\pi}>1 \\ \sqrt{m_\pi^2-\omega^2}\arccos\left(-\frac{\omega}{m_\pi}\right) & \text{for}\quad -1\le\frac{\omega}{m_\pi}\le 1 \\ -\sqrt{\omega^2-m_\pi^2}\ln\left(-\frac{\omega}{m_\pi}+\sqrt{\frac{\omega^2}{m_\pi^2}-1}\right) & \frac{\omega}{m_\pi}<-1\end{cases} \qquad \text{(A.6)}
\end{aligned}$$

Furthermore, we use the notations

$$J_0'(\omega, m_\pi^2) = -\frac{\partial}{\partial m_\pi^2} J_0(\omega, m_\pi^2), \tag{A.7}$$

$$J_1'(\omega, m_\pi^2) = -\frac{\partial}{\partial m_\pi^2} \left(\omega J_0(\omega, m_\pi) + \Delta_\pi\right), \tag{A.8}$$

$$J_2'(\omega, m_\pi^2) = -\frac{1}{d-1}\frac{\partial}{\partial m_\pi^2} \left[(m_\pi^2 - \omega^2) J_0(\omega, m_\pi) - \omega\Delta_\pi\right]. \tag{A.9}$$

The divergences at $d = 4$ parametrized via dimensional regularization are collected in the function L:

$$L = \frac{\lambda^{d-4}}{16\pi^2}\left[\frac{1}{d-4} + \frac{1}{2}\left(\gamma_E - 1 - \ln 4\pi\right)\right], \tag{A.10}$$

where γ_E is the Euler-Mascheroni constant and λ is the renormalization scale.

A.2 The Coupling Constant c_A

We determine the strength of the $N\Delta$ axial coupling constant c_A from the strong decay width of the $\Delta(1232)$ resonance at tree level. In the rest frame of the Δ this width reads:

$$\Gamma_{\Delta\to N\pi} = \frac{c_A^2}{6\pi F_\pi^2}\left(E_\pi^2 - m_\pi^2\right)^{\frac{3}{2}} \cdot \frac{M_\Delta + M_N - E_\pi}{2M_\Delta}, \tag{A.11}$$

where the $\pi N\Delta$ vertex has been taken from eq.(2.13) and the associated pion energy function reads:

$$E_\pi = \frac{M_\Delta^2 - M_N^2 + m_\pi^2}{2M_\Delta}. \tag{A.12}$$

For the numerical determination of c_A we use the parameters M_Δ, M_N, m_π and F_π from table 2.1, a width of $\Gamma_{\Delta\to N\pi} = 100$ MeV [Y$^+$06] and arrive at the result $c_A = 1.5$.

Appendix B

Appendices to Chapter 3

B.1 Basic Integrals

The integrals required for one loop calculations in BChPT can be reduced to three basic integrals in d-dimensions:

$$\Delta_\pi\left(m\right) \equiv \frac{1}{i}\int\frac{d^dl}{(2\pi)^d}\,\frac{1}{m^2-l^2-i\epsilon}, \tag{B.1}$$

$$\Delta_N\left(M\right) \equiv \frac{1}{i}\int\frac{d^dl}{(2\pi)^d}\,\frac{1}{M^2-l^2-i\epsilon}, \tag{B.2}$$

$$H_{11}\left(M,p,m\right) \equiv \frac{1}{i}\int\frac{d^dl}{(2\pi)^d}\,\frac{1}{\left(m^2-l^2-i\epsilon\right)\left(M^2-(l-p)^2-i\epsilon\right)}, \tag{B.3}$$

where m (M) is a mass function involving the mass of the quasi Goldstone Boson (of the Baryon) and p^μ denotes the four-momentum of the Baryon. The propagators are shifted into the complex energy-plane by a small amount ϵ to ensure causality. Utilizing the $\overline{\rm MS}$ renormalization scheme of ref.[GSS88] with

$$L=\frac{\lambda^{d-4}}{16\pi^2}\left[\frac{1}{d-4}+\frac{1}{2}\left(\gamma_E-1-\ln 4\pi\right)\right], \tag{B.4}$$

one obtains the dimensionally regularized results

$$\Delta_\pi(m) = 2m^2\left(L+\frac{1}{16\pi^2}\ln\frac{m}{\lambda}\right)+\mathcal{O}(d-4), \tag{B.5}$$

$$\Delta_N(M) = 2M^2\left(L+\frac{1}{16\pi^2}\ln\frac{M}{\lambda}\right)+\mathcal{O}(d-4), \tag{B.6}$$

$$\begin{aligned} H_{11}(M,p,m) = {} & -2L-\frac{1}{16\pi^2}\Bigg[-1+\log\frac{M^2}{\lambda^2}+\frac{p^2-M^2+m^2}{p^2}\log\frac{m}{M} \\ & +\frac{2mM}{p^2}\sqrt{1-\left(\frac{p^2-M^2-m^2}{2mM}\right)^2}\arccos\left(\frac{m^2+M^2-p^2}{2mM}\right)\Bigg] \\ & +\mathcal{O}(d-4). \end{aligned} \tag{B.7}$$

More complicated integral expressions needed during the calculations in this work are defined via

$$\frac{1}{i}\int\frac{d^dl}{(2\pi)^d}\,\frac{\{l^\mu,l^\mu l^\nu\}}{(m^2-l^2-i\epsilon)(M^2-(l-p)^2-i\epsilon)} = \{p^\mu H_{11}^{(1)},g^{\mu\nu}H_{11}^{(2)}+p^\mu p^\nu H_{11}^{(3)}\}, \tag{B.8}$$

$$\begin{aligned} \frac{1}{i}\int\frac{d^dl}{(2\pi)^d}\,\frac{l^\mu l^\nu l^\alpha}{(m^2-l^2-i\epsilon)(M^2-(l-p)^2-i\epsilon)} = {} & \left(p^\mu g^{\mu\alpha}+p^\nu g^{\mu\alpha}+p^\alpha g^{\mu\nu}\right)H_{11}^{(4)} \\ & +p^\mu p^\nu p^\alpha\,H_{11}^{(5)}. \end{aligned} \tag{B.9}$$

The integrals $H_{11}^{(i)}$ are related to the three basis integrals of eqs.(B.2-B.3) via the tensor-identities

$$H_{11}^{(1)}(M,p,m) = \frac{1}{2p^2}\left[\Delta_\pi - \Delta_N + \left(m^2+p^2-M^2\right) H_{11}(M,p,m)\right], \tag{B.10}$$

$$H_{11}^{(2)}(M,p,m) = \frac{1}{2(d-1)}\left[-\Delta_N + 2m^2 H_{11}(M,p,m) - \left(m^2+p^2-M^2\right) H_{11}^{(1)}\right], \tag{B.11}$$

$$H_{11}^{(3)}(M,p,m) = \frac{1}{p^2(d-1)}\left[\left(1-\frac{d}{2}\right)\Delta_N - m^2 H_{11}(M,p,m) + \frac{d}{2}\left(m^2+p^2-M^2\right) H_{11}^{(1)}(M,p,m)\right], \tag{B.12}$$

$$H_{11}^{(4)}(M,p,m) = \frac{1}{2p^2}\left[\left(m^2+p^2-M^2\right) H_{11}^{(2)}(M,p,m) + \frac{1}{d}\left(m^2\Delta_\pi - M^2\Delta_N\right)\right], \tag{B.13}$$

$$H_{11}^{(5)}(M,p,m) = \frac{1}{2p^2}\left[\left(m^2+p^2-M^2\right) H_{11}^{(3)}(M,p,m) - 4H_{11}^{(4)}(M,p,m) - \Delta_N\right] \tag{B.14}$$

Finally, we note that the integrals involving more than one baryon propagator can be related to the ones defined above via derivatives with respect to the nucleon- resp. the pion mass squared.

B.2 Regulator Functions

The infrared regular parts of the basic πN integral given above is defined as:

$$R_{11}(M,p,m) \equiv \int_{x=1}^{\infty} dx \int \frac{d^d l}{(2\pi)^d}\left[xM^2 + (x^2-x)p^2 + (1-x)m^2 - l^2\right]^{-2}. \tag{B.15}$$

The analytic expressions for the regular parts of the basic loop functions read

$$R\left(H_{11}(M,p,m)\right) = R_{11}(M,p,m) = \frac{1}{32\pi^2 p^2}\left[\left(M^2+p^2-m^2\right)\left(32\pi^2 L - 1 + 2\log\frac{M}{\lambda}\right) - 4mM\sqrt{1-\frac{\left(M^2-p^2+m^2\right)^2}{4m^2M^2}}\left(\arccos\left(-\frac{M^2-p^2+m^2}{2mM}\right) - \arccos\left(\frac{p^2-M^2+m^2}{2mp}\right)\right)\right], \tag{B.16}$$

$$R(\Delta_\pi) = 0, \tag{B.17}$$

$$R(\Delta_N) = -\Delta_N \tag{B.18}$$

The tensor reduction for the $R_{11}^{(i)}$ follows from the one given above if all the $H_{11}^{(i)}$ are replaced by their regular parts.

B.3 Proof of Eq.(3.1)

The contributions from one loop diagrams of a certain order n to a dimensionless observable O take the general form

$$O^{(n)} = \frac{\Gamma_{\mu_1\cdots\mu_k}}{(4\pi F_\pi)^2}\int \frac{dl^d}{(2\pi)^d}\frac{l^{\mu_1}l^{\mu_2}\ldots l^{\mu_k}}{\Pi^i N^j}, \tag{B.19}$$

where $\Gamma_{\mu_1\cdots\mu_k}$ is a dimensionless Dirac operator of chiral dimension zero, $\Pi = m_\pi^2 - l^2$ is the pion propagator and $N = M_0^2 - (p-l)^2$ is the propagator of the nucleon. The general order n result for O is the sum of the right hand side of eq.(B.19) over all k, i and j with

$$4 + k - 2(i+j) \quad = \quad n, \tag{B.20}$$

at $d \to 4$ for dimensional reasons. We are now going to show all properties of eq.(3.1) for arbitrary k, i, j and thus for the sum by relating eq.(B.19) to the basic integral $H_{11}(M_0, M_0, m_\pi)$ of eq.(B.3) (for simplicity we only discuss onshell nucleons $p^2 = M_0^2$, however the proof can straightforwardly be generalized to the case of offshell nucleons).
The first step on this way is to rewrite the integral of eq.(B.19) as

$$(-1)^{i+j} \frac{\partial^{i-1}}{\partial {m_\pi^2}^{i-1}} \frac{\partial^{j-1}}{\partial {M_0^2}^{j-1}} \int \frac{dl^d}{(2\pi)^d} \frac{l^{\mu_1} l^{\mu_2} \dots l^{\mu_k}}{\Pi N}. \tag{B.21}$$

The integral of this equation would in complete analogy of eqs.(B.8) and (B.9) be a sum over integral functions multiplied with structures like $g^{\mu_1\mu_2} g^{\mu_3\mu_4} \cdots$ and $\frac{p^{\mu_1}}{M_0} \frac{p^{\mu_2}}{M_0} \cdots$ and compositions thereof. In order to perform a tensor reduction of this integral we would have to multiply both sides (eq.(B.21) and the result in terms of Dirac structures times integral functions $H_{11}^{(i)}$) either with $g^{\mu_1\mu_2} \cdots$, $\frac{p^{\mu_1}}{M_0} \cdots$ or mixtures, to make a scalar out of both sides. While the right hand side just gives some dimensionless number times the integral functions, we find on the left hand side:

$$g_{\mu_1\mu_2} l^{\mu_1} l^{\mu_2} \quad = \quad m_\pi^2 - \Pi, \tag{B.22}$$

$$\frac{p_{\mu_1}}{M_0} l^{\mu_1} \quad = \quad \frac{1}{2} \left(N - \Pi + m_\pi^2 \right). \tag{B.23}$$

Since all terms in the tensor reduction which go like Π and N just correspond to eq.(B.19) with a different set of k, i and j, we are only interested in the terms $\sim m_\pi^2$ of the tensor reduction. $O^{(n)}$ thus consists of terms of the form

$$(-1)^{i+j} M_0^{k-2\rho} \frac{\partial^{i-1}}{\partial {m_\pi^2}^{i-1}} \frac{\partial^{j-1}}{\partial {M_0^2}^{j-1}} {m_\pi^2}^{\rho} H_{11}(M_0, M_0, m_\pi). \tag{B.24}$$

where $\frac{k}{2} \leq \rho \leq k$ ($\rho = \frac{k}{2}$ corresponds to a contraction of all open Dirac indices with terms like $\frac{p^\mu}{M_0}$, while $\rho = k$ results from a contraction with $g^{\mu_1\mu_2}$ structures only). Note that a contractions with $\frac{p_{\mu_1}}{M_0}$ does not generate a divergence or a scale dependence beyond m_π^0. This can be seen from eq.(B.23) via

$$\frac{p_{\mu_1}}{M_0} \int \frac{dl^d}{(2\pi)^d} \frac{l^{\mu_1}}{\Pi N} \quad = \quad \frac{1}{2} \left[m_\pi^2 H_{11}(M_0, M_0, m_\pi) + \Delta_\pi - \Delta_N \right]. \tag{B.25}$$

Where one can check with the help of the basic functions eqs.(B.2)-(B.3) that it does not contain an L term or a scale dependent logarithm beyond m_π^0. The generalization of this statement for arbitrary i and j follows by the same argument.
All statement made in eq.(3.1) can now be derived from eq.(B.24):

1. The highest power of m_π at which a UV-divergence L can appear is m_π^n: All divergences in $O^{(n)}$ are generated through eq.(B.24) out of the term $-2L$ of $H_{11}(M_0, M_0, m_\pi)$, see eq.(B.3). Thus the L terms in $O^{(n)}$ come from $j = 1$ and $\rho > i$ terms, where the maximal power of m_π is generated for $i = 1$. From the argument of eq.(B.25) one can see that only terms with $\rho = \frac{k}{2}$ can generate a term $\sim L$ in the final result. Inserting those values for the indices in eqs.(B.20) and (B.24) one finds that the maximum power in the pion mass at which a divergence L appears in $O^{(n)}$ is m_π^n.

2. A term $\sim \log \lambda$ can only appear at m_π^r with $r \leq n$: The proof for this statement goes exactly as above, since all basic integrals contain scale dependent logarithms only together with L in terms of the form $L - \frac{1}{16\pi^2} \log \lambda$.

3. A term $\sim \log m_\pi$ can only appear at m_π^s with $s \geq n$: Logarithms of the pion mass originate from a term $m_\pi^2 \log m_\pi$ in $H_{11}(M_0, M_0, m_\pi)$. The minimal power of m_π is realized by $j = 1$ and $\rho = \frac{k}{2}$. With these indices we find from eqs.(B.20) and (B.24) that the minimal power of the pion mass in front of a logarithm of the pion mass is $m_\pi^{2\,\frac{k}{2}+1-i}$ with $k = n + 2(i-1)$ and such m_π^n, where n is even.

4. The lowest possible odd power in the pion mass is n: All odd powers in the pion mass are generated out of the $\arccos$ structure of $H_{11}(M_0, M_0, m_\pi)$ with a leading term linear in m_π. For the general $O^{(n)}$ now the same argument holds as for the $\log m_\pi$ above.

Appendix C

Appendices to Chapter 4

C.1 Regulator Functions

In this section we give the relevant regular parts of the loop integrals which appear in a calculation of the nucleon form factors at next-to-leading one loop order. The full regulator functions can be found in appendix B.2. We note that for our $\mathcal{O}(p^4)$ calculation of nucleon form factors we only need to know these expressions up to the power[1] of m_π^2, t in order to obtain a properly renormalized, scale independent result, which at the same time is also consistent with the requirements of power-counting. The regulator function needed for our $\mathcal{O}(p^4)$ BChPT calculation (see Appendix D.2) reads

$$R_{11}^{(1)}(M_0^2, m_\pi^2, p^2) = \left(1+\frac{m_\pi^2}{M_0^2}\right) L + \frac{1}{16\pi^2}\left[\log\frac{M_0}{\lambda} + \frac{1}{2}\frac{m_\pi^2}{M_0^2}\left(2\log\frac{M_0}{\lambda}-1\right)\right] + ..., \quad \text{(C.1)}$$

The derivatives of the regulator functions needed for the calculation (see Appendix D.2) read

$$\begin{aligned}
\frac{\partial}{\partial M_0^2} R_{11}(\tilde{M}, \tilde{p}, m_\pi) &= \frac{1}{M_0^2}\left(1+\frac{t}{6M_0^2}\right) L + \frac{1}{32\pi^2 M_0^2}\left(1+2\log\frac{M_0}{\lambda}-\frac{m_\pi^2}{M_0^2}\right) \\
&\quad + \frac{t}{96\pi^2 M_0^4}\log\frac{M_0}{\lambda} + ..., && \text{(C.2)} \\
\frac{\partial}{\partial M_0^2} R_{11}^{(2)}(\tilde{M}, \tilde{p}, m_\pi) &= \frac{1}{2}\left(1+\frac{m_\pi^2}{M_0^2}\right) L + \frac{1}{32\pi^2}\left[\log\frac{M_0}{\lambda} + \frac{1}{2}\left(2\log\frac{M_0}{\lambda}-1\right)\right] - \frac{t}{384\pi^2 M_0^2} \\
&\quad + ..., && \text{(C.3)} \\
\frac{\partial}{\partial M_0^2} R_{11}^{(3)}(\tilde{M}, \tilde{p}, m_\pi) &= -\frac{m_\pi^2}{M_0^4} L + \frac{1}{16\pi^2 M_0^2}\left[\frac{1}{2} + \frac{m_\pi^2}{M_0^2}\left(-\log\frac{M_0}{\lambda}+1\right)\right] + \frac{t}{192\pi^2 M_0^4} + ..., && \text{(C.4)} \\
\frac{\partial}{\partial m_\pi^2} R_{11}^{(2)}(M_0, \tilde{p}, \tilde{m}) &= \left(\frac{1}{2} - \frac{m_\pi^2}{M_0^2} + \frac{t}{4M_0^2}\right) L + \frac{1}{96\pi^2}\left[3\log\frac{M_0}{\lambda} - 3 - \left(6\log\frac{M_0}{\lambda}+3\right)\frac{m_\pi^2}{M_0^2}\right] \\
&\quad + \frac{t}{576\pi^2 M_0^2}\left(9\log\frac{M_0}{\lambda}-1\right) + ..., && \text{(C.5)} \\
\frac{\partial}{\partial m_\pi^2} R_{11}^{(3)}(M_0, \tilde{p}, \tilde{m}) &= \frac{1}{2M_0^4}\left(-4m_\pi^2+t\right) L + \frac{1}{32\pi^2 M_0^2}\left(1+4\frac{m_\pi^2}{M_0^2}\log\frac{M_0}{\lambda}\right) \\
&\quad + \frac{t}{288\pi^2 M_0^4}\left(-9\log\frac{M_0}{\lambda}+5\right) + ..., && \text{(C.6)} \\
& && \text{(C.7)}
\end{aligned}$$

[1] Strictly speaking $F_1(t)$ is renormalized up to terms $\sim m_\pi^2 t^0$ and $\sim m_\pi^0 t^1$ at order p^3, whereas those structures in $F_2(t)$ are only renormalized at order p^4, see chapter 3.

One can clearly observe that all contributions are polynomial in m_π^2 (and therefore polynomial in the quark mass) and polynomial in t, as expected. Their addition to the $\overline{\rm MS}$ results therefore just amounts to a redefinition of the the coupling constants of the effective field theory and does not affect the nonanalytic quark mass dependencies, which are the scheme independent signatures of chiral dynamics.

C.2 Amplitudes

The five $\mathcal{O}(p^3)$ and three $\mathcal{O}(p^4)$ amplitudes corresponding to the diagrams of figures 4.1 and 4.2 written in terms of the basic integrals

$$I_{11}^{(i)}\left(M^2,m^2,p^2\right)=H_{11}^{(i)}\left(M^2,m^2,p^2\right)+R_{11}^{(i)}\left(M^2,m^2,p^2\right)\ ,\quad i=0\ldots3, \tag{C.8}$$

of Appendices B.1 and C.1 read

$$\begin{aligned}
Amp^a &= \frac{g_A^2}{F_\pi^2}\eta^\dagger\ (3\cdot\mathbb{1}-\tau^a)\,\eta\bar u(p_2)\int_{-\frac12}^{\frac12}du\Bigg\{\gamma^\mu\frac18\Bigg[\Delta_\pi-4M_0^2I_{11}^{(1)}(M_0,M_0,m_\pi)\\
&\quad+4m_\pi^2M_0^2\frac{\partial}{\partial\tilde M^2}I_{11}(\tilde M,\tilde p,m_\pi)-8M_0^2\frac{\partial}{\partial\tilde M^2}I_{11}^{(2)}(\tilde M,\tilde p,m_\pi)\\
&\quad-8M_0^4\frac{\partial}{\partial\tilde M^2}I_{11}^{(3)}(\tilde M,\tilde p,m_\pi)\Bigg]+\frac{i}{2M_N}\sigma^{\mu\nu}q_\nu\frac{M_N}{M_0}\left[M_0^4\frac{\partial}{\partial\tilde M^2}I_{11}^{(3)}(\tilde M,\tilde p,m_\pi)\right]\Bigg\}u(p_2),
\end{aligned} \tag{C.9}$$

$$Amp^{b+c} = \frac{g_A^2}{F_\pi^2}\eta^\dagger\tau^a\eta\,\bar u(p_2)\,\gamma^\mu\left[\Delta_\pi-2M_0^2I_{11}^{(1)}(M_0,M_0,m_\pi)\right]u(p_1), \tag{C.10}$$

$$\begin{aligned}
Amp^d &= \frac{g_A^2}{F_\pi^2}\eta^\dagger\tau^a\eta\,\bar u(p_2)\int_{-\frac12}^{\frac12}du\Bigg\{\gamma^\mu\Bigg[-\frac{\partial}{\partial m_\pi^2}\frac{\tilde m^2}{d}\Delta_\pi(\tilde m)+4M_0^2\frac{\partial}{\partial m_\pi^2}I_{11}^{(2)}(M_0,\tilde p,\tilde m)\\
&\quad+4M_0^4\frac{\partial}{\partial m_\pi^2}I_{11}^{(3)}(M_0,\tilde p,\tilde m)\Bigg]\\
&\quad+\frac{i}{2M_N}\sigma^{\mu\nu}q_\nu\frac{M_N}{M_0}\left[-4M_0^4\frac{\partial}{\partial m_\pi^2}I_{11}^{(3)}(M_0,\tilde p,\tilde m)\right]\Bigg\}u(p_1),
\end{aligned} \tag{C.11}$$

$$Amp^e = -\frac{1}{2F_\pi^2}\eta^\dagger\tau^a\eta\,\bar u(p_2)\,\gamma^\mu\Delta_\pi\,u(p_1), \tag{C.12}$$

$$Amp^f = \frac{1}{F_\pi^2}\eta^\dagger\tau^a\eta\,\bar u(p_2)\,\gamma^\mu\int_{-\frac12}^{\frac12}du\frac{\partial}{\partial m_\pi^2}\frac{\tilde m^2}{d}\Delta_\pi(\tilde m)\,u(p_1), \tag{C.13}$$

$$
\begin{aligned}
Amp^g &= \frac{g_A^2}{F_\pi^2}\eta^\dagger\,\left[(3\cdot\mathbb{1}-\tau^a)\,c_6+6c_7\cdot\mathbb{1}\right]\eta\,\bar{u}(p_1)\int_{-\frac{1}{2}}^{\frac{1}{2}}du\Bigg\{\gamma^\mu\Bigg[-\frac{tM_0^2}{4}\frac{\partial}{\partial\tilde{M}^2}I_{11}^{(3)}(\tilde{M},\tilde{p},m_\pi)\Bigg] \\
&\quad+\frac{i}{2M_N}\sigma^{\mu\nu}q_\nu\frac{1}{8}\frac{M_N}{M_0}\Bigg[-\Delta_\pi+4M_0^2I_{11}^{(1)}(\tilde{M},\tilde{p},m_\pi)+4m_\pi^2M_0^2\frac{\partial}{\partial\tilde{M}^2}I_{11}(\tilde{M},\tilde{p},m_\pi) \\
&\quad-16M_0^2\frac{\partial}{\partial\tilde{M}^2}I_{11}^{(2)}(\tilde{M},\tilde{p},m_\pi)+8tM_0^2\left(\frac{1}{4}-u^2\right)\frac{\partial}{\partial\tilde{M}^2}I_{11}^{(3)}(\tilde{M},\tilde{p},m_\pi)\Bigg]\Bigg\}u(p_1), \qquad \text{(C.14)} \\
Amp^h &= \frac{1}{F_\pi^2}\eta^\dagger\,(\mathbb{1}+\tau^a)\,\eta\,\bar{u}(p_2)\gamma^\mu\left[\frac{3m_\pi^2c_2}{4M_0}\left(\Delta_\pi-\frac{m_\pi^2}{32\pi^2}\right)\right]u(p_1) \\
&\quad-\frac{1}{2F_\pi^2}\eta^\dagger\tau^a\eta\,\bar{u}(p_2)\left[\frac{i}{2M_N}\sigma^{\mu\nu}q_\nu c_6\frac{M_N}{M_0}\Delta_\pi\right]u(p_1), \qquad \text{(C.15)} \\
Amp^i &= \frac{4M_0c_4}{F_\pi^2}\eta^\dagger\tau^a\eta\,\bar{u}(p_2)\left[\frac{i}{2M_N}\sigma^{\mu\nu}q_\nu\frac{M_N}{M_0}\int_{-\frac{1}{2}}^{\frac{1}{2}}du\frac{\partial}{\partial m_\pi^2}\frac{\tilde{m}^2}{d}\Delta_\pi(\tilde{m})\right]u(p_1). \qquad \text{(C.16)}
\end{aligned}
$$

with

$$
\begin{aligned}
\tilde{M}^2 = \quad \tilde{p}^2 &= M_0^2+\left(u^2-\frac{1}{4}\right)t, \qquad \text{(C.17)} \\
\tilde{m}^2 &= m_\pi^2+\left(u^2-\frac{1}{4}\right)t. \qquad \text{(C.18)}
\end{aligned}
$$

The nucleon Z-factor reads:

$$
\begin{aligned}
\mathcal{Z}_N &= 1-\frac{3g_A^2}{4F_\pi^2}\Bigg[2m_\pi^2\left(-\left(m_\pi^2-2M_0^2\right)\frac{\partial}{\partial M_0^2}I_{11}(M_0,p,m_\pi)+I_{11}(M_0,M_0,m_\pi)\right)_{p\to M_0}+\Delta_\pi\Bigg] \\
&\quad-\frac{3m_\pi^2c_2}{2M_0F_\pi^2}\left(\Delta_\pi-\frac{m_\pi^2}{32\pi^2}\right)+\mathcal{O}(p^5). \qquad \text{(C.19)}
\end{aligned}
$$

C.3 Explicit Representation of the Form Factors

C.3.1 Isovector form factors

We employ the definitions

$$F_1^v(t) = 1 + B_{c1}^v t + A_1^{(3)}(t) + A_1^{(4)}(t) + \mathcal{O}(p^5), \tag{C.20}$$

$$F_2^v(t) = \frac{M^{(n)}}{M_0}\left[c_6 + B_{c2}^v t + A_2^{(3)}(t) + A_2^{(4)}(t) + \mathcal{O}(p^5)\right], \tag{C.21}$$

and obtain for the t-dependent functions

$$\begin{aligned}
A_1^{(3)}(t) = {} & \frac{g_A^2}{192\pi^2 F_\pi^2}\int_{u=-\frac{1}{2}}^{u=\frac{1}{2}}\frac{du}{\tilde{M}^4}\Bigg[-96M^6+12\left(8\tilde{m}^2+5\tilde{M}^2\right)M^4 \\
& +\left(36\tilde{M}^4-24\tilde{m}^2\tilde{M}^2\right)M^2-6m_\pi^2\left(4M^4-\tilde{M}^2M^2+9\tilde{M}^4\right)+29t\tilde{M}^4\Bigg] \\
& +\frac{g_A^2 m_\pi^3}{32\pi^2F_\pi^2M^2}\int_{u=-\frac{1}{2}}^{u=\frac{1}{2}}\frac{du}{\tilde{M}^6\sqrt{\left(m_\pi^2-4M^2\right)\left(m_\pi^2-4\tilde{M}^2\right)}}\Bigg[M^4\sqrt{4M^2-m_\pi^2}\Big(-2\tilde{M}^4 \\
& +12M^2\tilde{M}^2+m_\pi^2\left(\tilde{M}^2-4M^2\right)\Big)\arccos\left(\frac{m_\pi}{2\tilde{M}}\right) \\
& -3\left(3m_\pi^2-10M^2\right)\tilde{M}^6\sqrt{4\tilde{M}^2-m_\pi^2}\arccos\left(\frac{m_\pi}{2M}\right)\Bigg] \\
& -\frac{g_A^2M^2}{8\pi^2F_\pi^2}\int_{u=-\frac{1}{2}}^{u=\frac{1}{2}}\frac{du}{\tilde{M}^6\sqrt{2M^2\left(\tilde{m}^2+\tilde{M}^2\right)-M^4-\left(\tilde{m}^2-\tilde{M}^2\right)^2}}\Bigg[4M^8 \\
& -3\left(4\tilde{m}^2+3\tilde{M}^2\right)M^6+\left(12\tilde{m}^4+7\tilde{M}^2\tilde{m}^2+5\tilde{M}^4\right)M^4+\Big(-4\tilde{m}^6+\tilde{M}^2\tilde{m}^4 \\
& +2\tilde{M}^4\tilde{m}^2+\tilde{M}^6\Big)M^2+\tilde{M}^2\left(\tilde{m}^2-\tilde{M}^2\right)^3\Bigg]\arccos\left(\frac{M^2-\tilde{M}^2+\tilde{m}^2}{2M\tilde{m}}\right) \\
& +\frac{1}{32\pi^2F_\pi^2M^2}\int_{u=-\frac{1}{2}}^{u=\frac{1}{2}}\frac{du}{\tilde{M}^6}\Bigg[g_A^2\left(-2\tilde{M}^6+4m_\pi^2M^2\tilde{M}^2+m_\pi^4\left(\tilde{M}^2-4M^2\right)\right)M^4\log\frac{\tilde{M}}{M} \\
& -4\Big(g_A^2\Big(\left(M^2+\tilde{m}^2\right)\tilde{M}^6+2M^2\tilde{m}^2\tilde{M}^4-M^2\left(5M^4-2\tilde{m}^2M^2+\tilde{m}^4\right)\tilde{M}^2 \\
& +4M^4\left(M^2-\tilde{m}^2\right)^2\Big)-\tilde{m}^2\tilde{M}^6\Big)M^2\log\frac{\tilde{m}}{m_\pi}+g_A^2\Big(4tM^2\tilde{M}^6 \\
& -4m_\pi^2M^2\left(M^4+3\tilde{M}^4\right)\tilde{M}^2+4M^4\Big(-\tilde{M}^6-2\tilde{m}^2\tilde{M}^4+\left(5M^4-2\tilde{m}^2M^2+\tilde{m}^4\right)\tilde{M}^2 \\
& -4M^2\left(M^2-\tilde{m}^2\right)^2\Big)+m_\pi^4\left(4M^6-\tilde{M}^2M^4+9\tilde{M}^6\right)\Big)\log\frac{m_\pi}{M} \\
& -\frac{2}{3}M^2\tilde{M}^6t\left(\left(5g_A^2+1\right)\log\frac{m_\pi}{M}+g_A^2\right)\Bigg],
\end{aligned} \tag{C.22}$$

$$
\begin{aligned}
A_1^{(4)}(t) &= -\frac{g_A^2 c_6 m_\pi^3 t M_0^2}{32\pi^2 F_\pi^2}\int_{u=-\frac{1}{2}}^{u=\frac{1}{2}}\frac{du}{\tilde{M}^6}\frac{m_\pi^2-3\tilde{M}^2}{\sqrt{4\tilde{M}^2-m_\pi^2}}\arccos\left(\frac{m_\pi}{2\tilde{M}}\right)\\
&+\frac{g_A^2 c_6 t}{64\pi^2 F_\pi^2}\int_{u=-\frac{1}{2}}^{u=\frac{1}{2}}\frac{du}{\tilde{M}^6}\Bigg[\tilde{M}^6-M_0^2\tilde{M}^4-2m_\pi^2M_0^2\tilde{M}^2\\
&+2m_\pi^2M_0^2\left(m_\pi^2-\tilde{M}^2\right)\log\frac{m_\pi}{\tilde{M}}\Bigg], \qquad \text{(C.23)}
\end{aligned}
$$

for the isovector Dirac form factor and

$$
\begin{aligned}
A_2^{(3)}(t) &= \frac{g_A^2 M M_0}{(4\pi F_\pi)^2}\int_{u=-\frac{1}{2}}^{u=\frac{1}{2}}\frac{du}{\tilde{M}^4}\left[8M^4+2m_\pi^2M^2-\left(8\tilde{m}^2+3\tilde{M}^2\right)M^2-5\tilde{M}^4\right]\\
&+\frac{g_A^2M^3M_0}{8\pi^2F_\pi^2}\int_{u=-\frac{1}{2}}^{u=\frac{1}{2}}\frac{du}{\tilde{M}^6}\Bigg[m_\pi^2\left(m_\pi^2-\tilde{M}^2\right)\log\frac{\tilde{M}}{M}+\Big(4\left(M^2-\tilde{m}^2\right)^2\\
&+\tilde{M}^2\left(m_\pi^2-4M^2\right)-m_\pi^4\Big)\log\frac{m_\pi}{M}+4\Big(\left(M^2-\tilde{m}^2\right)^2-M^2\tilde{M}^2\Big)\log\frac{\tilde{m}}{m_\pi}\Bigg]\\
&+\frac{g_A^2M^3M_0}{8\pi^2F_\pi^2}\int_{u=-\frac{1}{2}}^{u=\frac{1}{2}}\frac{du}{\tilde{M}^6}\Bigg[\\
&4\frac{M^6-\left(3\tilde{m}^2+2\tilde{M}^2\right)M^4+\left(3\tilde{m}^4+\tilde{M}^2\tilde{m}^2+\tilde{M}^4\right)M^2-\tilde{m}^6+\tilde{m}^4\tilde{M}^2}{\sqrt{2M^2\left(\tilde{M}^2+\tilde{m}^2\right)-\left(\tilde{M}^2-\tilde{m}^2\right)^2-M^4}}\\
&\times\arccos\left(\frac{M^2+\tilde{m}^2-\tilde{M}^2}{2\tilde{m}M}\right)-\frac{m_\pi^3\left(3\tilde{M}^2-m_\pi^2\right)}{\sqrt{4\tilde{M}^2-m_\pi^2}}\arccos\left(\frac{m_\pi}{2\tilde{M}}\right)\Bigg], \qquad \text{(C.24)}
\end{aligned}
$$

$$
\begin{aligned}
A_2^{(4)}(t) &= \frac{1}{192\pi^2F_\pi^2M_0^2}\int_{u=-\frac{1}{2}}^{u=\frac{1}{2}}\frac{du}{\tilde{M}^6}\Bigg[-8M_0^2\Big(\left(2c_4M_0-6g_A^2\right)t\\
&+3m_\pi^2\left(2c_6g_A^2+7g_A^2+c_6-4c_4M_0\right)\Big)\tilde{M}^6\log\frac{m_\pi}{M_0}-6g_A^2\Big(4M_0^2\tilde{M}^6\left(2t-7m_\pi^2\right)\\
&+c_6m_\pi^2\left(\left(4M_0^6-2\tilde{M}^2M_0^4-7\tilde{M}^6\right)m_\pi^2+2M_0^2\tilde{M}^2\left(-2M_0^4+\tilde{M}^2M_0^2+\tilde{M}^4\right)\right)\Big)\log\frac{m_\pi}{M_0}\\
&+96c_4\tilde{m}^2M_0^3\tilde{M}^6\log\frac{\tilde{m}}{m_\pi}+g_A^2M_0^2\Bigg[-2\left(12m_\pi^2+13t\right)\tilde{M}^6\\
&+c_6\Bigg(\left(3M_0^2(1-4u^2)-4\tilde{M}^2\right)t\tilde{M}^4+12m_\pi^2\left(2M_0^2-3\tilde{M}^2\right)\left(M_0^2+\tilde{M}^2\right)\tilde{M}^2\Bigg)\\
&+12c_6M_0^2\Big(-2\tilde{M}^6+m_\pi^4\left(2M_0^2-\tilde{M}^2\right)+m_\pi^2\left(\tilde{M}^4-2M_0^2\tilde{M}^2\right)\Big)\log\frac{\tilde{M}}{M_0}\Bigg]\Bigg]\\
&+\frac{g_A^2c_6m_\pi^3}{32\pi^2F_\pi^2M_0^2}\int_{u=-\frac{1}{2}}^{u=\frac{1}{2}}\frac{du}{\tilde{M}^6\sqrt{\left(4M_0^2-m_\pi^2\right)\left(4\tilde{M}^2-m_\pi^2\right)}}\Bigg[M_0^4\sqrt{4M_0^2-m_\pi^2}\left(m_\pi^2-3\tilde{M}^2\right)\\
&\left(4M_0^2-2\tilde{M}^2\right)\arccos\left(\frac{m_\pi}{2\tilde{M}}\right)-\left(7m_\pi^2-22M_0^2\right)\tilde{M}^6\sqrt{4\tilde{M}^2-m_\pi^2}\arccos\left(\frac{m_\pi}{2M_0}\right)\Bigg], \qquad \text{(C.25)}
\end{aligned}
$$

for the isovector Pauli form factor, where $\tilde{M}^2 = M^2 + \left(u^2-\frac{1}{4}\right)t$. Note that the mass-function M in eqs.(C.22,C.24) depends again on the chiral order at which eq.(C.21) is studied.

C.3.2 Isoscalar form factors

In complete analogy to the isovector sector we define

$$F_1^s(t) = 1 + B_{c1}^s t + B_1^{(3)}(t) + B_1^{(4)}(t) + \mathcal{O}(p^5), \tag{C.26}$$

$$F_2^s(t) = \frac{M^{(n)}}{M_0}\left[\kappa_s^0 + B_{c2}^s t + B_2^{(3)}(t) + B_2^{(4)}(t) + \mathcal{O}(p^5)\right]. \tag{C.27}$$

and find the following explicit expressions:

$$\begin{aligned} B_1^{(3)}(t) &= \frac{g_A^2}{64\pi^2 F_\pi^2}\int_{-\frac{1}{2}}^{\frac{1}{2}}\frac{du}{\tilde{M}^6}\Bigg[6m_\pi^2\left(3m_\pi^2-4M^2\right)\frac{\tilde{M}^6}{M^2}\log\frac{m_\pi}{M} - t\tilde{M}^6 \\ &\quad +6\left(M^2-\tilde{M}^2\right)\left(m_\pi^2\left(4M^2+3\tilde{M}^2\right)+2M^2\tilde{M}^2\right)\tilde{M}^2 \\ &\quad +6M^2\left(2\tilde{M}^6\log\frac{\tilde{M}}{M}+\left(m_\pi^2\tilde{M}^2\left(m_\pi^2+4M^2\right)-4m_\pi^4M^2\right)\log\frac{m_\pi}{\tilde{M}}\right)\Bigg] \\ &\quad -\frac{3g_A^2m_\pi^3}{32\pi^2F_\pi^2M^2}\int_{-\frac{1}{2}}^{\frac{1}{2}}\frac{du}{\tilde{M}^6}\Bigg[\frac{3m_\pi^2-10M^2}{\sqrt{4M^2-m_\pi^2}}\tilde{M}^6\arccos\left(\frac{m_\pi}{2M}\right) \\ &\quad +\frac{-2\tilde{M}^4+12M^2\tilde{M}^2+m_\pi^2\left(\tilde{M}^2-4M^2\right)}{\sqrt{4\tilde{M}^2-m_\pi^2}}M^4\arccos\left(\frac{m_\pi}{2\tilde{M}}\right)\Bigg] \end{aligned} \tag{C.28}$$

$$\begin{aligned} B_1^{(4)}(t) &= -\frac{3\kappa_S^0g_A^2t}{64\pi^2F_\pi^2}\int_{-\frac{1}{2}}^{\frac{1}{2}}\frac{du}{\tilde{M}^6}\left[\tilde{M}^6-M_0^2\tilde{M}^4-2m_\pi^2M_0^2\tilde{M}^2+2m_\pi^2M_0^2\left(m_\pi^2-\tilde{M}^2\right)\log\frac{m_\pi}{\tilde{M}}\right] \\ &\quad +\frac{3\kappa_S^0g_A^2m_\pi^3M_0^2t}{32\pi^2F_\pi^2}\int_{-\frac{1}{2}}^{\frac{1}{2}}\frac{du}{\tilde{M}^6}\frac{m_\pi^2-3\tilde{M}^2}{\sqrt{4\tilde{M}^2-m_\pi^2}}\arccos\left(\frac{m_\pi}{2\tilde{M}}\right) \end{aligned} \tag{C.29}$$

for the isovector Dirac form factor and

$$\begin{aligned} B_2^{(3)}(t) &= \frac{g_A^2M_0}{32\pi^2F_\pi^2M}\int_{-\frac{1}{2}}^{\frac{1}{2}}\frac{du}{\tilde{M}^6}\Bigg[6M^2\tilde{M}^2+t\tilde{M}^6-6M^4\tilde{M}^4-12m^2M^4\tilde{M}^2 \\ &\quad +12m_\pi^2M^4\left(m_\pi^2-\tilde{M}^2\right)\log\frac{m_\pi}{\tilde{M}}\Bigg] \\ &\quad -\frac{3g_A^2m_\pi^3M^3M_0}{8\pi^2F_\pi^2}\int_{-\frac{1}{2}}^{\frac{1}{2}}\frac{du}{\tilde{M}^6}\frac{m_\pi^2-3\tilde{M}^2}{\sqrt{4\tilde{M}^2-m_\pi^2}}\arccos\left(\frac{m_\pi}{2\tilde{M}}\right) \end{aligned} \tag{C.30}$$

$$\begin{aligned} B_2^{(4)}(t) &= \frac{3g_A^2m_\pi^2}{8\pi^2F_\pi^2}+\frac{\kappa_S^0g_A^2}{64\pi^2F_\pi^2M_0^2}\int_{-\frac{1}{2}}^{\frac{1}{2}}\frac{du}{\tilde{M}^6}\Bigg[6m_\pi^2\left(m_\pi^2-2M_0^2\right)\tilde{M}^6\log\frac{m_\pi}{M_0} \\ &\quad +M_0^2\tilde{M}^2\left(\tilde{M}^2t\left(3(4u^2-1)M_0^2+4\tilde{M}^2\right)-6m^2\left(M_0^2\left(2\tilde{M}^2-4tu^2+t\right)-2\tilde{M}^4\right)\right) \\ &\quad +6M_0^4\left(4\tilde{M}^6\log\frac{\tilde{M}}{M_0}+m_\pi^2\left(\left(m_\pi^2-\tilde{M}^2\right)\left(2\tilde{M}^2-4tu^2+t\right)\log\frac{m_\pi}{\tilde{M}}\right)\right)\Bigg] \\ &\quad -\frac{3\kappa_S^0g_A^2m_\pi^3}{32\pi^2F_\pi^2M_0^2}\int_{-\frac{1}{2}}^{\frac{1}{2}}\frac{du}{\tilde{M}^6}\Bigg[\frac{m_\pi^2-2M_0^2}{\sqrt{4M_0^2-m_\pi^2}}\tilde{M}^6\arccos\left(\frac{m_\pi}{2M_0}\right) \\ &\quad +M_0^4\left(m_\pi^2-3\tilde{M}^2\right)\left(2\tilde{M}^2-4tu^2+t\right)\arccos\left(\frac{m_\pi}{2\tilde{M}}\right)\Bigg]. \end{aligned} \tag{C.31}$$

for the isovector Pauli form factor. Note that the mass-function M in eqs.(C.28,C.30) depends again on the chiral order at which eq.(C.27) is studied.

Appendix D

Appendices to Chapter 5

D.1 Regulator Functions

In this appendix we give the explicit expressions for the relevant parts of the regulator functions needed in order to $\overline{\text{IR}}$ renormalize the $\mathcal{O}(p^2)$ results for the generalized form factors of the nucleon. We note that at the order we are working we only need to know these functions up to the power[1] of m_π^2, t in order to obtain a properly renormalized, scale independent result, which at the same time is also consistent with the requirements of power-counting. The full expressions can be found in section B.2 of the appendix. The relevant parts of the regulator functions needed for our $\mathcal{O}(p^2)$ BChPT calculation (see Appendix D.2) read

$$R_{11}(M_0^2, m_\pi^2, p^2) = \left(2 - \frac{m_\pi^2}{M_0^2}\right) L + \frac{1}{16\pi^2}\left[2\log\frac{M_0}{\lambda} - 1 - \frac{1}{2}\frac{m_\pi^2}{M_0^2}\left(2\log\frac{M_0}{\lambda} + 3\right)\right] + ..., \quad \text{(D.1)}$$

$$R_{11}^{(1)}(M_0^2, m_\pi^2, p^2) = \left(1 + \frac{m_\pi^2}{M_0^2}\right) L + \frac{1}{16\pi^2}\left[\log\frac{M_0}{\lambda} + \frac{1}{2}\frac{m_\pi^2}{M_0^2}\left(2\log\frac{M_0}{\lambda} - 1\right)\right] + ..., \quad \text{(D.2)}$$

$$R_{11}^{(2)}(M_0^2, m_\pi^2, p^2) = \left(\frac{1}{3}M_0^2 + \frac{1}{2}m_\pi^2\right) L + \frac{1}{48\pi^2}\left[\frac{M_0^2}{3}\left(3\log\frac{M_0}{\lambda} - 1\right) + \frac{3}{2}m_\pi^2\left(\log\frac{M_0}{\lambda} - 1\right)\right] + ..., \quad \text{(D.3)}$$

$$R_{11}^{(3)}(M_0^2, m_\pi^2, p^2) = \frac{2}{3}L + \frac{1}{48\pi^2}\left[2\log\frac{M_0}{\lambda} + \frac{1}{3} + \frac{3}{2}\frac{m_\pi^2}{M_0^2}\right] + ..., \quad \text{(D.4)}$$

The derivatives of the regulator functions needed for the calculation (see Appendix D.2) are

$$R_{11}^{(2)\prime}(\tilde{M}^2, m_\pi^2, \tilde{p}^2) = \frac{1}{2}\left(1 + \frac{m_\pi^2}{M_0^2}\right) L + \frac{1}{32\pi^2}\left[\log\frac{M_0}{\lambda} + \frac{m_\pi^2}{2M_0^2}\left(2\log\frac{M_0}{\lambda} - 1\right)\right] - \frac{t}{384\pi^2 M_0^2} + ..., \quad \text{(D.5)}$$

$$R_{11}^{(3)\prime}(\tilde{M}^2, m_\pi^2, \tilde{p}^2) = -\frac{m_\pi^2}{M_0^4}L + \frac{1}{16\pi^2 M_0^2}\left[\frac{1}{2} + \frac{m_\pi^2}{M_0^2}\left(-\log\frac{M_0}{\lambda} + 1\right)\right] + \frac{t}{192\pi^2 M_0^4} + ..., \quad \text{(D.6)}$$

$$R_{11}^{(4)\prime}(\tilde{M}^2, m_\pi^2, \tilde{p}^2) = \frac{1}{3}L + \frac{1}{16\pi^2}\left[\frac{1}{3}\log\frac{M_0}{\lambda} + \frac{1}{18} + \frac{m_\pi^2}{4M_0^2}\right] - \frac{t}{576\pi^2 M_0^2} + ..., \quad \text{(D.7)}$$

$$R_{11}^{(5)\prime}(\tilde{M}^2, m_\pi^2, \tilde{p}^2) = \frac{1}{16\pi^2 M_0^2}\left[\frac{1}{3} - \frac{m_\pi^2}{2M_0^2}\right] + \frac{t}{288\pi^2 M_0^4} + ... \quad \text{(D.8)}$$

[1] Strictly speaking we need to know the regular terms contained in the generalized form factors $A_{2,0}^{s,v}(t)$ up to power $m_\pi^2 t^0$ and $m_\pi^0 t^1$, whereas for $B_{2,0}^{s,v}(t)$ and $C_{2,0}^{s,v}(t)$ only the leading terms $m_\pi^0 t^0$ are required, see chapter 3 and eq.(5.6).

One can clearly observe that all contributions are polynomial in m_π^2 (and therefore polynomial in the quark mass and t, as expected. Their addition to the $\overline{\rm MS}$ results therefore just amounts to a redefinition of the coupling constants [BL99] of the effective field theory and does not affect the nonanalytic quark mass dependencies, which are the scheme-independent signatures of chiral dynamics.

D.2 Isovector Amplitudes in $\mathcal{O}(p^2)$ BChPT

The five $\mathcal{O}(p^2)$ amplitudes in the isovector channel corresponding to the five diagrams of figure 5.1 written in terms of the basic integrals

$$I_{11}^{(i)}\left(M^2,m^2,p^2\right)=H_{11}^{(i)}\left(M^2,m^2,p^2\right)+R_{11}^{(i)}\left(M^2,m^2,p^2\right)\ ,\quad i=0\ldots5, \tag{D.9}$$

of Appendices B.1 and D.1 read

$$\begin{aligned}
Amp^{a+b} =& -i\,\frac{\Delta a_{2,0}^v\ g_A}{F_\pi^2}\ \eta^\dagger\frac{\tau^a}{2}\eta\ \overline{u}(p')\,\gamma_{\{\mu}\overline{p}_{\nu\}}\,u(p)\,\Big[2m_\pi^2 I_{11}(M_0^2,m_\pi^2,p^2) \qquad (D.10)\\
&-m_\pi^2 I_{11}^{(1)}(M_0^2,m_\pi^2,p^2)+2I_{11}^{(2)}(M_0^2,m_\pi^2,p^2)\Big],\\
Amp^{c} =& \,i\,\frac{a_{2,0}^v g_A^2}{4F_\pi^2}\ \eta^\dagger\frac{\tau^a}{2}\eta\ \overline{u}(p')\int_{-\frac{1}{2}}^{\frac{1}{2}}du \qquad (D.11)\\
&\Bigg\{\gamma_{\{\mu}\overline{p}_{\nu\}}\Bigg[-\Delta_\pi+4M_0^2\Big(I_{11}^{(1)}(M_0^2,m_\pi^2,p^2)-I_{11}^{(3)}(M_0^2,m_\pi^2,p^2)\\
&+(2M_0^2-\tilde{M}^2)\left(I_{11}^{(3)\prime}(\tilde{M}^2,m_\pi^2,\tilde{p}^2)-I_{11}^{(5)\prime}(\tilde{M}^2,m_\pi^2,\tilde{p}^2)\right)\\
&+(d-2)\left(I_{11}^{(4)\prime}(\tilde{M}^2,m_\pi^2,\tilde{p}^2)-I_{11}^{(2)\prime}(\tilde{M}^2,m_\pi^2,\tilde{p}^2)\right)\Big)\Bigg]\\
&+\,i\,\Delta^\alpha\sigma_{\alpha\{\mu}\overline{p}_{\nu\}}\,4M_0^3\left(I_{11}^{(3)\prime}(\tilde{M}^2,m_\pi^2,\tilde{p}^2)-I_{11}^{(5)\prime}(\tilde{M}^2,m_\pi^2,\tilde{p}^2)\right)\\
&-\Delta_{\{\mu}\Delta_{\nu\}}\left(8M_0^3\,u^2\,I_{11}^{(5)\prime}(\tilde{M}^2,m_\pi^2,\tilde{p}^2)\right)\Bigg\}\,u(p),\\
Amp^{d} =& -\,i\,\frac{a_{2,0}^v}{F_\pi^2}\ \eta^\dagger\frac{\tau^a}{2}\eta\ \overline{u}(p')\,\gamma_{\{\mu}\overline{p}_{\nu\}}\,u(p)\,\Delta_\pi, \qquad (D.12)\\
Amp^{e} =& \,i\,a_{2,0}^v\ \eta^\dagger\frac{\tau^a}{2}\eta\ \overline{u}(p')\,\gamma_{\{\mu}\overline{p}_{\nu\}}\,u(p)\,\mathcal{Z}_{\mathcal{N}}. \qquad (D.13)
\end{aligned}$$

Note that the various couplings and parameters are defined in section 5.3. η denotes the isospin doublet of proton and neutron. The variables in the integral functions are given as

$$\tilde{p}^2\ =\ \tilde{M}^2\ \ =\ \ M_0^2+\left(u^2-\frac{1}{4}\right)t, \tag{D.14}$$

where $t=q^2$ corresponds to the momentum transfer by the tensor fields. $\mathcal{Z}_{\mathcal{N}}$ denotes the Z-factor of the nucleon, calculated to the required $\mathcal{O}(p^3)$ accuracy in BChPT. It is obtained from the self-energy Σ_N at this order via the prescription

$$\mathcal{Z}_{\mathcal{N}}=1+\left.\frac{\partial\Sigma_N}{\partial\not{p}}\right|_{\not{p}=M_0}+\mathcal{O}(p^4), \tag{D.15}$$

with

$$\Sigma_N=\frac{3g_A^2}{4F_\pi^2}(M_0+\not{p})\big[m_\pi^2 I_{11}(M_0^2,m_\pi^2,p^2)+(M_0-\not{p})\not{p}\,I_{11}^{(1)}(M_0^2,m_\pi^2,p^2)-\Delta_N\big]+\mathcal{O}(p^4). \tag{D.16}$$

D.3 BChPT Results in the Isoscalar Channel

D.3.1 Isoscalar amplitudes in $\mathcal{O}(p^2)$ BChPT

To $\mathcal{O}(p^2)$ in BChPT the results in the isoscalar channel are quite simple. The amplitudes corresponding to the Feynman diagrams of Fig.5.1 can be be simply expressed in terms of results already obtained in the isovector channel discussed in the previous section D.2. They read

$$\begin{aligned}
\overline{Amp}_{a+b} &= 0 + \mathcal{O}(p^3), && \text{(D.17)}\\
\overline{Amp}_{c} &= -3\,\frac{a^s_{2,0}\eta^\dagger \mathbb{1}\eta}{a^v_{2,0}\eta^\dagger\tau^a\eta}\,Amp^c + \mathcal{O}(p^3), && \text{(D.18)}\\
\overline{Amp}_{d} &= 0 + \mathcal{O}(p^3), && \text{(D.19)}\\
\overline{Amp}_{e} &= \frac{a^s_{2,0}\eta^\dagger \mathbb{1}\eta}{a^v_{2,0}\eta^\dagger\tau^a\eta}\,Amp^e + \mathcal{O}(p^3). && \text{(D.20)}
\end{aligned}$$

Note that the various couplings and parameters are defined in section 5.3.

D.3.2 Estimate of $\mathcal{O}(p^3)$ contributions

The contributions from the (higher order) Feynman diagram shown in figure 5.2 to the generalized isoscalar form factors read

$$\begin{aligned}
\Delta A^s_{h.o.}(t,m_\pi) &= \frac{g_A^2 x^0_\pi}{32\pi^2 F_{\pi^2}}\int_{-\frac{1}{2}}^{\frac{1}{2}}\frac{du}{\tilde{p}^8}\Bigg\{2\tilde{p}^8\left(3m_\pi^2+M_0^2\right)-t\tilde{p}^8+4M_0^2\left(2M_0^2+\tilde{m}^2\right)\tilde{p}^6\\
&-2M_0^2\left(11M_0^4-7\tilde{m}^2M_0^2+2\tilde{m}^4\right)\tilde{p}^4+12M_0^4\left(M_0^2-\tilde{m}^2\right)^2\tilde{p}^2\\
&+2M_0^2\Big[-\tilde{p}^8+3\tilde{p}^4\left(3M_0^4-\tilde{m}^4\right)-2\tilde{p}^2\left(M_0^2-\tilde{m}^2\right)\left(7M_0^4-2\tilde{m}^2M_0^2+\tilde{m}^4\right)\\
&+6M_0^2\left(M_0^2-\tilde{m}^2\right)^3\Big]\log\frac{\tilde{m}}{M_0}+\frac{2M_0^2}{\sqrt{2M_0^2\left(\tilde{p}^2+\tilde{m}^2\right)-\left(\tilde{p}^2-\tilde{m}^2\right)^2-M_0^4}}\\
&\Big[6M_0^{10}-4M_0^8\left(6\tilde{m}^2+5\tilde{p}^2\right)+M_0^6\left(36\tilde{m}^4+38\tilde{m}^2\tilde{p}^2+23\tilde{p}^4\right)\\
&-M_0^4\left(24\tilde{m}^6+18\tilde{p}^2\tilde{m}^4+11\tilde{p}^4\tilde{m}^2+9\tilde{p}^6\right)+M_0^2\left(6\tilde{m}^8+2\tilde{p}^2\tilde{m}^6\right.\\
&\left.-5\tilde{p}^4\tilde{m}^4-2\tilde{p}^6\tilde{m}^2-\tilde{p}^8\right)+\tilde{p}^2\left(\tilde{p}^2-\tilde{m}^2\right)^3\left(\tilde{p}^2+2\tilde{m}^2\right)\Big]\arccos\left(\frac{M_0^2+\tilde{m}^2-\tilde{p}^2}{2M_0\tilde{m}}\right)\Bigg\}, \qquad \text{(D.21)}
\end{aligned}$$

$$
\begin{aligned}
\Delta B^s_{h.o.}(t,m_\pi) &= \frac{g_A^2 x_\pi^0}{96\pi^2 F_\pi^2}\,\frac{M_N(m_\pi)}{M_0}\int_{-\frac{1}{2}}^{\frac{1}{2}} du\,\Bigg\{-6M_0^2+18m_\pi^2\left(2\log\frac{M_0}{\lambda}-3\right)+t\left(11-6\log\frac{M_0}{\lambda}\right)\\
&-\frac{36M_0^4}{\tilde{p}^8\sqrt{2\left(\tilde{m}^2+\tilde{p}^2\right)M_0^2-\left(\tilde{p}^2-\tilde{m}^2\right)^2-M_0^4}}\Big[M_0^8-\left(4\tilde{m}^2+3\tilde{p}^2\right)M_0^6\\
&+\left(6\tilde{m}^4+5\tilde{p}^2\tilde{m}^2+3\tilde{p}^4\right)M_0^4-\left(4\tilde{m}^6+\tilde{p}^2\tilde{m}^4+\tilde{p}^4\tilde{m}^2+\tilde{p}^6\right)M_0^2\\
&+\tilde{m}^8-\tilde{m}^6\tilde{p}^2\Big]\arccos\left(\frac{M_0^2+\tilde{m}^2-\tilde{p}^2}{2M_0\tilde{m}}\right)-\frac{6M_0^4}{\tilde{p}^8}\Big[2\tilde{p}^6-3\left(3M_0^2-\tilde{m}^2\right)\tilde{p}^4\\
&+6\left(M_0^2-\tilde{m}^2\right)^2\tilde{p}^2+6\left(M_0^2\tilde{p}^4-2M_0^2\left(M_0^2-\tilde{m}^2\right)\tilde{p}^2+\left(M_0^2-\tilde{m}^2\right)^3\right)\log\frac{\tilde{m}}{M_0}\Big]\Bigg\},\\
&+B_{33}^r(\lambda)\,\frac{M_N(m_\pi)}{M_0}\,\frac{m_\pi^2}{\left(4\pi F_\pi\right)^2}+B_{34}^r(\lambda)\,\frac{M_N(m_\pi)}{M_0}\,\frac{t}{\left(4\pi F_\pi\right)^2},
\end{aligned}
\tag{D.22}
$$

$$
\begin{aligned}
\Delta C^s_{h.o.}(t,m_\pi) &= \frac{g_A^2 x_\pi^0 M_0^2}{96\pi^2 F_\pi^2}\,\frac{M_N(m_\pi)}{M_0}\int_{-\frac{1}{2}}^{\frac{1}{2}}\frac{du}{\tilde{p}^8}\,\Bigg\{5\tilde{p}^8-9M_0^2\tilde{p}^6-6u^2\tilde{p}^2\Big[3\tilde{p}^6-2M_0^2\tilde{p}^4\\
&-3M_0^2\left(M_0^2-3\tilde{m}^2\right)\tilde{p}^2-6\left(M_0^3-M_0\tilde{m}^2\right)^2\Big]-9\left(4u^2-1\right)\tilde{p}^8\log\frac{\tilde{m}}{M_0}\\
&+9M_0^2\Big[4u^2\left(-\tilde{m}^2\tilde{p}^4+2\tilde{m}^2\tilde{p}^2\left(\tilde{m}^2-M_0^2\right)+\left(M_0^2-\tilde{m}^2\right)^3\right)\\
&-\tilde{p}^4\left(M_0^2-\tilde{m}^2\right)\Big]\log\frac{\tilde{m}}{M_0}+\frac{9M_0^2}{\sqrt{2M_0^2\left(\tilde{m}^2+\tilde{p}^2\right)-\left(\tilde{p}^2-\tilde{m}^2\right)^2-M_0^4}}\Big[4u^2M_0^8\\
&-4\left(4\tilde{m}^2+\tilde{p}^2\right)u^2M_0^6-\left(-24u^2\tilde{m}^4+4u^2\tilde{p}^2\tilde{m}^2+\tilde{p}^4\right)M_0^4\\
&+\left(-16u^2\tilde{m}^6+20u^2\tilde{p}^2\tilde{m}^4+2\left(1-2u^2\right)\tilde{m}^2\tilde{p}^4+\tilde{p}^6\right)M_0^2\\
&+\tilde{m}^2\left(\tilde{m}^2-\tilde{p}^2\right)\left(4u^2\tilde{m}^4-8u^2\tilde{m}^2\tilde{p}^2+\left(4u^2-1\right)\tilde{p}^4\right)\Big]\arccos\left(\frac{M_0^2+\tilde{m}^2-\tilde{p}^2}{2M_0\tilde{m}}\right)\Bigg\},
\end{aligned}
\tag{D.23}
$$

with the new variable

$$
\tilde{m}^2 = m_\pi^2+\left(u^2-\frac{1}{4}\right)t. \tag{D.24}
$$

We note that the contributions of $\Delta A^s_{2,0}(t,m_\pi)$, $\Delta C^s_{2,0}(t,m_\pi)$ are finite at $\mathcal{O}(p^3)$ in BChPT, while $\Delta B^s_{2,0}(t,m_\pi)$ contains two new counter-terms, $B^r_{33}(\lambda)$ and $B^r_{34}(\lambda)$, at this order.

Bibliography

[A$^+$67] W. W. Ash et al., *Measurement of the γNN^* Form Factors*, Phys. Lett. **B24** (1967), 165.

[A$^+$05a] C. Alexandrou et al., *First principles calculations of nucleon and pion form factors: Understanding the building blocks of nuclear matter from lattice QCD*, J. Phys. Conf. Ser. **16** (2005), 174–178.

[A$^+$05b] C. Alexandrou et al., *The N to Delta electromagnetic transition form factors from lattice QCD*, Phys. Rev. Lett. **94** (2005), 021601.

[ACK06] S. Ando, J.-W. Chen, and C.-W. Kao, *Leading chiral corrections to the nucleon generalized parton distributions*, Phys. Rev. **D74** (2006), 094013.

[AK$^+$04] A. Ali Khan et al., *The nucleon mass in N(f) = 2 lattice QCD: Finite size effects from chiral perturbation theory*, Nucl. Phys. **B689** (2004), 175–194.

[AKNT06] C. Alexandrou, G. Koutsou, J. W. Negele, and A. Tsapalis, *The nucleon electromagnetic form factors from lattice QCD*, Phys. Rev. **D74** (2006), 034508.

[Ale] C. Alexandrou, *private communication*.

[AS02] D. Arndt and M. J. Savage, *Chiral Corrections to Matrix Elements of Twist-2 Operators*, Nucl. Phys. **A697** (2002), 429–439.

[B$^+$68] W. Bartel et al., *Electroproduction of pions near the Delta(1236) isobar and the form-factor of G*(M)(q**2) of the (gamma N Delta) vertex*, Phys. Lett. **B28** (1968), 148–151.

[B$^+$72] K. Baetzner et al., *Separation of sigma(s) and sigma(t) in the region of the delta(1236) resonance and determination of the magnetic dipole transition form-factor*, Phys. Lett. **B39** (1972), 575–578.

[B$^+$00] R. Beck et al., *Determination of the E2/M1 ratio in the gamma N –> Delta(1232) transition from a simultaneous measurement of p(gamma(pol.),p)pi0 and p(gamma(pol.),pi+)n*, Phys. Rev. **C61** (2000), 035204.

[BC88] J. Bijnens and F. Cornet, *Two pion production in photon-photon collisions*, Nucl. Phys. **B296** (1988), 557.

[Ber03] A. M. Bernstein, *Deviation of the nucleon shape from spherical symmetry: Experimental status*, Eur. Phys. J. **A17** (2003), 349–355.

[Ber07] V. Bernard, *Chiral Perturbation Theory and Baryon Properties*, arXiv:0706.0312 [hep-ph].

[BFHM98] V. Bernard, H. W. Fearing, T. R. Hemmert, and U.-G. Meißner, *The form factors of the nucleon at small momentum transfer*, Nucl. Phys. **A635** (1998), 121–145.

[BHM03] V. Bernard, T. R. Hemmert, and U.-G. Meißner, *Infrared regularization with spin-3/2 fields*, Phys. Lett. **B565** (2003), 137–145.

[BHM05] V. Bernard, T. R. Hemmert, and U.-G. Meißner, *Chiral extrapolations and the covariant small scale expansion*, Phys. Lett. **B622** (2005), 141–150.

[BHM07] M. A. Belushkin, H. W. Hammer, and U. G. Meissner, *Dispersion analysis of the nucleon form factors including meson continua*, Phys. Rev. **C75** (2007), 035202.

[BJ02] A. V. Belitsky and X. Ji, *Chiral structure of nucleon gravitational form factors*, Phys. Lett. **B538** (2002), 289–297.

[BKKM92] V. Bernard, N. Kaiser, J. Kambor, and U.-G. Meißner, *Chiral structure of the nucleon*, Nucl. Phys. **B388** (1992), 315–345.

[BKM95] V. Bernard, N. Kaiser, and U.-G. Meißner, *Chiral dynamics in nucleons and nuclei*, Int. J. Mod. Phys. **E4** (1995), 193–346.

[BL99] T. Becher and H. Leutwyler, *Baryon chiral perturbation theory in manifestly Lorentz invariant form*, Eur. Phys. J. **C9** (1999), 643–671.

[BM06] V. Bernard and U.-G. Meißner, *Chiral perturbation theory*, arXiv:hep-ph/0611231.

[BPT03] S. Boffi, B. Pasquini, and M. Traini, *Linking generalized parton distributions to constituent quark models*, Nucl. Phys. **B649** (2003), 243–262.

[BR05] A. V. Belitsky and A. V. Radyushkin, *Unraveling hadron structure with generalized parton distributions*, Phys. Rept. **418** (2005), 1–387.

[BSS94] M. N. Butler, M. J. Savage, and R. P. Springer, *Electromagnetic moments of the baryon decuplet*, Phys. Rev. **D49** (1994), 3459–3465.

[Buc99] A. J. Buchmann, *N –> Delta quadrupole transition in the constituent quark model*, arXiv:hep-ph/9909385.

[CJ01] J.-W. Chen and X.-D. Ji, *Is the Sullivan process compatible with QCD chiral dynamics?*, Phys. Lett. **B523** (2001), 107–110.

[CJ02] J.-W. Chen and X.-D. Ji, *Leading chiral contributions to the spin structure of the proton*, Phys. Rev. Lett. **88** (2002), 052003.

[CP74] D. G. Caldi and H. Pagels, *Chiral Perturbation Theory and the Magnetic Moments of the Baryon Octet*, Phys. Rev. **D10** (1974), 3739.

[DGH07] M. Dorati, T. A. Gail, and T. R. Hemmert, *Chiral Perturbation Theory and the first moments of the Generalized Parton Distriputions in a Nucleon*, arXiv:nucl-th/0703073.

[DGHH] M. Dorati, T.A. Gail, Ph. Hagler, and T.R. Hemmert, *Moments of nucleon GPDs at next-to-leading one-loop order*, in preparation.

[DH] M. Dorati and T.R. Hemmert, *Generalized Axial Form Factors of the Nucleon*, in preparation.

[DHKT99] D. Drechsel, O. Hanstein, S. S. Kamalov, and L. Tiator, *A unitary isobar model for pion photo- and electroproduction on the proton up to 1-GeV*, Nucl. Phys. **A645** (1999), 145–174.

[DHL88] J. F. Donoghue, B. R. Holstein, and Y. C. Lin, *The reaction gamma gamma → pi0 pi0 and chiral loops*, Phys. Rev. **D37** (1988), 2423.

[Die03] M. Diehl, *Generalized parton distributions*, Phys. Rept. **388** (2003), 41–277.

[dJ06] K. de Jager, *Nucleon form factor experiments and the pion cloud*, arXiv:nucl-ex/0612026.

[DL91] J. F. Donoghue and H. Leutwyler, *Energy and momentum in chiral theories*, Z. Phys. **C52** (1991), 343–351.

[DMN+01] W. Detmold, W. Melnitchouk, J. W. Negele, D. B. Renner, and A. W. Thomas, *Chiral extrapolation of lattice moments of proton quark distributions*, Phys. Rev. Lett. **87** (2001), 172001.

[DMS05] M. Diehl, A. Manashov, and A. Schafer, *Generalized parton distributions for the pion in chiral perturbation theory*, Phys. Lett. **B622** (2005), 69–82.

[DMS06a] M. Diehl, A. Manashov, and A. Schafer, *Chiral perturbation theory for nucleon generalized parton distributions*, Eur. Phys. J. **A29** (2006), 315–326.

[DMS06b] M. Diehl, A. Manashov, and A. Schafer, *Generalized parton distributions for the nucleon in chiral perturbation theory*, arXiv:hep-ph/0611101.

[Dor05] M. Dorati, *Laureau Thesis*, University of Pavia, Pavia, Italy (2005).

[E+06] R. G. Edwards et al., *Nucleon structure in the chiral regime with domain wall fermions on an improved staggered sea*, arXiv:hep-lat/0610007.

[FGJS03] T. Fuchs, J. Gegelia, G. Japaridze, and S. Scherer, *Renormalization of relativistic baryon chiral perturbation theory and power counting*, Phys. Rev. **D68** (2003), 056005.

[FGML73] H. Fritzsch, M. Gell-Mann, and H. Leutwyler, *Advantages of the Color Octet Gluon Picture*, Phys. Lett. **B47** (1973), 365–368.

[FGS04] T. Fuchs, J. Gegelia, and S. Scherer, *Electromagnetic form factors of the nucleon in relativistic baryon chiral perturbation theory*, J. Phys. **G30** (2004), 1407–1426.

[FMMS00] Nadia Fettes, Ulf-G. Meissner, Martin Mojzis, and Sven Steininger, *The chiral effective pion nucleon Lagrangian of order p**4*, Ann. Phys. **283** (2000), 273–302.

[FMS98] N. Fettes, U.-G. Meißner, and S. Steininger, *Pion nucleon scattering in chiral perturbation theory. I: Isospin-symmetric case*, Nucl. Phys. **A640** (1998), 199–234.

[FW03] J. Friedrich and T. Walcher, *A coherent interpretation of the form factors of the nucleon in terms of a pion cloud and constituent quarks*, Eur. Phys. J. **A17** (2003), 607–623.

[G+04] M. Gockeler et al., *Generalized parton distributions from lattice QCD*, Phys. Rev. Lett. **92** (2004), 042002.

[G+05] M. Gockeler et al., *Nucleon electromagnetic form factors on the lattice and in chiral effective field theory*, Phys. Rev. **D71** (2005), 034508.

[G+07] K. Goeke et al., *The pion mass dependence of the nucleon form-factors of the energy momentum tensor in the chiral quark-soliton model*, arXiv:hep-ph/0702031.

[Geo84] H. Georgi, *Weak interactions and modern particle theory*, Benjamin/Cummings, Menlo Park, USA, 1984.

[GH06] T. A. Gail and T. R. Hemmert, *Signatures of chiral dynamics in the nucleon to Delta transition*, Eur. Phys. J. **A28** (2006), 91–105.

[GH07] T. A. Gail and T. R. Hemmert, *The electromagnetic nucleon to Delta transition in chiral effective field theory*, AIP Conf. Proc. **904** (2007), 151–157.

[GHKP99] G. C. Gellas, T. R. Hemmert, C. N. Ktorides, and G. I. Poulis, *The Delta nucleon transition form factors in chiral perturbation theory*, Phys. Rev. **D60** (1999), 054022.

[GL84] J. Gasser and H. Leutwyler, *Chiral Perturbation Theory to One Loop*, Ann. Phys. **158** (1984), 142.

[GMOR68] M. Gell-Mann, R. J. Oakes, and B. Renner, *Behavior of current divergences under SU(3) x SU(3)*, Phys. Rev. **175** (1968), 2195–2199.

[GRS99] M. Gluck, E. Reya, and I. Schienbein, *Pionic parton distributions revisited*, Eur. Phys. J. **C10** (1999), 313–317.

[GSS88] J. Gasser, M. E. Sainio, and A. Svarc, *Nucleons with chiral loops*, Nucl. Phys. **B307** (1988), 779.

[H$^+$] T.R. Hemmert et al., *The energy momentum tensor of a nucleon from the viewpoint of ChPT*, in preparation.

[H$^+$03] P. Hagler et al., *Moments of nucleon generalized parton distributions in lattice QCD*, Phys. Rev. **D68** (2003), 034505.

[H$^+$07] P. Hagler et al., *Nucleon Generalized Parton Distributions from Full Lattice QCD*, arXiv:0705.4295 [hep-lat].

[HGHP04] R. P. Hildebrandt, H. W. Griesshammer, T. R. Hemmert, and B. Pasquini, *Signatures of chiral dynamics in low energy Compton scattering off the nucleon*, Eur. Phys. J. **A20** (2004), 293–315.

[HHK98] T. R. Hemmert, B. R. Holstein, and J. Kambor, *Chiral Lagrangians and Delta(1232) interactions: Formalism*, J. Phys. **G24** (1998), 1831–1859.

[HPW03] T. R. Hemmert, M. Procura, and W. Weise, *Quark mass dependence of the nucleon axial-vector coupling constant*, Phys. Rev. **D68** (2003), 075009.

[HW02] T. R. Hemmert and W. Weise, *Chiral magnetism of the nucleon*, Eur. Phys. J. **A15** (2002), 487–504.

[J$^+$02] K. Joo et al., *Q**2 dependence of quadrupole strength in the gamma* p –> Delta(1232)+ –> p pi0 transition*, Phys. Rev. Lett. **88** (2002), 122001.

[Ji97] X.-D. Ji, *Gauge invariant decomposition of nucleon spin*, Phys. Rev. Lett. **78** (1997), 610–613.

[Ji98] X.-D. Ji, *Off-forward parton distributions*, J. Phys. **G24** (1998), 1181–1205.

[JM91] E. E. Jenkins and A. V. Manohar, *Baryon chiral perturbation theory using a heavy fermion Lagrangian*, Phys. Lett. **B255** (1991), 558–562.

[JS73] H. F. Jones and M. D. Scadron, *Multipole gamma N Delta form-factors and resonant photoproduction and electroproduction*, Ann. Phys. **81** (1973), 1–14.

[K$^+$06] A. Ali Khan et al., *The axial charge of the nucleon on the lattice and in chiral perturbation theory*, PoS **LAT2005** (2006), 349.

[Kai03] N. Kaiser, *Spectral functions of isoscalar scalar and isovector electromagnetic form factors of the nucleon at two-loop order*, Phys. Rev. **C68** (2003), 025202.

[KM01] B. Kubis and Ulf-G. Meissner, *Low energy analysis of the nucleon electromagnetic form factors*, Nucl. Phys. **A679** (2001), 698–734.

[KP02] N. Kivel and M. V. Polyakov, *One loop chiral corrections to hard exclusive processes. I: Pion case*, arXiv:hep-ph/0203264.

[Kra90] A. Krause, *Baryon matrix elements of the vector current in chiral perturbation theory*, Helv. Phys. Acta **63** (1990), 3–70.

[KY99] S. S. Kamalov and S. N. Yang, *Pion cloud and the Q**2 dependence of gamma* N <–> Delta transition form factors*, Phys. Rev. Lett. **83** (1999), 4494–4497.

[KYD+01] S. S. Kamalov, S. N. Yang, D. Drechsel, O. Hanstein, and L. Tiator, *gamma* N –> Delta transition form factors: A new analysis of the JLab data on p(e,e' p)pi0 at Q**2 = 2.8-(GeV/c)**2 and 4.0-(GeV/c)**2*, Phys. Rev. **C64** (2001), 032201.

[L+04] LHPC et al., *Transverse structure of nucleon parton distributions from lattice QCD*, Phys. Rev. Lett. **93** (2004), 112001.

[LQ] LHPC and QCDSF, - *FORTHCOMMING* -.

[LTW97] D.-H. Lu, A. W. Thomas, and A. G. Williams, *Chiral bag model approach to Delta electroproduction*, Phys. Rev. **C55** (1997), 3108–3114.

[Lus06] M. Luscher, *Lattice QCD with light Wilson quarks*, PoS **LAT2005** (2006), 002.

[MB99] J. A. McGovern and M. C. Birse, *On the absence of fifth-order contributions to the nucleon mass in heavy-baryon chiral perturbation theory*, Phys. Lett. **B446** (1999), 300–305.

[MB06] J. A. McGovern and M. C. Birse, *Convergence of the chiral expansion for the nucleon mass*, Phys. Rev. **D74** (2006), 097501.

[Mus05] B. Musch, *Hadron masses: Lattice QCD and chiral effective field theory*, arXiv:hep-lat/0602029.

[P+01] Th. Pospischil et al., *Measurement of the recoil polarization in the p(e(pol.),e' p(pol.))pi0 reaction at the Delta(1232) resonance*, Phys. Rev. Lett. **86** (2001), 2959–2962.

[PBe07] C. N. Papanicolas and E. M. Bernstein (editors), *Shapes of hadrons*, American Institute of Physics, Melville, New York, 2007.

[PHW04] M. Procura, T. R. Hemmert, and W. Weise, *Nucleon mass, sigma term and lattice QCD*, Phys. Rev. **D69** (2004), 034505.

[PMHW07] M. Procura, B. U. Musch, T. R. Hemmert, and W. Weise, *Chiral extrapolation of g(A) with explicit Delta(1232) degrees of freedom*, Phys. Rev. **D75** (2007), 014503.

[PMW+06] M. Procura, B. U. Musch, T. Wollenweber, T. R. Hemmert, and W. Weise, *Nucleon mass: From lattice QCD to the chiral limit*, Phys. Rev. **D73** (2006), 114510.

[PPV06] C. F. Perdrisat, V. Punjabi, and M. Vanderhaeghen, *Nucleon electromagnetic form factors*, arXiv:hep-ph/0612014.

[PV05] V. Pascalutsa and M. Vanderhaeghen, *Electromagnetic nucleon to Delta transition in chiral effective field theory*, Phys. Rev. Lett. **95** (2005), 232001.

[PV06] V. Pascalutsa and M. Vanderhaeghen, *Chiral effective-field theory in the Delta(1232) region. I: Pion electroproduction on the nucleon*, Phys. Rev. **D73** (2006), 034003.

[RS41] W. Rarita and J. S. Schwinger, *On a theory of particles with half integral spin*, Phys. Rev. **60** (1941), 61.

[S+71] R. Siddle et al., *Coincidence π^0 electroproduction experiments in the first resonance region at momentum transfers of 0.3, 0.45, 0.60, 0.76 GeV/c^2*, Nucl. Phys. **B35** (1971), 93–119.

[S+75] S. Stein et al., *Electron scattering at 4-degrees with energies of 4.5-GeV - 20-GeV*, Phys. Rev. **D12** (1975), 1884.

[S+05] N. F. Sparveris et al., *Investigation of the conjectured nucleon deformation at low momentum transfer*, Phys. Rev. Lett. **94** (2005), 022003.

[S+06] S. Stave et al., *Lowest Q**2 measurement of the gamma* p –> delta reaction: Probing the pionic contribution*, Eur. Phys. J. **A30** (2006), 471–476.

[Sch03] S. Scherer, *Introduction to chiral perturbation theory*, Adv. Nucl. Phys. **27** (2003), 277.

[SDGS07a] M. R. Schindler, D. Djukanovic, J. Gegelia, and S. Scherer, *Chiral expansion of the nucleon mass to order O(q**6)*, Phys. Lett. **B649** (2007), 390–393.

[SDGS07b] M. R. Schindler, D. Djukanovic, J. Gegelia, and S. Scherer, *Infrared renormalization of two-loop integrals and the chiral expansion of the nucleon mass*, arXiv:0707.4296 [hep-ph].

[SL96] T. Sato and T. S. H. Lee, *Meson-exchange model for pi N scattering and gamma N –> pi N reaction*, Phys. Rev. **C54** (1996), 2660–2684.

[SL01a] T. Sato and T. S. H. Lee, *Dynamical study of the Delta excitation in N(e,e' pi) reactions*, Phys. Rev. **C63** (2001), 055201.

[SL01b] T. Sato and T. S. H. Lee, *Dynamical study of the Delta excitation in N(e,e' pi) reactions*, Phys. Rev. **C63** (2001), 055201.

[SUW+00] A. Silva, D. Urbano, T. Watabe, M. Fiolhais, and K. Goeke, *The electroproduction of the Delta(1232) in the chiral quark-soliton model*, Nucl. Phys. **A675** (2000), 637–657.

[TDKY03] L. Tiator, D. Drechsel, S. S. Kamalov, and S. N. Yang, *Electromagnetic form-factors of the Delta(1232) excitation*, Eur. Phys. J. **A17** (2003), 357–363.

[Ter99] O. V. Teryaev, *Spin structure of nucleon and equivalence principle*, arXiv:hep-ph/9904376.

[Wei76] S. Weinberg, *Implications of Dynamical Symmetry Breaking*, Phys. Rev. **D13** (1976), 974–996.

[Wei79] S. Weinberg, *Implications of Dynamical Symmetry Breaking: An Addendum*, Phys. Rev. **D19** (1979), 1277–1280.

[WW87] A. Wirzba and W. Weise, *The E2 / M1 transition ratio for gamma N → Delta (1232) in a modified Skyrme model*, Phys. Lett. **B188** (1987), 6.

[xpr] *http://www-spires.dur.ac.uk/hepdata/pdf3.html*.

[Y+06] W. M. Yao et al., *Review of particle physics*, J. Phys. **G33** (2006), 1–1232.

Acknowledgements – Danksagungen

Finally, this last page is dedicated to all those who directly influenced this work and without whom it would not have been possible in this form. In particular, I am grateful to

- Prof. Dr. Wolfram Weise who initiated, supported and supervised this work for motivating and insightful discussions.
- Dr. Thomas Hemmert who is the reason why this work is written in the first person *plural*. All results of this work were developed in interesting and inspiring discussion with him.
- Marina Dorati who also is part of the "we" in chapter five of this work and influenced many other passages by her views.
- Bernhard Musch, Michael Thaler and Stefan Fritsch who reliably and patiently took care about the computer infrastructure at T39.
- Bernhard Musch again for sharing his profound knowledge about statistical uncertainies with me.
- Everybody else who was a member of the "Institut für theoretische Physik T39" during the years of my stay there for delightful discussions about many topics: Norbert Kaiser, Philipp Hägler, Bertram Klein, Massimiliano Procura, Chihiro Sasaki, Ying Cui, Youngshin Kwon, Alexander Laschka, Simon Rößner, Nino Bratovic, Thomas Hell, Philip de Homont, Jorge Martin Camalich, Akinobu Dote, Harald Grießammer, Paolo Finelli, Claudia Ratti, Rainer Härtle, Johannes Eiglsperger, Robert Hildebrandt, Monika Mühlbauer, Bernhard Langwallner, Stefan Christlmeier, Tim Wollenweber, Claudia Hagedorn, Daisuke Jido, Edisher Lipartia, Robin Nissler, Bugra Borasoy, Alberto Polleri and Susanne Tillich.
- Constantia Alexandrou for providing us with detailed informations about the lattice simulations of the form factors of the nucleon and Lothar Tiator for the discussions about the experimental data situation for the $N\Delta$ transition form factors.
- Meinen Eltern und Großeltern für die vielfältige, nicht zuletzt finanzielle Unterstützung während meines gesamten Studiums.